SCHOOL ON ADVANCED MODELING OF SEISMIC HAZARD IN AFRICA
National Research Institute of Astronomy and Geophysics (NRIAG), Helwan, Cairo, 24-29 October 2014

Scenario based seismic (and tsunami) hazard assessment

Fabio Romanelli
(A. Magrin, A. Peresan, F. Vaccari, G.F. Panza and many others)

1 - Department of Mathematics & Geosciences, University of di Trieste
2 - ICTP - SAND Group - The Abdus Salam International Centre for Theoretical Physics

romanel@units.it

UNIVERSITÀ DEGLI STUDI DI TRIESTE

the road to (earthquake) safety...

Know the input - Bound the output...

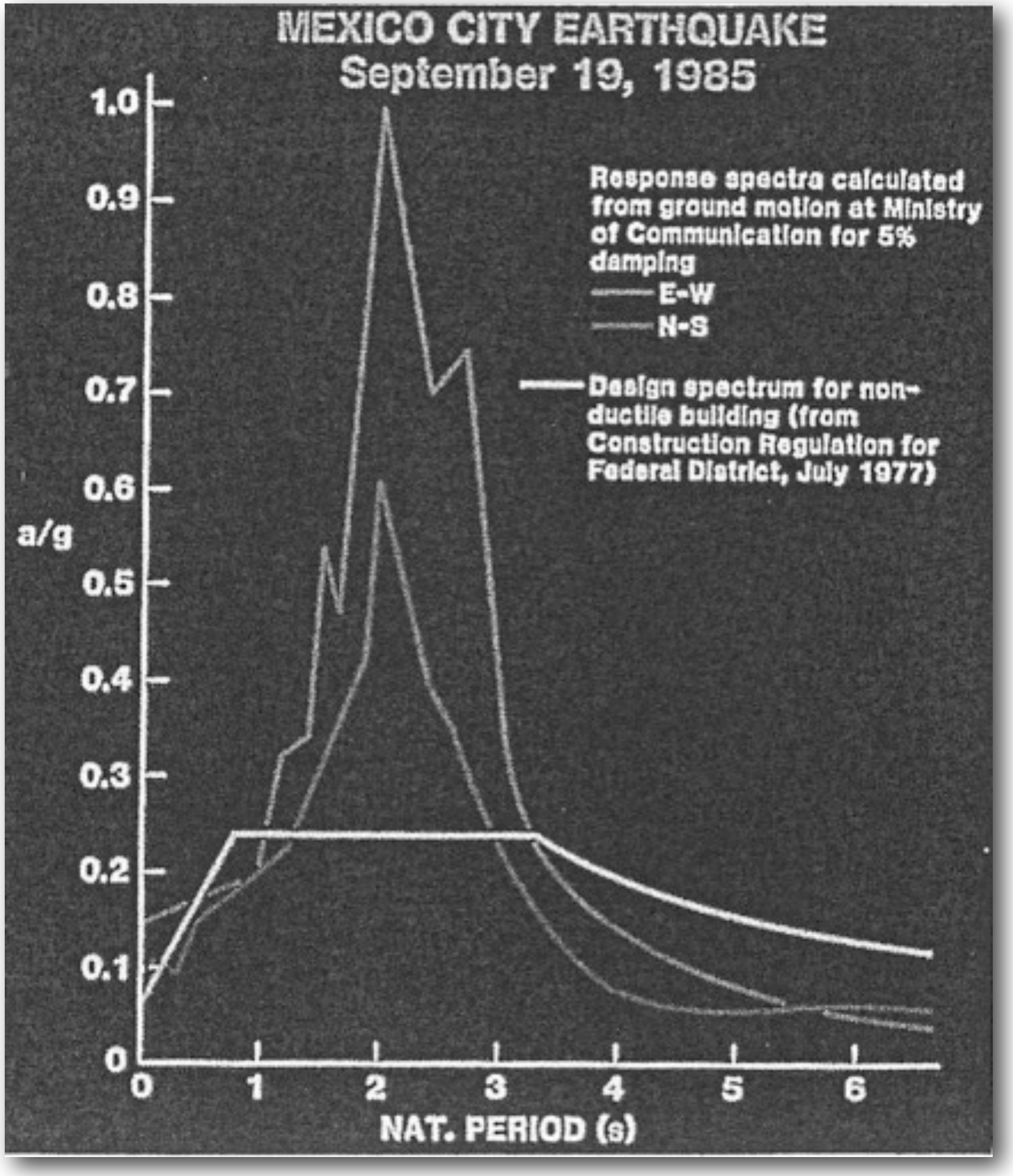

Mitigate the difference...

the road to (earthquake) safety...

Know the input - Bound the output...

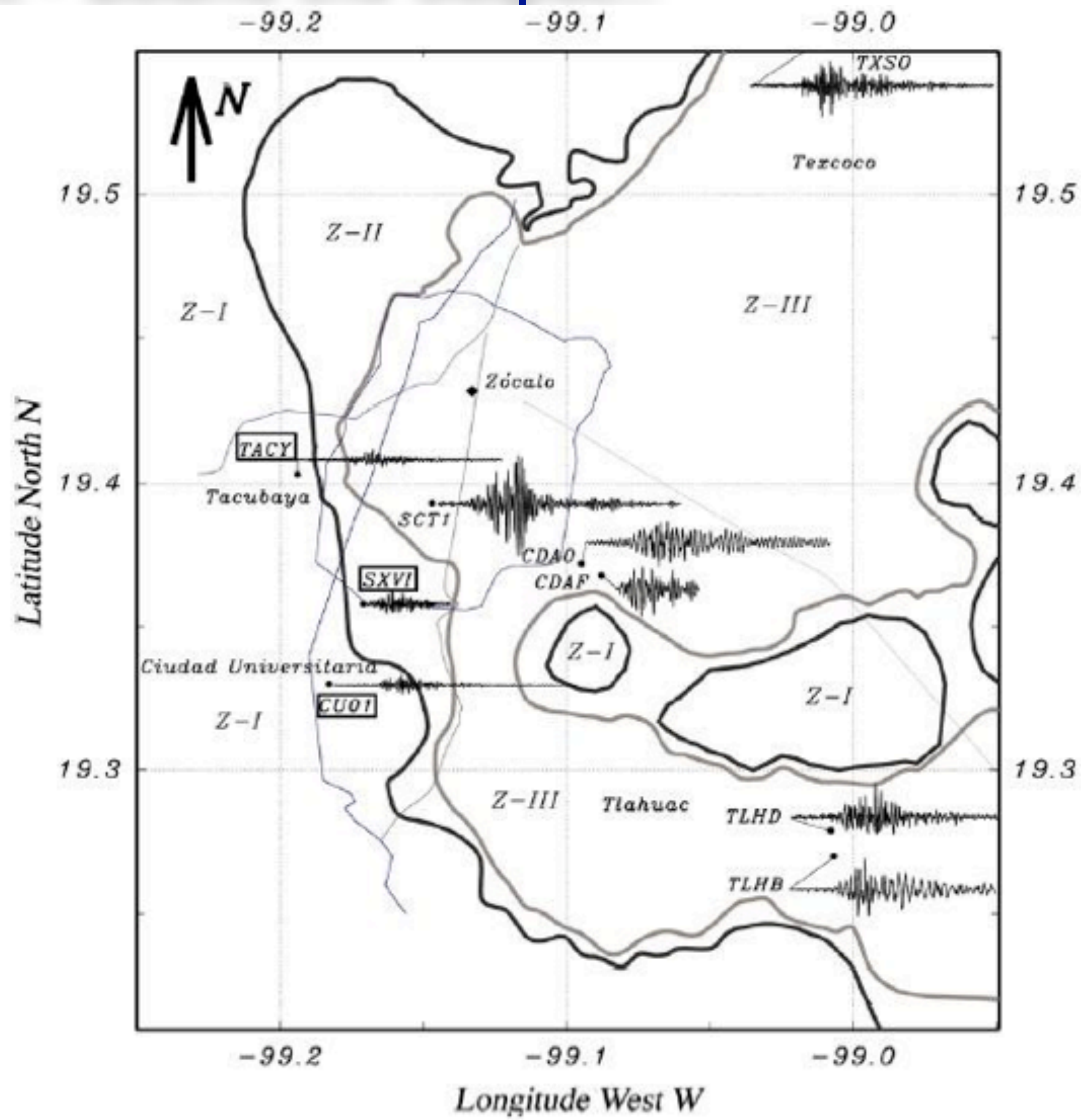

Mitigate the difference...

the road to (earthquake) safety...

Know the input - Bound the output...

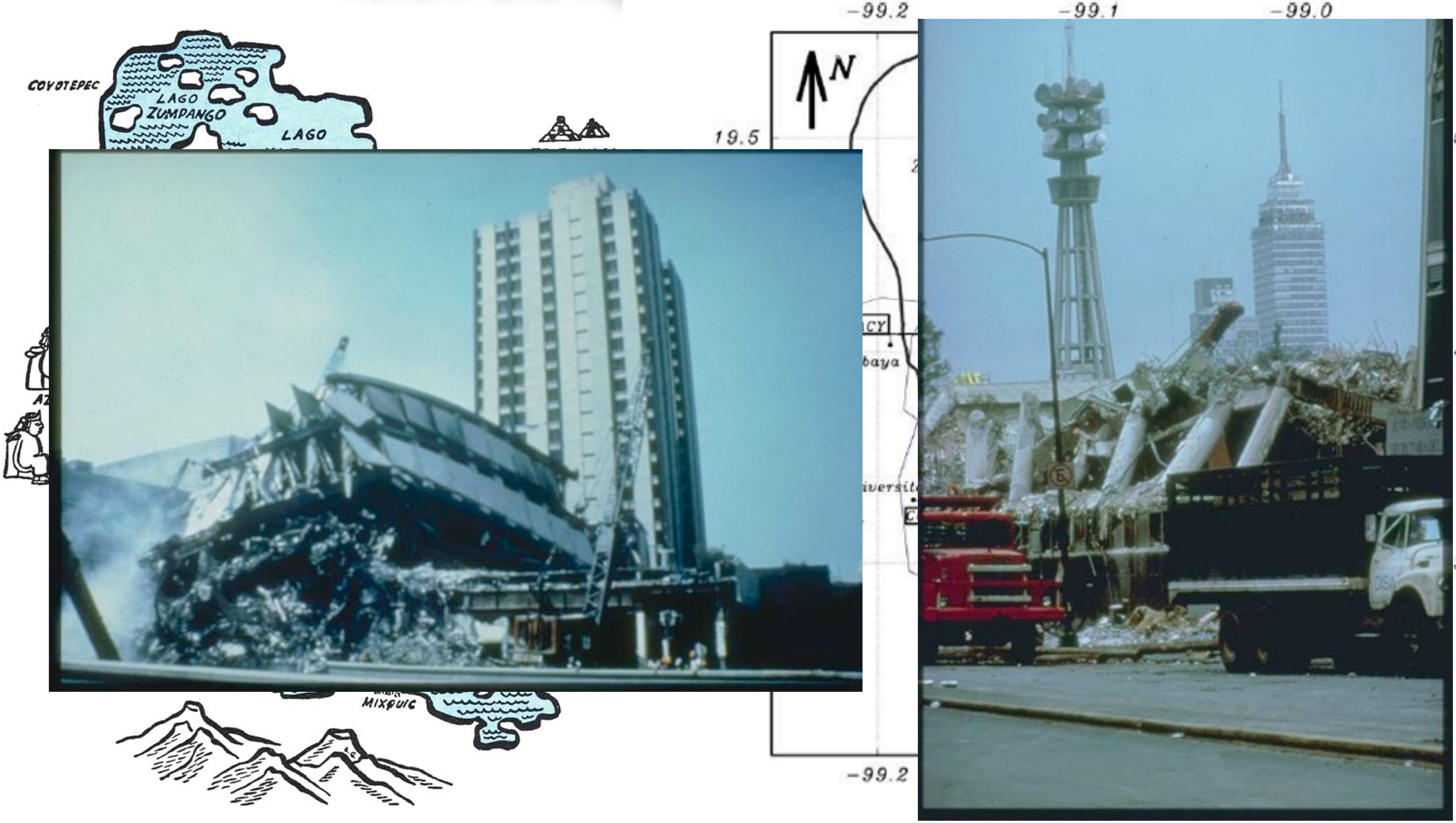

Mitigate the difference...

Response spectra

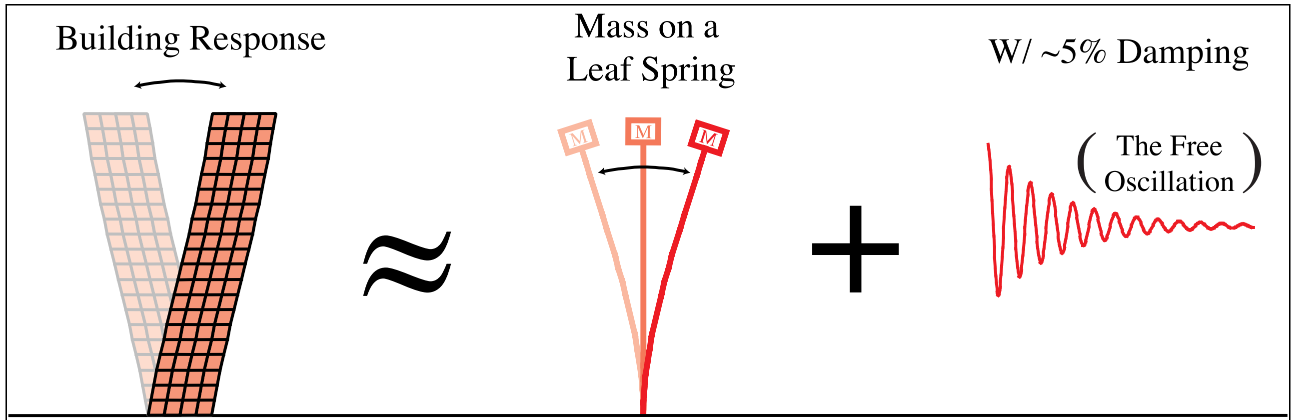

Figure 1. The response-spectrum value is the peak motion (displacement, velocity, or acceleration) of a damped single-degree of freedom harmonic oscillator (with a particular damping and resonant period) subjected to a prescribed ground motion.

Response spectra

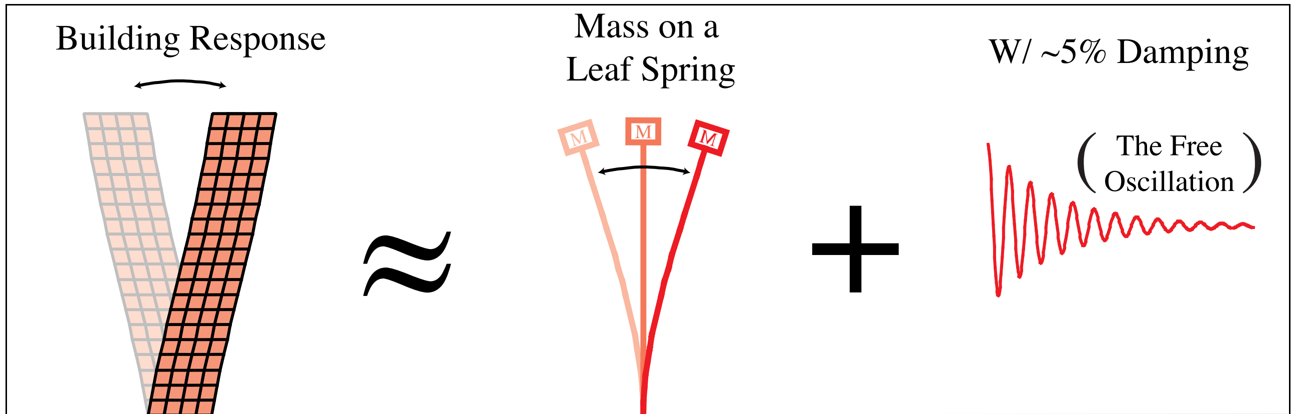

Figure 1. The response-spectrum value is the peak motion (displacement, velocity, or acceleration) of a damped single-degree of freedom harmonic oscillator (with a particular damping and resonant period) subjected to a prescribed ground motion.

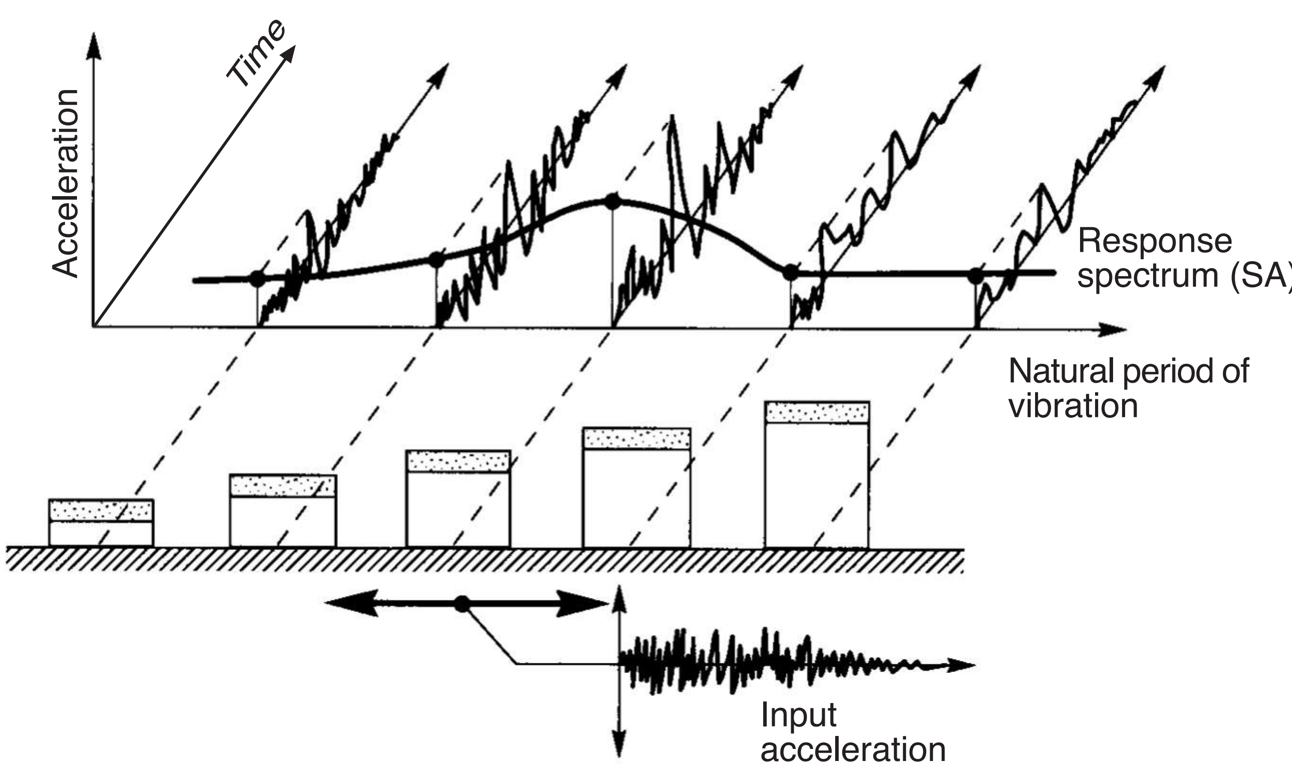

Response spectra

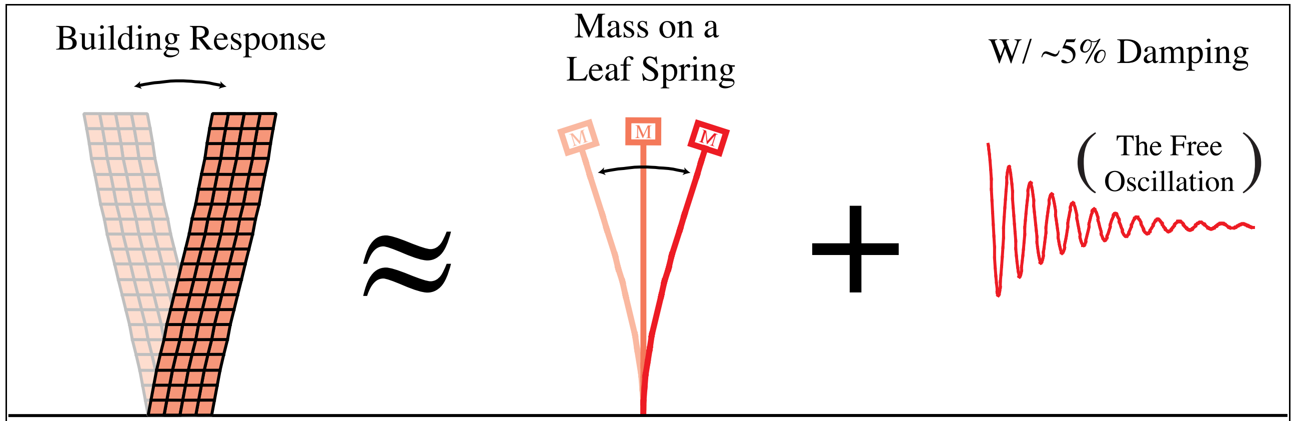

Figure 1. The response-spectrum value is the peak motion (displacement, velocity, or acceleration) of a damped single-degree of freedom harmonic oscillator (with a particular damping and resonant period) subjected to a prescribed ground motion.

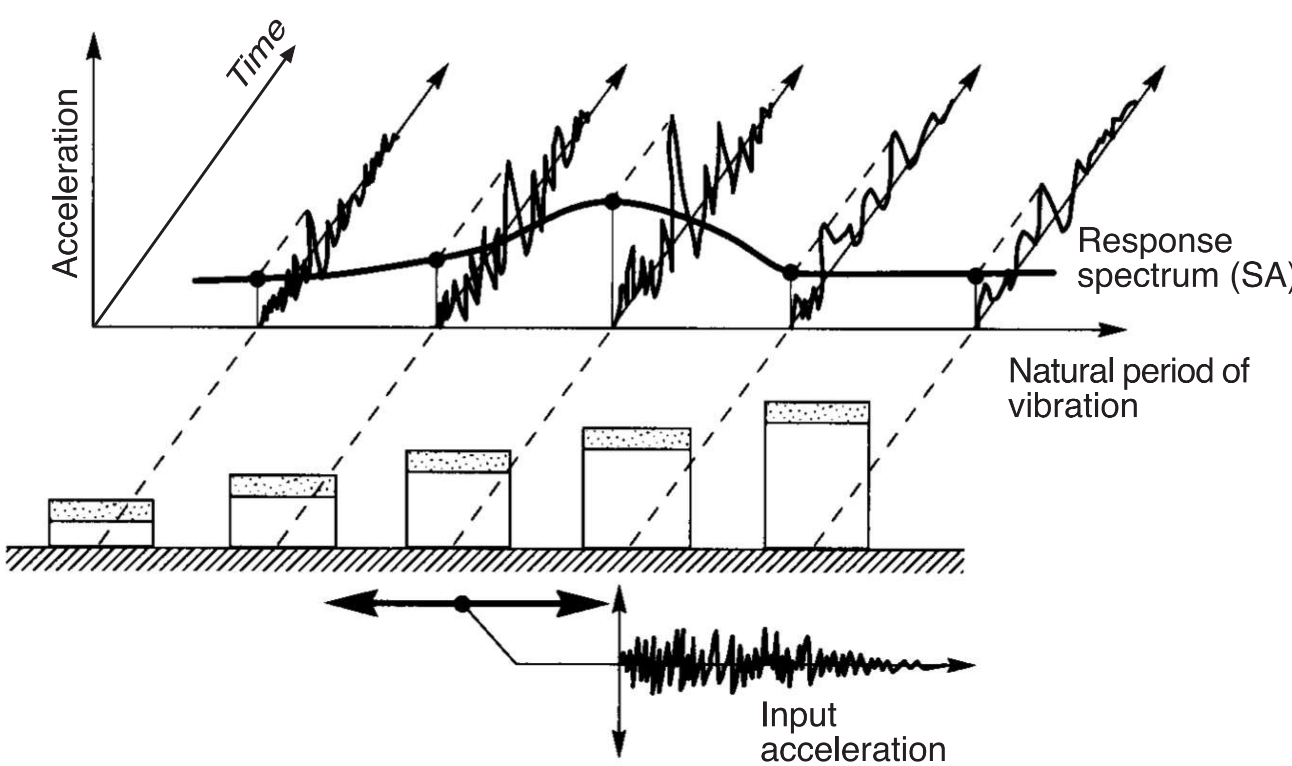

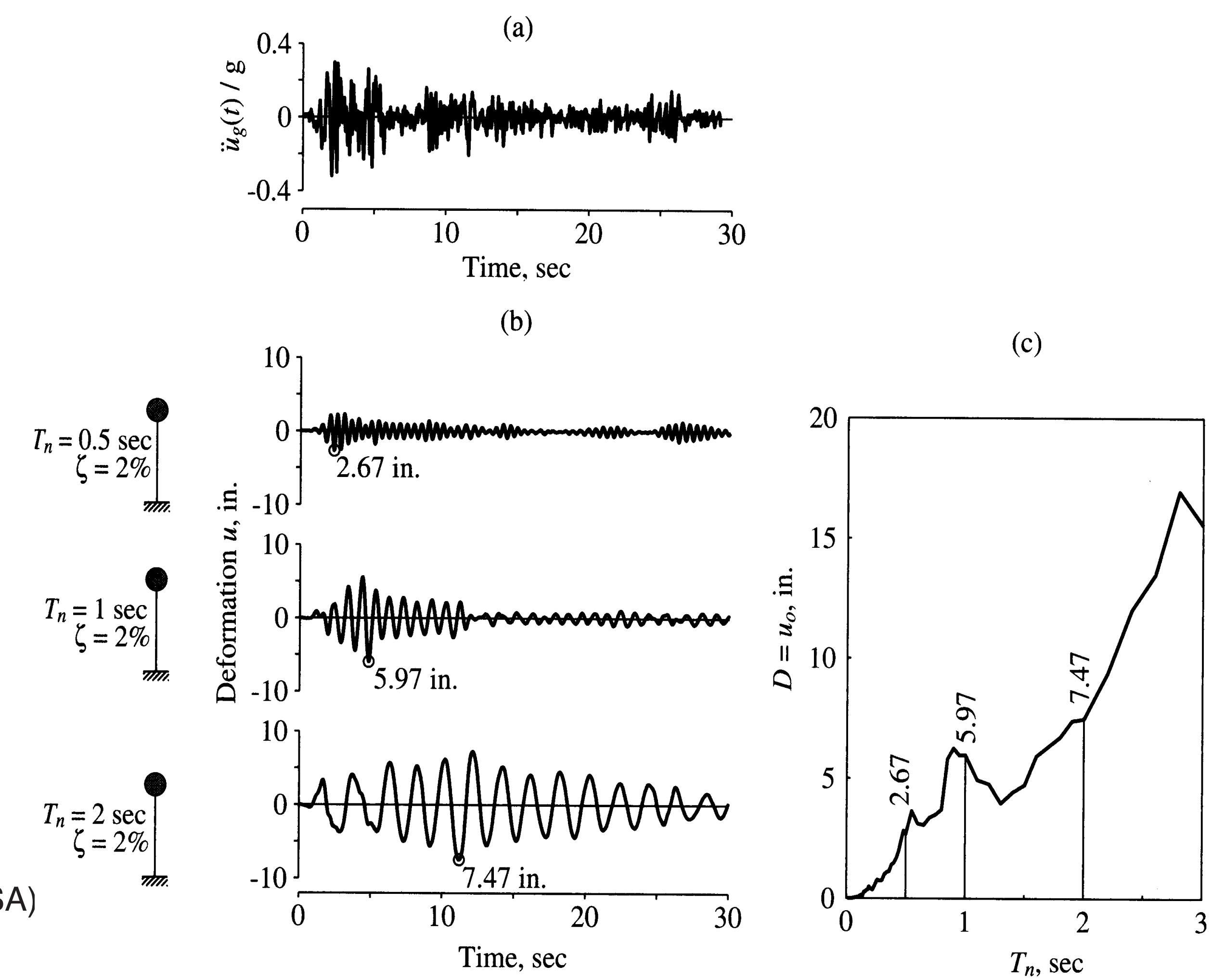

Figure 6.6.1 (a) Ground acceleration; (b) deformation response of three SDF systems with $\zeta = 2\%$ and $T_n = 0.5$, 1, and 2 sec; (c) deformation response spectrum for $\zeta = 2\%$.

SITE EFFECTS

Surface topography effects (convexity)

sensitivity to:

a) type of wavefield

b) angle of incidence

c) shape and sharpness

SITE EFFECTS

Surface topography effects (convexity)

sensitivity to:

a) type of wavefield
b) angle of incidence
c) shape and sharpness

SITE EFFECTS

Soft surface layering

a) 1-D: trapping of waves for impedance contrast
(vertical resonances)
$fn=(2n+1)\beta/4H$
$A \approx (\rho 2\ v2)/(\rho 1\ v1)$

b) 2-D 3-D: complex energy focusing
for diffraction effects
(basin edge waves)

Weak (and strong) motion

a) S/B spectral ratio
(Borcherdt, 1970)

b) generalized inversion scheme
(Andrews, 1986)

c) coda waves analysis
(Margheriti et al., 1994)

d) parametrized source and path inversion
(Boatwright et al., 1991)

e) H/V spectral ratio (receiver function)
(Lermo et al., 1993)

Empirical techniques for Site effect estimation

Empirical techniques for Site effect estimation

Weak (and strong) motion

a) S/B spectral ratio
(Borcherdt, 1970)
b) generalized inversion scheme
(Andrews, 1986)
c) coda waves analysis
(Margheriti et al., 1994)
d) parametrized source and path inversion
(Boatwright et al., 1991)
e) H/V spectral ratio (receiver function)
(Lermo et al., 1993)

Microtremors

a) peak frequencies examination
b) S/B spectral ratio
c) H/V spectral ratio
(Nagoshi, 1971; Nakamura, 1989)
d) array analysis
(Malagnini et al., 1993)

Weak (and strong) motion

a) S/B spectral ratio
(Borcherdt, 1970)

b) generalized inversion scheme
(Andrews, 1986)

c) coda waves analysis
(Margheriti et al., 1994)

d) parametrized source and path inversion
(Boatwright et al., 1991)

e) H/V spectral ratio (receiver function)
(Lermo et al., 1993)

Empirical techniques for Site effect estimation

$$R_{ij} = So_i(\omega) \cdot P_{ij}(\omega) \cdot S_j(\omega)$$

Microtremors

a) peak frequencies examination

b) S/B spectral ratio

c) H/V spectral ratio
(Nagoshi, 1971; Nakamura, 1989)

d) array analysis
(Malagnini et al., 1993)

Road map

Road map

- Some remarks on SHA
  - Source & site effects
  - Integrated methodology

Road map

- Some remarks on SHA
  - Source & site effects
  - Integrated methodology
- A bird's eye on Scenario Based SHA
  - Scenarios at regional scale
  - Detailed scenarios, that take into account local soil conditions
  - Tsunami physics

Source effects...

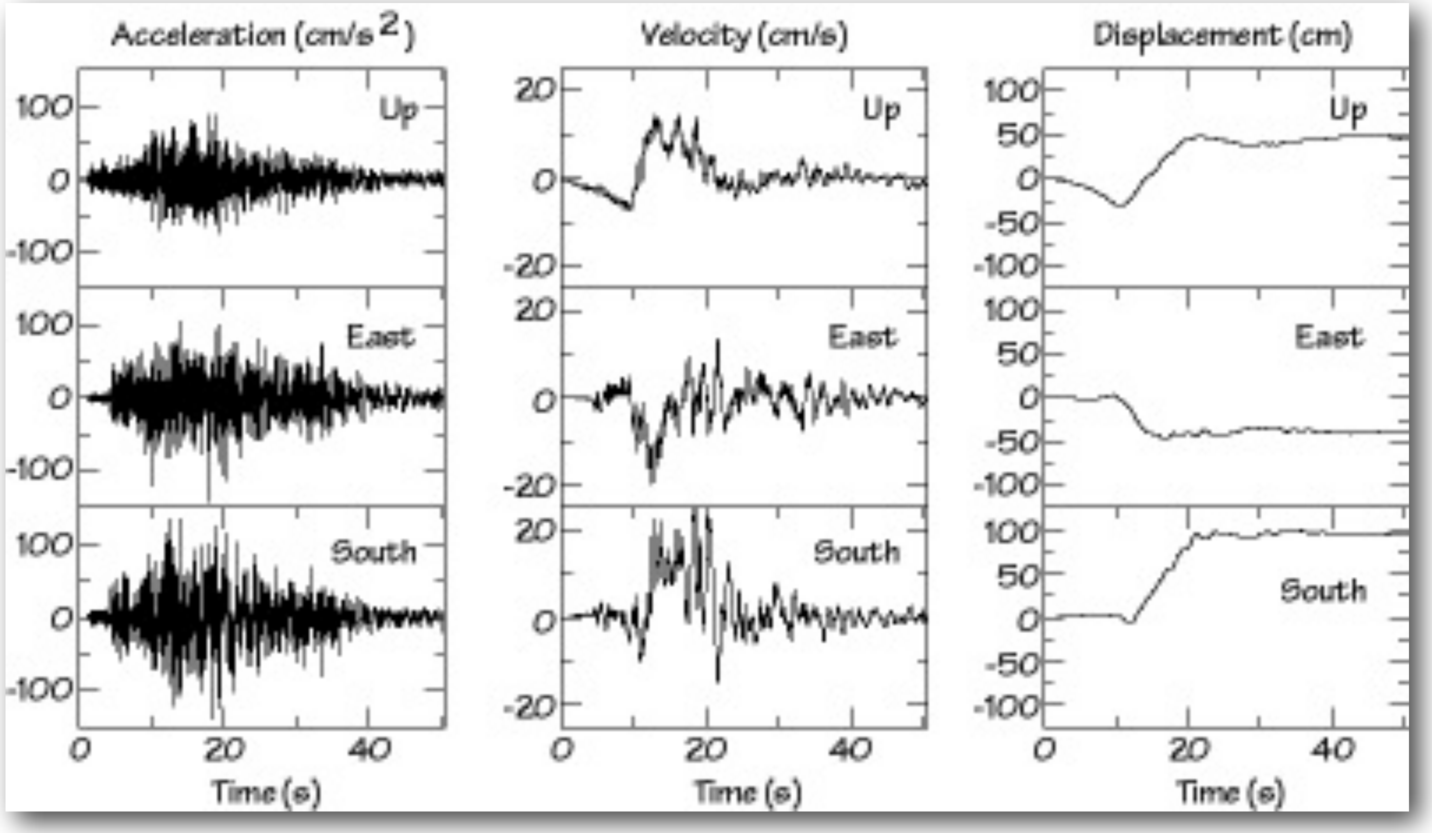

Michoacan, 1985

Source effects...

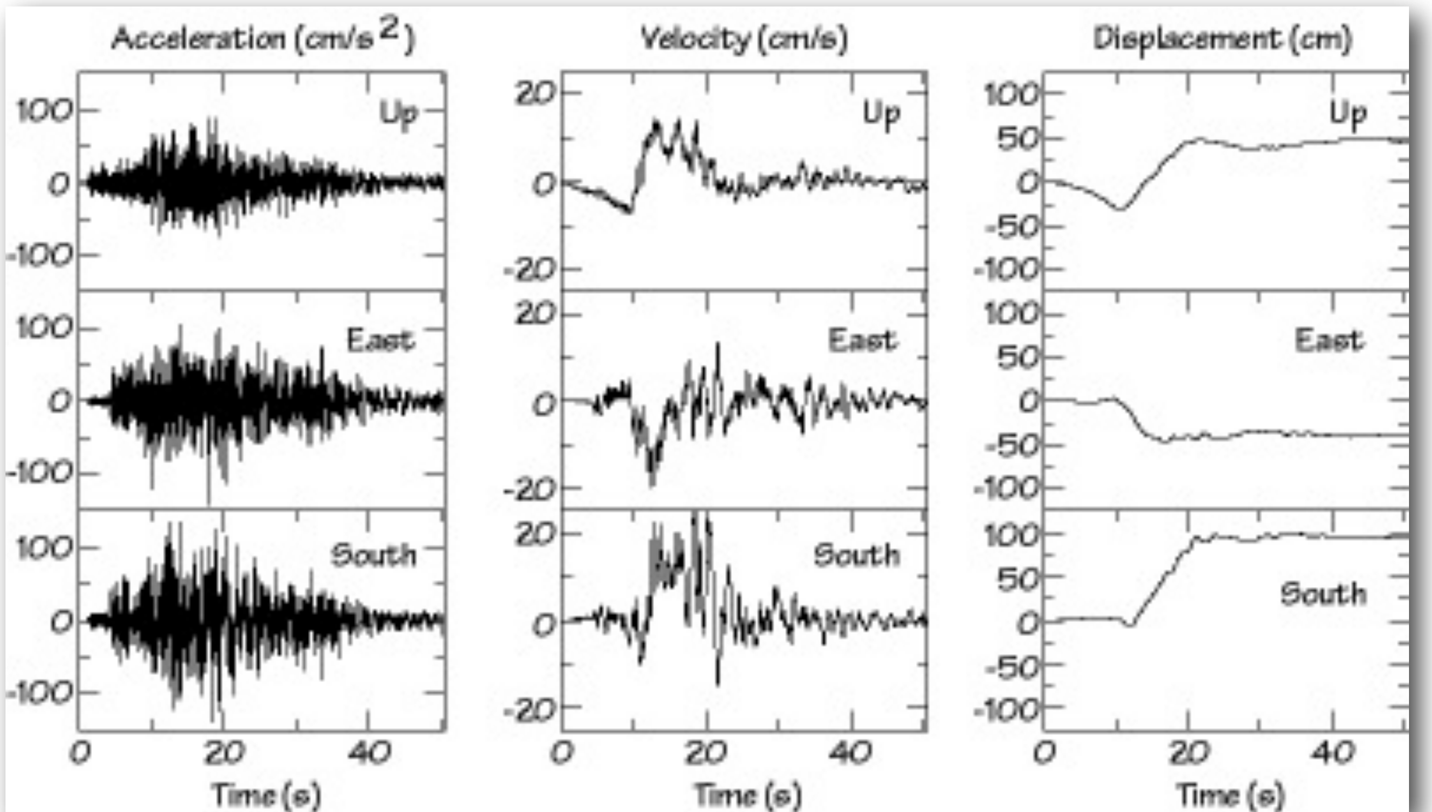

Michoacan, 1985

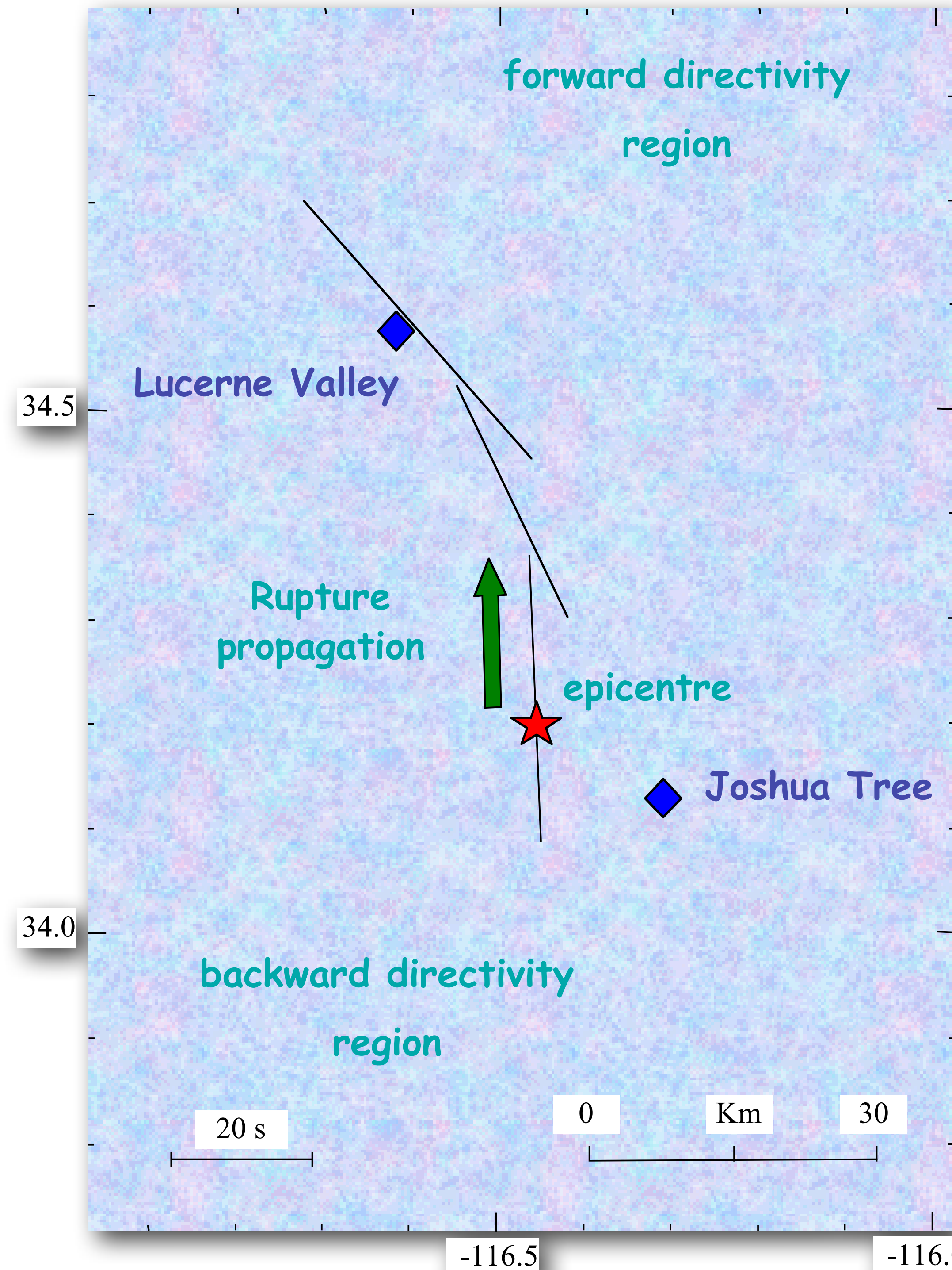

Landers, 1992

Source effects...

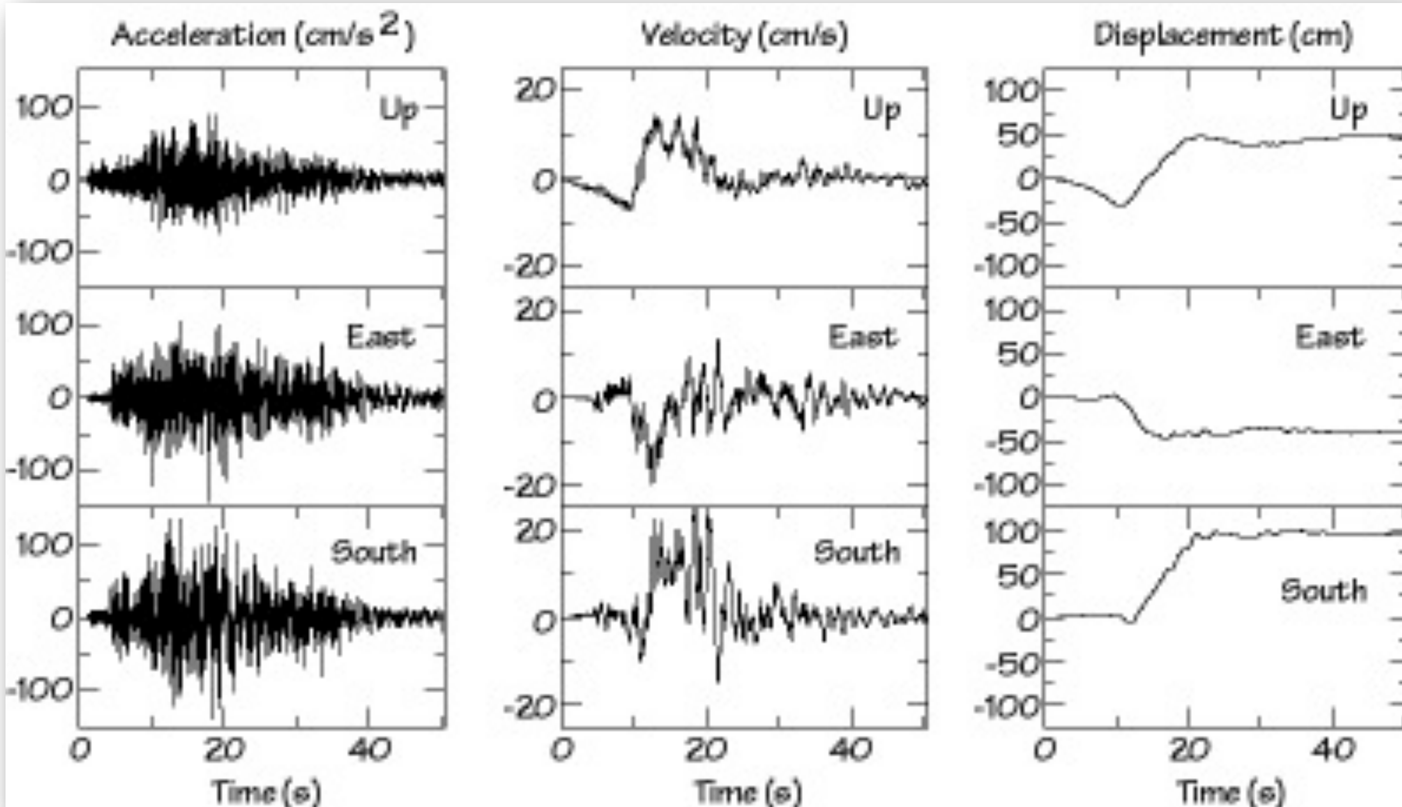

Michoacan, 1985

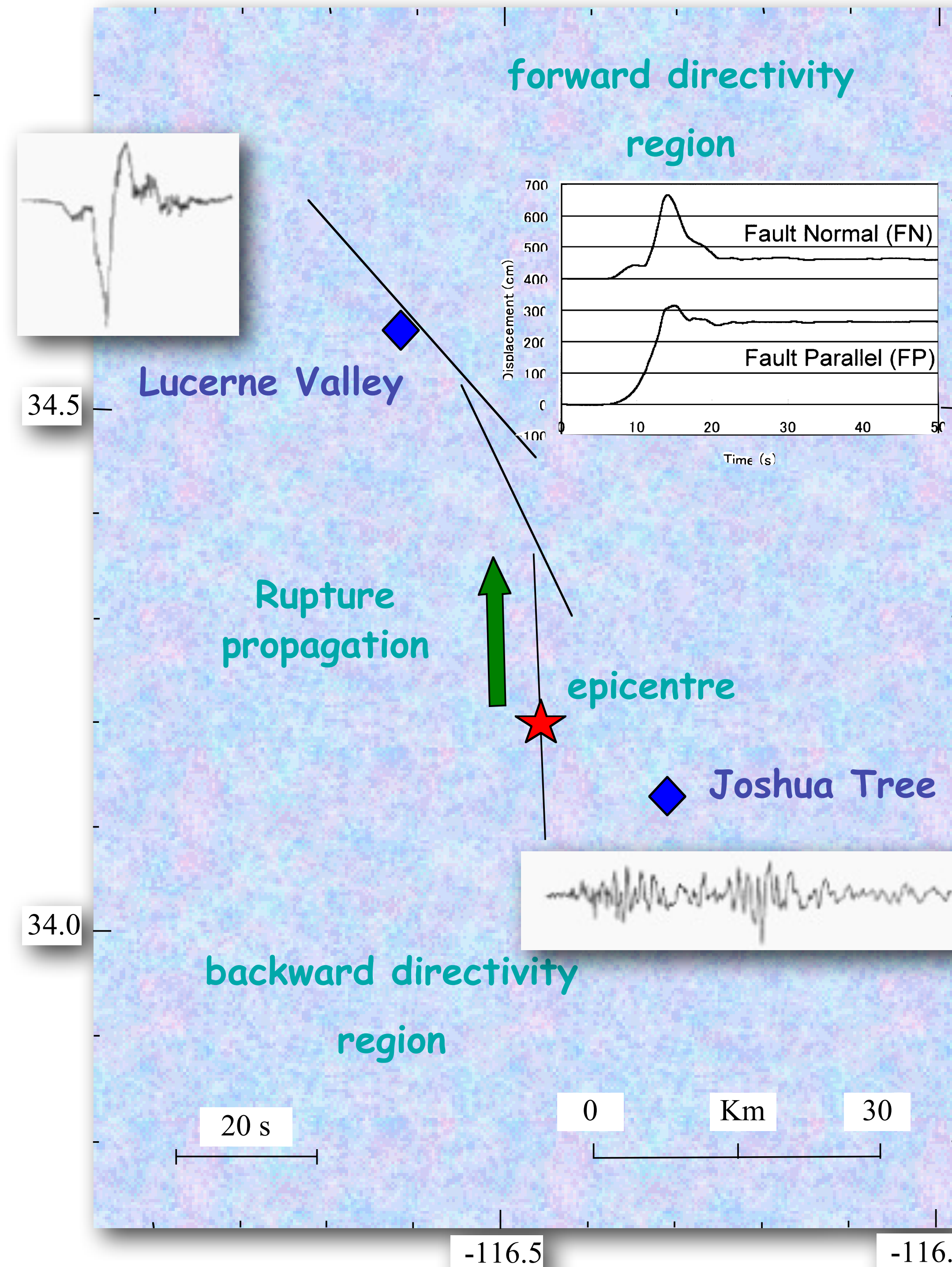

Landers, 1992

Source effects...

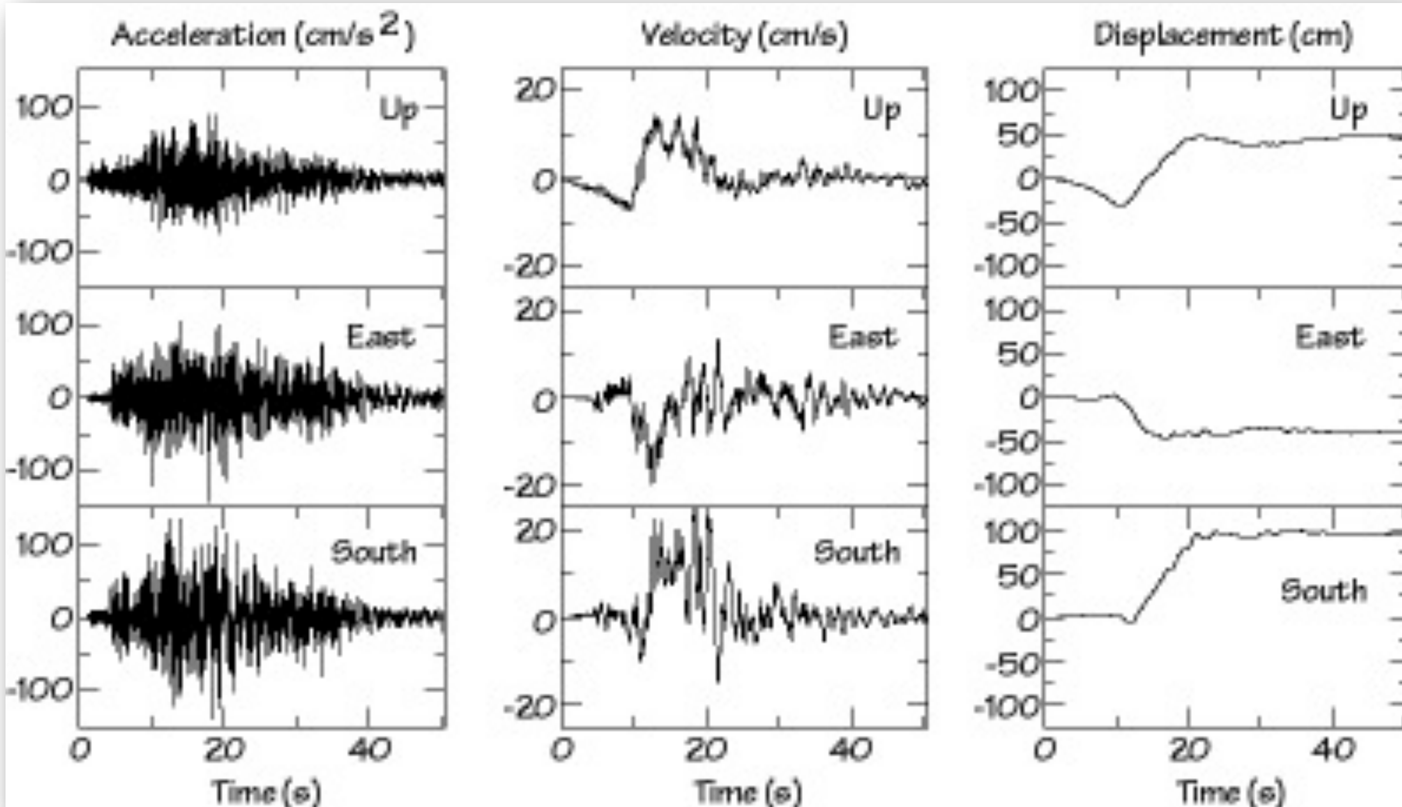

Michoacan, 1985

Fling & Directivity
aka
Near-field & Near-source

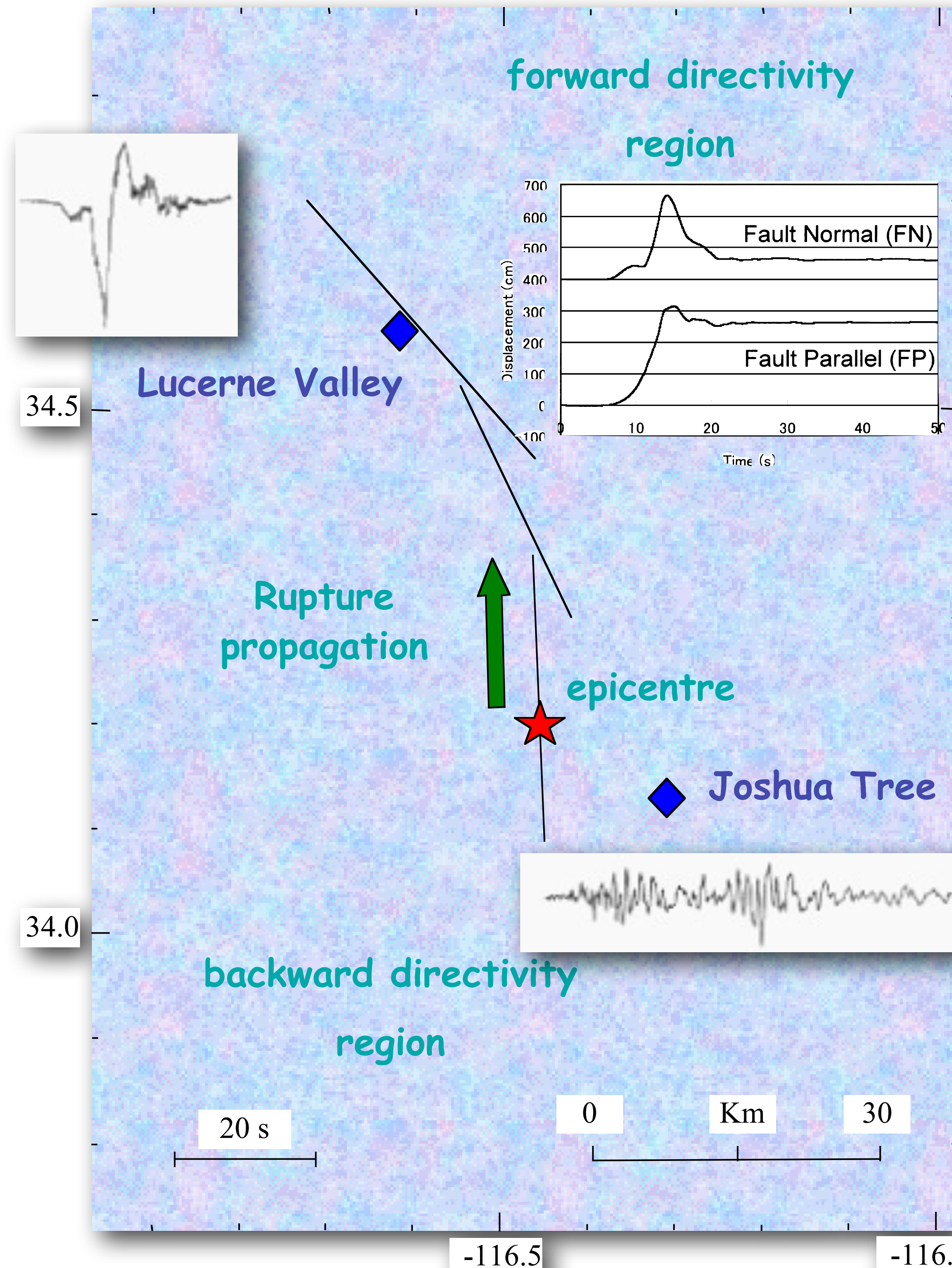

Landers, 1992

Source effects...

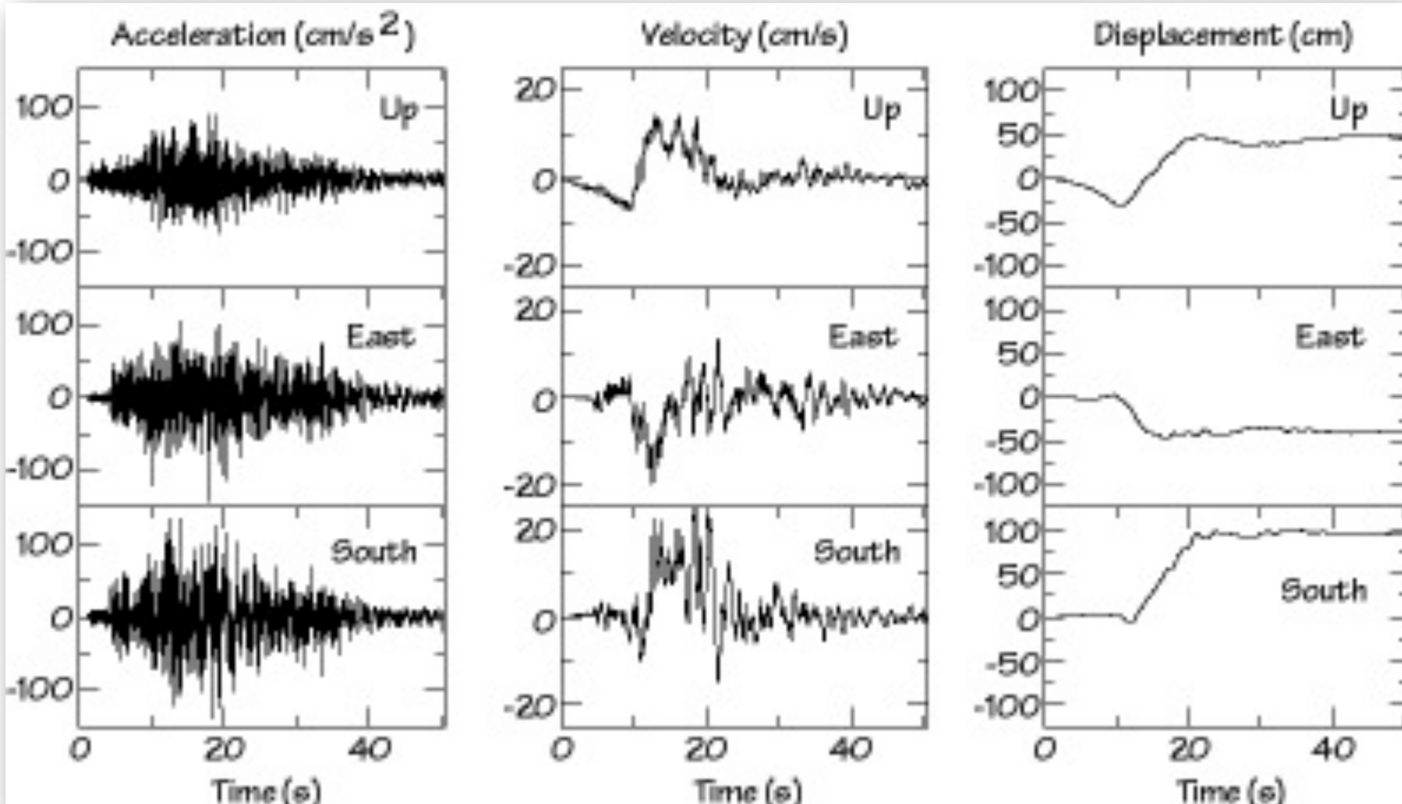

Michoacan, 1985

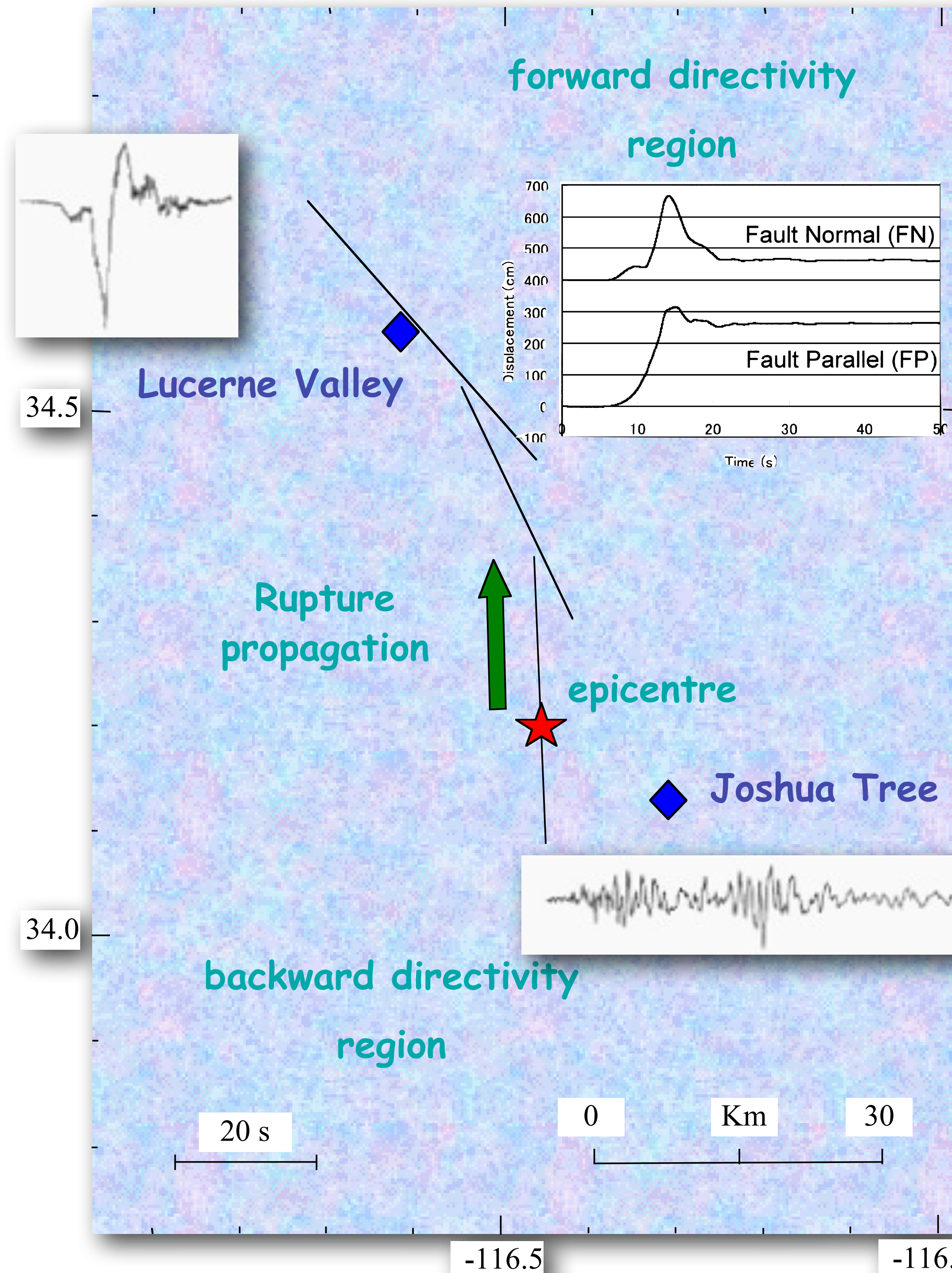

Landers, 1992

Fling & Directivity

aka

Near-field & Near-source

Sir Georges Stokes

Hugo Benioff

Near fault ground motion

Peer report, 2001

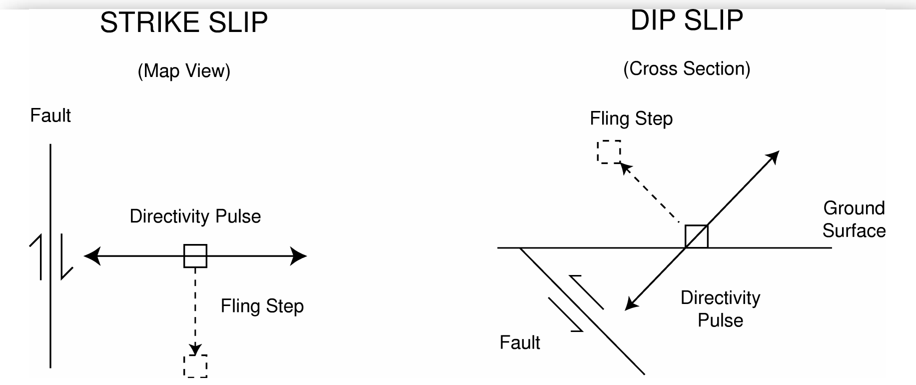

Fig. 4.3. Schematic diagram showing the orientations of fling step and directivity pulse for strike-slip and dip-slip faulting.

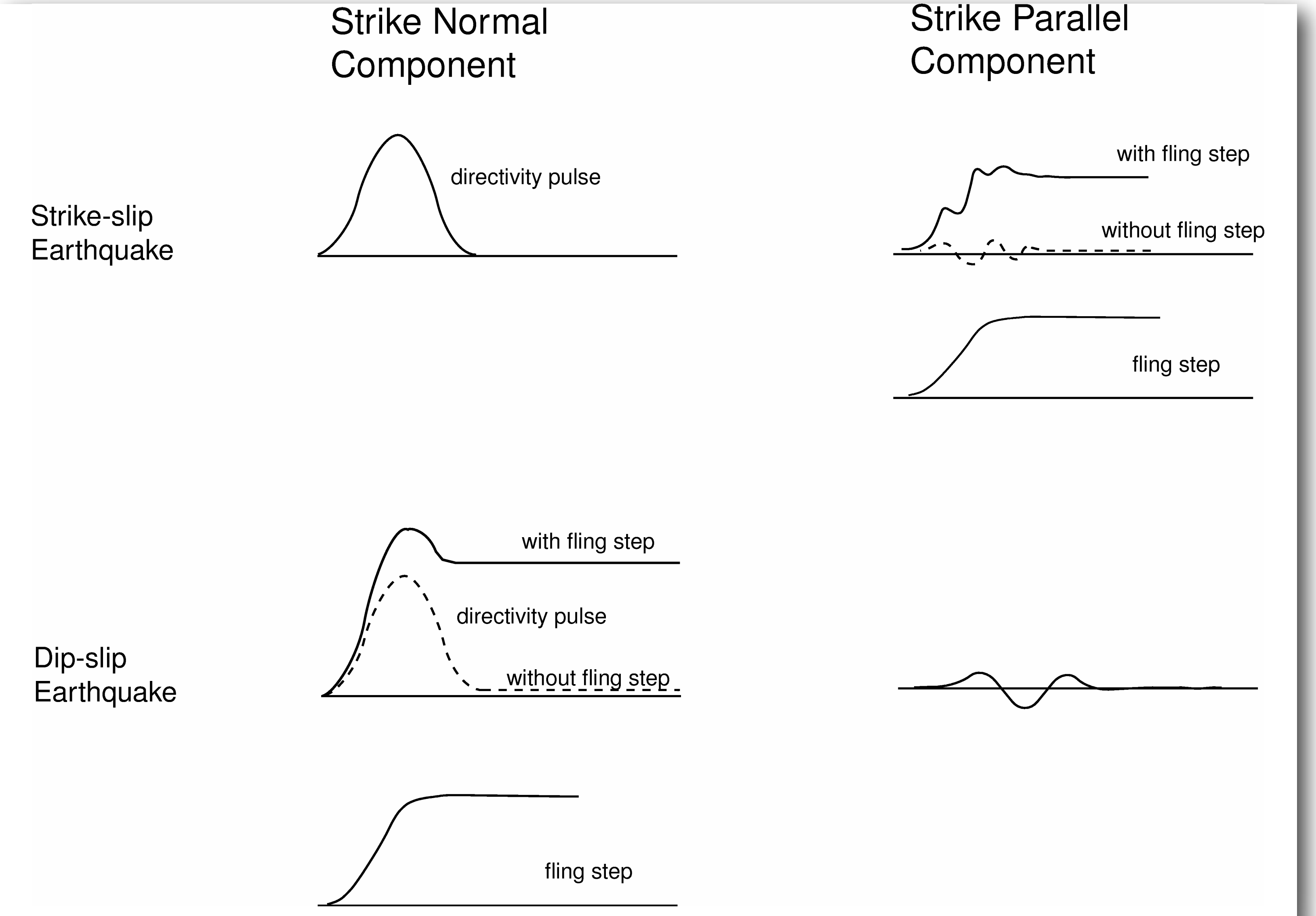

Fig. 4.4. Schematic diagram of time histories for strike-slip and dip-slip faulting in which the fling step and directivity pulse are shown together and separately.

Regression example...

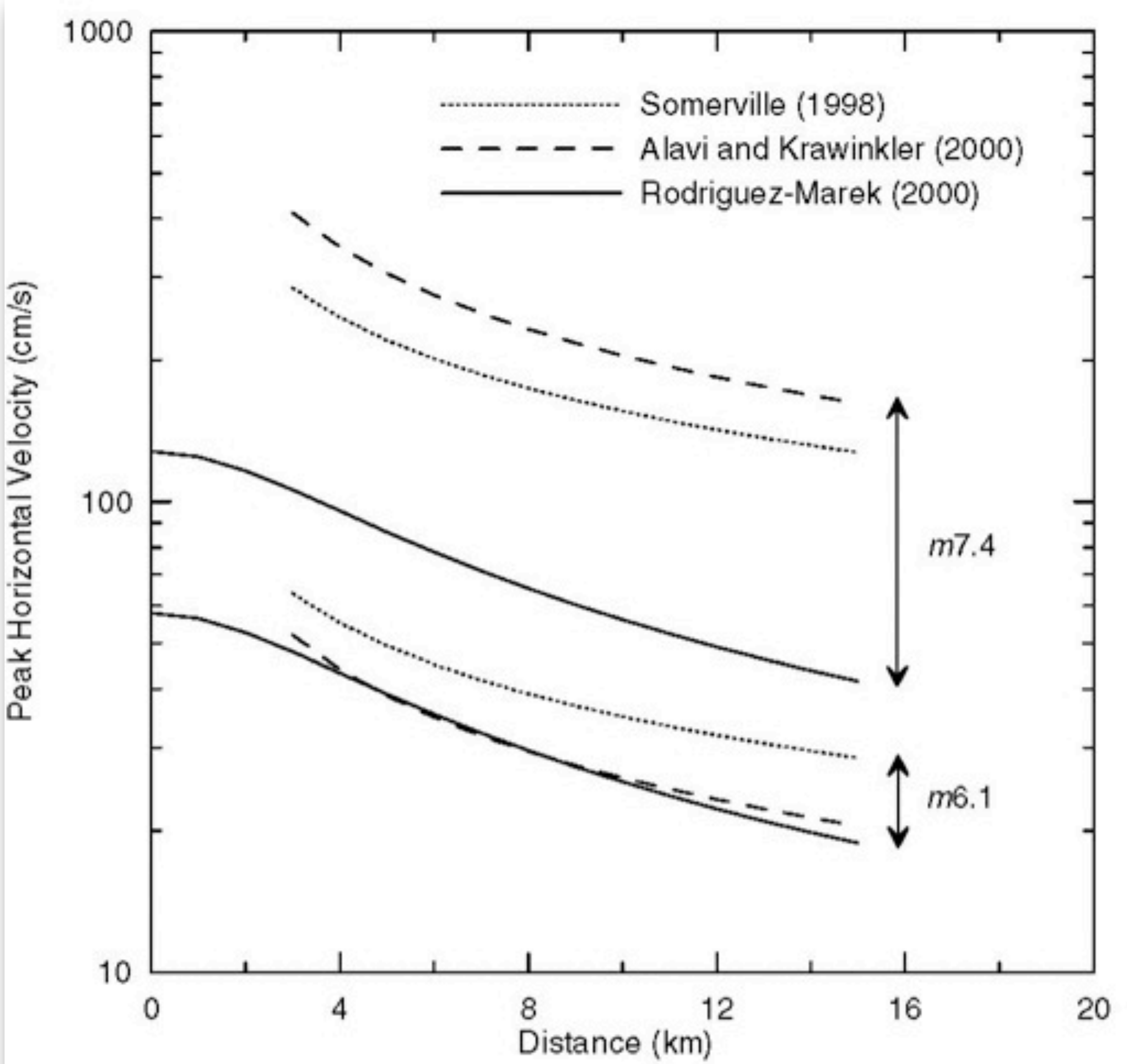

Rodriguez-Marek (2000):

$$\ln(PHV) = 2.44 + 0.5\,m - 0.41\,\ln(r^2 + 3.93^2)$$

Somerville (1998):

$$\ln(PHV) = -2.31 + 1.15\,m - 0.5\,\ln(r)$$

Alavi and Krawinkler (2000):

$$\ln(PHV) = -5.11 + 1.59\,m - 0.58\,\ln(r)$$

Peer report, 2001

Amplification patterns...

....may vary greatly among the earthquake scenarios, considering different source locations (and rupture ...)

SCEC
Phase 3
Report

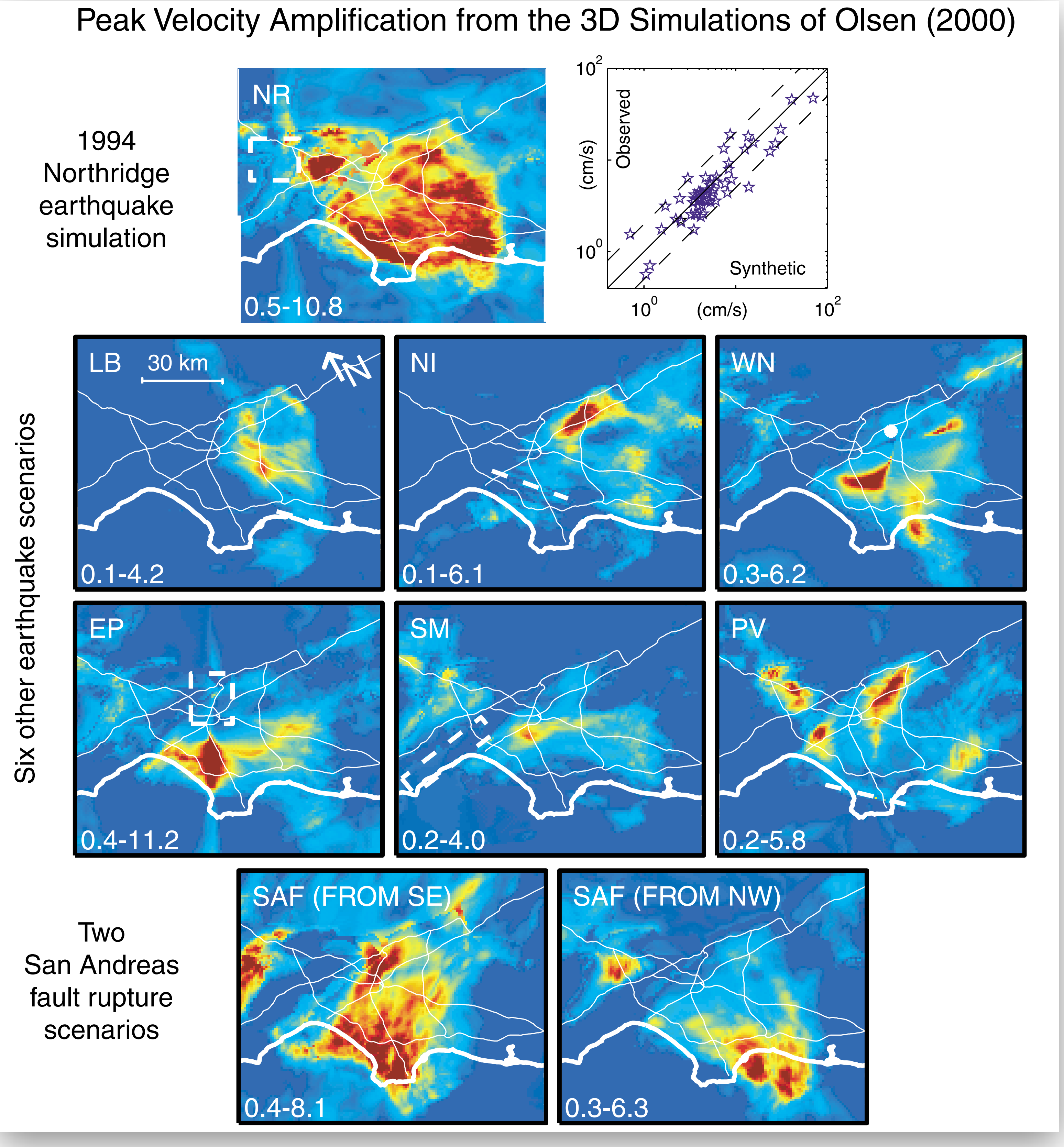

Important issues in SRE

- Near surface effects: impedance contrast, velocity

Important issues in SRE

- Near surface effects: impedance contrast, velocity
  - geological maps, v_{30}

Important issues in SRE

- Near surface effects: impedance contrast, velocity
    - geological maps, v_{30}
- Basin effects

Important issues in SRE

- Near surface effects: impedance contrast, velocity
  - geological maps, v_{30}
- Basin effects
  - Basin-edge induced waves

Important issues in SRE

- Near surface effects: impedance contrast, velocity
  - geological maps, v_{30}
- Basin effects
  - Basin-edge induced waves
  - Subsurface focusing

Important issues in SRE

- Near surface effects: impedance contrast, velocity
  - geological maps, v_{30}
- Basin effects
  - Basin-edge induced waves
  - Subsurface focusing

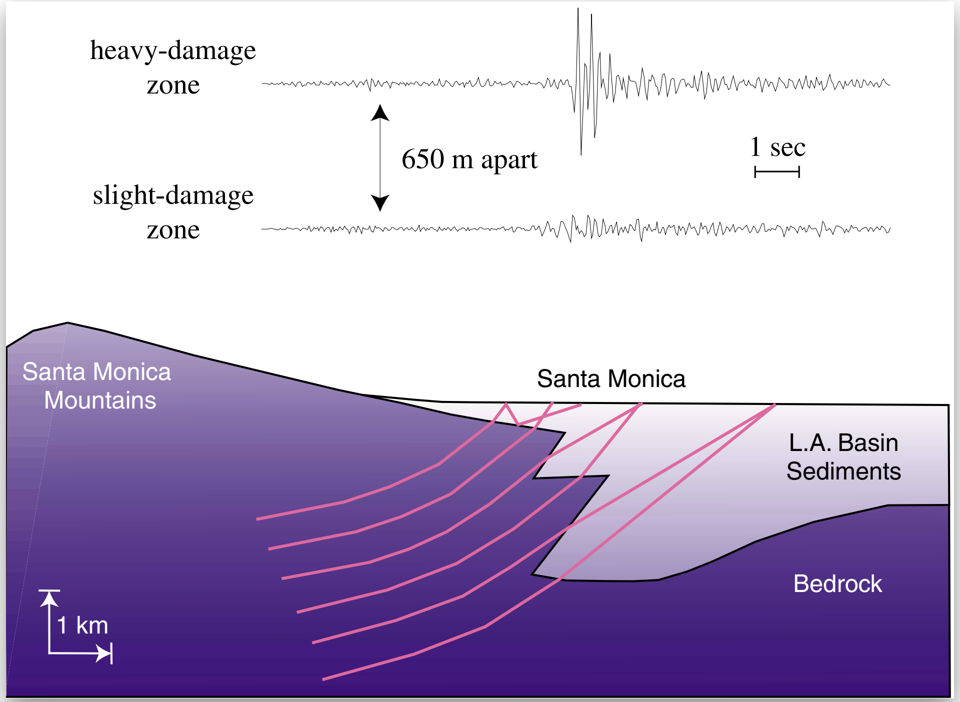

Important issues in SRE

- Near surface effects: impedance contrast, velocity
  - geological maps, v_{30}
- Basin effects
  - Basin-edge induced waves
  - Subsurface focusing

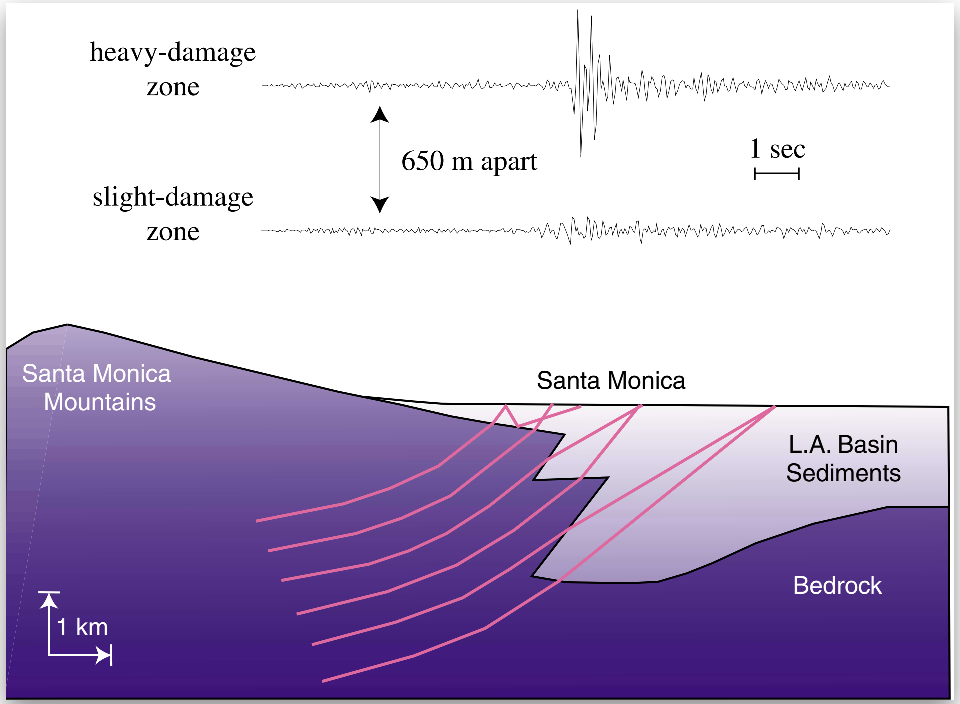

In SHA the site effect should be defined as the average behavior, relative to other sites, given all potentially damaging earthquakes.

This produces an intrinsic variability with respect to different earthquake locations, that cannot exceed the difference between sites

PGA as a demand parameter…

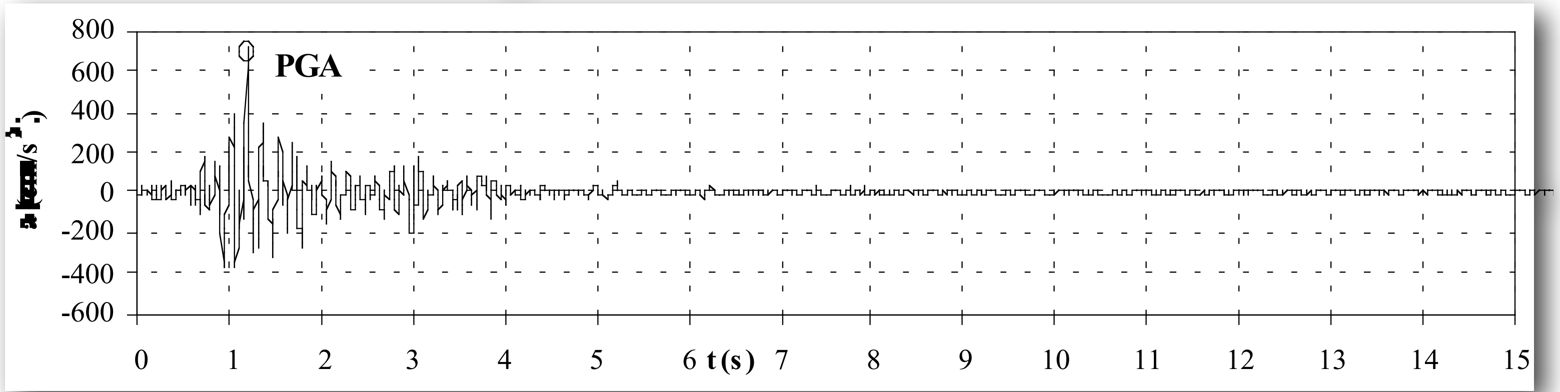

Figure 1 – Acceleration time history. Rocca NS record. 1971 Ancona earthquake (M_L=4.7)

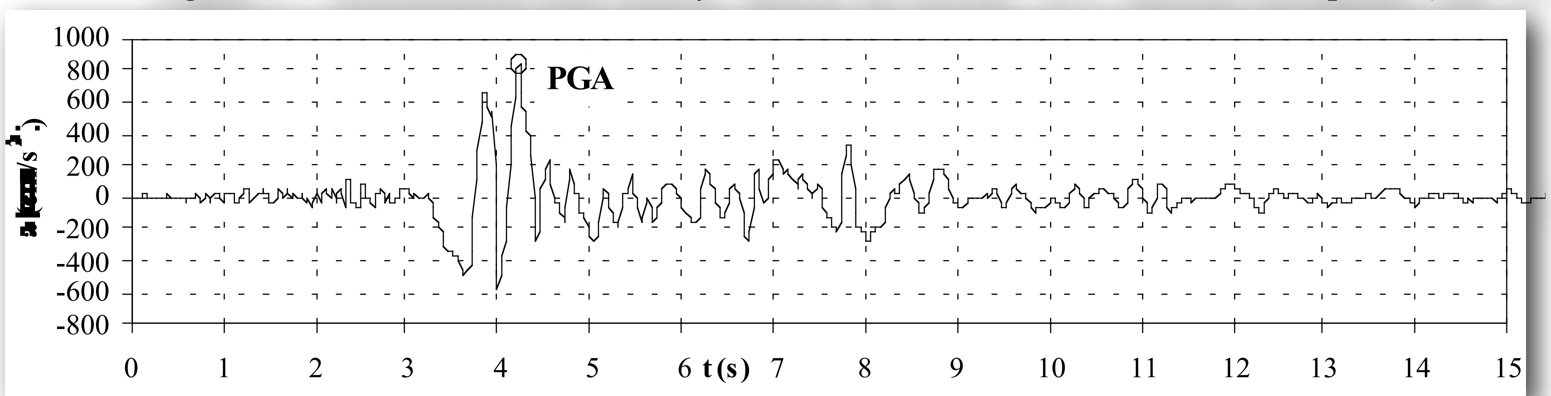

Figure 2 – Acceleration time history. Sylmar N360 record. 1994 Northridge earthquake (M_w=6.7)

PGA as a demand parameter…

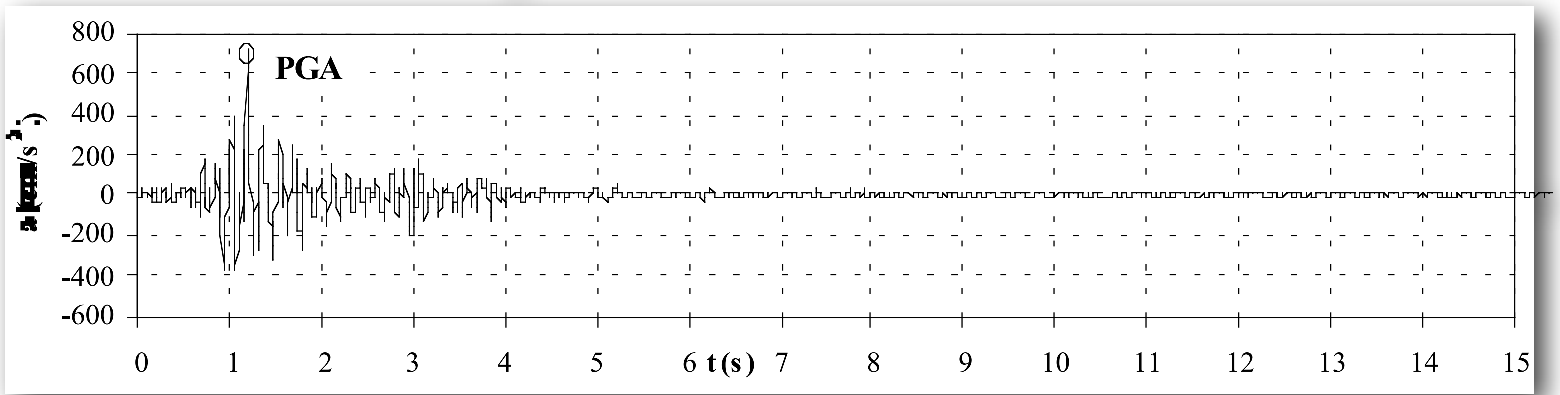

Figure 1 – Acceleration time history. Rocca NS record. 1971 Ancona earthquake (M_L=4.7)

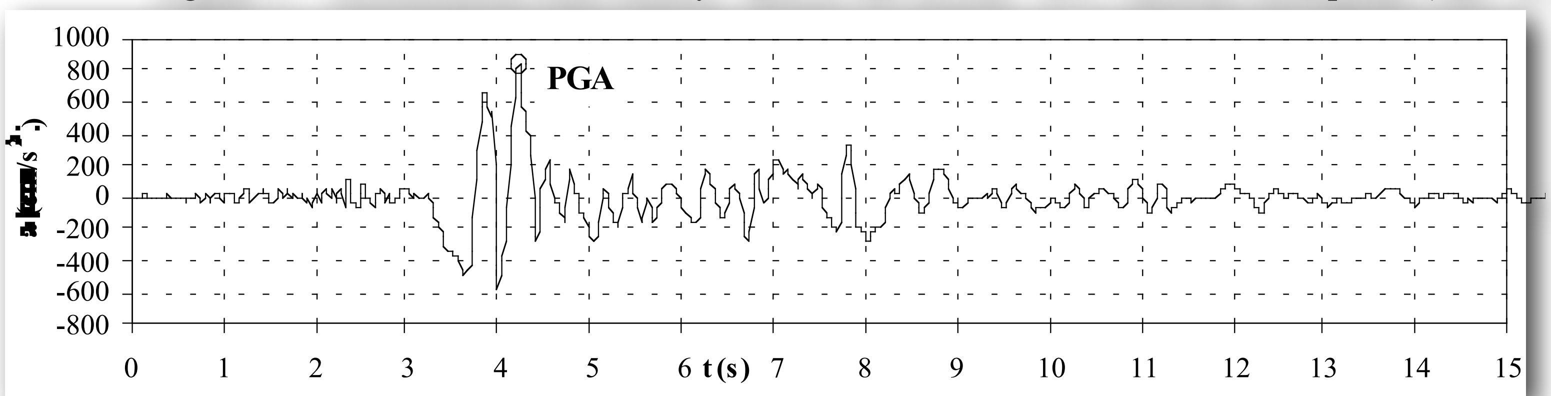

Figure 2 – Acceleration time history. Sylmar N360 record. 1994 Northridge earthquake (M_w=6.7)

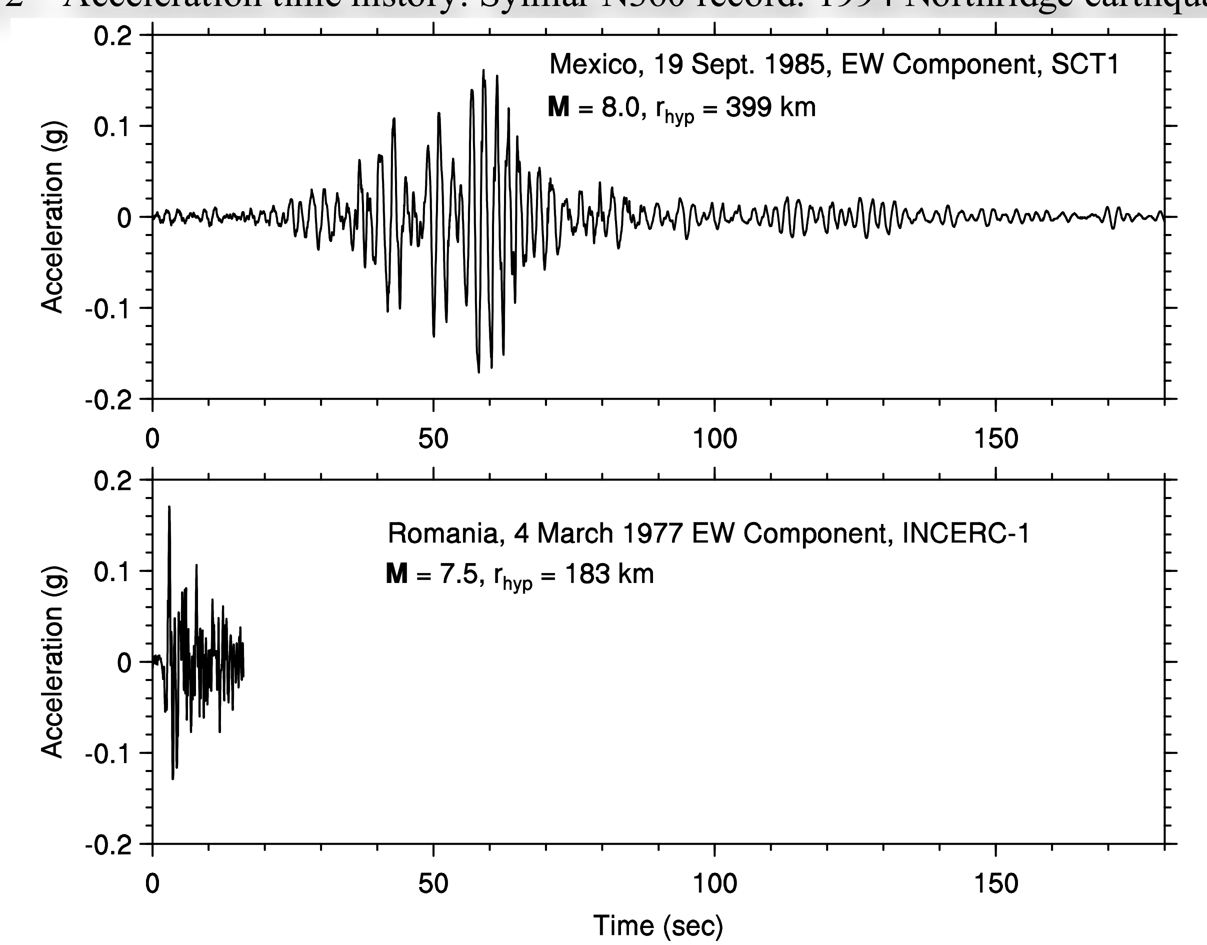

Tsukidate

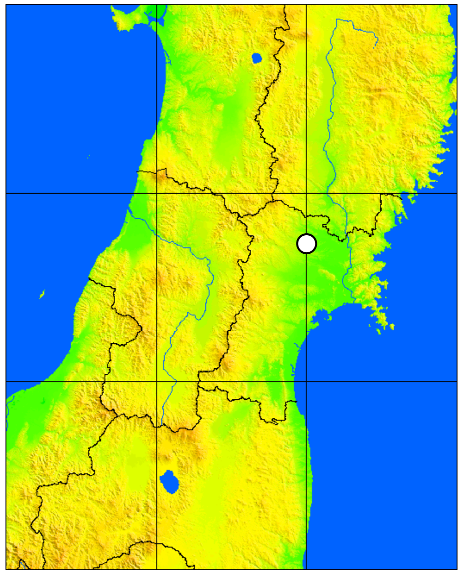

Courtesy of Kazuhiko Kawashima

Comparison with Type II Design Spectra, JRA Design Specifications of Bridges

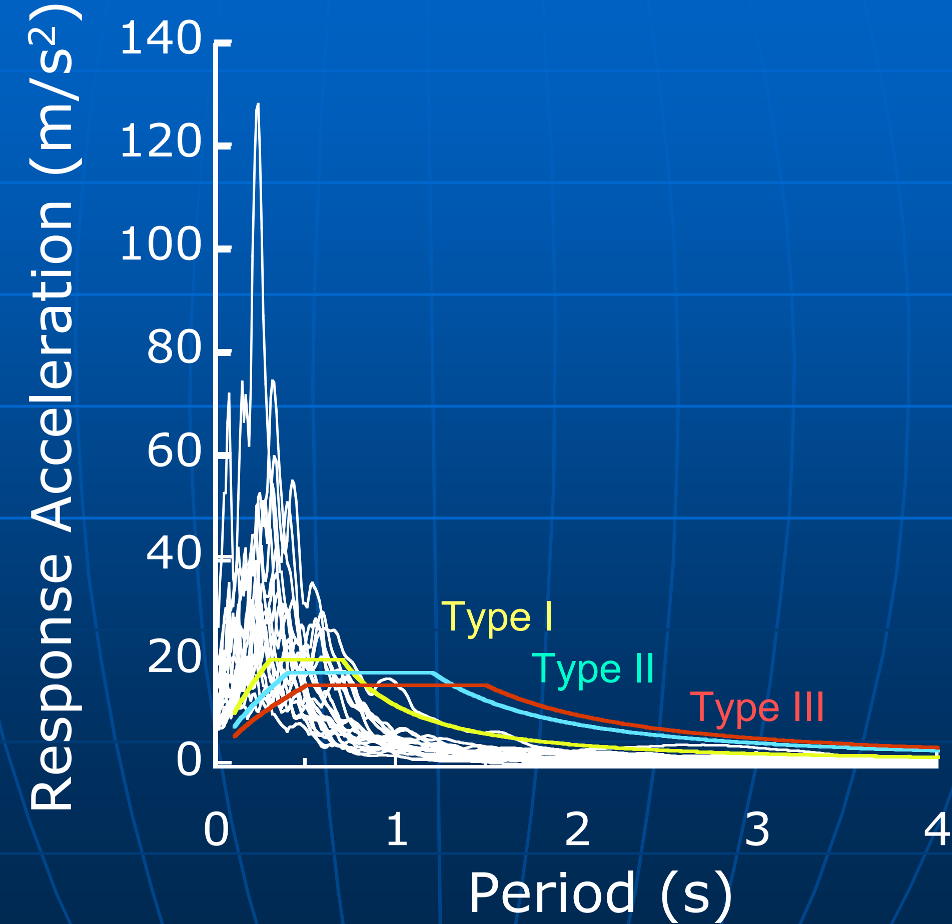

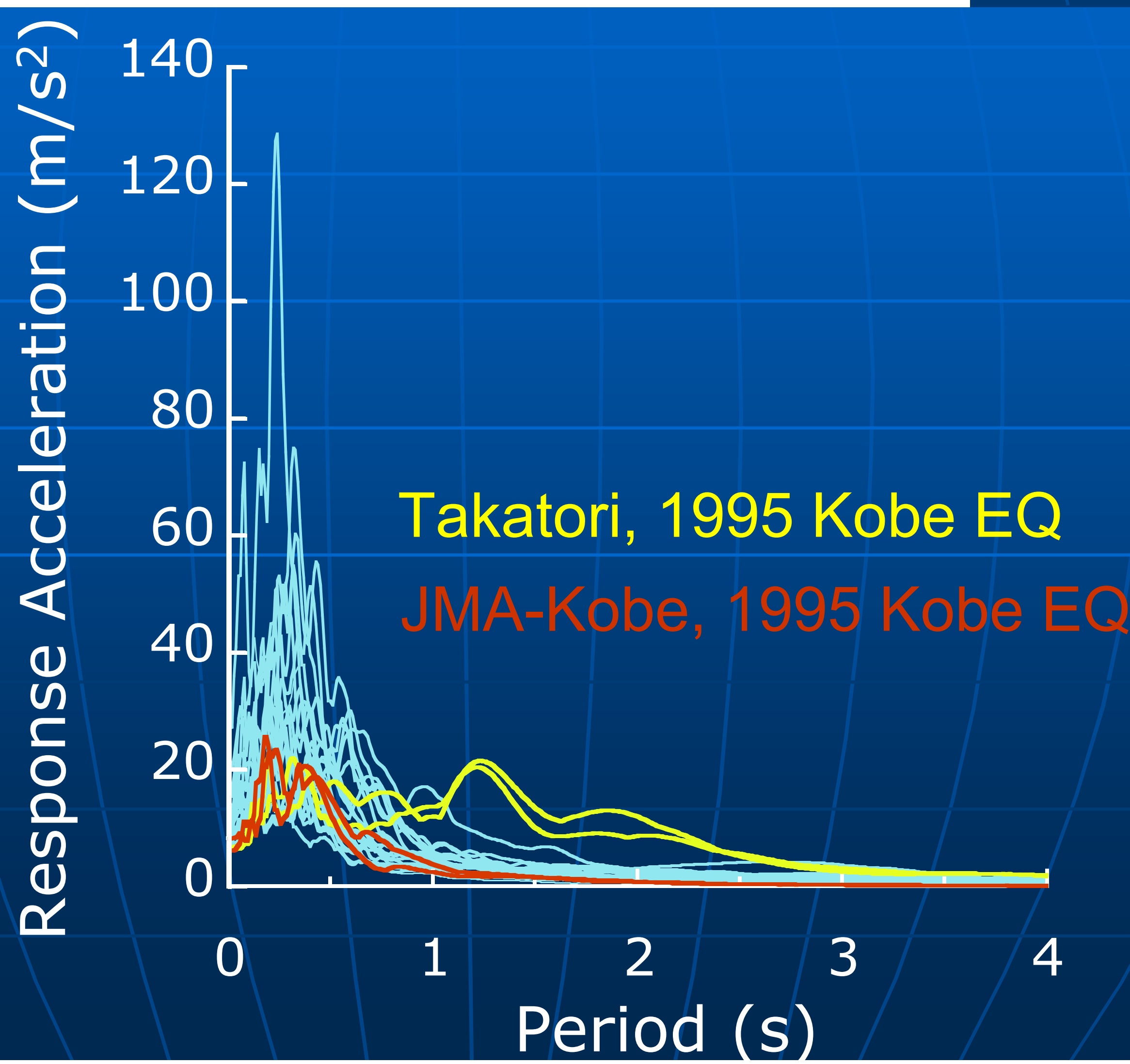

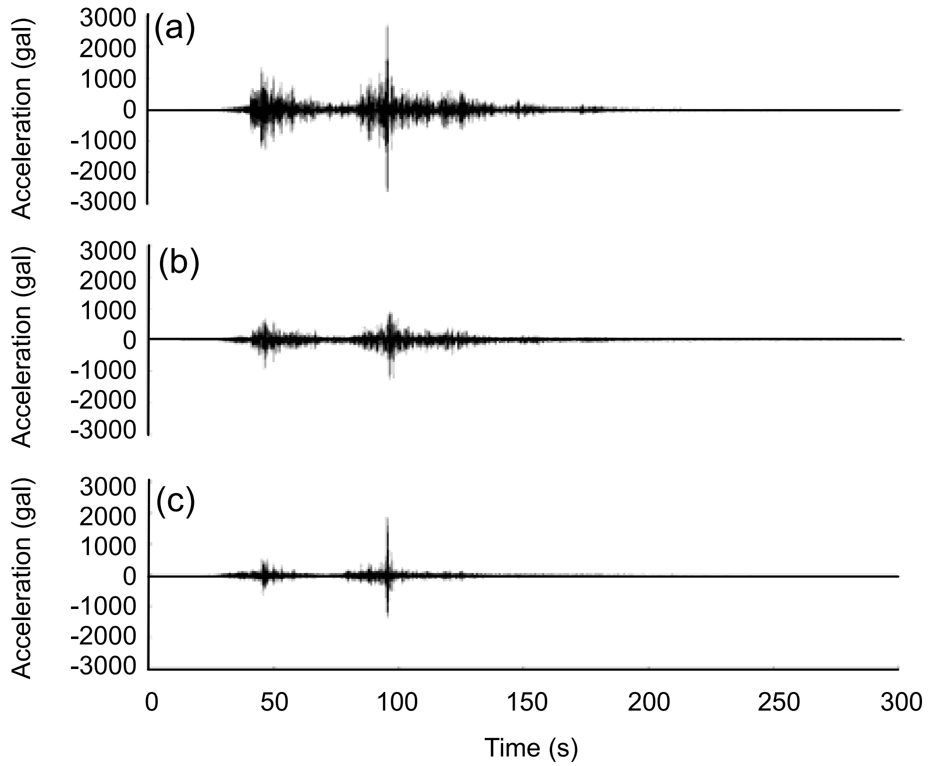

SHA dualism

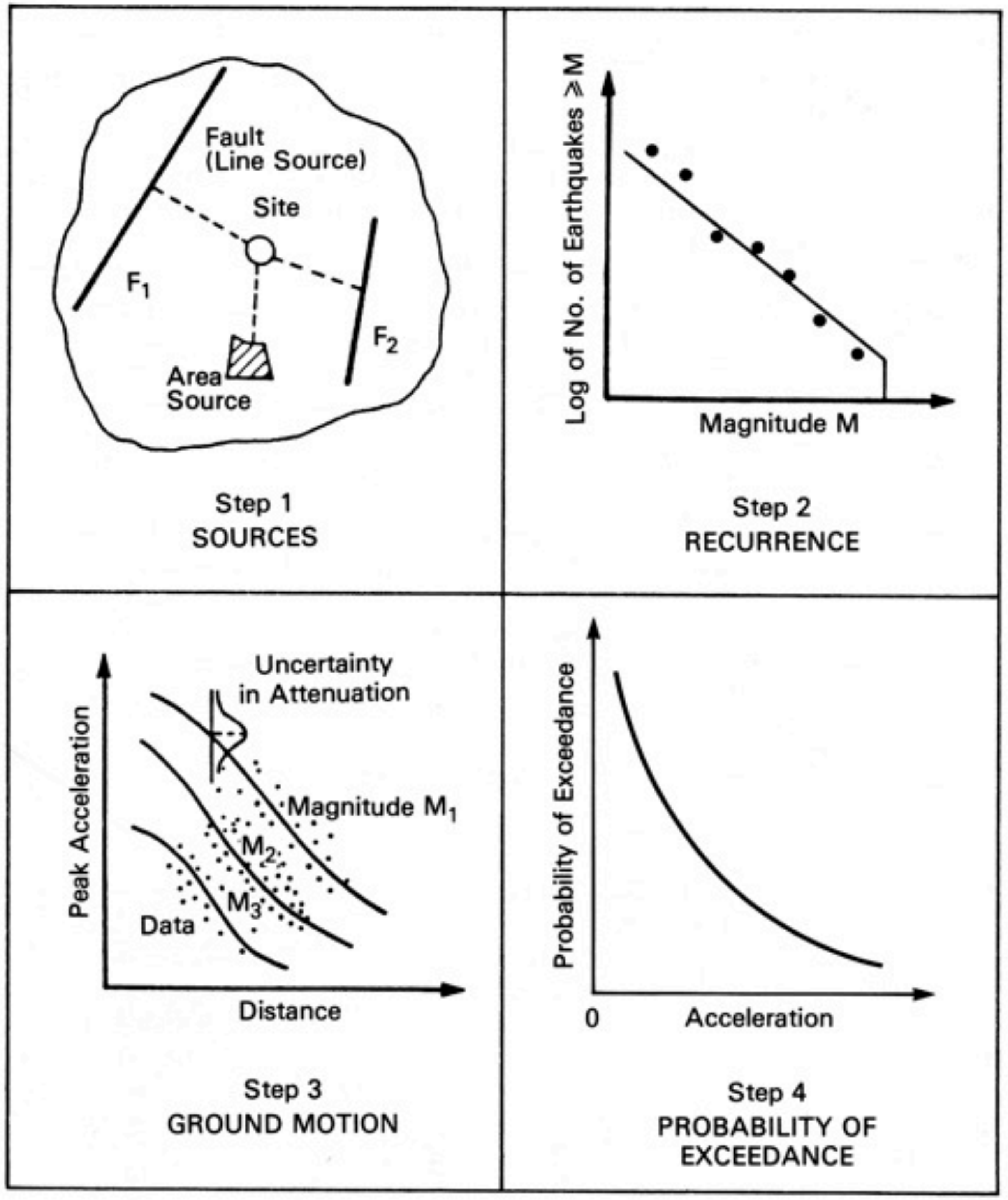

FIGURE 10.2 Basic steps of probabilistic seismic hazard analysis (after TERA Corporation 1978).

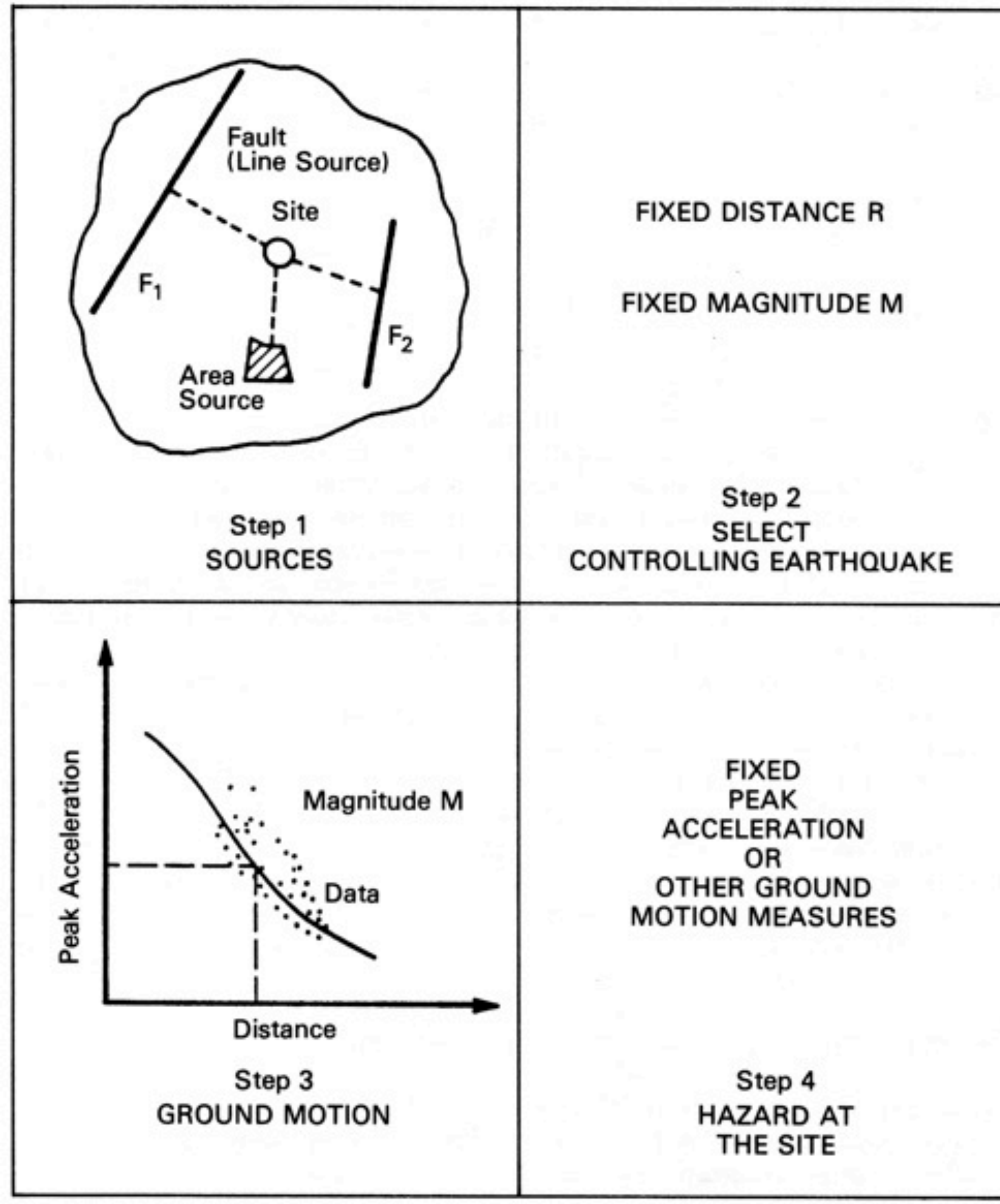

FIGURE 4.1 Basic steps of deterministic seismic hazard analysis (after TERA Corporation 1978).

Probabilistic and Deterministic procedures (after Reiter, 1990)

SHA dualism

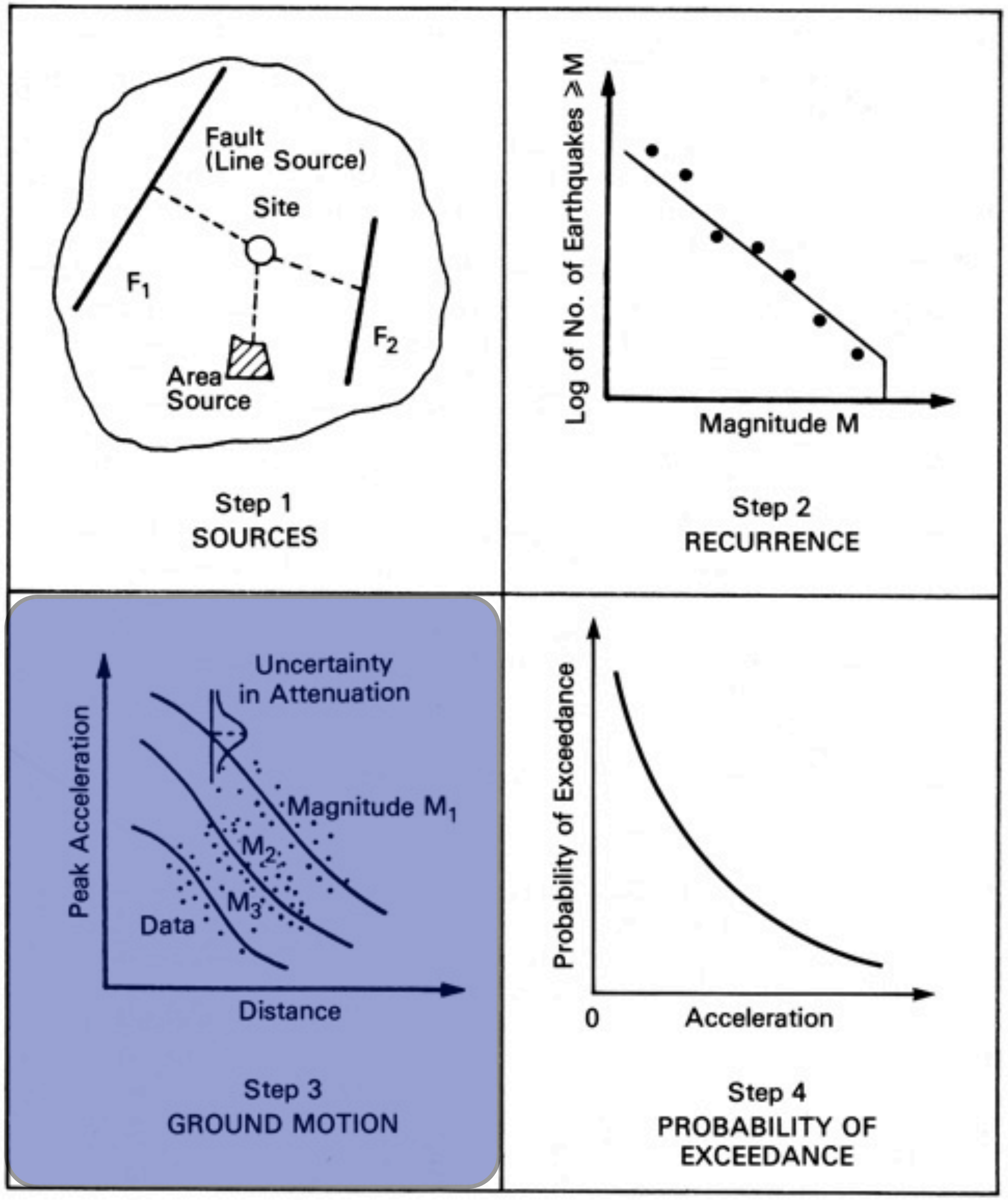

FIGURE 10.2 Basic steps of probabilistic seismic hazard analysis (after TERA Corporation 1978).

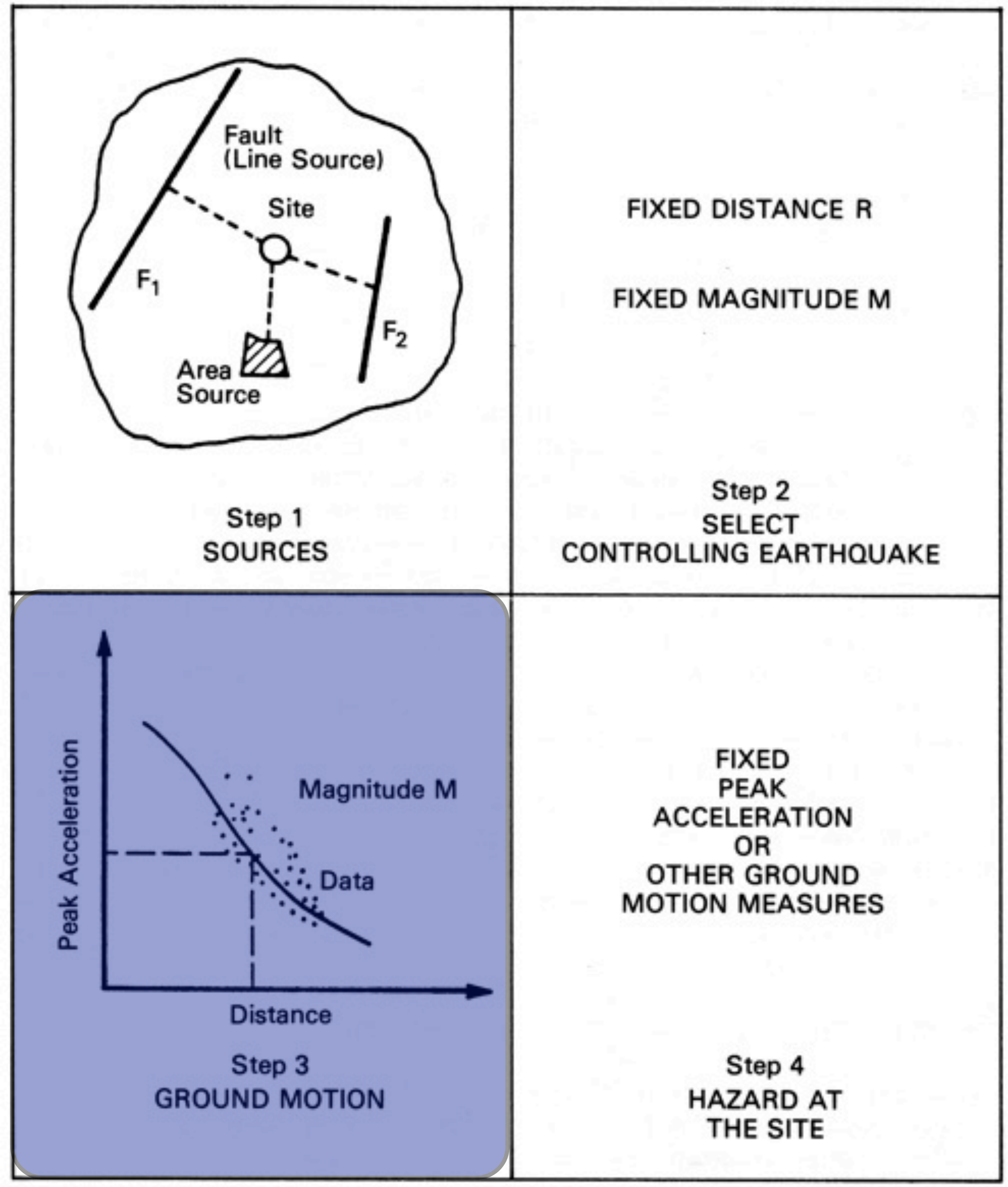

FIGURE 4.1 Basic steps of deterministic seismic hazard analysis (after TERA Corporation 1978).

Probabilistic and Deterministic procedures (after Reiter, 1990)

Modern PSHA & DSHA dualism

Modern PSHA & DSHA dualism

PSHA	Waveform modelling

Modern PSHA & DSHA dualism

PSHA	Waveform modelling
Accounts for all potentially damaging earthquakes in a region	Focus on selected controlling earthquakes

Modern PSHA & DSHA dualism

PSHA	Waveform modelling
Accounts for all potentially damaging earthquakes in a region	Focus on selected controlling earthquakes
(Single) parameter	Complete time series

Modern PSHA & DSHA dualism

PSHA	Waveform modelling
Accounts for all potentially damaging earthquakes in a region	Focus on selected controlling earthquakes
(Single) parameter	Complete time series
Deeply rooted in engineering practice (e.g. building codes)	Dynamic analyses of critical facilities

Modern PSHA & DSHA dualism

PSHA	Waveform modelling
Accounts for all potentially damaging earthquakes in a region	Focus on selected controlling earthquakes
(Single) parameter	Complete time series
Deeply rooted in engineering practice (e.g. building codes)	Dynamic analyses of critical facilities

← Study of attenuation relationships

Modern PSHA & DSHA dualism

PSHA	Waveform modelling
Accounts for all potentially damaging earthquakes in a region	Focus on selected controlling earthquakes
(Single) parameter	Complete time series
Deeply rooted in engineering practice (e.g. building codes)	Dynamic analyses of critical facilities

Deaggregation, recursive analysis → ← Study of attenuation relationships

Modern PSHA & DSHA dualism

PSHA	Waveform modelling
Accounts for all potentially damaging earthquakes in a region	Focus on selected controlling earthquakes
(Single) parameter	Complete time series
Deeply rooted in engineering practice (e.g. building codes)	Dynamic analyses of critical facilities

Deaggregation, recursive analysis ➡ ⬅ Study of attenuation relationships

e.g. see "Cybershake" project at SCEC web:
http://scec.usc.edu/research/cme/groups/broadband

PBDE

PBDE

SHA produces response spectral ordinates (or other intensity measures) for each of the annual probabilities that are specified for performance-based design.

PBDE

SHA produces response spectral ordinates (or other intensity measures) for each of the annual probabilities that are specified for performance-based design.

In PBDE, the ground motions may need to be specified not only as intensity measures such as response spectra, but also by suites of strong motion time histories for input into time-domain nonlinear analyses of structures.

PBDE

SHA produces response spectral ordinates (or other intensity measures) for each of the annual probabilities that are specified for performance-based design.

In PBDE, the ground motions may need to be specified not only as intensity measures such as response spectra, but also by suites of strong motion time histories for input into time-domain nonlinear analyses of structures.

It is necessary to use a suite of time histories having phasing and spectral shapes that are appropriate for the characteristics of the earthquake source, wave propagation path, and site conditions that control the design spectrum.

Time & Space scales... and actions

MYrs Decades Seconds

Time & Space scales... and actions

MYrs	Decades	Seconds
Geodynamics	Geodesy	Seismology

Time & Space scales... and actions

MYrs Decades Seconds

Geodynamics Geodesy Seismology

Strain rates Slip rates

Time & Space scales... and actions

MYrs Decades Seconds

Geodynamics Geodesy Seismology

Strain rates Slip rates

Time	Space	Action

Time & Space scales... and actions

MYrs Decades Seconds

Geodynamics Geodesy Seismology

Strain rates Slip rates

Time	Space	Action
No	National	Seismic Codes

Time & Space scales... and actions

MYrs Decades Seconds

Geodynamics Geodesy Seismology

Strain rates Slip rates

Time	Space	Action
No	National	Seismic Codes
Decades	Regional	IT alerts

Time & Space scales... and actions

MYrs Decades Seconds

Geodynamics Geodesy Seismology

Strain rates Slip rates

Time	Space	Action
No	National	Seismic Codes
Decades	Regional	IT alerts
Seconds	Urban	Red Alert

Ground motion - USA & backprojection

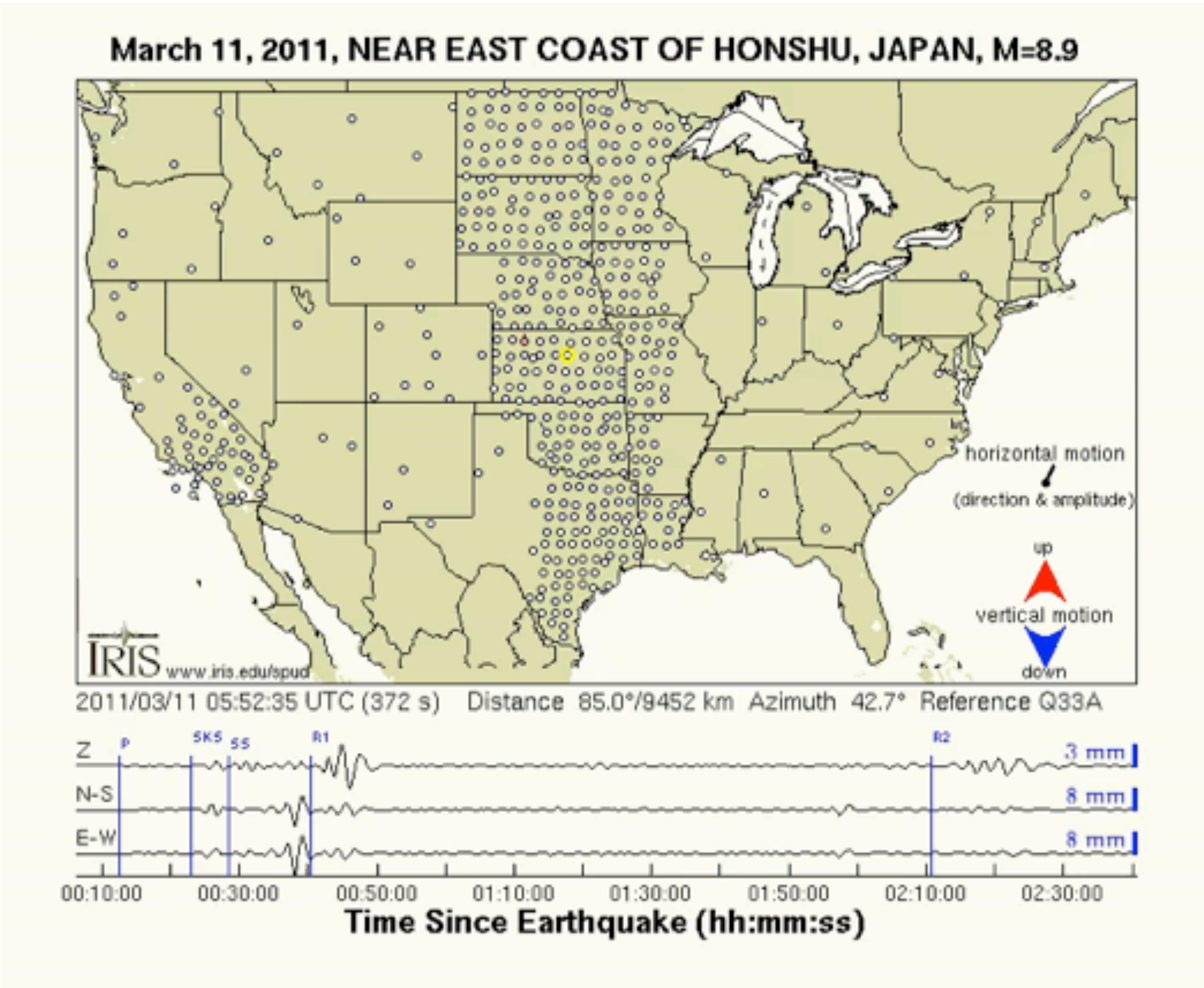

Courtesy of Dun Wang and Jim Mori

Ground motion - USA & backprojection

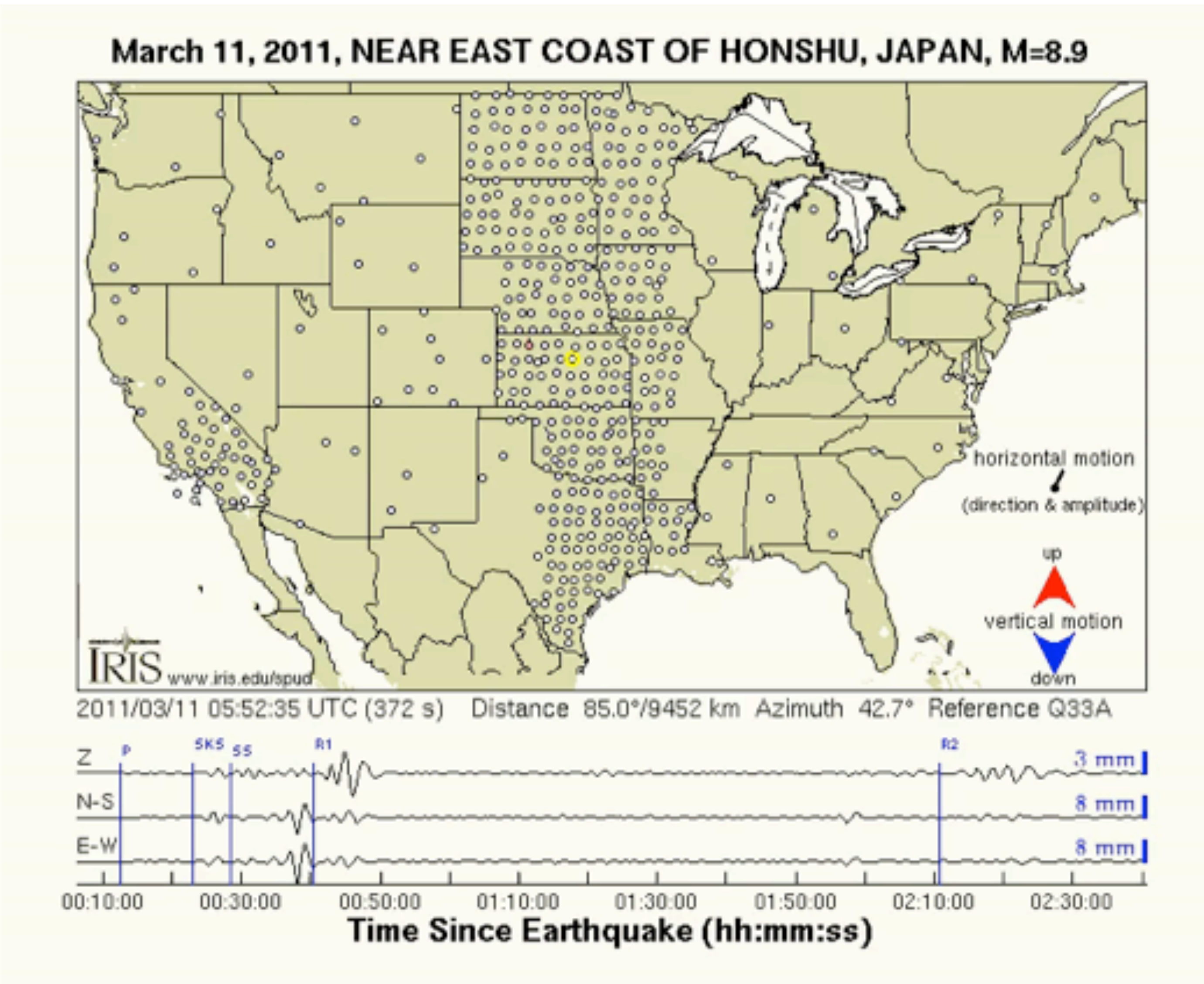

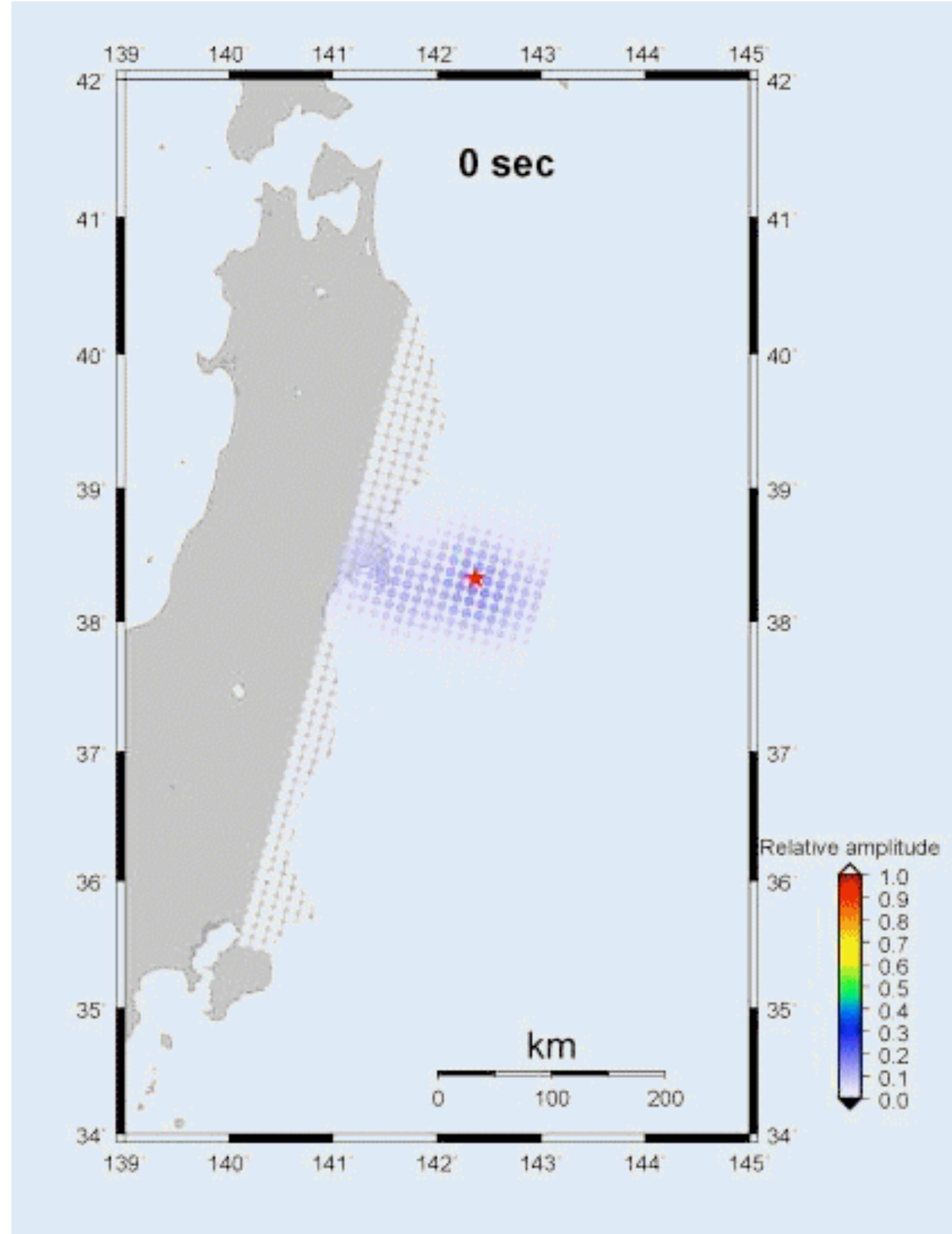

Courtesy of Dun Wang and Jim Mori

Ground motion animation: time scales...

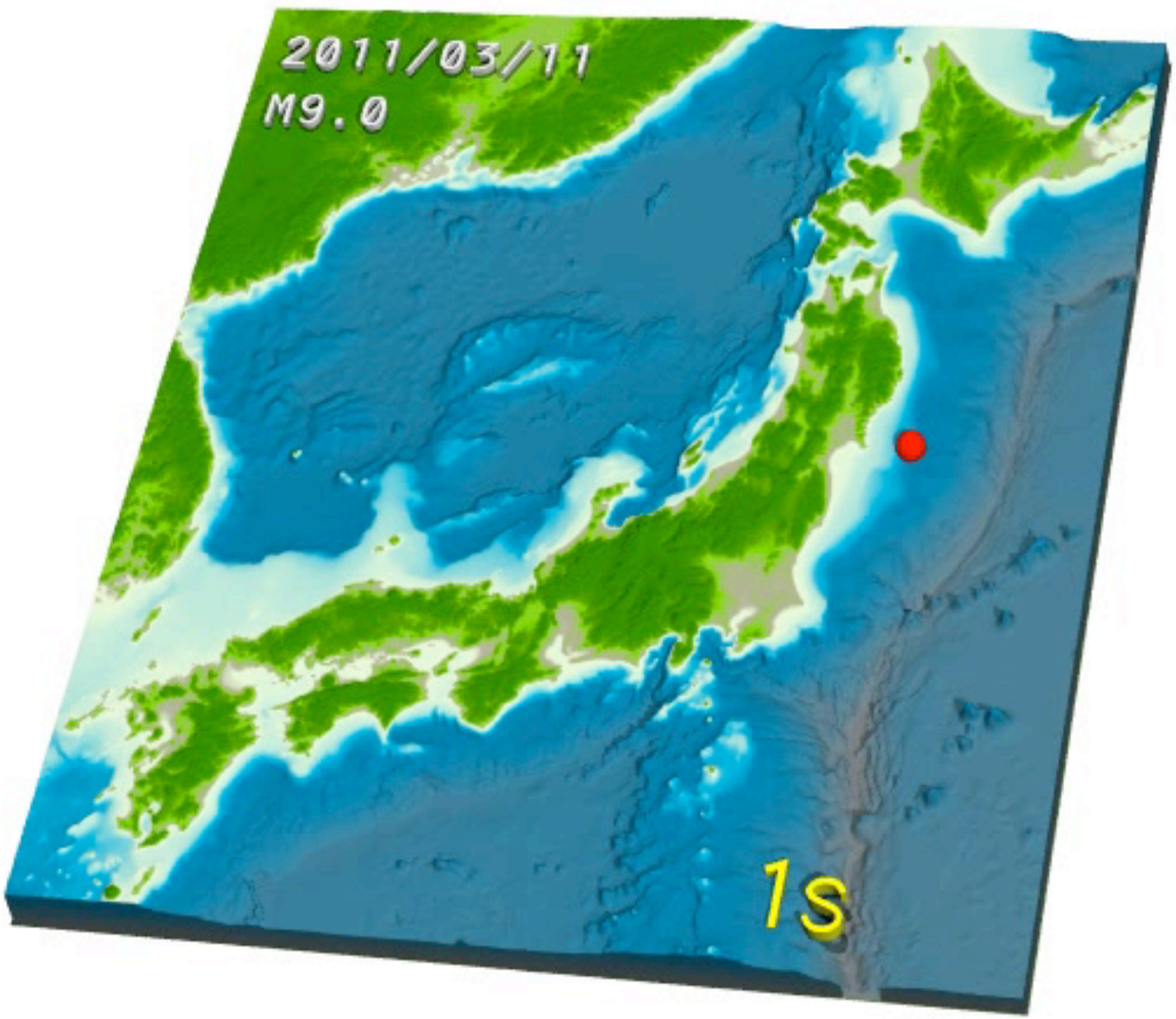

Courtesy of Takashi Furumura

Tsunami animation: time scales...

http://outreach.eri.u-tokyo.ac.jp/eqvolc/201103_tohoku/eng/

http://supersites.earthobservations.org/honshu.php

http://eqseis.geosc.psu.edu/~cammon/Japan2011EQ/

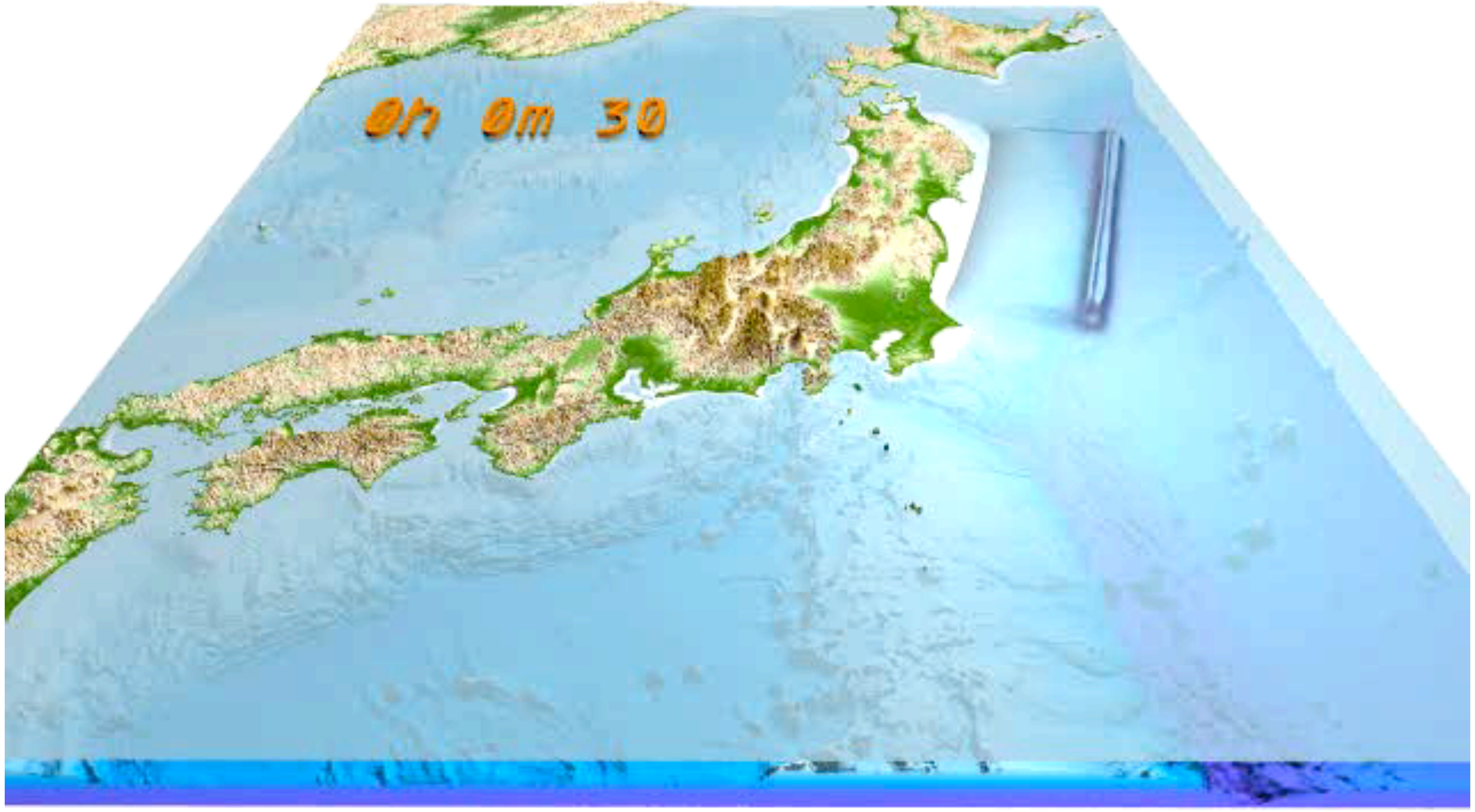

"Earthquake Research Institute, University of Tokyo, Prof. Takashi Furumura and Project Researcher Takuto Maeda"

Regional Scale - Seismograms computation

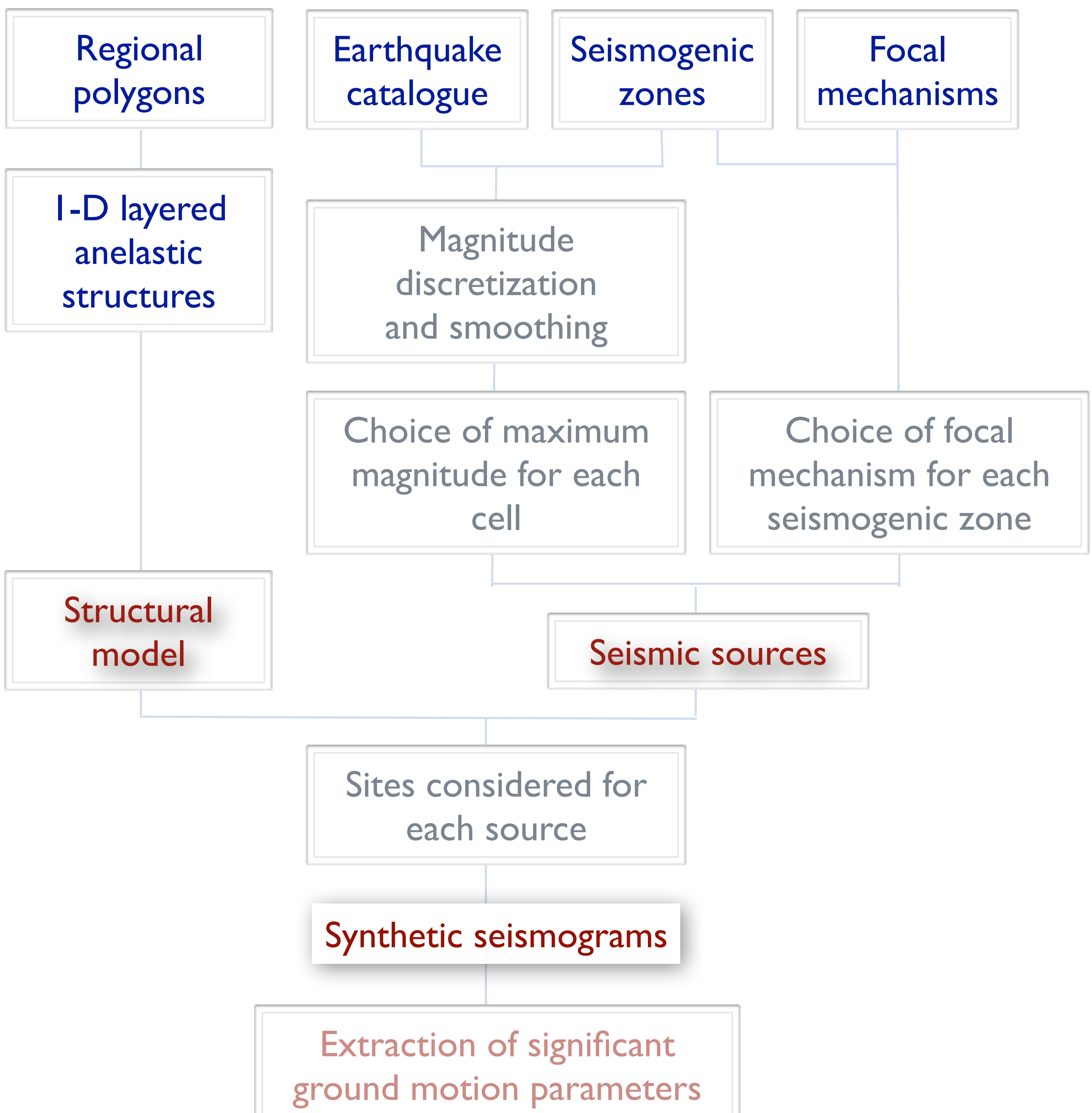

Regional Scale - Seismograms computation

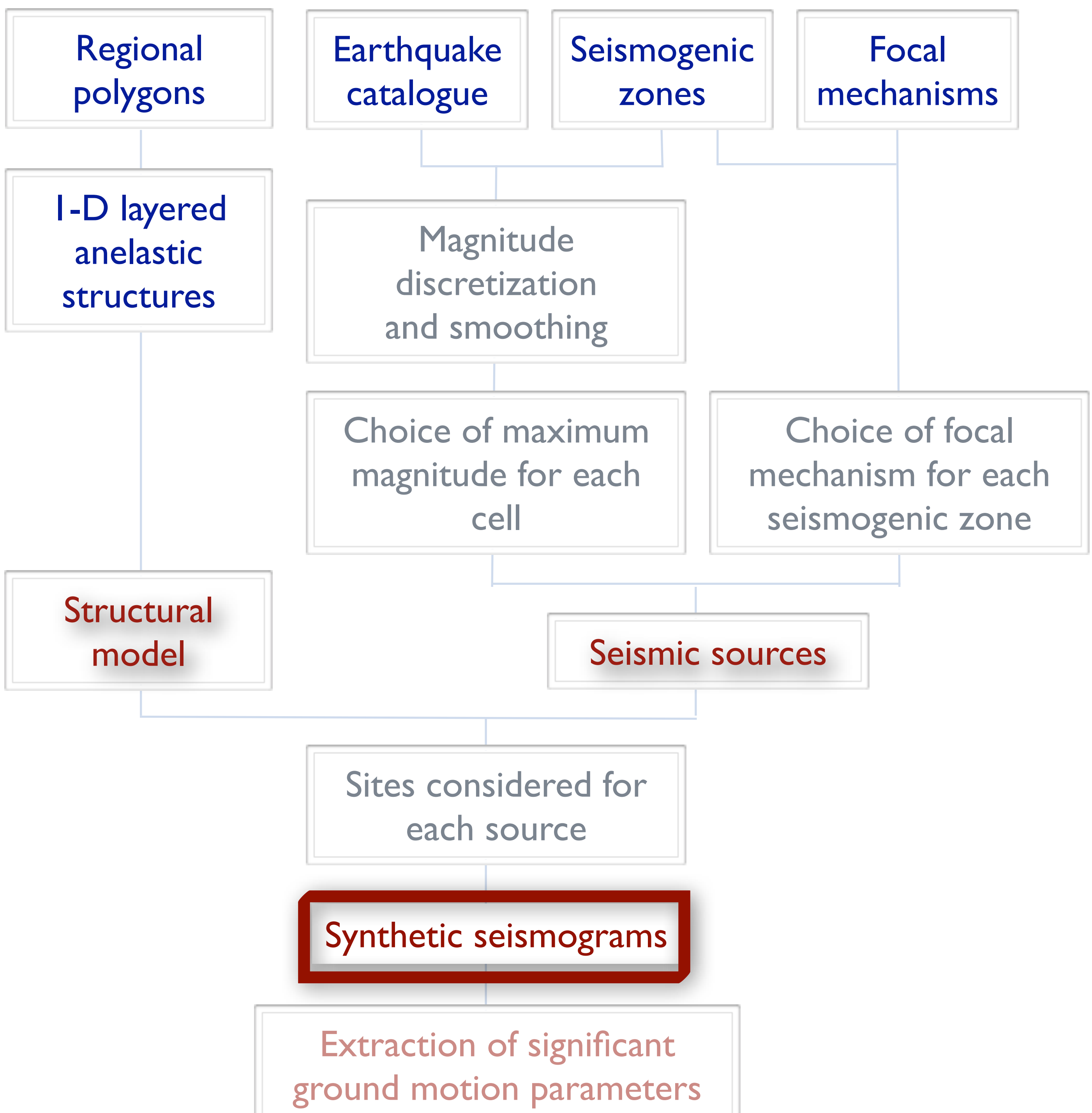

Equivalent Forces

The observable seismic radiation is through energy release as the fault surface moves: formation and propagation of a crack. This complex dynamical problem can be studied by kinematical equivalent approaches.

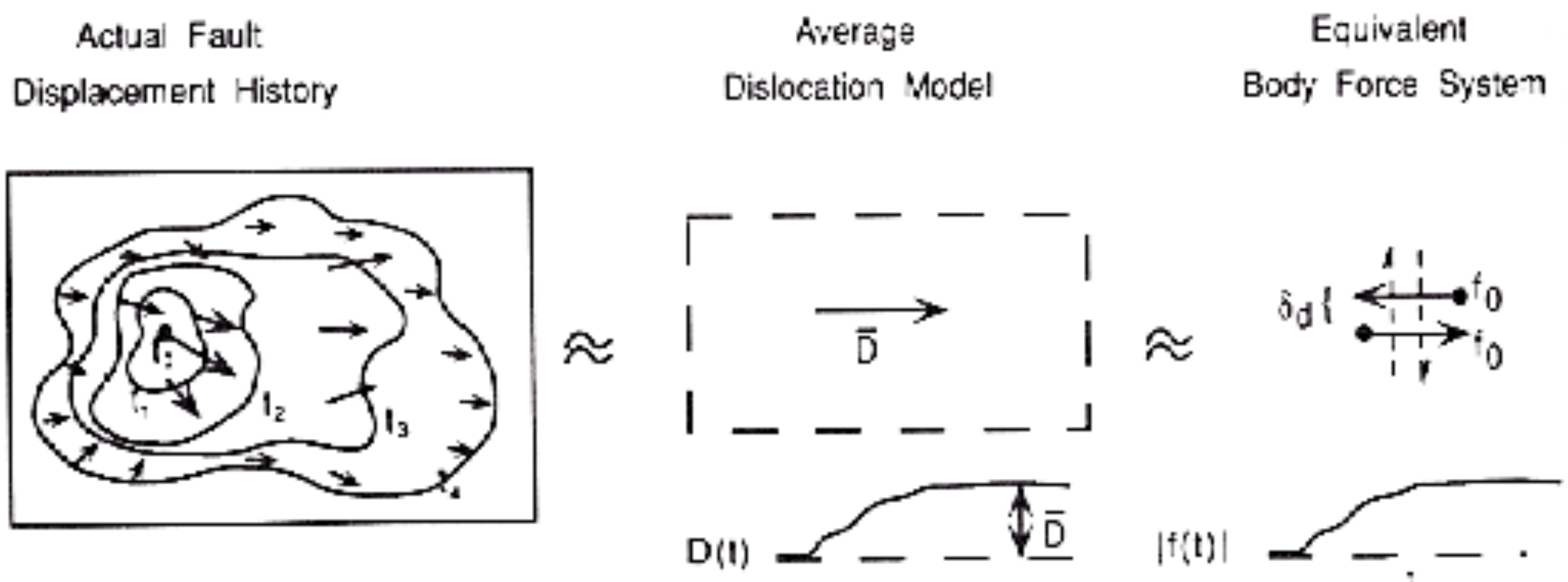

The scope is to develop a representation of the displacement generated in an elastic body in terms of the quantities that originated it: body forces and applied tractions and displacements over the surface of the body.

The actual slip process will be described by superposition of equivalent body forces acting in space (over a fault) and time (rise time).

Final source representation

$$u_n(x,t) = \iint_\Sigma [u_i] c_{ijpq} \nu_j * \frac{\partial G_{np}}{\partial \xi_q} d\Sigma$$

$$m_{pq} = [u_i] c_{ijpq} \nu_j \qquad u_n(x,t) = \iint_\Sigma m_{pq} * \frac{\partial G_{np}}{\partial \xi_q} d\Sigma$$

And if the source can be considered a point-source (for distances greater than fault dimensions), the contributions from different surface elements can be considered in phase.

Thus for an effective point source, one can define the moment tensor:

$$M_{pq} = \iint_\Sigma m_{pq} d\Sigma$$

$$u_n(x,t) = M_{pq} * G_{np,q}$$

GF for double couple

An important case to consider in detail is the radiation pattern expected when the source is a double-couple. The result for a moment time function $M_0(t)$ is:

$$u = \frac{A^{NF}}{4\pi\rho|\mathbf{x}|^4}\int_{|\mathbf{x}|/\alpha}^{|\mathbf{x}|/\beta}\tau M_0(t-\tau)d\tau + \\ + \frac{A_P^{IF}}{4\pi\rho\alpha^2|\mathbf{x}|^2}M_0\left(t-\frac{|\mathbf{x}|}{\alpha}\right) - \frac{A_S^{IF}}{4\pi\rho\beta^2|\mathbf{x}|^2}M_0\left(t-\frac{|\mathbf{x}|}{\beta}\right) + \\ + \frac{A_P^{FF}}{4\pi\rho\alpha^3|\mathbf{x}|}\dot{M}_0\left(t-\frac{|\mathbf{x}|}{\alpha}\right) - \frac{A_S^{FF}}{4\pi\rho\beta^3|\mathbf{x}|}\dot{M}_0\left(t-\frac{|\mathbf{x}|}{\beta}\right)$$

$$A^{NF} = 9\sin 2\theta\cos\phi\,\hat{\mathbf{r}} - 6\left(\cos 2\theta\cos\phi\,\hat{\boldsymbol{\theta}} - \cos\theta\sin\phi\,\hat{\boldsymbol{\phi}}\right)$$

$$A_P^{IF} = 4\sin 2\theta\cos\phi\,\hat{\mathbf{r}} - 2\left(\cos 2\theta\cos\phi\,\hat{\boldsymbol{\theta}} - \cos\theta\sin\phi\,\hat{\boldsymbol{\phi}}\right)$$

$$A_S^{IF} = -3\sin 2\theta\cos\phi\,\hat{\mathbf{r}} + 3\left(\cos 2\theta\cos\phi\,\hat{\boldsymbol{\theta}} - \cos\theta\sin\phi\,\hat{\boldsymbol{\phi}}\right)$$

$$A_P^{FF} = \sin 2\theta\cos\phi\,\hat{\mathbf{r}}$$

$$A_S^{FF} = \cos 2\theta\cos\phi\,\hat{\boldsymbol{\theta}} - \cos\theta\sin\phi\,\hat{\boldsymbol{\phi}}$$

GF for double couple

An important case to consider in detail is the radiation pattern expected when the source is a double-couple. The result for a moment time function $M_0(t)$ is:

$$u = \frac{A^{NF}}{4\pi\rho|\mathbf{x}|^4}\int_{|\mathbf{x}|/\alpha}^{|\mathbf{x}|/\beta}\tau M_0(t-\tau)d\tau +$$

$$+\frac{A_P^{IF}}{4\pi\rho\alpha^2|\mathbf{x}|^2}M_0\left(t-\frac{|\mathbf{x}|}{\alpha}\right)-\frac{A_S^{IF}}{4\pi\rho\beta^2|\mathbf{x}|^2}M_0\left(t-\frac{|\mathbf{x}|}{\beta}\right)+$$

$$+\frac{A_P^{FF}}{4\pi\rho\alpha^3|\mathbf{x}|}\dot{M}_0\left(t-\frac{|\mathbf{x}|}{\alpha}\right)-\frac{A_S^{FF}}{4\pi\rho\beta^3|\mathbf{x}|}\dot{M}_0\left(t-\frac{|\mathbf{x}|}{\beta}\right)$$

$$A^{NF} = 9\sin 2\theta\cos\phi\,\hat{\mathbf{r}} - 6\left(\cos 2\theta\cos\phi\,\hat{\boldsymbol{\theta}} - \cos\theta\sin\phi\,\hat{\boldsymbol{\phi}}\right)$$

Near field term

$$A_P^{IF} = 4\sin 2\theta\cos\phi\,\hat{\mathbf{r}} - 2\left(\cos 2\theta\cos\phi\,\hat{\boldsymbol{\theta}} - \cos\theta\sin\phi\,\hat{\boldsymbol{\phi}}\right)$$

$$A_S^{IF} = -3\sin 2\theta\cos\phi\,\hat{\mathbf{r}} + 3\left(\cos 2\theta\cos\phi\,\hat{\boldsymbol{\theta}} - \cos\theta\sin\phi\,\hat{\boldsymbol{\phi}}\right)$$

$$A_P^{FF} = \sin 2\theta\cos\phi\,\hat{\mathbf{r}}$$

$$A_S^{FF} = \cos 2\theta\cos\phi\,\hat{\boldsymbol{\theta}} - \cos\theta\sin\phi\,\hat{\boldsymbol{\phi}}$$

GF for double couple

An important case to consider in detail is the radiation pattern expected when the source is a double-couple. The result for a moment time function $M_0(t)$ is:

$$u = \frac{A^{NF}}{4\pi\rho|\mathbf{x}|^4}\int_{|\mathbf{x}|/\alpha}^{|\mathbf{x}|/\beta}\tau M_0(t-\tau)d\tau + \frac{A_P^{IF}}{4\pi\rho\alpha^2|\mathbf{x}|^2}M_0\left(t-\frac{|\mathbf{x}|}{\alpha}\right) - \frac{A_S^{IF}}{4\pi\rho\beta^2|\mathbf{x}|^2}M_0\left(t-\frac{|\mathbf{x}|}{\beta}\right) + \frac{A_P^{FF}}{4\pi\rho\alpha^3|\mathbf{x}|}\dot{M}_0\left(t-\frac{|\mathbf{x}|}{\alpha}\right) - \frac{A_S^{FF}}{4\pi\rho\beta^3|\mathbf{x}|}\dot{M}_0\left(t-\frac{|\mathbf{x}|}{\beta}\right)$$

$$A^{NF} = 9\sin 2\theta\cos\phi\,\hat{\mathbf{r}} - 6\left(\cos 2\theta\cos\phi\,\hat{\theta} - \cos\theta\sin\phi\,\hat{\phi}\right)$$

Near field term

$$A_P^{IF} = 4\sin 2\theta\cos\phi\,\hat{\mathbf{r}} - 2\left(\cos 2\theta\cos\phi\,\hat{\theta} - \cos\theta\sin\phi\,\hat{\phi}\right)$$

$$A_S^{IF} = -3\sin 2\theta\cos\phi\,\hat{\mathbf{r}} + 3\left(\cos 2\theta\cos\phi\,\hat{\theta} - \cos\theta\sin\phi\,\hat{\phi}\right)$$

Intermediate field term

$$A_P^{FF} = \sin 2\theta\cos\phi\,\hat{\mathbf{r}}$$

$$A_S^{FF} = \cos 2\theta\cos\phi\,\hat{\theta} - \cos\theta\sin\phi\,\hat{\phi}$$

GF for double couple

An important case to consider in detail is the radiation pattern expected when the source is a double-couple. The result for a moment time function $M_0(t)$ is:

$$u = \frac{A^{NF}}{4\pi\rho|\mathbf{x}|^4} \int_{|\mathbf{x}|/\alpha}^{|\mathbf{x}|/\beta} \tau M_0(t-\tau)d\tau + \frac{A_P^{IF}}{4\pi\rho\alpha^2|\mathbf{x}|^2} M_0\left(t - \frac{|\mathbf{x}|}{\alpha}\right) - \frac{A_S^{IF}}{4\pi\rho\beta^2|\mathbf{x}|^2} M_0\left(t - \frac{|\mathbf{x}|}{\beta}\right) + \frac{A_P^{FF}}{4\pi\rho\alpha^3|\mathbf{x}|} \dot{M}_0\left(t - \frac{|\mathbf{x}|}{\alpha}\right) - \frac{A_S^{FF}}{4\pi\rho\beta^3|\mathbf{x}|} \dot{M}_0\left(t - \frac{|\mathbf{x}|}{\beta}\right)$$

$$A^{NF} = 9\sin 2\theta\cos\phi\,\hat{\mathbf{r}} - 6\left(\cos 2\theta\cos\phi\,\hat{\theta} - \cos\theta\sin\phi\,\hat{\phi}\right)$$

Near field term

$$A_P^{IF} = 4\sin 2\theta\cos\phi\,\hat{\mathbf{r}} - 2\left(\cos 2\theta\cos\phi\,\hat{\theta} - \cos\theta\sin\phi\,\hat{\phi}\right)$$

$$A_S^{IF} = -3\sin 2\theta\cos\phi\,\hat{\mathbf{r}} + 3\left(\cos 2\theta\cos\phi\,\hat{\theta} - \cos\theta\sin\phi\,\hat{\phi}\right)$$

Intermediate field term

$$A_P^{FF} = \sin 2\theta\cos\phi\,\hat{\mathbf{r}}$$

$$A_S^{FF} = \cos 2\theta\cos\phi\,\hat{\theta} - \cos\theta\sin\phi\,\hat{\phi}$$

Far field term

NF DC (static) Radiation pattern

The static final displacement for a shear dislocation of strength M_0 is:

$$\mathbf{u} = \frac{M_0(\infty)}{4\pi\rho|\mathbf{x}|^2}\left[A^{NF}\left(\frac{1}{2\beta^2}-\frac{1}{2\alpha^2}\right)+\frac{A_P^{IF}}{\alpha^2}+\frac{A_S^{IF}}{\beta^2}\right]=$$

$$= \frac{M_0(\infty)}{4\pi\rho|\mathbf{x}|^2}\left[\left(\frac{3}{2\beta^2}-\frac{1}{2\alpha^2}\right)\sin 2\theta\cos\phi\,\hat{\mathbf{r}}+\frac{1}{\alpha^2}\left(\cos 2\theta\cos\phi\,\hat{\boldsymbol{\theta}}-\cos\theta\sin\phi\,\hat{\boldsymbol{\phi}}\right)\right]$$

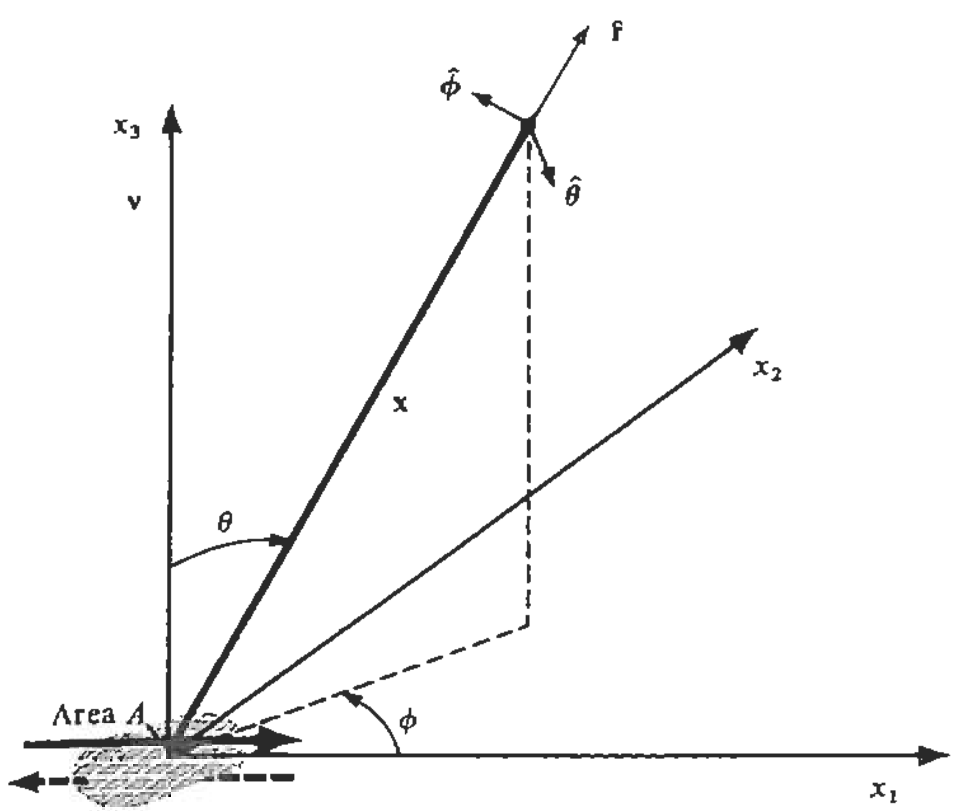

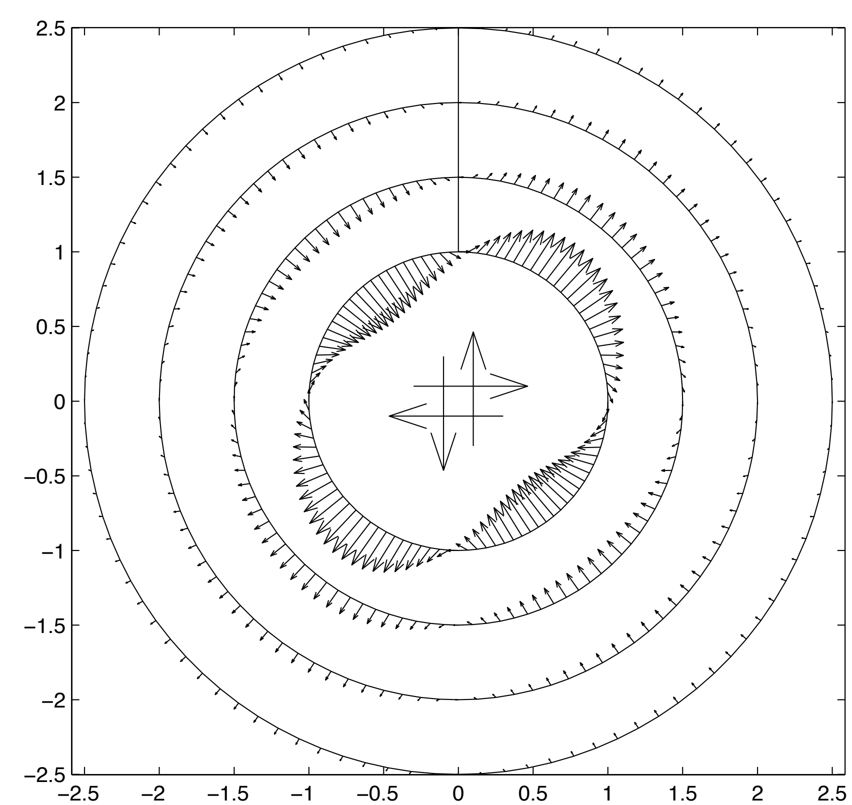

Figure 7: Near-field Static Displacement Field From a Point Double Couple Source ($\phi = 0$ plane); $\alpha = 3^{1/2}$, $\beta = 1$, $r = 0.1,\ 0.15,\ 0.20,\ 0.25$, $\rho = 1/4\pi$, $M_\infty = 1$; self-scaled displacements

Coseismic deformation

L'Aquila (Italy) earthquake, Mw 6.3.
Horizontal and Vertical surface displacement from InSAR Data
(assuming horizontal displacement is perpendicular to the fault strike ~N48W).

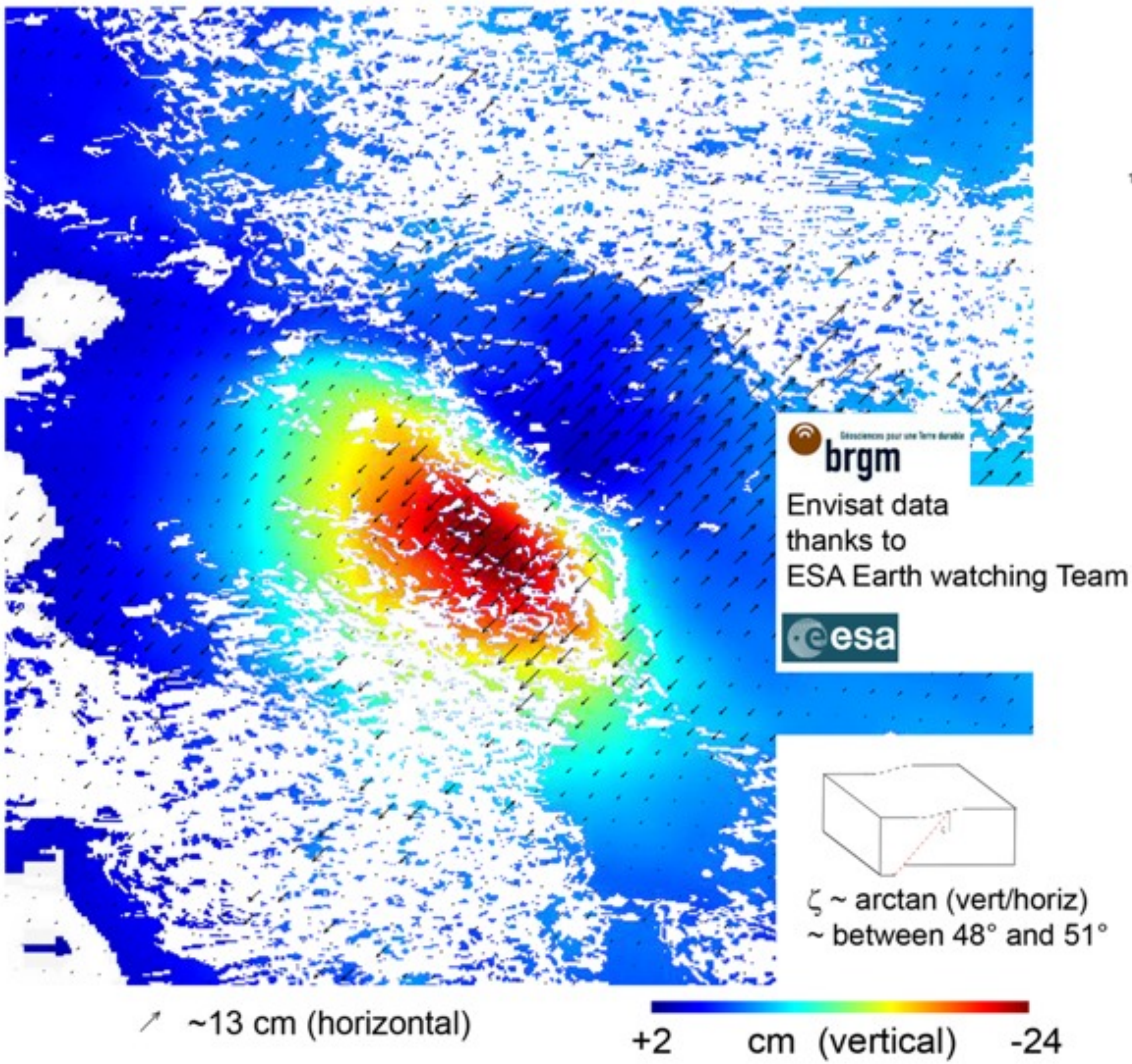

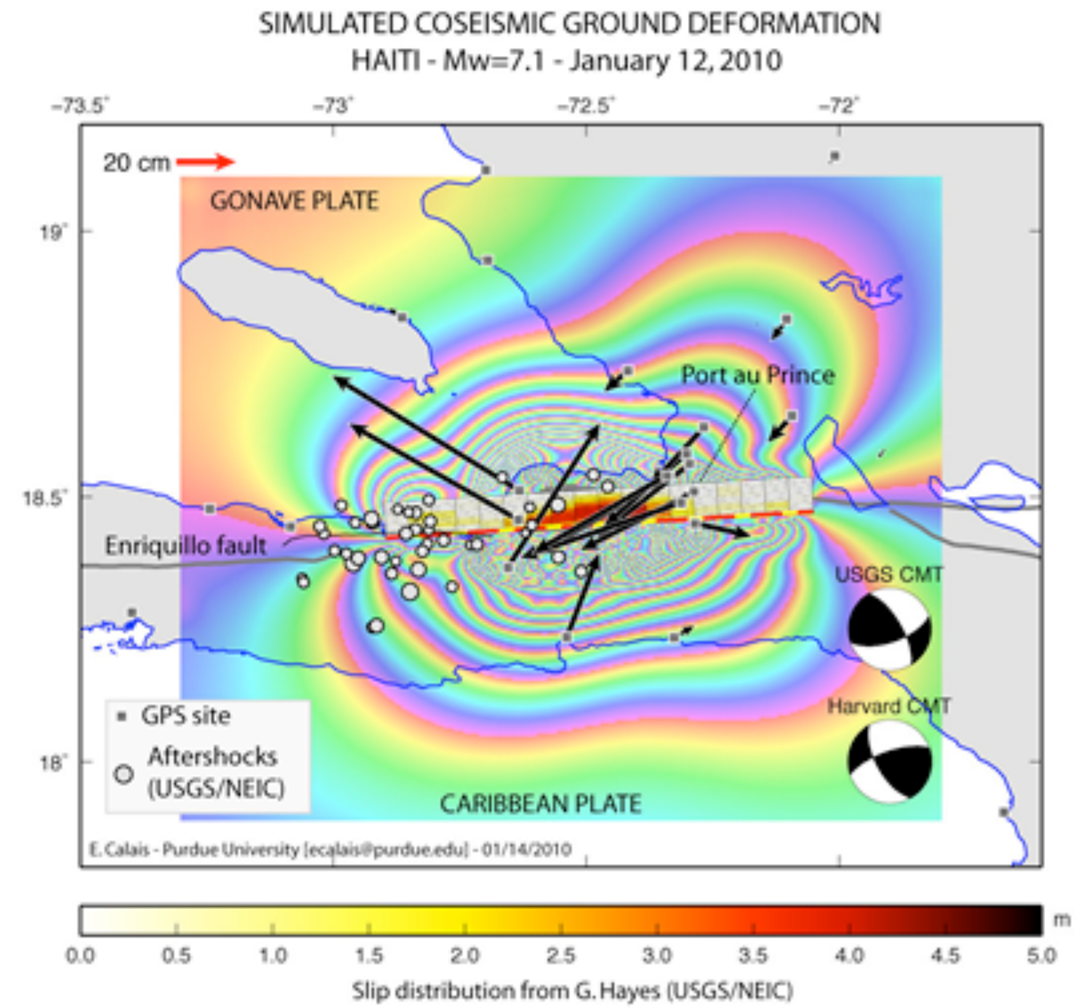

Coseismic deformation

L'Aquila (Italy) earthquake, Mw 6.3.
Horizontal and Vertical surface displacement from InSAR Data
(assuming horizontal displacement is perpendicular to the fault strike ~N48W).

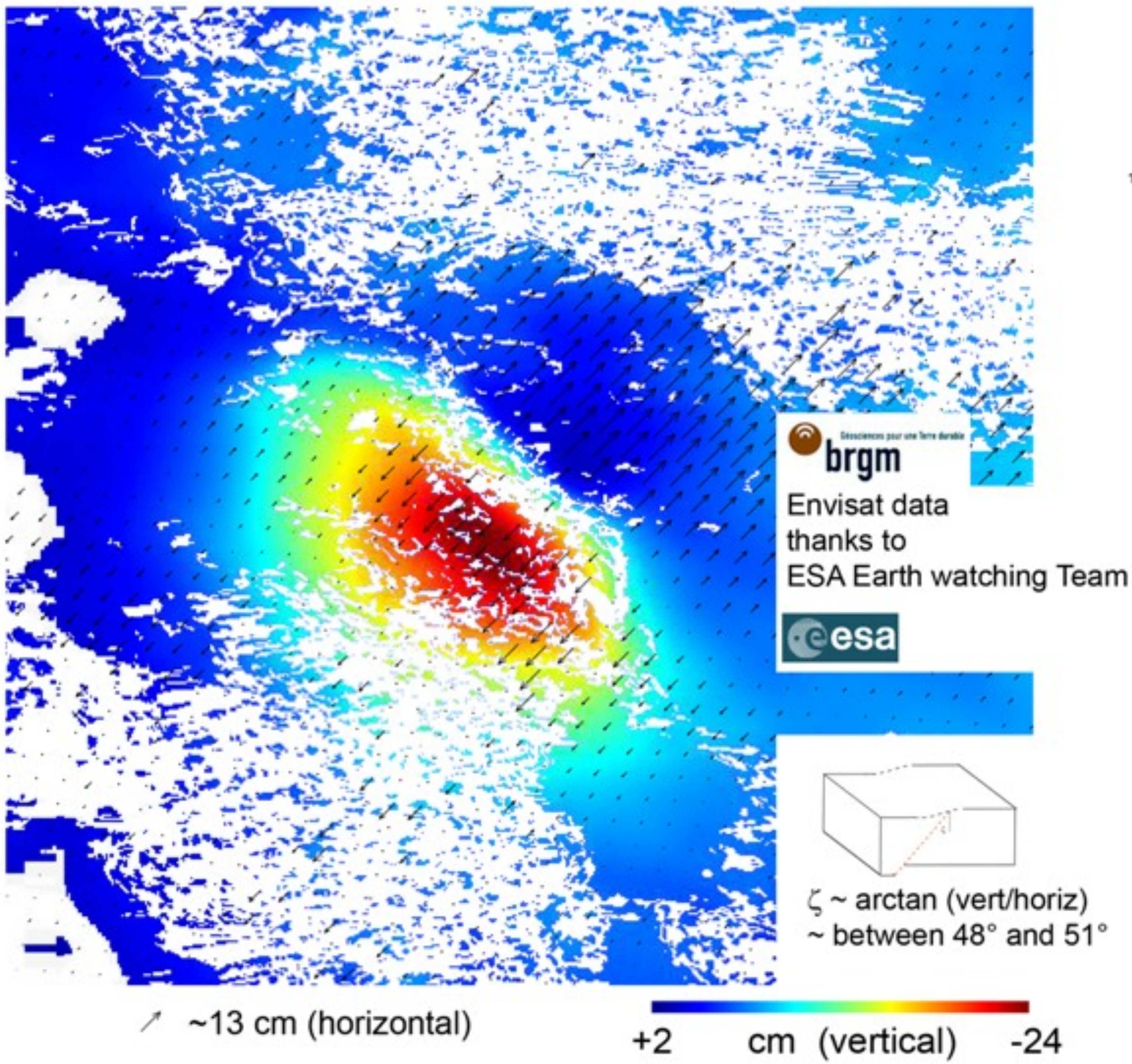

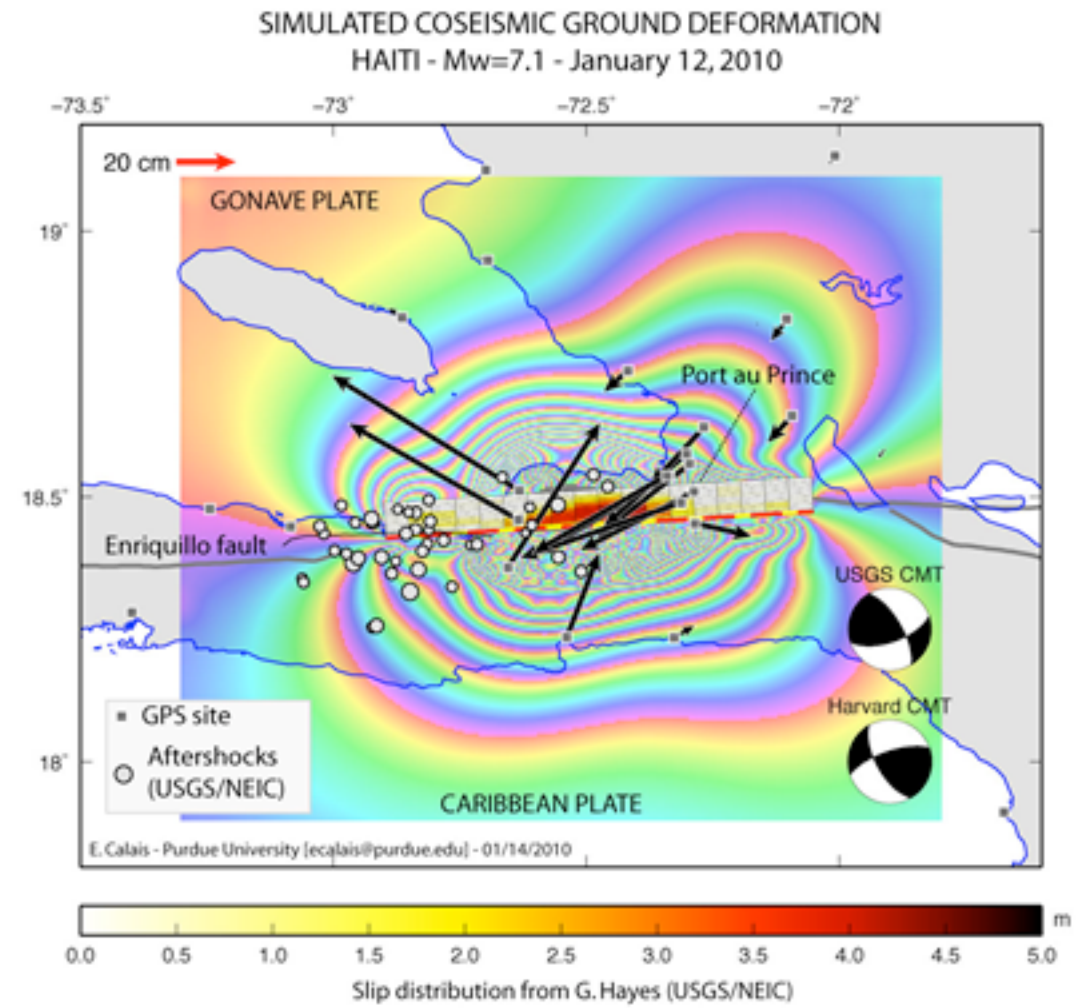

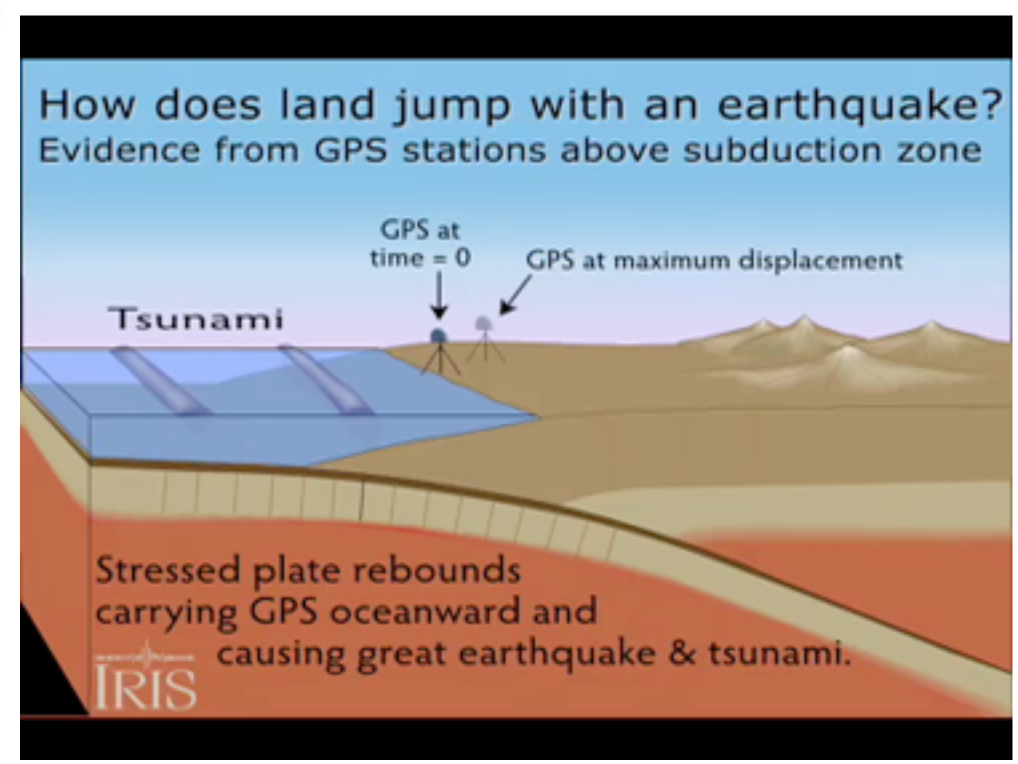

Co- & Post- seismic: Tohoku-oki

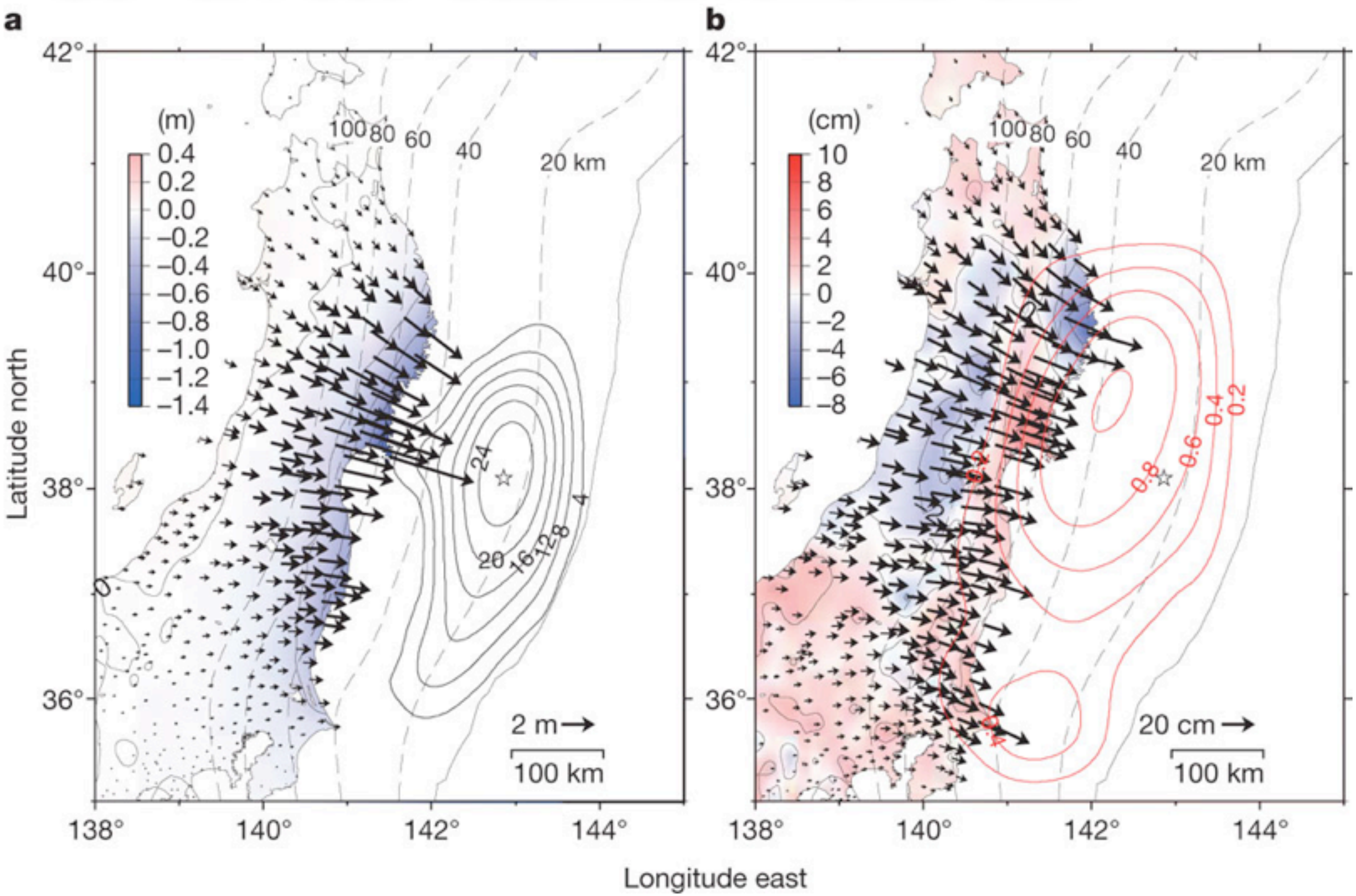

a, Coseismic displacements for 10–11 March 2011, relative to the Fukue site. The black arrows indicate the horizontal coseismic movements of the GPS sites. The colour shading indicates vertical displacement. The star marks the location of the earthquake epicentre. The dotted lines indicate the isodepth contours of the plate boundary at 20-km intervals28. The solid contours show the coseismic slip distribution in metres.

b, Postseismic displacements for 12–25 March 2011, relative to the Fukue site. The red contours show the afterslip distribution in metres. All other markings represent the same as in a.

From: Ozawa et al., 2011,, Nature, 475, 373–376.

Far field for a point DC point source

From the representation theorem we have:

$$u_n(\mathbf{x},t) = M_{pq} * G_{np,q}$$

that, in the far field and in a spherical coordinate system becomes:

$$\mathbf{u}(\mathbf{x},t) = \frac{1}{4\pi\rho\alpha^3}\left(\sin 2\theta \cos\phi \hat{\mathbf{r}}\right)\frac{\dot{M}(t - r/\alpha)}{r} +$$

$$\frac{1}{4\pi\rho\beta^3}\left(\cos 2\theta \cos\phi \hat{\boldsymbol{\theta}} - \cos\theta \sin\phi \hat{\boldsymbol{\phi}}\right)\frac{\dot{M}(t - r/\beta)}{r}$$

and both P and S radiation fields are proportional to the time derivative of the moment function (moment rate). If the moment function is a ramp of duration τ (**rise time**), the propagating disturbance in the far-field will be a **boxcar,** with the same duration, and whose amplitude is varying depending on the radiation pattern.

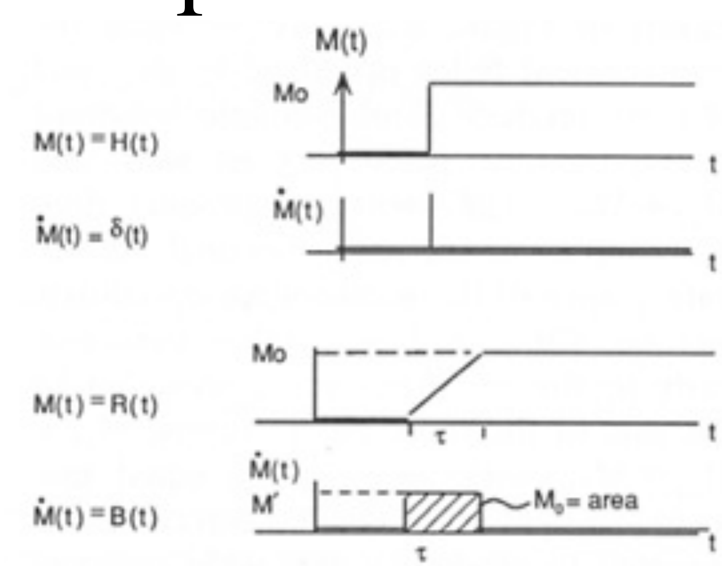

FIGURE 8.21 Far-field *P*- and *S*-wave displacements are proportional to $\dot{M}(t)$, the time derivative of the moment function $M(t) = \mu A(t)D(t)$. Simple step and ramp moment functions generate far-field impulses or boxcar ground motions.

FF DC Radiation pattern

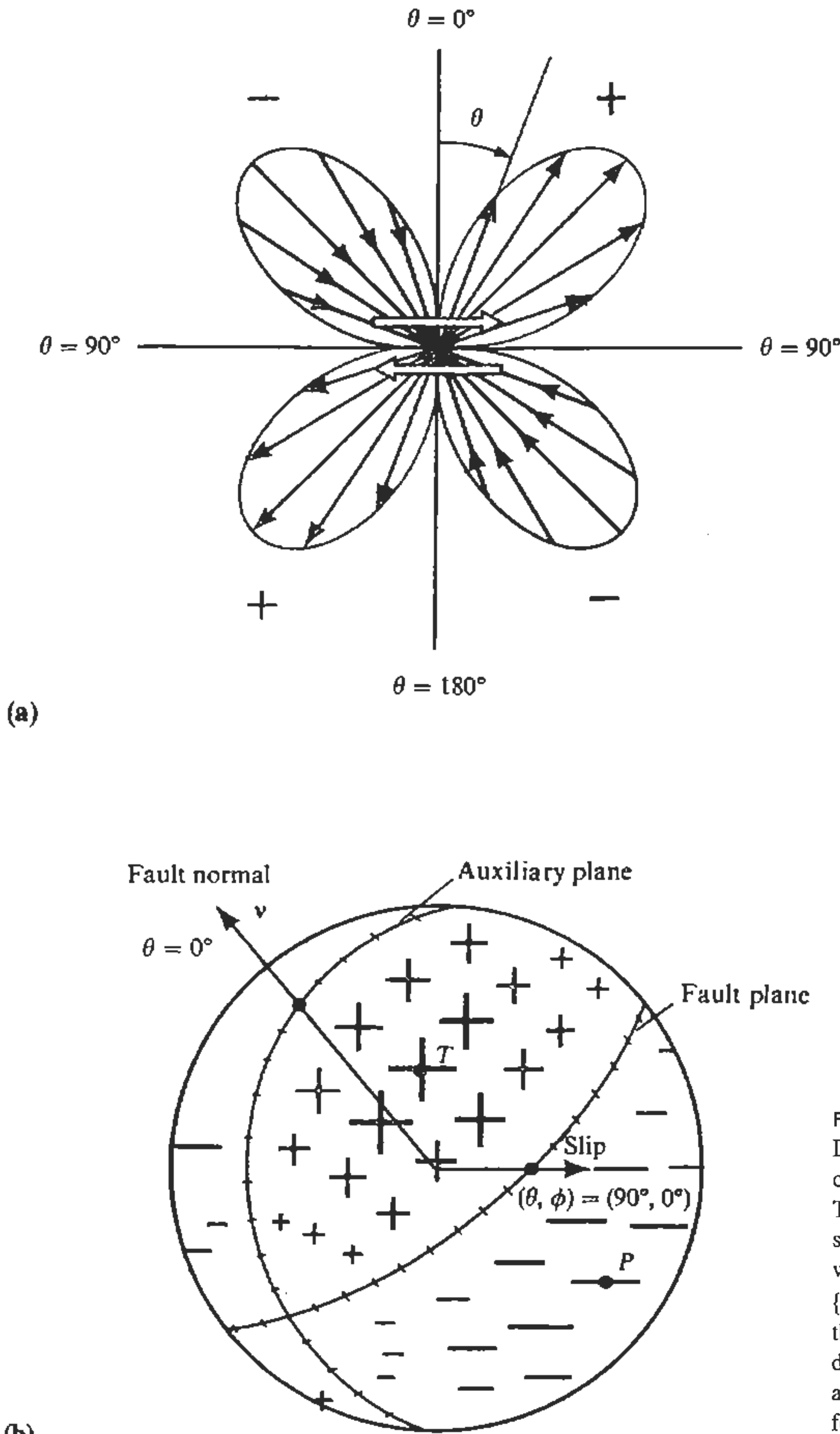

FIGURE **4.5**
Diagrams for the radiation pattern of the radial component of displacement due to a double couple, i.e., $\sin 2\theta \cos\phi\, \hat{\mathbf{r}}$. (**a**) The lobes are a locus of points having a distance from the origin that is proportional to $\sin 2\theta$. The diagram is for a plane of constant azimuth, and the pair of arrows at the center denotes the shear dislocation. Note the alternating quadrants of inward and outward directions. In terms of far-field P-wave displacement, plus signs denote outward displacement (if $\dot{M}_0(t - r/\alpha)$ is positive), and minus signs denote inward displacement. (**b**) View of the radiatiou pattern over a sphere centered on the origin. Plus and minus signs of various sizes denote variation (with θ, ϕ) of outward and inward motions. The fault plane and the auxiliary plane are nodal lines (on which $\sin 2\theta \cos\phi = 0$). An equal-area projection has been used (see Fig. 4.17). Point P marks the pressure axis, and T the tension axis.

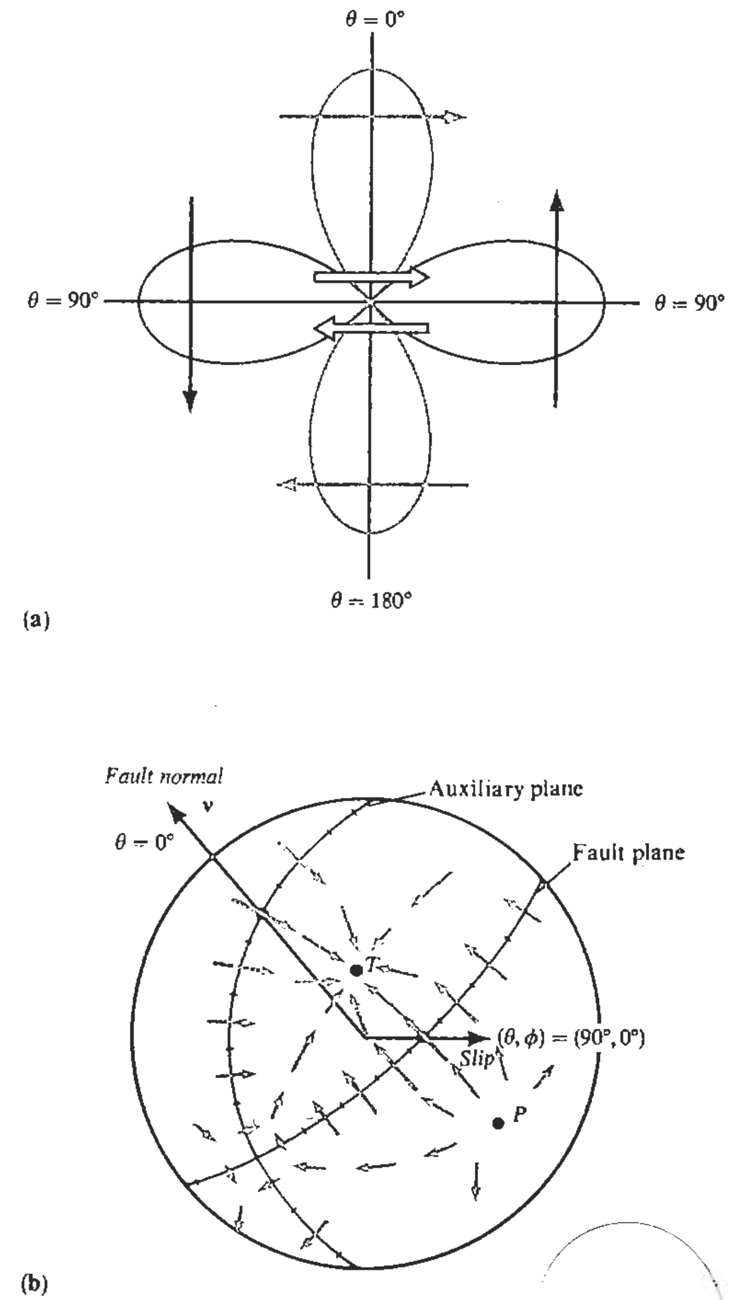

FIGURE **4.6**
Diagrams for the radiation pattern of the transverse component of displacement due to a double couple, i.e., $\cos 2\theta \cos\phi\, \hat{\boldsymbol{\theta}} - \cos\theta \sin\phi\, \hat{\boldsymbol{\phi}}$. (**a**) The four-lobed pattern in plane $\{\phi = 0, \phi = \pi\}$. The central pair of arrows shows the sense of shear dislocation, and arrows imposed on each lobe show the direction of particle displacement associated with the lobe. If applied to the far-field S-wave displacement, it is assumed that $\dot{M}_0(t - r/\beta)$ is positive. (**b**) Off the two planes $\theta = \pi/2$ and $\{\phi = 0, \phi = \pi\}$, the $\hat{\phi}$ component is nonzero, hence (a) is of limited use. This diagram is a view of the radiation pattern over a whole sphere centered on the origin, and arrows (with varying size and direction) in the spherical surface denote the variation (with θ, ϕ) of the transverse motions. There are no nodal lines (where there is zero motion), but nodal points do occur. Note that the nodal point for transverse motion at $(\theta, \phi) = (45°, 0)$ is a maximum in the radiation pattern for longitudinal motion (Fig. 4.5b). But the maximum transverse motion (e.g., at $\theta = 0$) occurs on a nodal line for the longitudinal motion. The stereographic projection has been used (see Fig. 4.16). It is a conformal projection, meaning that it preserves the angles at which curves intersect and the shapes of small regions, but it does not preserve relative areas.

Methodology - Modal Summation Technique

- Expression of the displacement generated by a double-couple point source in a flat layered halfspace

$$u_y^L(x,z,\omega) = \sum_{m=1}^{\infty} \frac{e^{-i3\pi/4}}{\sqrt{8\pi\omega}} \frac{e^{-ik_m x}}{\sqrt{x}} \frac{\left(\chi_m^L(h_s,\omega)\right)}{\sqrt{c_m v_m I_m}} \frac{\left(F_y(z,\omega)\right)}{\sqrt{v_m I_m}}$$

$$u_x^R(x,z,\omega) = \sum_{m=1}^{\infty} \frac{e^{-i3\pi/4}}{\sqrt{8\pi\omega}} \frac{e^{-ik_m x}}{\sqrt{x}} \frac{\left(\chi_m^R(h_s,\omega)\right)}{\sqrt{c_m v_m I_m}} \frac{\left(F_x(z,\omega)\right)}{\sqrt{v_m I_m}}$$

$$u_z^R(x,z,\omega) = \sum_{m=1}^{\infty} \frac{e^{-i\pi/4}}{\sqrt{8\pi\omega}} \frac{e^{-ik_m x}}{\sqrt{x}} \frac{\left(\chi_m^R(h_s,\omega)\right)}{\sqrt{c_m v_m I_m}} \frac{\left(F_z(z,\omega)\right)}{\sqrt{v_m I_m}}$$

Methodology - Modal Summation Technique

- Expression of the displacement generated by a double-couple point source in a flat layered halfspace

$$u_y^L(x,z,\omega) = \sum_{m=1}^{\infty} \frac{e^{-i3\pi/4}}{\sqrt{8\pi\omega}} \frac{e^{-ik_m x}}{\sqrt{x}} \frac{\left(\chi_m^L(h_s,\omega)\right)}{\sqrt{c_m v_m I_m}} \frac{\left(F_y(z,\omega)\right)}{\sqrt{v_m I_m}}$$

$$u_x^R(x,z,\omega) = \sum_{m=1}^{\infty} \frac{e^{-i3\pi/4}}{\sqrt{8\pi\omega}} \frac{e^{-ik_m x}}{\sqrt{x}} \frac{\left(\chi_m^R(h_s,\omega)\right)}{\sqrt{c_m v_m I_m}} \frac{\left(F_x(z,\omega)\right)}{\sqrt{v_m I_m}}$$

$$u_z^R(x,z,\omega) = \sum_{m=1}^{\infty} \frac{e^{-i\pi/4}}{\sqrt{8\pi\omega}} \frac{e^{-ik_m x}}{\sqrt{x}} \frac{\left(\chi_m^R(h_s,\omega)\right)}{\sqrt{c_m v_m I_m}} \frac{\left(F_z(z,\omega)\right)}{\sqrt{v_m I_m}}$$

source

Methodology - Modal Summation Technique

- Expression of the displacement generated by a double-couple point source in a flat layered halfspace

$$u_y^L(x,z,\omega) = \sum_{m=1}^{\infty} \frac{e^{-i3\pi/4}}{\sqrt{8\pi\omega}} \frac{e^{-ik_m x}}{\sqrt{x}} \frac{\left(\chi_m^L(h_s,\omega)\right)}{\sqrt{c_m v_m I_m}} \frac{\left(F_y(z,\omega)\right)}{\sqrt{v_m I_m}}$$

$$u_x^R(x,z,\omega) = \sum_{m=1}^{\infty} \frac{e^{-i3\pi/4}}{\sqrt{8\pi\omega}} \frac{e^{-ik_m x}}{\sqrt{x}} \frac{\left(\chi_m^R(h_s,\omega)\right)}{\sqrt{c_m v_m I_m}} \frac{\left(F_x(z,\omega)\right)}{\sqrt{v_m I_m}}$$

$$u_z^R(x,z,\omega) = \sum_{m=1}^{\infty} \frac{e^{-i\pi/4}}{\sqrt{8\pi\omega}} \frac{e^{-ik_m x}}{\sqrt{x}} \frac{\left(\chi_m^R(h_s,\omega)\right)}{\sqrt{c_m v_m I_m}} \frac{\left(F_z(z,\omega)\right)}{\sqrt{v_m I_m}}$$

source (yellow) structure (blue)

Methodology - Modal Summation Technique

- Expression of the displacement generated by a double-couple point source in a flat layered halfspace

$$u_y^L(x,z,\omega) = \sum_{m=1}^{\infty} \frac{e^{-i3\pi/4}}{\sqrt{8\pi\omega}} \frac{e^{-ik_m x}}{\sqrt{x}} \frac{\left(\chi_m^L(h_s,\omega)\right)}{\sqrt{c_m v_m I_m}} \frac{\left(F_y(z,\omega)\right)}{\sqrt{v_m I_m}}$$

$$u_x^R(x,z,\omega) = \sum_{m=1}^{\infty} \frac{e^{-i3\pi/4}}{\sqrt{8\pi\omega}} \frac{e^{-ik_m x}}{\sqrt{x}} \frac{\left(\chi_m^R(h_s,\omega)\right)}{\sqrt{c_m v_m I_m}} \frac{\left(F_x(z,\omega)\right)}{\sqrt{v_m I_m}}$$

$$u_z^R(x,z,\omega) = \sum_{m=1}^{\infty} \frac{e^{-i\pi/4}}{\sqrt{8\pi\omega}} \frac{e^{-ik_m x}}{\sqrt{x}} \frac{\left(\chi_m^R(h_s,\omega)\right)}{\sqrt{c_m v_m I_m}} \frac{\left(F_z(z,\omega)\right)}{\sqrt{v_m I_m}}$$

source — structure — receiver

Methodology - Modal Summation Technique

- Source definition and examples of radiation pattern

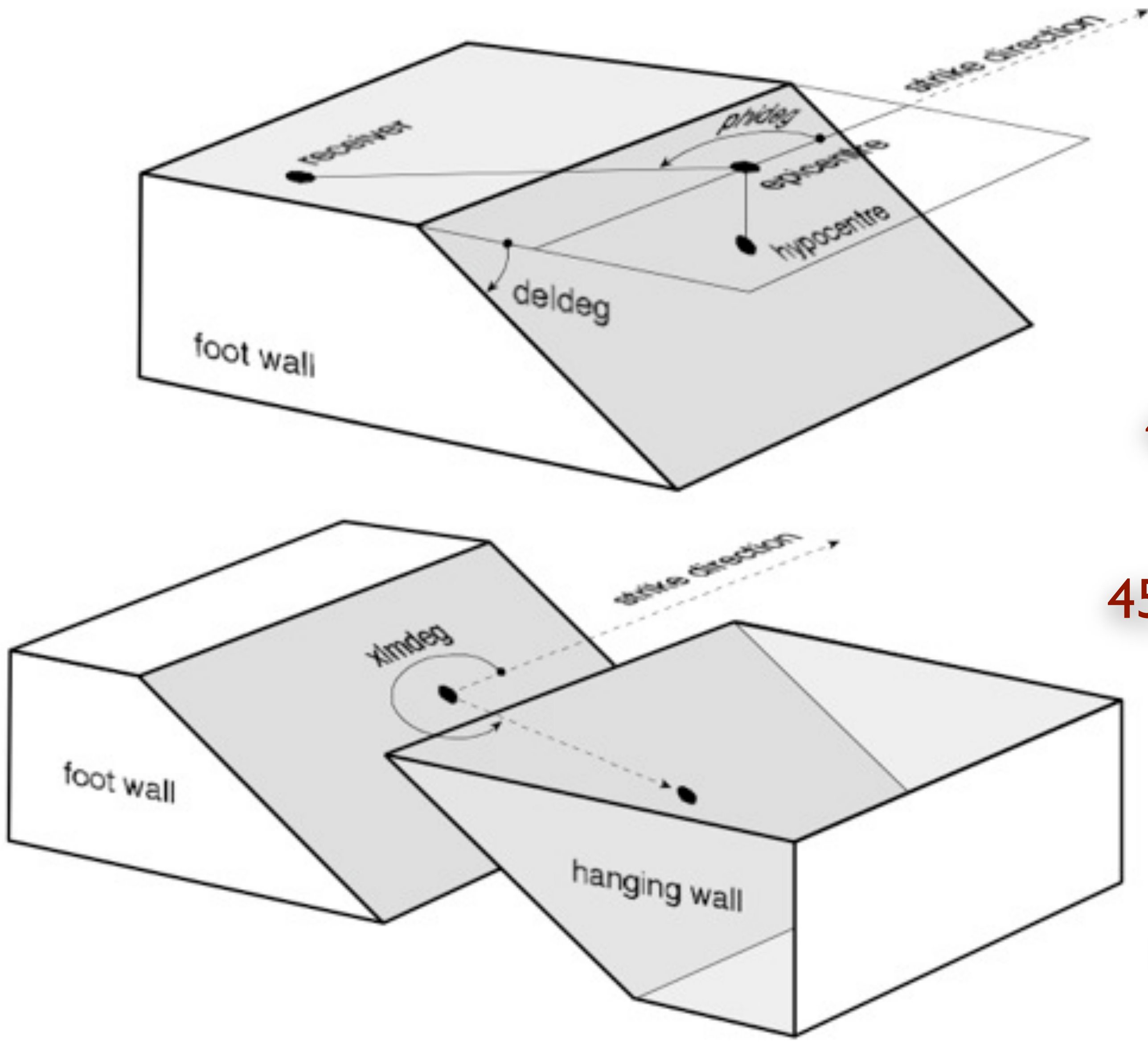

$$\left(\chi_m^L(h_s,\omega)\right) \quad \left(\chi_m^R(h_s,\omega)\right)$$

Love Rayleigh

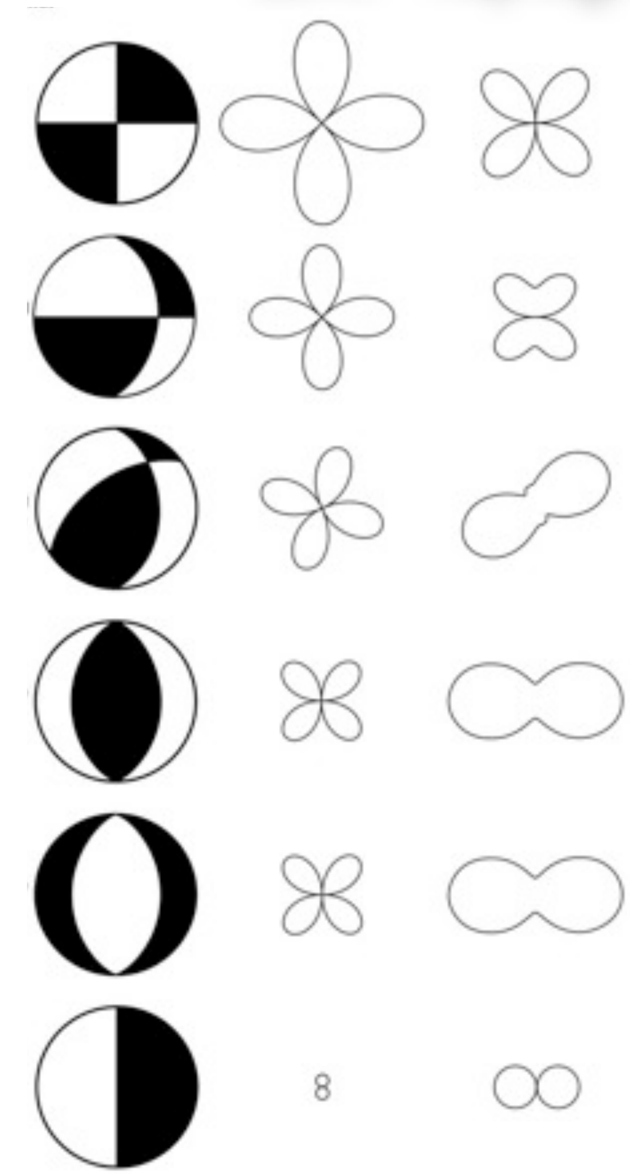

vertical strike-slip

45° dipping strike-slip

45° dipping oblique slip

45° dip-slip (thrust)

45° dip-slip (normal)

vertical dip-slip

Methodology - Modal Summation Technique

- Expression of the source radiation pattern

$$\chi_L = i(d_{1L}\sin\varphi + d_{2L}\cos\varphi) + d_{3L}\sin 2\varphi + d_{4L}\cos 2\varphi$$

$$\chi_R = d_0 + i(d_{1R}\sin\varphi + d_{2R}\cos\varphi) + d_{3R}\sin 2\varphi + d_{4R}\cos 2\varphi$$

$$\left(\chi_m^L(h_s,\omega)\right) \quad \left(\chi_m^R(h_s,\omega)\right)$$

Methodology - Modal Summation Technique

- Expression of the source radiation pattern

$$\chi_L = i(d_{1L}\sin\varphi + d_{2L}\cos\varphi) + d_{3L}\sin 2\varphi + d_{4L}\cos 2\varphi$$

$$\chi_R = d_0 + i(d_{1R}\sin\varphi + d_{2R}\cos\varphi) + d_{3R}\sin 2\varphi + d_{4R}\cos 2\varphi$$

where

$$d_{1L} = G(h_s)\cos\lambda\sin\delta$$

$$d_{2L} = -G(h_s)\sin\lambda\cos 2\delta$$

$$d_{3L} = \frac{1}{2}V(h_s)\sin\lambda\sin 2\delta$$

$$d_{4L} = V(h_s)\cos\lambda\sin\delta$$

$$d_0 = \frac{1}{2}B(h_s)\sin\lambda\sin 2\delta$$

$$d_{1R} = -C(h_s)\sin\lambda\cos 2\delta$$

$$d_{2R} = -C(h_s)\cos\lambda\cos\delta$$

$$d_{3R} = A(h_s)\cos\lambda\sin\delta$$

$$d_{4R} = -\frac{1}{2}A(h_s)\sin\lambda\sin 2\delta$$

$$\left(\chi_m^L(h_s,\omega)\right) \quad \left(\chi_m^R(h_s,\omega)\right)$$

Methodology - Modal Summation Technique

- Expression of the source radiation pattern

$$\chi_L = i(d_{1L}\sin\varphi + d_{2L}\cos\varphi) + d_{3L}\sin 2\varphi + d_{4L}\cos 2\varphi$$

$$\chi_R = d_0 + i(d_{1R}\sin\varphi + d_{2R}\cos\varphi) + d_{3R}\sin 2\varphi + d_{4R}\cos 2\varphi$$

where

$$d_{1L} = G(h_s)\cos\lambda\sin\delta$$
$$d_{2L} = -G(h_s)\sin\lambda\cos 2\delta$$
$$d_{3L} = \frac{1}{2}V(h_s)\sin\lambda\sin 2\delta$$
$$d_{4L} = V(h_s)\cos\lambda\sin\delta$$

$$d_0 = \frac{1}{2}B(h_s)\sin\lambda\sin 2\delta$$
$$d_{1R} = -C(h_s)\sin\lambda\cos 2\delta$$
$$d_{2R} = -C(h_s)\cos\lambda\cos\delta$$
$$d_{3R} = A(h_s)\cos\lambda\sin\delta$$
$$d_{4R} = -\frac{1}{2}A(h_s)\sin\lambda\sin 2\delta$$

$$A(h_s) = -\frac{F_x{}^*(h_s)}{F_z(0)}$$
$$B(h_s) = -\left(3 - 4\frac{\beta^2(h_s)}{\alpha^2(h_s)}\right)\frac{F_x{}^*(h_s)}{F_z(0)} - \frac{2}{\rho(h_s)\,\alpha^2(h_s)}\frac{\sigma_{zz}{}^*(h_s)}{\dot{F}_z(0)/c}$$
$$C(h_s) = -\frac{1}{\mu(h_s)}\frac{\sigma_{zx}(h_s)}{\dot{F}_z(0)/c}$$
$$G(h_s) = -\frac{1}{\mu(h_s)}\frac{\sigma_{zy}{}^*(h_s)}{\dot{F}_y(0)/c}$$
$$V(h_s) = \frac{\dot{F}_y(h_s)}{\dot{F}_y(0)/c} = \frac{F_y(h_s)}{F_y(0)/c}$$

$$\left(\chi_m^L(h_s,\omega)\right) \quad \left(\chi_m^R(h_s,\omega)\right)$$

Methodology - Modal Summation Technique

- Example of quantities associated with a structure

$$\sqrt{c_m v_m I_m} \qquad \sqrt{v_m I_m}$$

Methodology - Modal Summation Technique

- Example of quantities associated with a structure

$$\sqrt{c_m v_m I_m} \qquad \sqrt{v_m I_m}$$

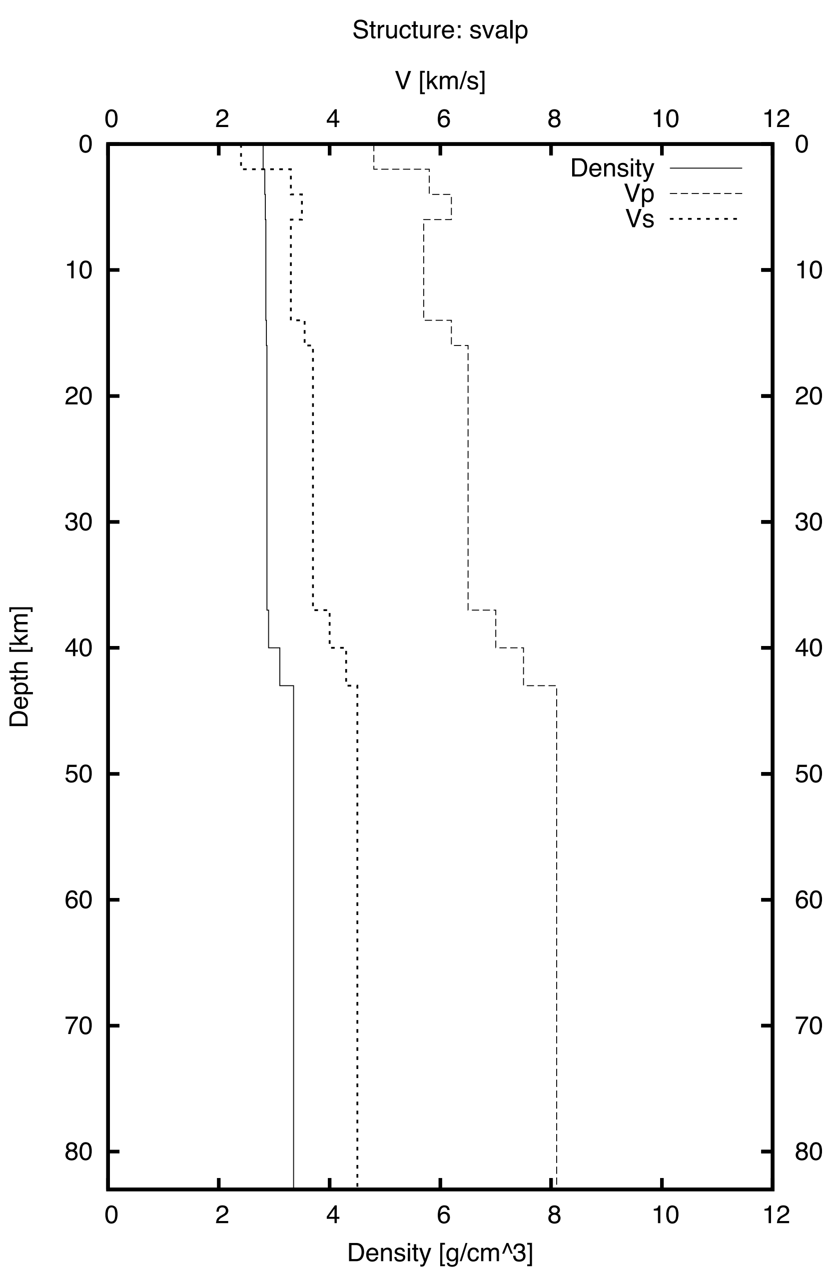

Methodology - Modal Summation Technique

- Example of quantities associated with a structure

$$\sqrt{c_m v_m I_m} \qquad \sqrt{v_m I_m}$$

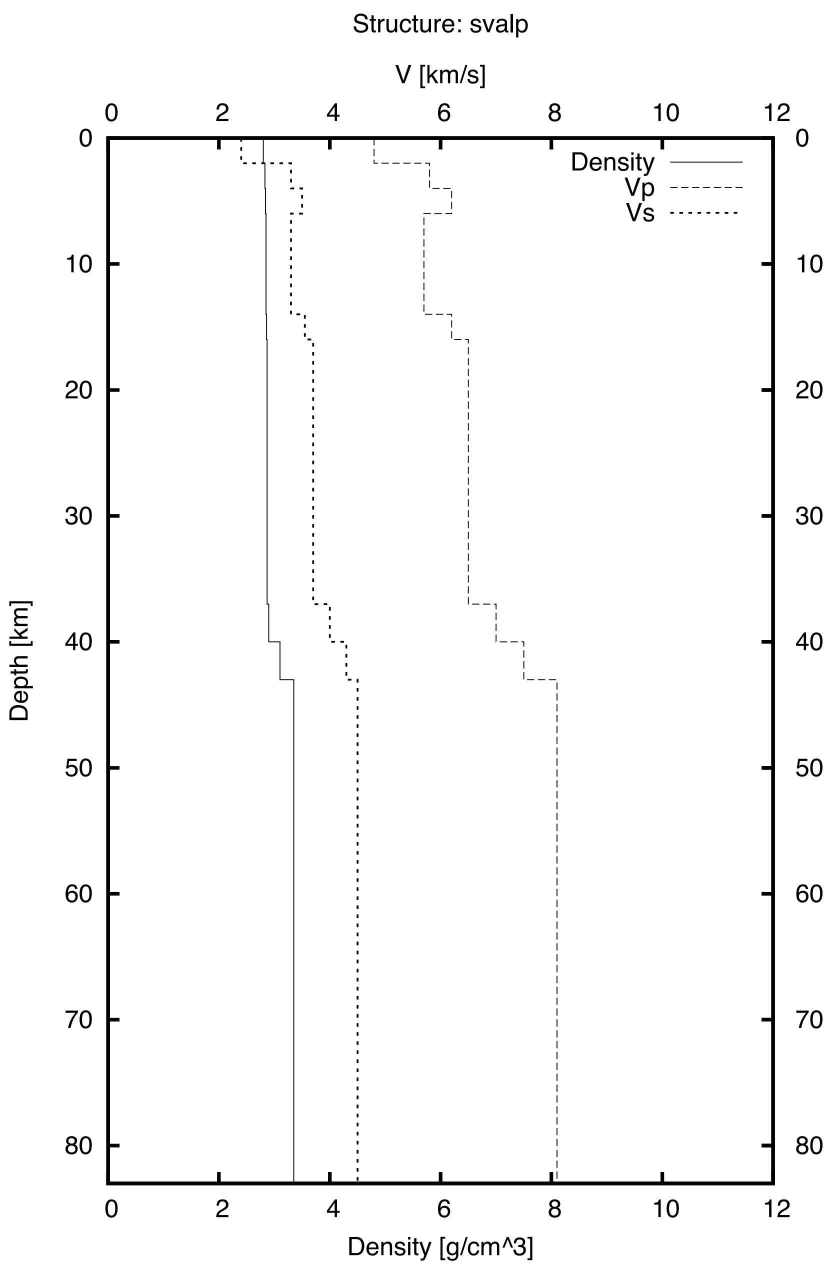

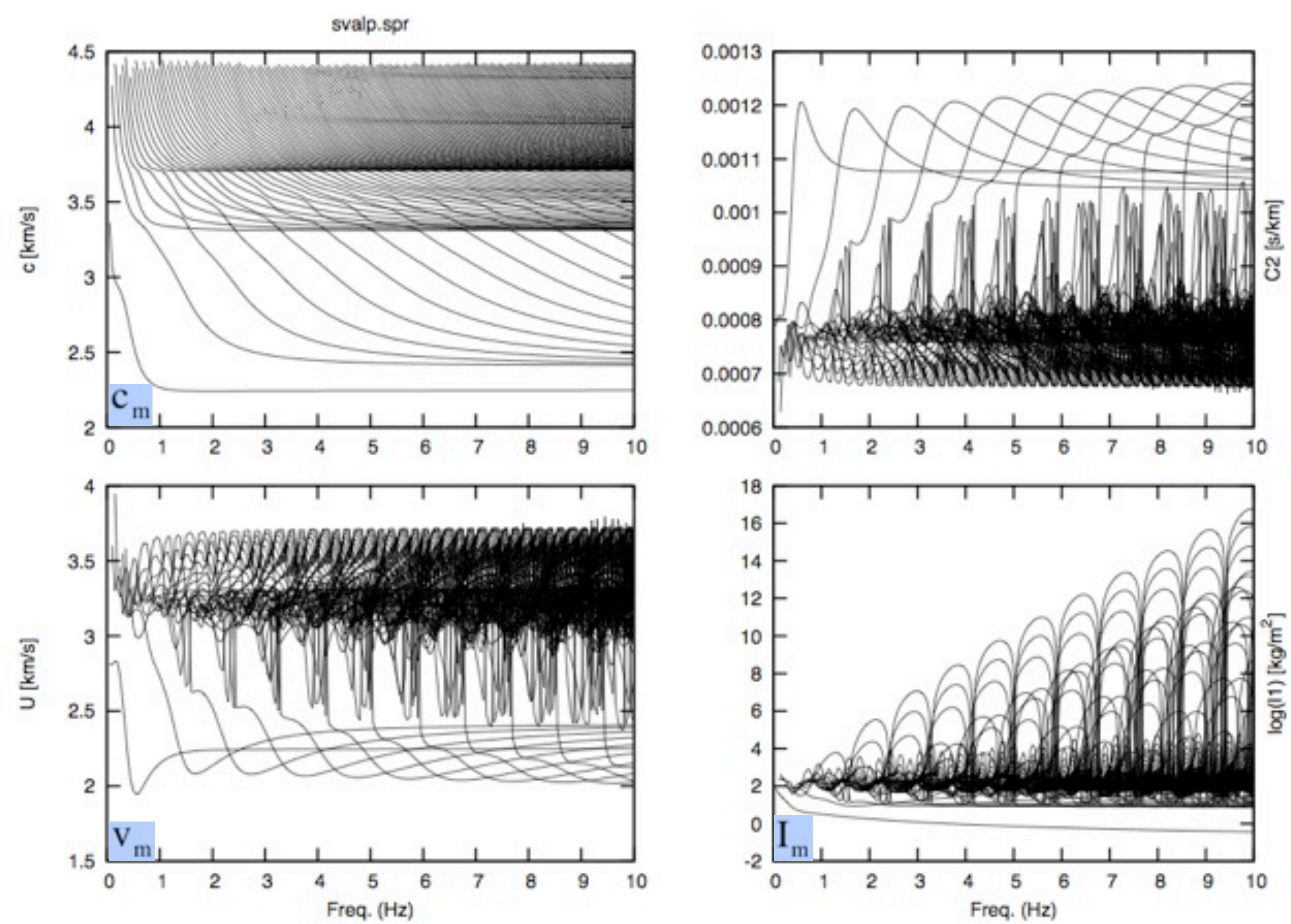

Methodology - Modal Summation Technique

- Phase velocity dispersion curve

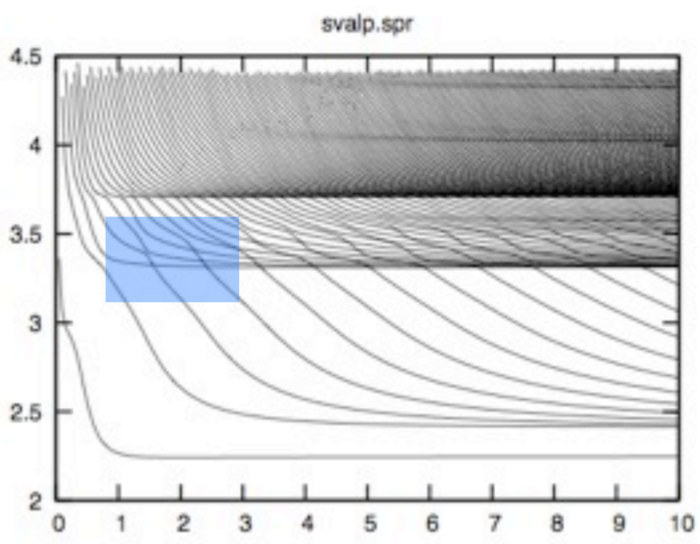

Methodology - Modal Summation Technique

- Phase velocity dispersion curve

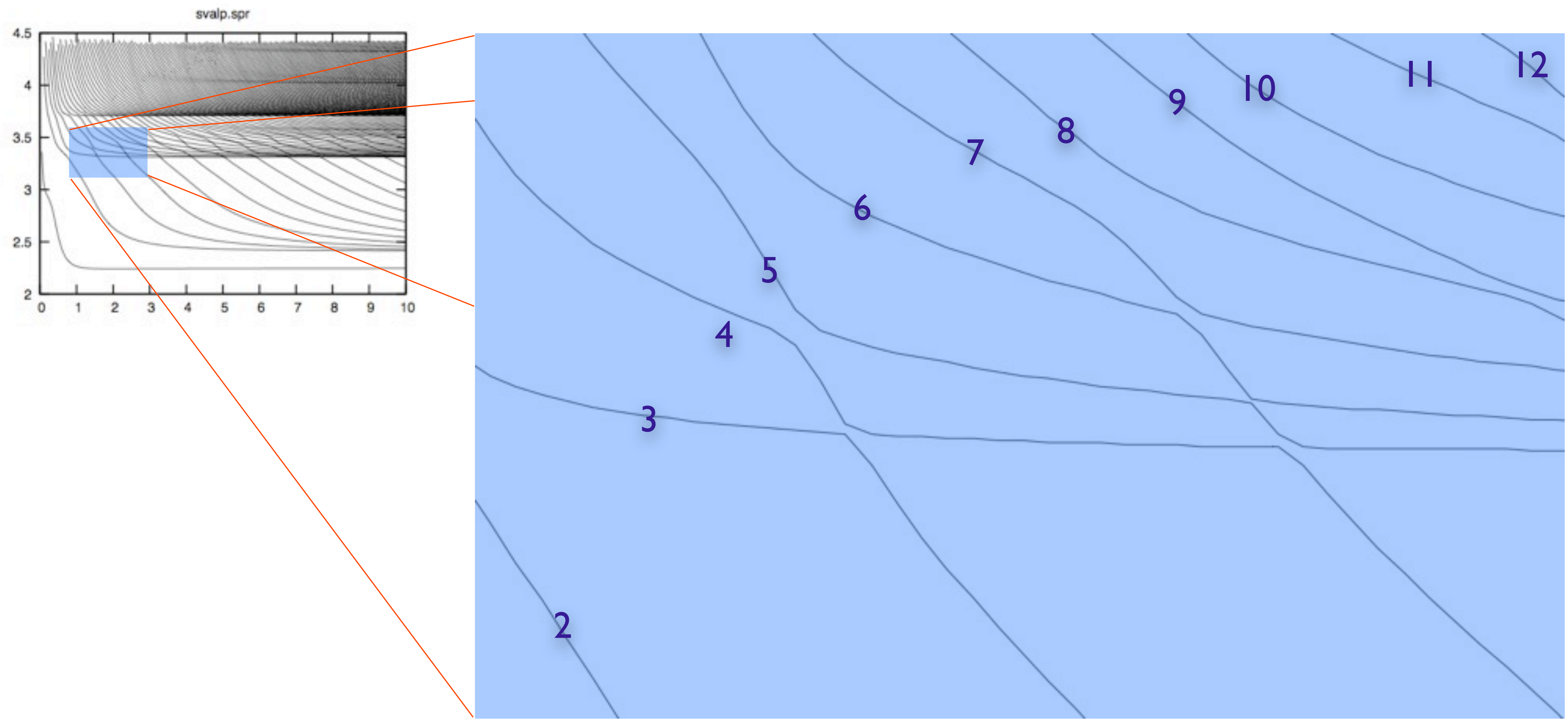

Methodology - Modal Summation Technique

- Phase velocity dispersion curve

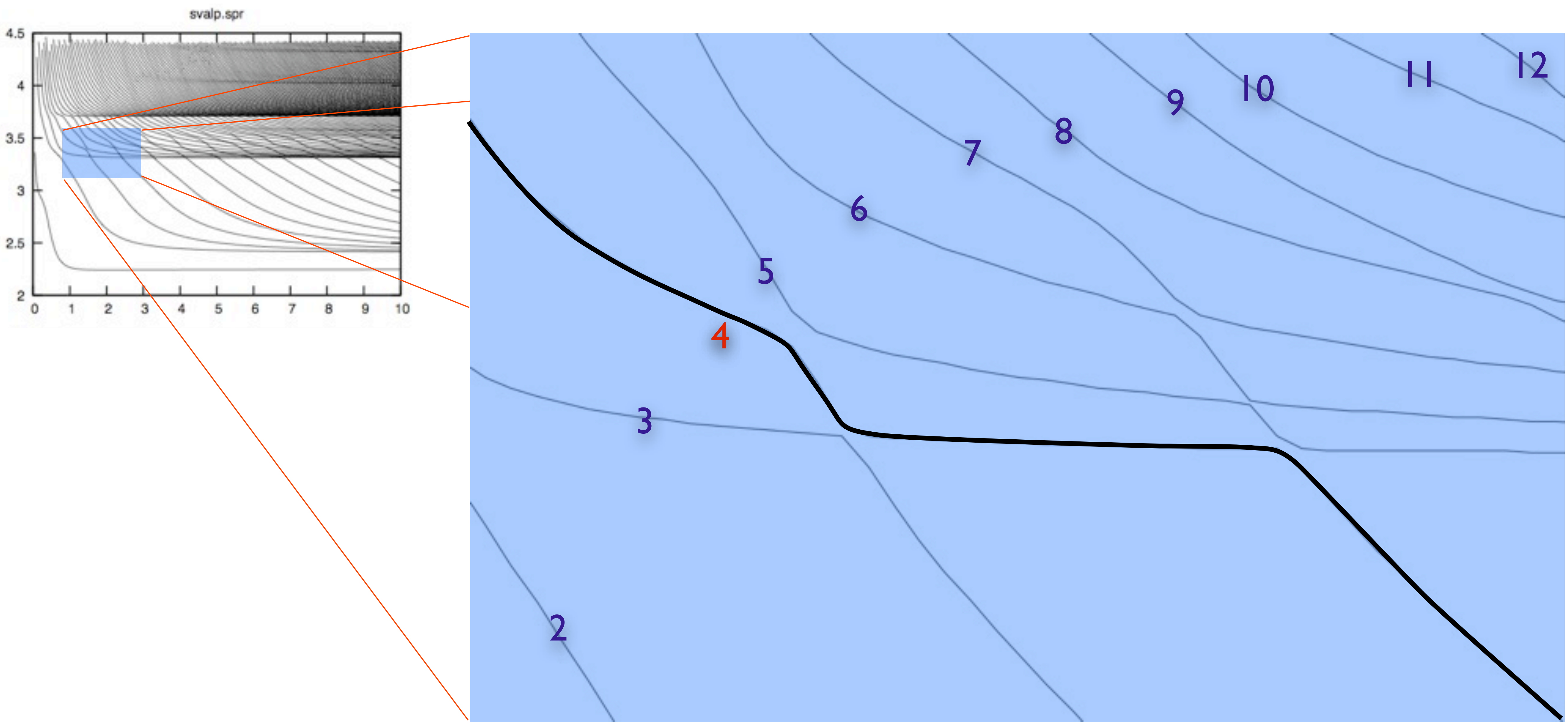

Methodology - Modal Summation Technique

- Phase velocity dispersion curve

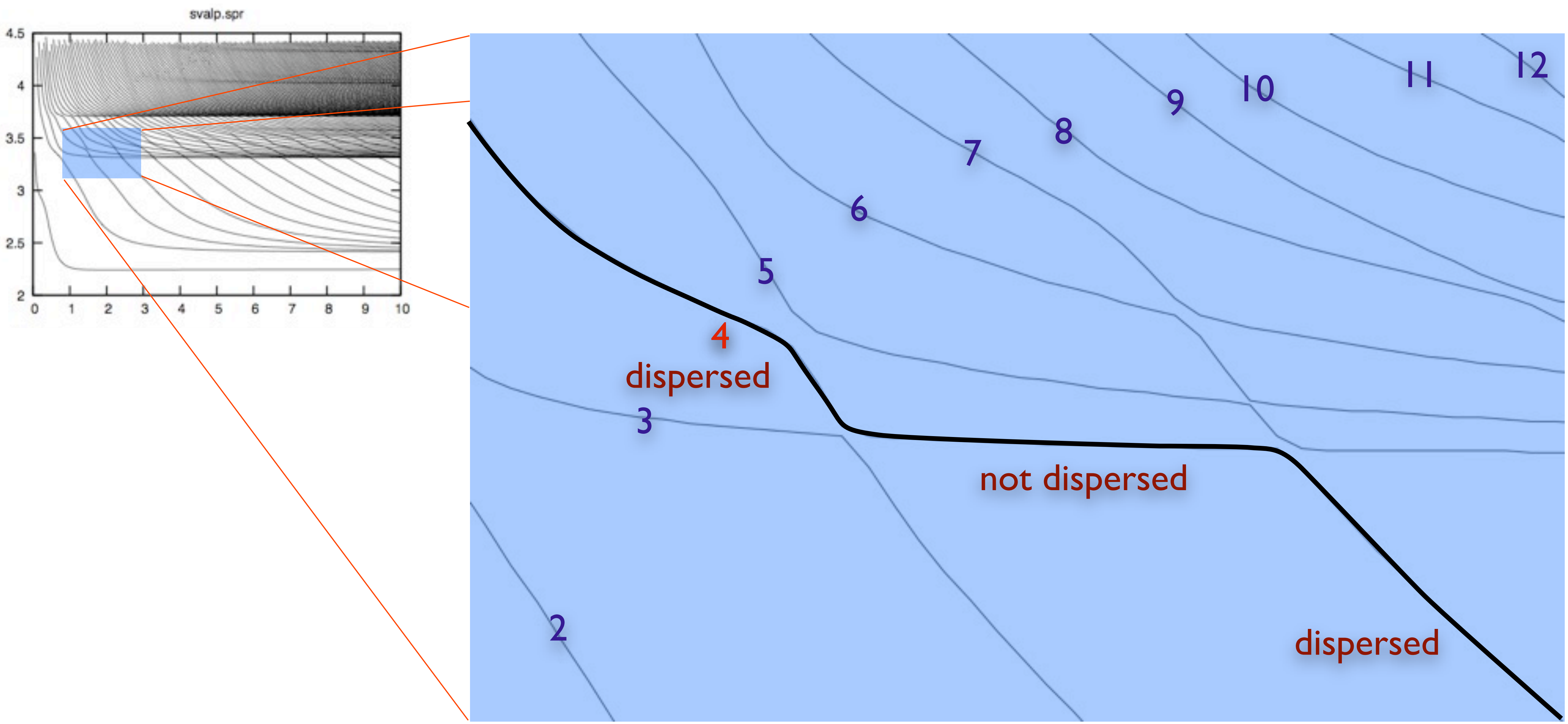

Methodology - Modal Summation Technique

- Phase velocity dispersion curve

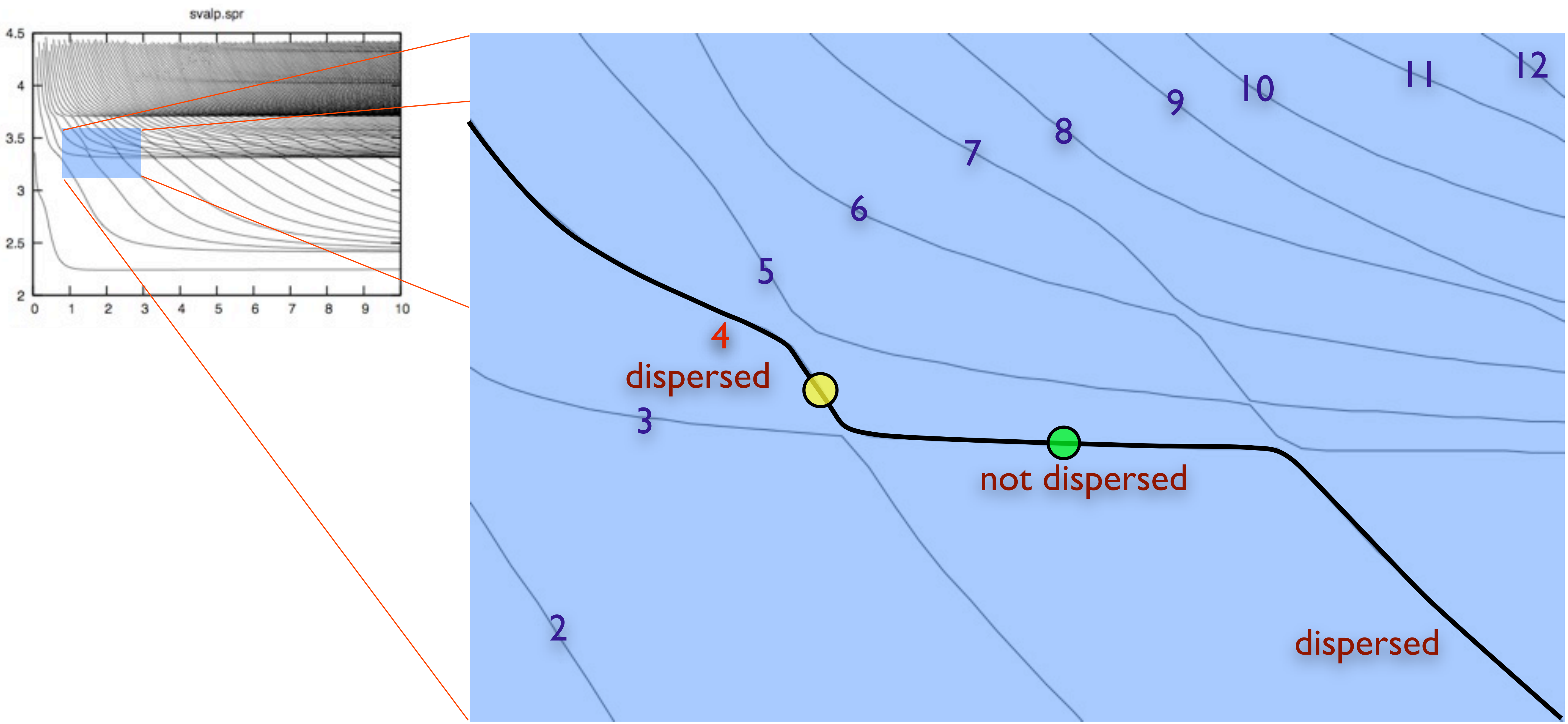

Methodology - Modal Summation Technique

- Eigenfunctions

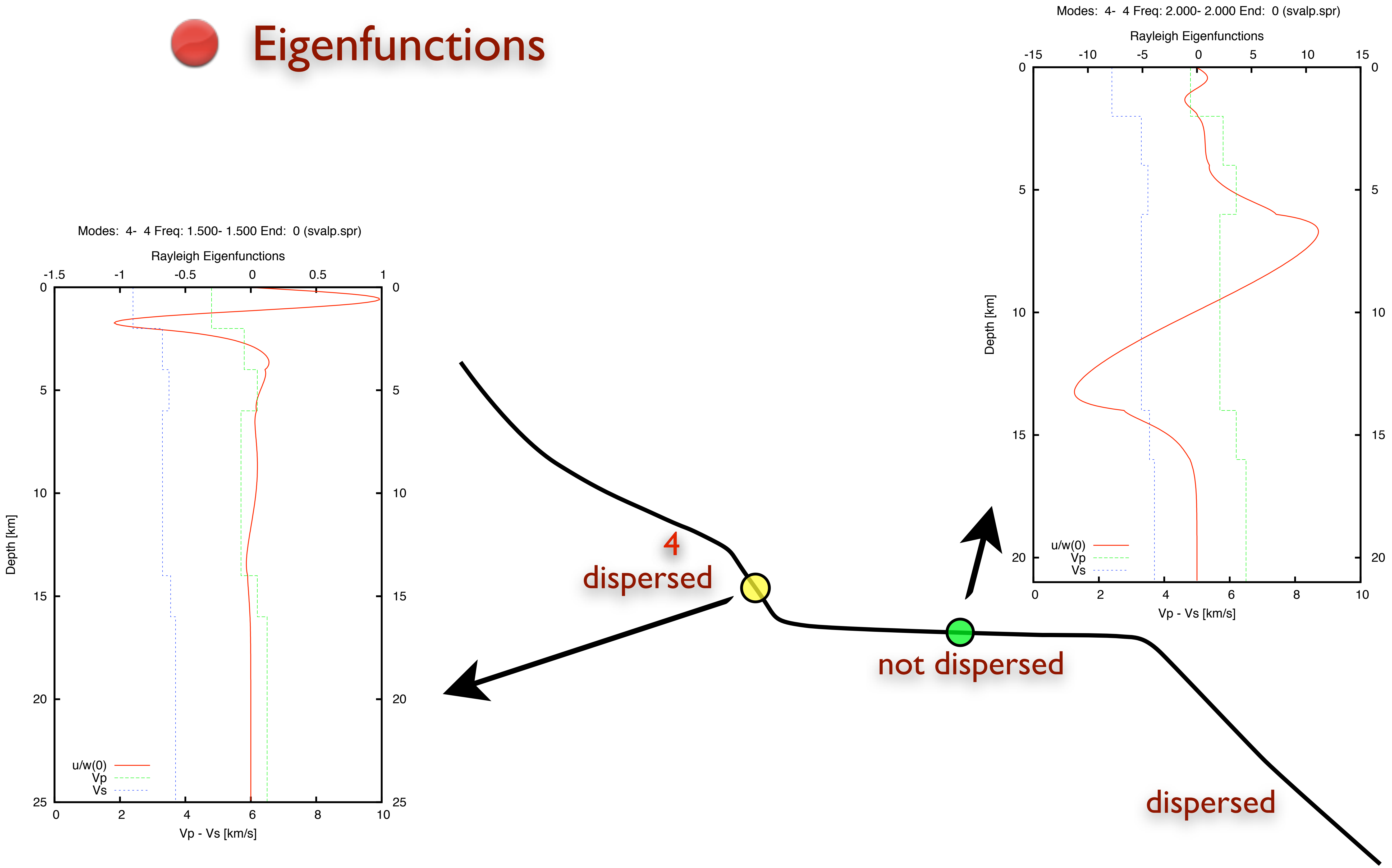

Haskell dislocation model

Haskell N. A. (1964). Total energy spectral density of elastic wave radiation from propagating faults, Bull. Seism. Soc. Am. **54**, 1811-1841

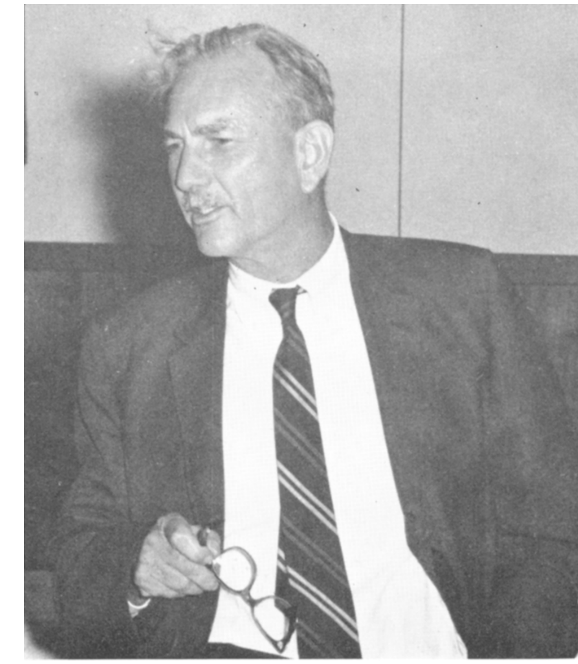

Norman A. Haskell

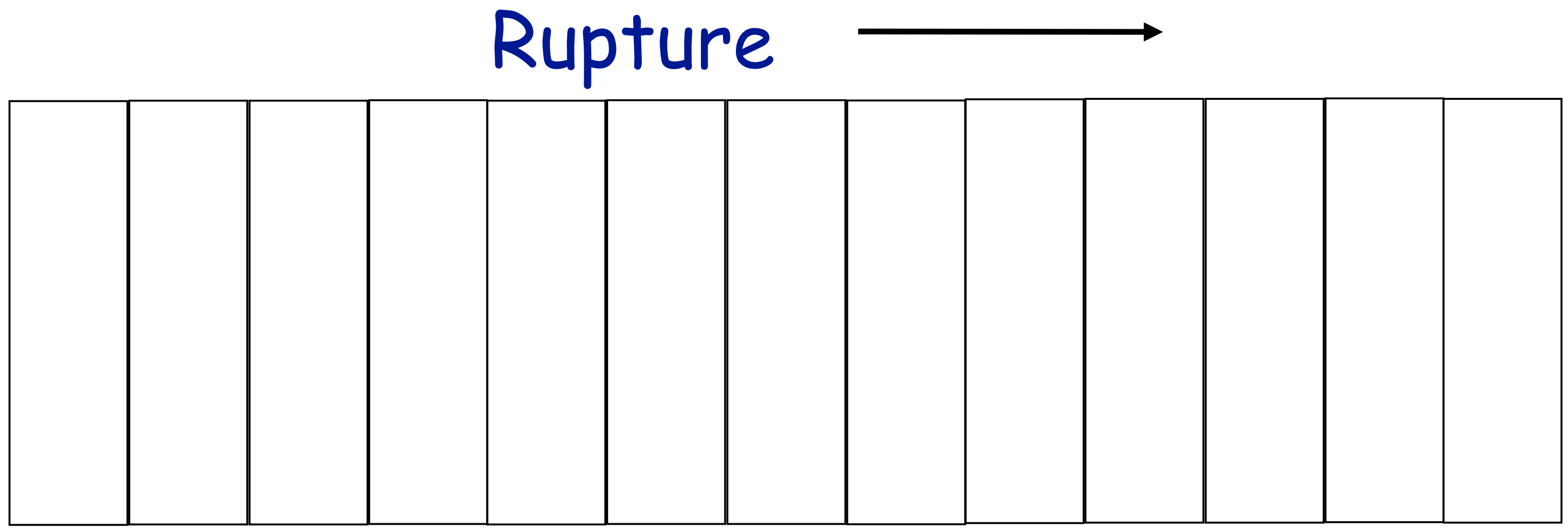

Sumatra earthquake, Dec 28, 2004

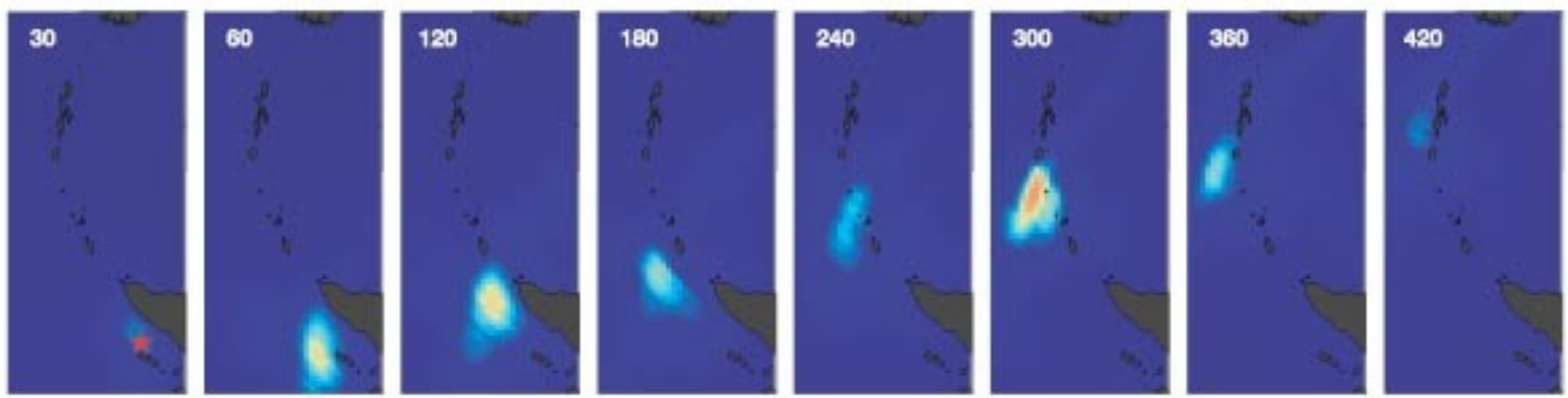

Ishii et al., Nature 2005 doi:10.1038/nature03675

Haskell dislocation model

Haskell N. A. (1964). Total energy spectral density of elastic wave radiation from propagating faults, Bull. Seism. Soc. Am. **54**, 1811-1841

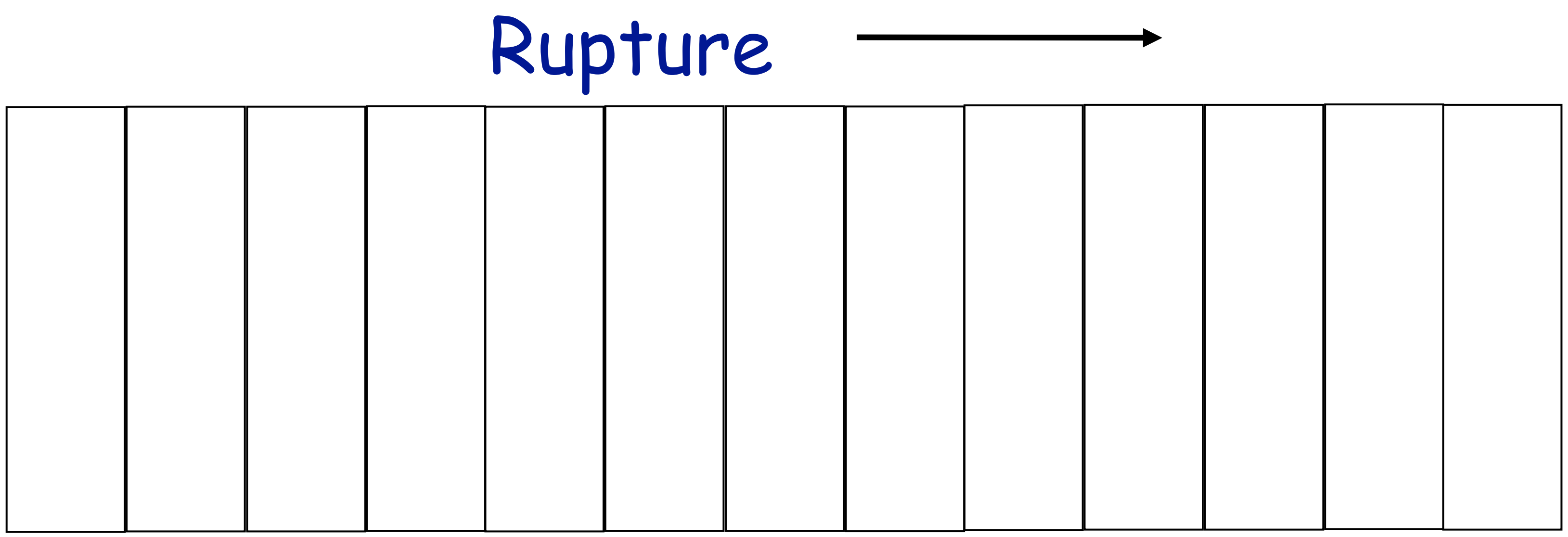

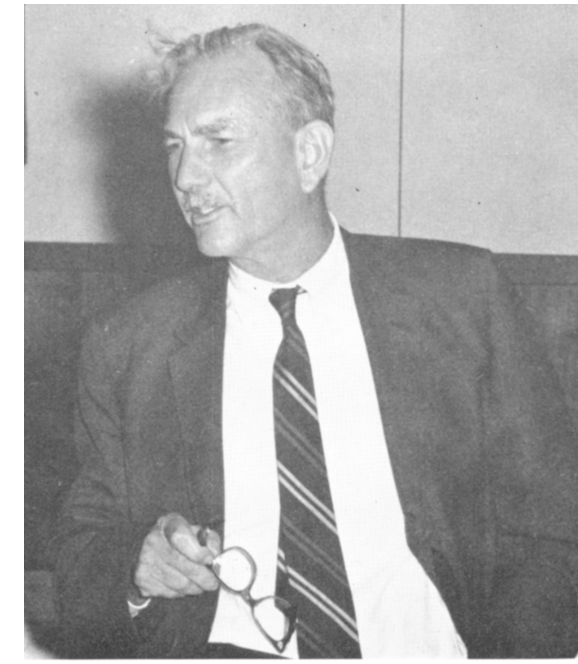

Norman A. Haskell

Sumatra earthquake, Dec 28, 2004

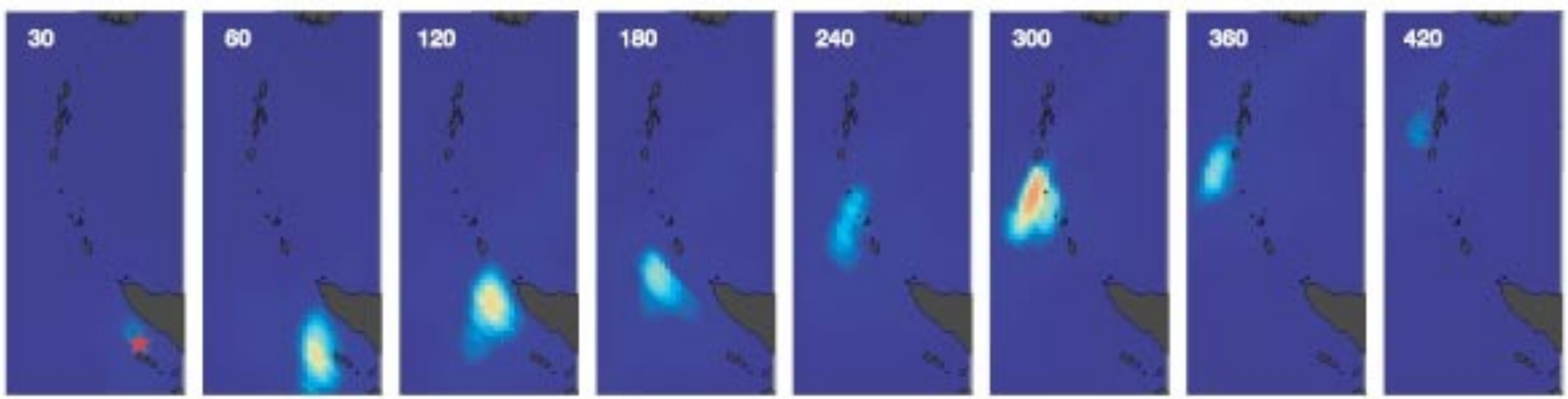

Ishii et al., Nature 2005 doi:10.1038/nature03675

Haskell source model: far field

For a single segment (point source)

$$\mathbf{u}(\mathbf{x},t) = \frac{1}{4\pi\rho\alpha^3}\left(\sin 2\theta \cos\phi \hat{\mathbf{r}}\right)\frac{\dot{M}(t - r/\alpha)}{r} +$$

$$\frac{1}{4\pi\rho\beta^3}\left(\cos 2\theta \cos\phi \hat{\boldsymbol{\theta}} - \cos\theta \sin\phi \hat{\boldsymbol{\phi}}\right)\frac{\dot{M}(t - r/\beta)}{r}$$

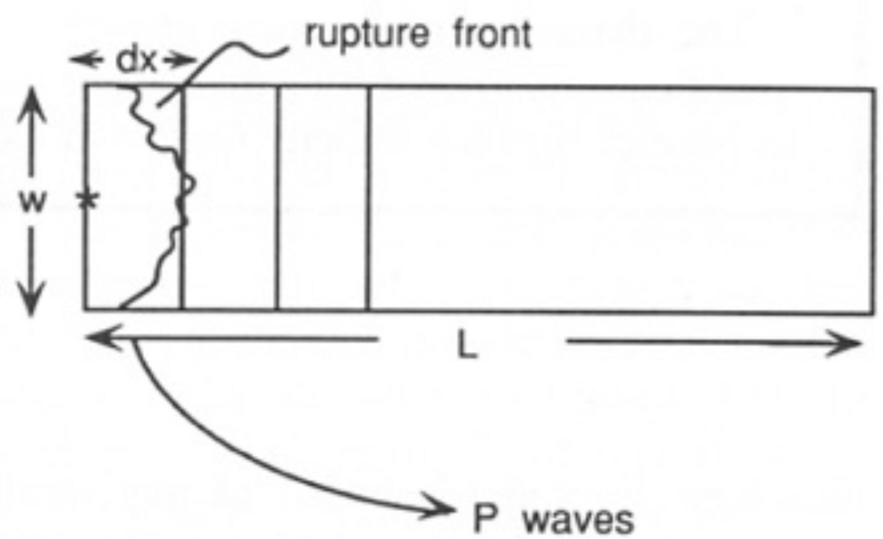

FIGURE 9.5 Geometry of a one-dimensional fault of width *w* and length *L*. The individual segments of the fault are of length *dx*, and the moment of a segment is *m dx*. The fault ruptures with velocity v_r.

Haskell source model: far field

For a single segment (point source)

$$\mathbf{u}(\mathbf{x},t) = \frac{1}{4\pi\rho\alpha^3}\left(\sin 2\theta \cos\phi \hat{\mathbf{r}}\right)\frac{\dot{M}(t - r/\alpha)}{r} +$$

$$\frac{1}{4\pi\rho\beta^3}\left(\cos 2\theta \cos\phi \hat{\boldsymbol{\theta}} - \cos\theta \sin\phi \hat{\boldsymbol{\phi}}\right)\frac{\dot{M}(t - r/\beta)}{r}$$

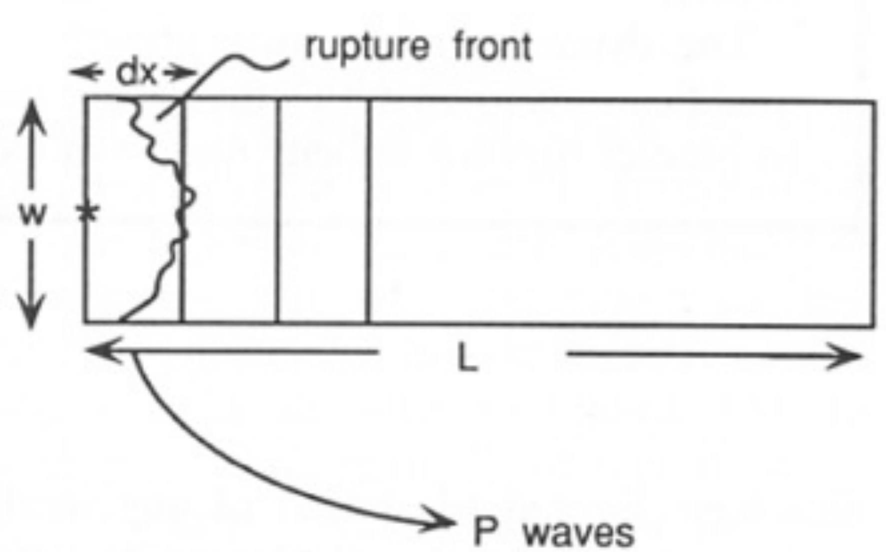

FIGURE 9.5 Geometry of a one-dimensional fault of width *w* and length *L*. The individual segments of the fault are of length *dx*, and the moment of a segment is *m dx*. The fault ruptures with velocity v_r.

$$u_r(r,t) = \sum_{i=1}^{N} u_i\left(r_i, t - r_i/\alpha - \Delta t_i\right) =$$

$$= \frac{R_i^P \mu}{4\pi\rho\alpha^3} W \sum_{i=1}^{N} \frac{\dot{D}_i}{r_i}\left(t - \Delta t_i\right) dx \approx$$

$$\approx \frac{R_i^P \mu}{4\pi\rho\alpha^3} \frac{W}{r} \sum_{i=1}^{N} \dot{D}(t) * \delta\left(t - \frac{x}{v_r}\right) dx \approx$$

$$\approx \frac{R_i^P \mu}{4\pi\rho\alpha^3} \frac{W}{r} \dot{D}(t) * \int_0^x \delta\left(t - \frac{x}{v_r}\right) dx =$$

$$= \frac{R_i^P \mu}{4\pi\rho\alpha^3} \frac{W}{r} v_r \dot{D}(t) * B(t;T_r)$$

Haskell source model: far field

$$u_r(r,t) \propto \dot{D}(t) * v_r H(z)\Big|_{t-x/v_r}^{t} = v_r \dot{D}(t) * B(t;T_r)$$

resulting in the convolution of two boxcars: the first with duration equal to the rise time and the second with duration equal to the **rupture time** (L/v_r)

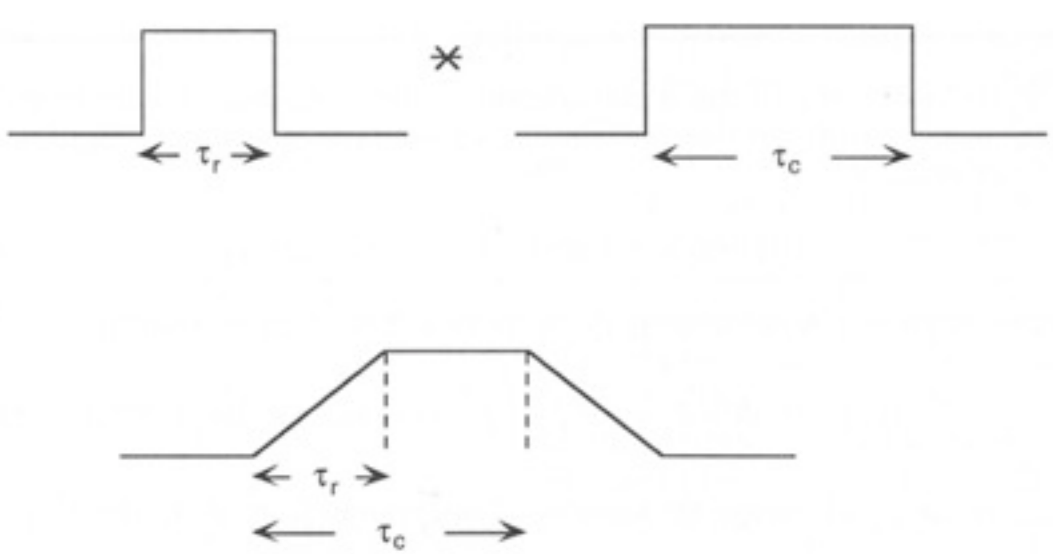

FIGURE 9.6 The convolution of two boxcars, one of length τ_r and the other of length τ_c ($\tau_c > \tau_r$). The result is a trapezoid with a rise time of τ_r, a top of length $\tau_c - \tau_r$, and a fall of width τ_r.

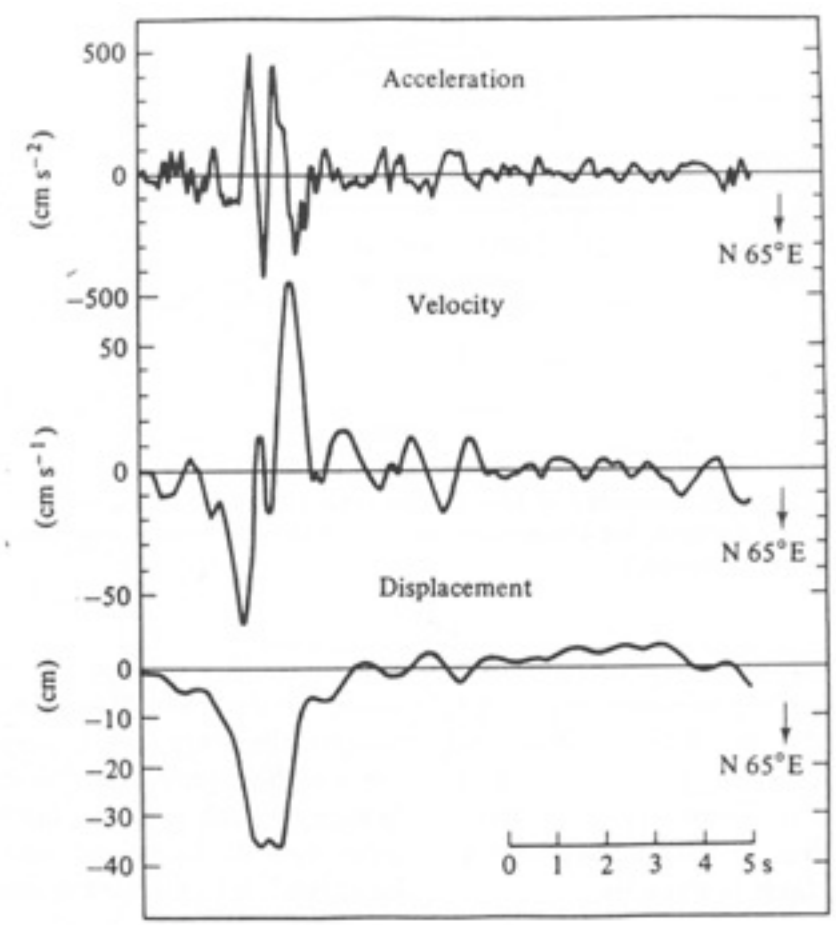

FIGURE 9.7 A recording of the ground motion near the epicenter of an earthquake at Parkfield, California. The station is located on a node for *P* waves and a maximum for *SH*. The displacement pulse is the *SH* wave. Note the trapezoidal shape. (From Aki, *J. Geophys. Res.* 73, 5359–5375, 1968; © copyright by the American Geophysical Union.)

Haskell source model: directivity

The body waves generated from a breaking segment will arrive at a receiver before than those that are radiated by a segment that ruptures later.
If the path to the station is not perpendicular, the waves generated by different segments will have different path lengths, and then unequal travel times.

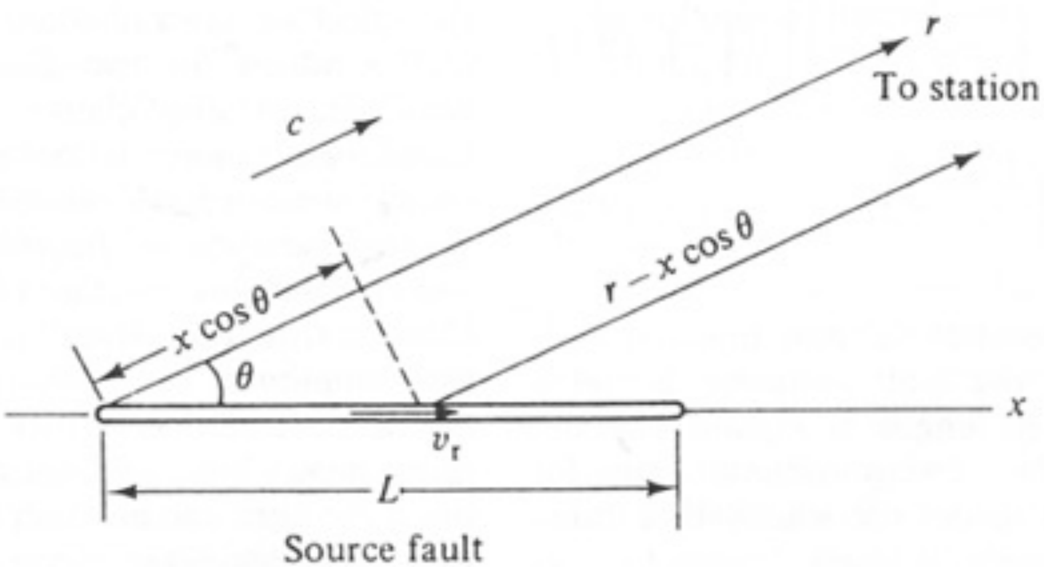

FIGURE 9.8 Geometry of a rupturing fault and the path to a remote recording station. (From Kasahara, 1981.)

$$T_r = \left[\frac{L}{v_r} + \left(\frac{r - L\cos\theta}{c}\right)\right] - \frac{r}{c} =$$

$$= \frac{L}{v_r} - \left(\frac{L\cos\theta}{c}\right) = \frac{L}{v_r}\left(1 - \frac{v_r}{c}\cos\theta\right)$$

Haskell source model: directivity

The body waves generated from a breaking segment will arrive at a receiver before than those that are radiated by a segment that ruptures later.
If the path to the station is not perpendicular, the waves generated by different segments will have different path lengths, and then unequal travel times.

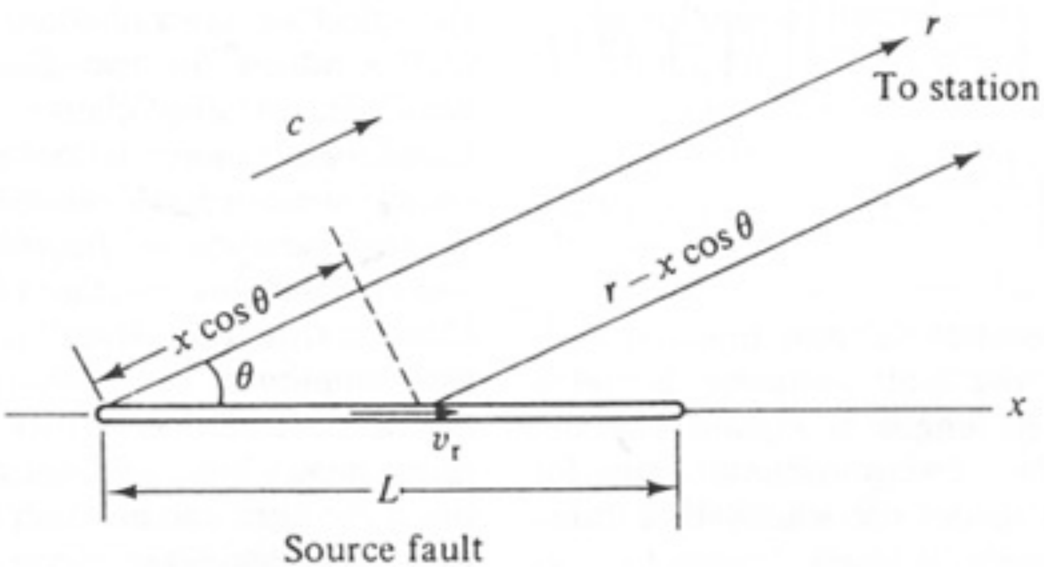

$$T_r = \left[\frac{L}{v_r} + \left(\frac{r - L\cos\theta}{c}\right)\right] - \frac{r}{c} =$$

$$= \frac{L}{v_r} - \left(\frac{L\cos\theta}{c}\right) = \frac{L}{v_r}\left(1 - \frac{v_r}{c}\cos\theta\right)$$

FIGURE 9.8 Geometry of a rupturing fault and the path to a remote recording station. (From Kasahara, 1981.)

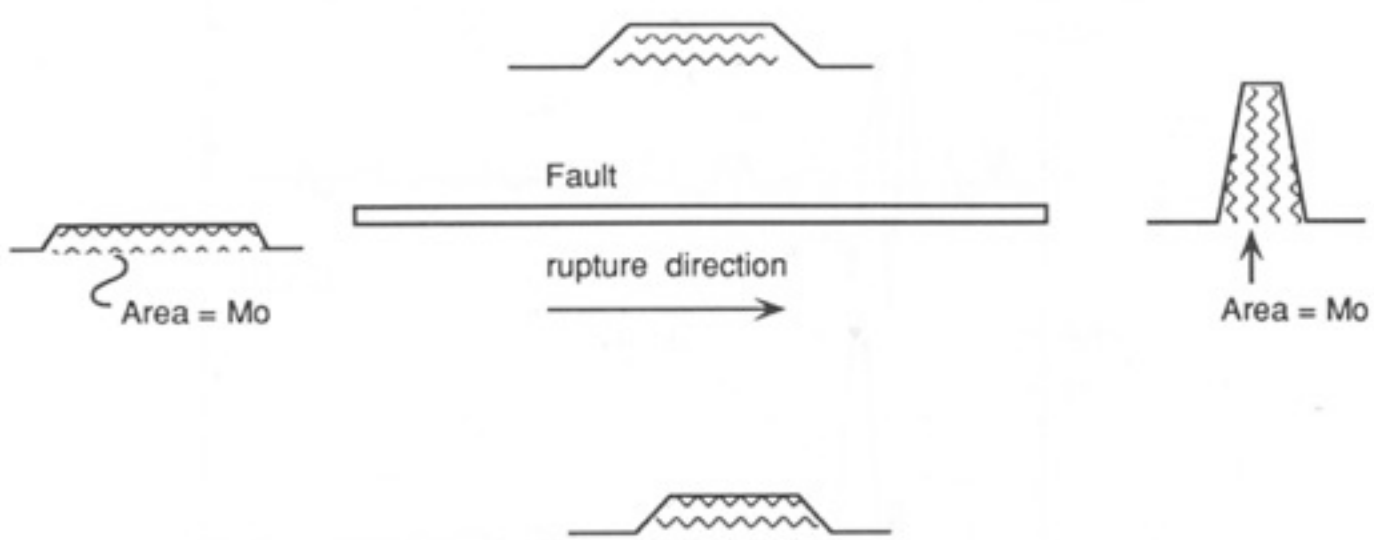

FIGURE 9.9 Azimuthal variability of the source time function for a unilaterally rupturing fault. The duration changes, but the area of the source time function is the seismic moment and is independent of azimuth.

Directivity example

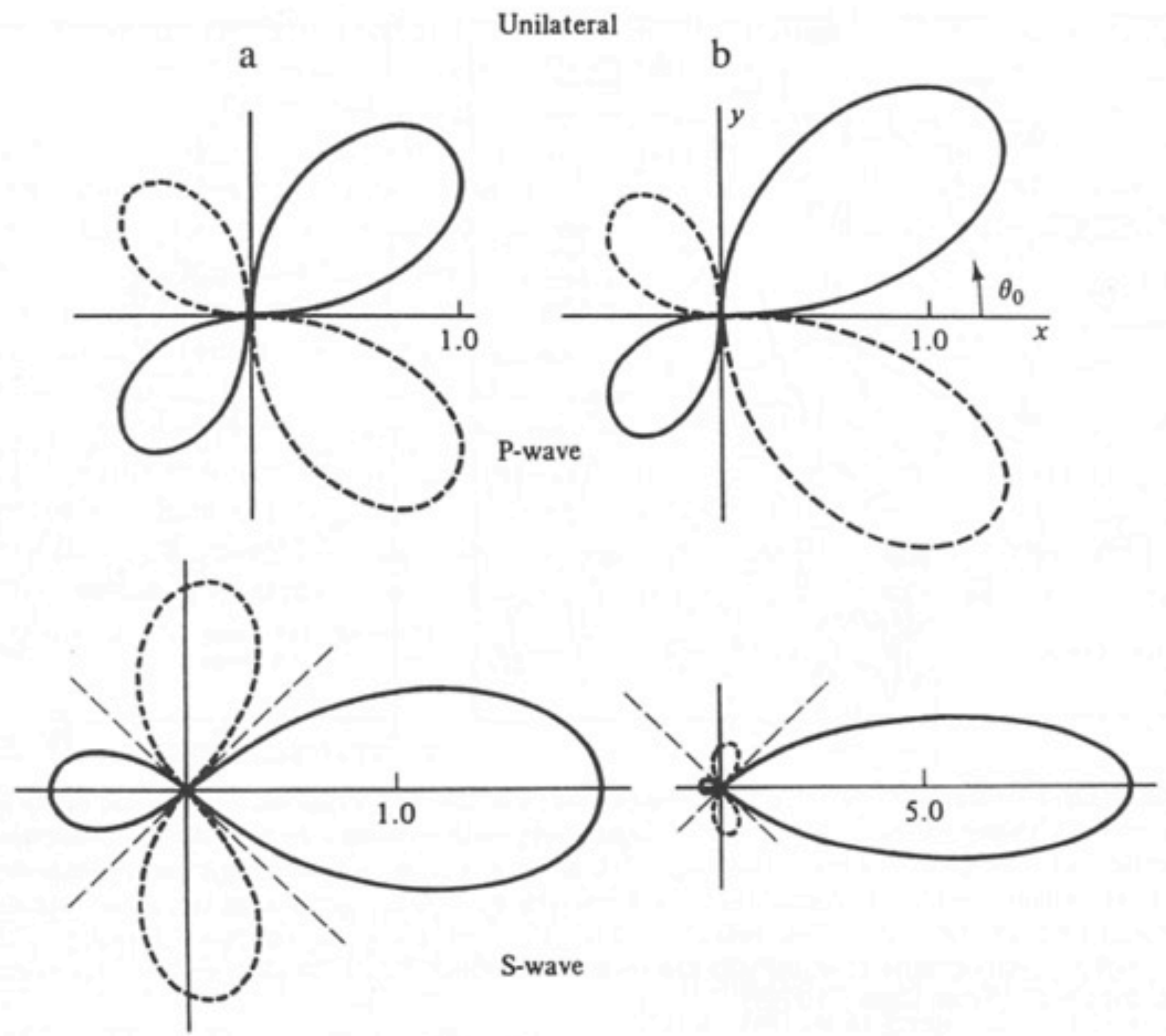

FIGURE 9.10 The variability of *P*- and *SH*-wave amplitude for a propagating fault (from left to right). For the column on the left $v_r/v_s = 0.5$, while for the column on the right $v_r/v_s = 0.9$. Note that the effects are amplified as rupture velocity approaches the propagation velocity. (From Kasahara, 1981.)

Ground motion scenarios

The two views in this movie show the cumulative velocities for a San Andreas earthquake TeraShake simulation, rupturing south to north and north to south. The crosshairs pinpoint the peak velocity magnitude as the simulation progresses.

www.scec.org

Ground motion scenarios

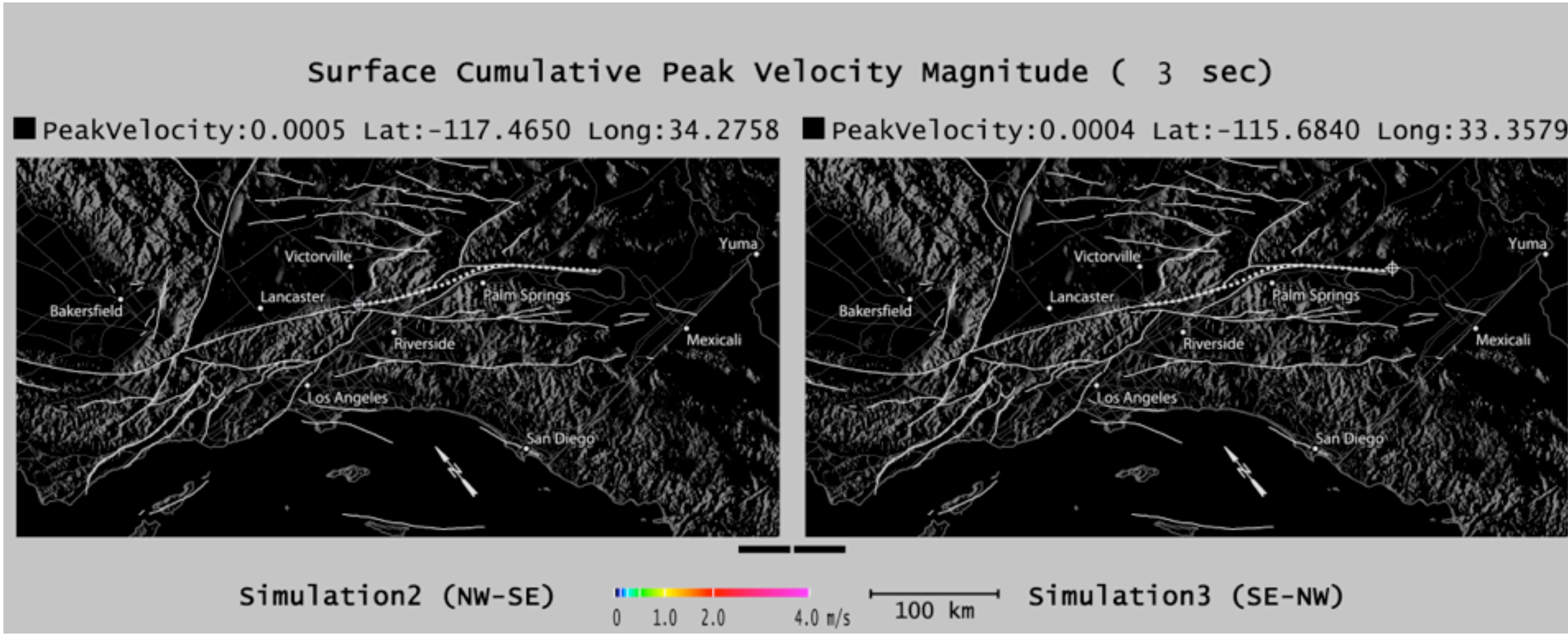

The two views in this movie show the cumulative velocities for a San Andreas earthquake TeraShake simulation, rupturing south to north and north to south. The crosshairs pinpoint the peak velocity magnitude as the simulation progresses.

www.scec.org

Source spectrum

The displacement pulse, corrected for the geometrical spreading and the radiation pattern can be written as:

$$u(t) = M_0\left(B(t;\tau) * B(t;T_R)\right)$$

and in the frequency domain:

$$U(\omega) = M_0 F(\omega) = M_0 \left|\frac{\sin\left(\frac{\omega\tau}{2}\right)}{\left(\frac{\omega\tau}{2}\right)}\right| \left|\frac{\sin\left(\frac{\omega L}{v_r 2}\right)}{\left(\frac{\omega L}{v_r 2}\right)}\right| \approx \begin{cases} M_0 & \omega < \frac{2}{T_r} \\ \frac{2M_0}{\omega T_R} & \frac{2}{T_r} < \omega < \frac{2}{\tau} \\ \frac{4M_0}{\omega^2 \tau T_R} & \omega > \frac{2}{\tau} \end{cases}$$

Source spectrum

$$U(\omega) \approx \begin{cases} M_0 & \omega < \dfrac{2}{T_r} \\ \dfrac{2M_0}{\omega T_R} & \dfrac{2}{T_r} < \omega < \dfrac{2}{\tau} \\ \dfrac{4M_0}{\omega^2 \tau T_R} & \omega > \dfrac{2}{\tau} \end{cases}$$

Figure 4.6-4: Approximation of the (sin *x*)/*x* function, and derivation of corner frequencies.

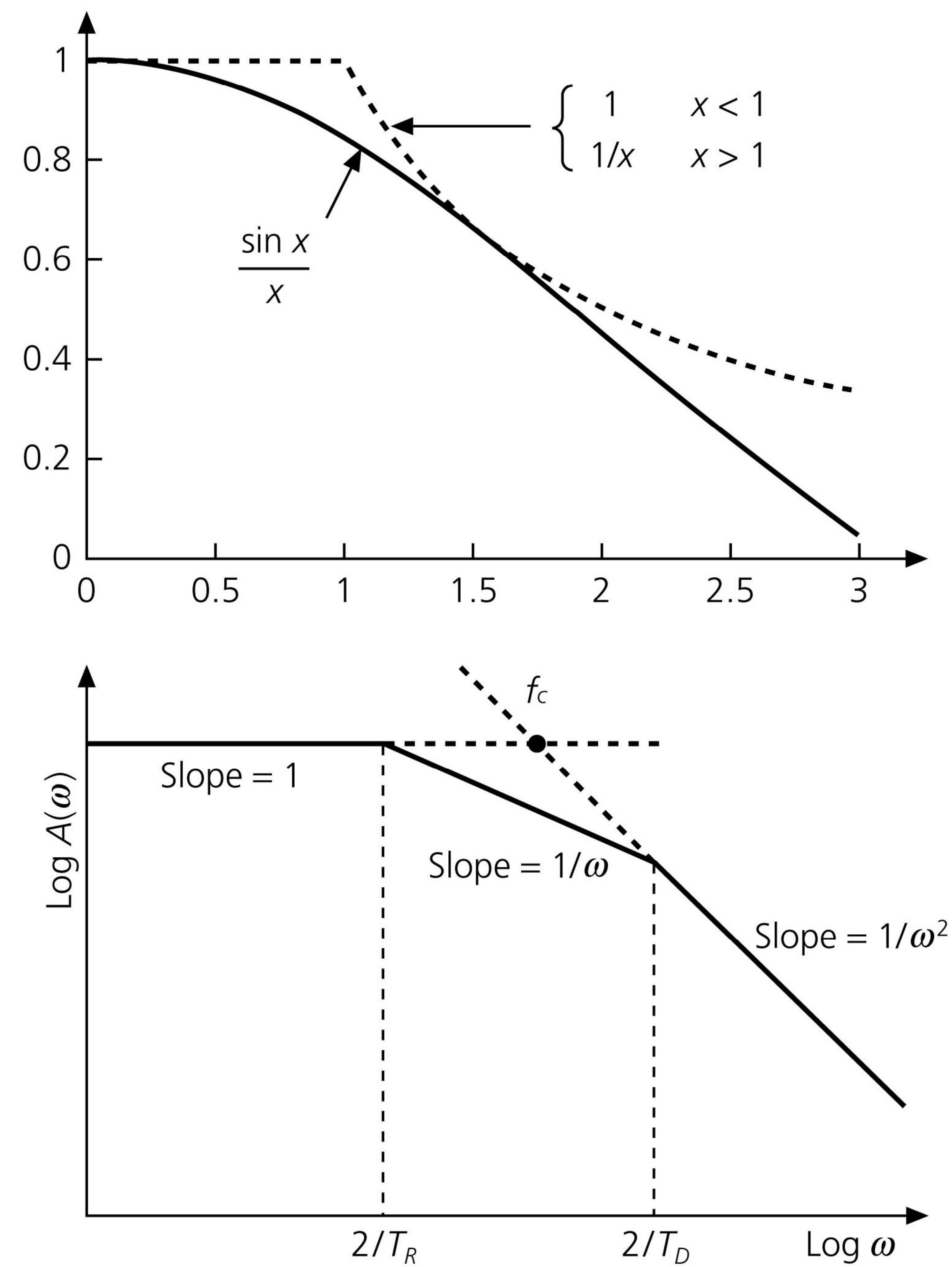

Source spectrum

$$U(\omega) \approx \begin{cases} M_0 & \omega < \dfrac{2}{T_r} \\[2ex] \dfrac{2M_0}{\omega T_R} & \dfrac{2}{T_r} < \omega < \dfrac{2}{\tau} \\[2ex] \dfrac{4M_0}{\omega^2 \tau T_R} & \omega > \dfrac{2}{\tau} \end{cases}$$

Figure 4.6-4: Approximation of the (sin *x*)/*x* function, and derivation of corner frequencies.

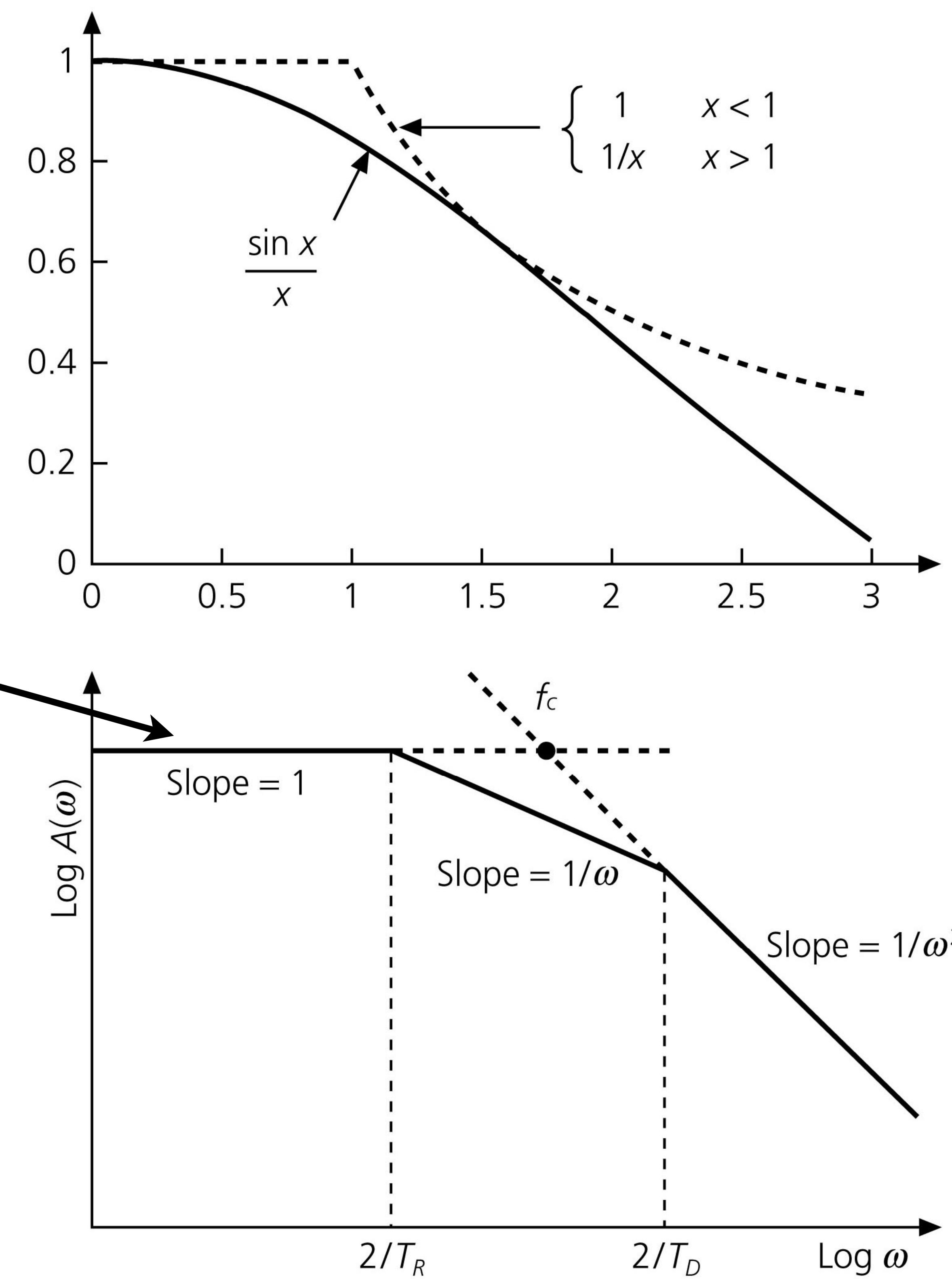

Source spectrum

$$U(\omega) \approx \begin{cases} M_0 & \omega < \dfrac{2}{T_r} \\ \dfrac{2M_0}{\omega T_R} & \dfrac{2}{T_r} < \omega < \dfrac{2}{\tau} \\ \dfrac{4M_0}{\omega^2 \tau T_R} & \omega > \dfrac{2}{\tau} \end{cases}$$

Figure 4.6-4: Approximation of the (sin *x*)/*x* function, and derivation of corner frequencies.

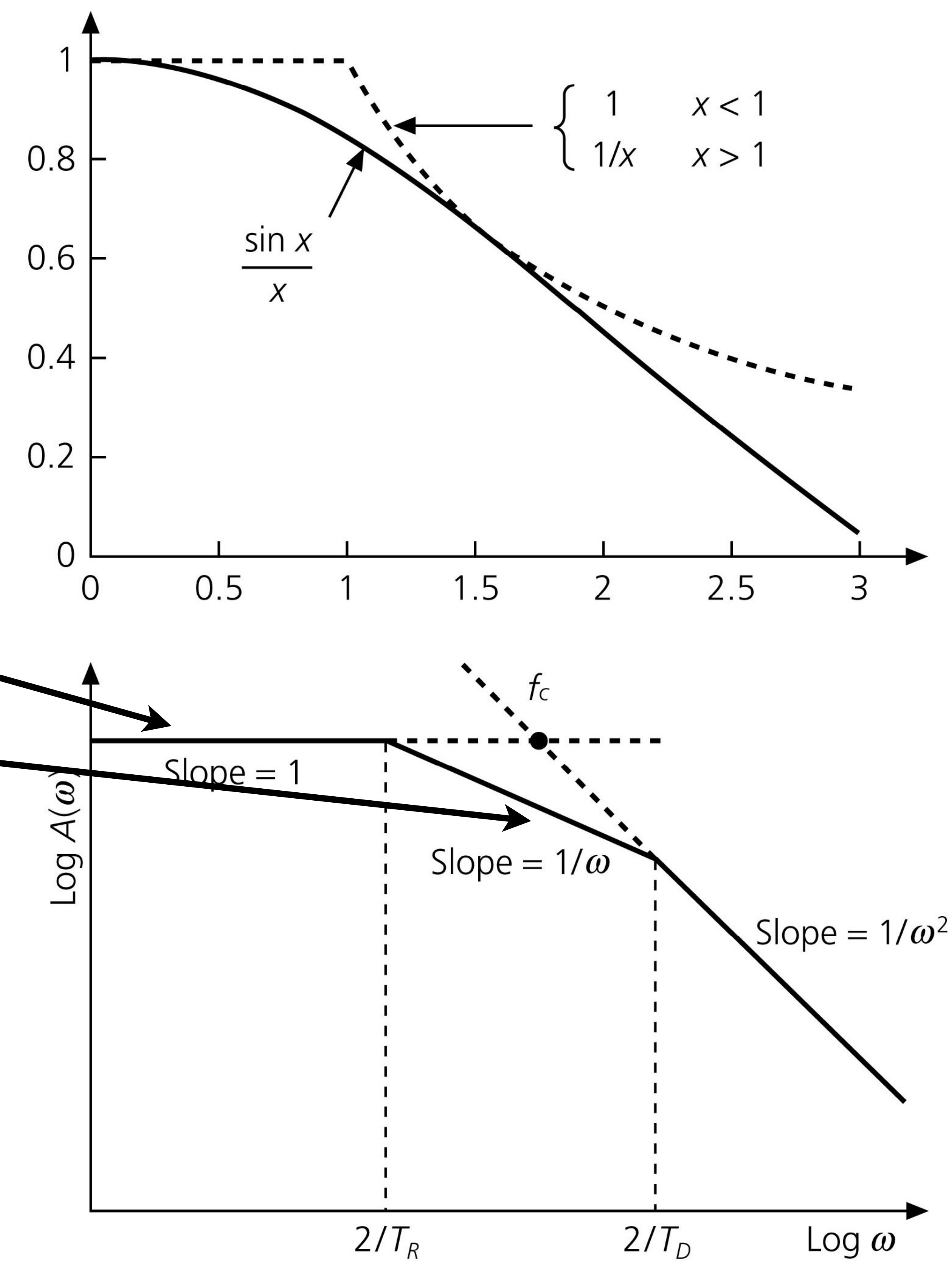

Source spectrum

$$U(\omega) \approx \begin{cases} M_0 & \omega < \dfrac{2}{T_r} \\ \dfrac{2M_0}{\omega T_R} & \dfrac{2}{T_r} < \omega < \dfrac{2}{\tau} \\ \dfrac{4M_0}{\omega^2 \tau T_R} & \omega > \dfrac{2}{\tau} \end{cases}$$

Figure 4.6-4: Approximation of the (sin *x*)/*x* function, and derivation of corner frequencies.

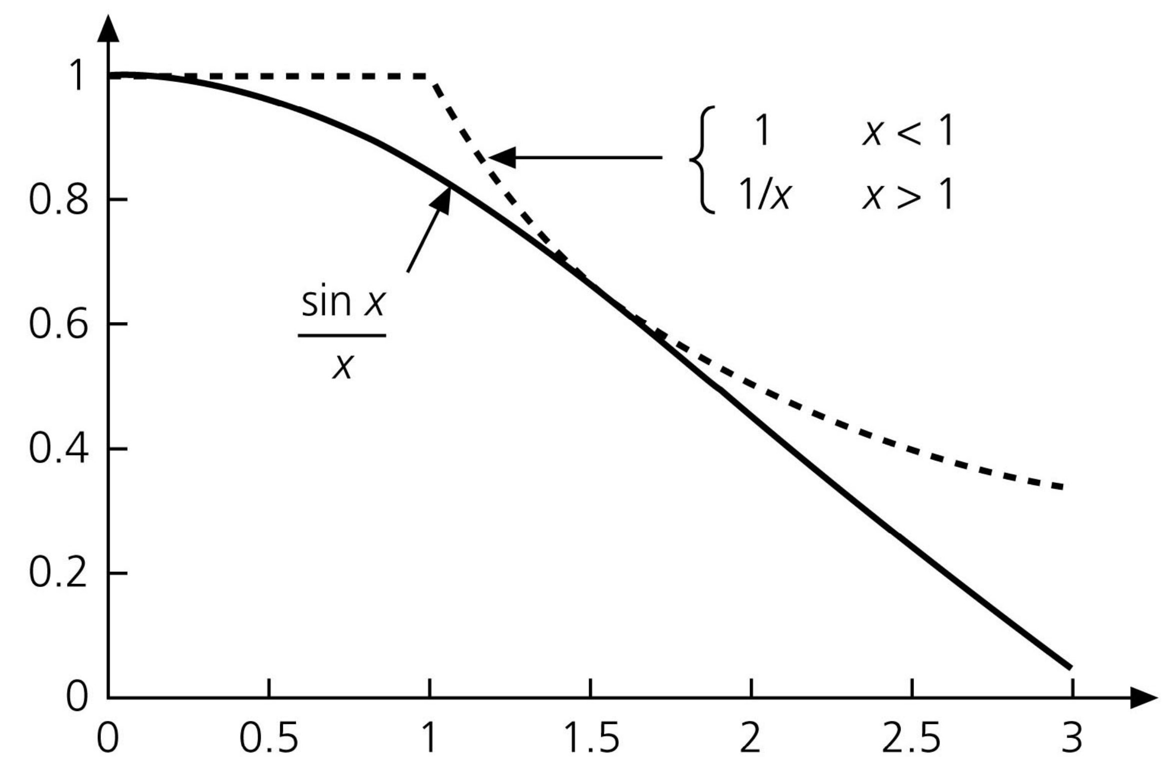

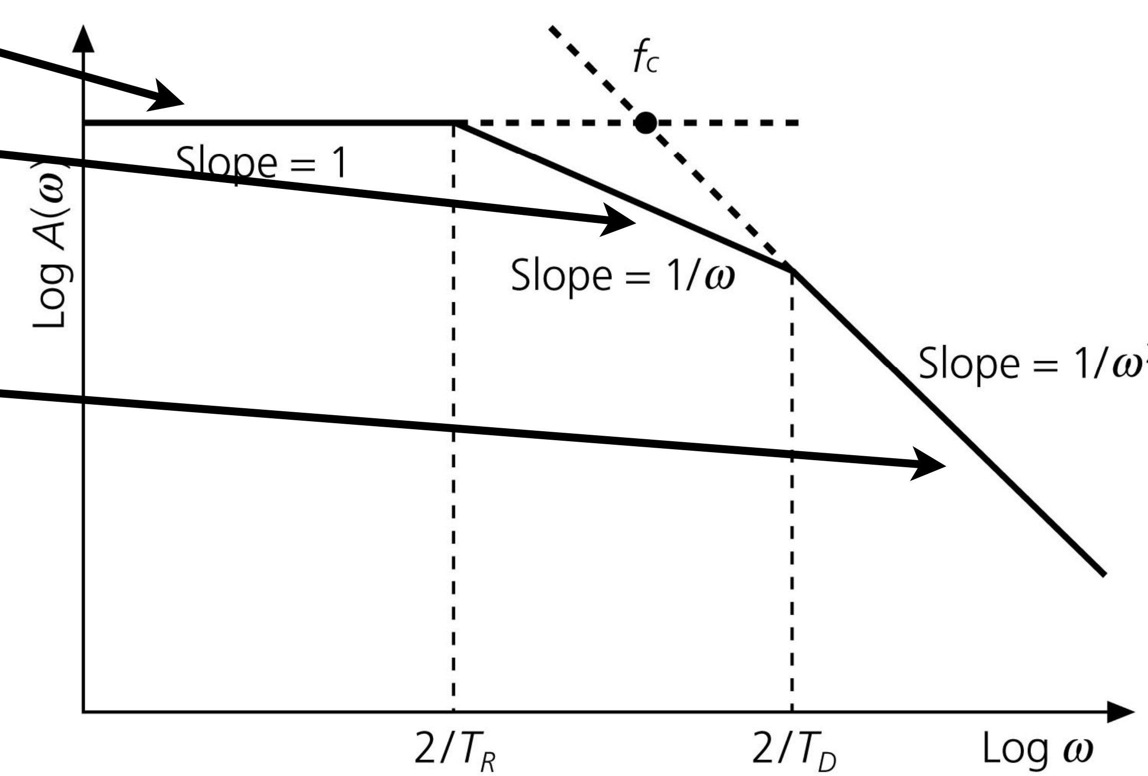

Magnitude saturation

There is no a-priory scale limitation or classification of magnitudes as for macroseismic intensities. In fact, nature limits the maximum size of tectonic earthquakes which is controlled by the maximum size of a brittle fracture in the lithosphere. A simple seismic shear source with linear rupture propagation has a typical "source spectrum”.

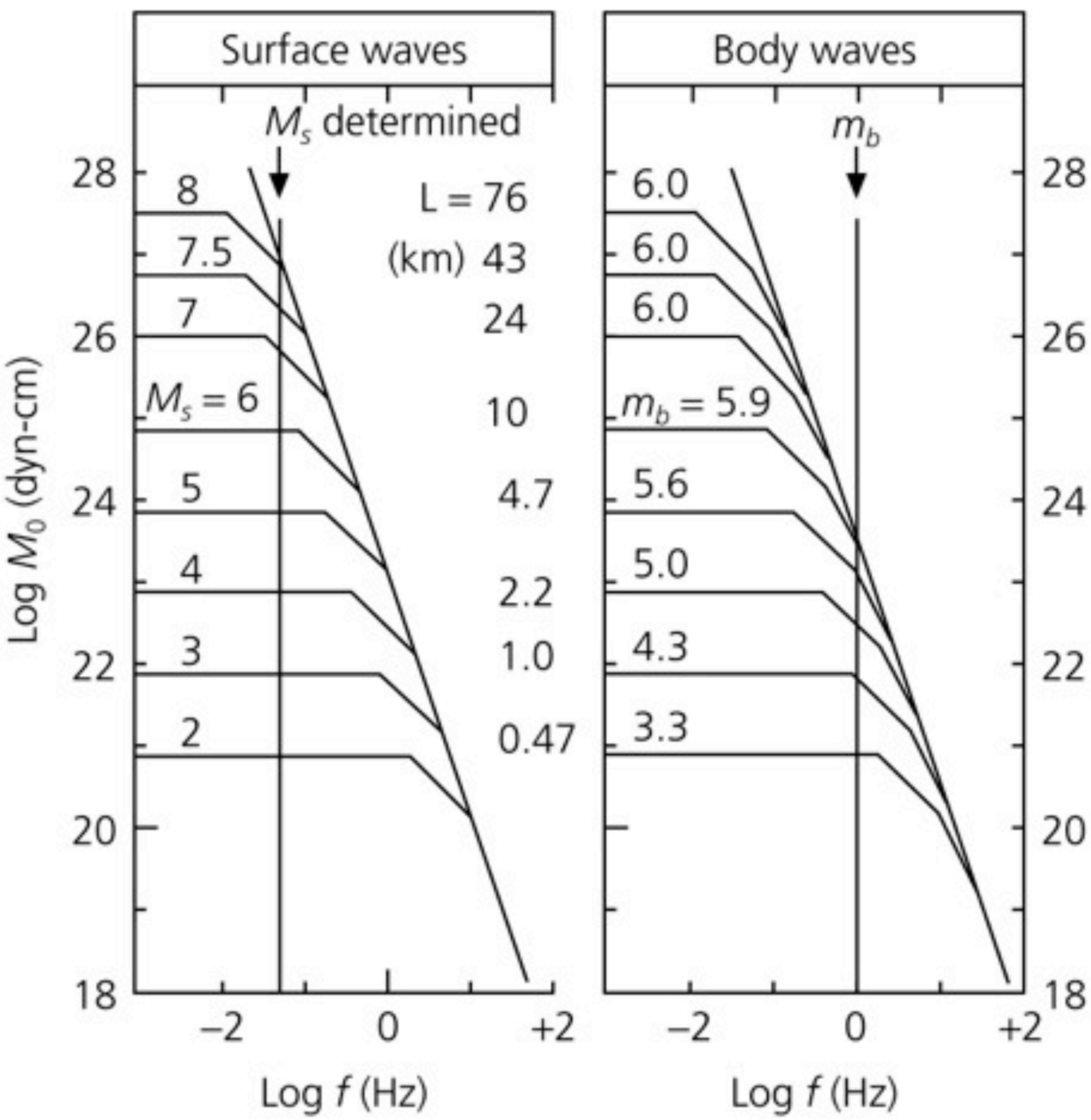

Ms is not linearly scaled with Mo for Ms > 6 due to the beginning of the so-called saturation effect for spectral amplitudes with frequencies f > fc. This saturation occurs already much earlier for mb which are determined from amplitude measurements around 1 Hz.

Empirical source spectra

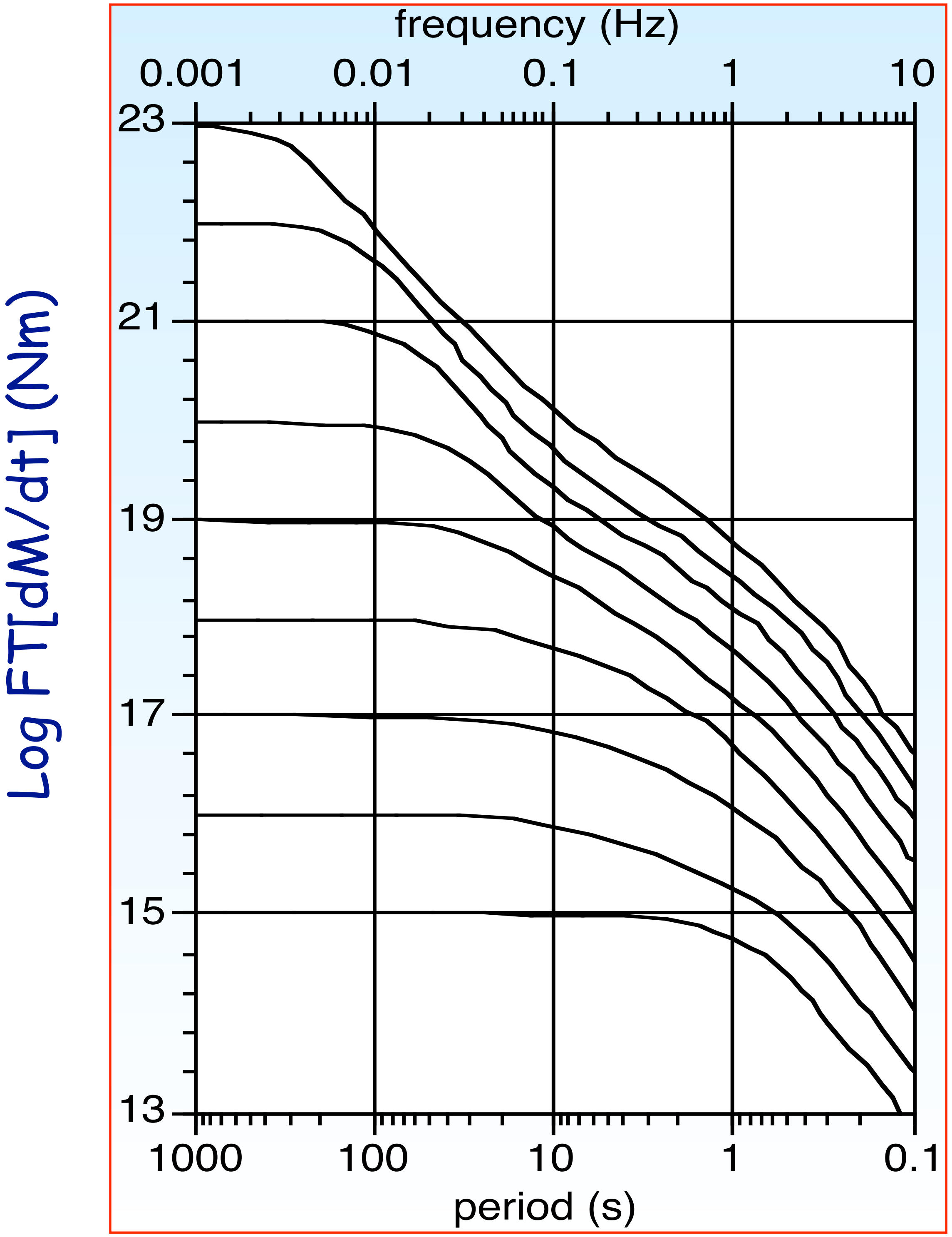

Empirical source spectra

represent a set of average amplitude curves respect to:

Tectonic setting

Source mechanism

Directivity effects

Source models

Method DWN (Pavlov, 2002)

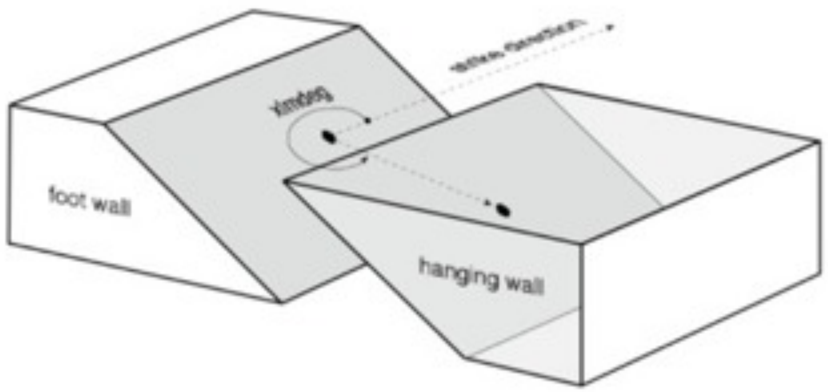

Point source approximation

FPS and radiation pattern

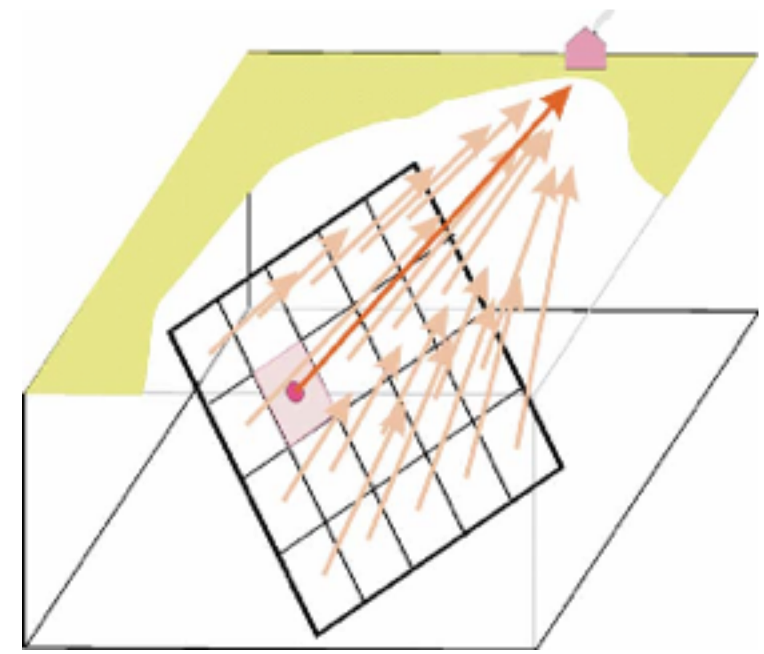

Extendend source kinematic model

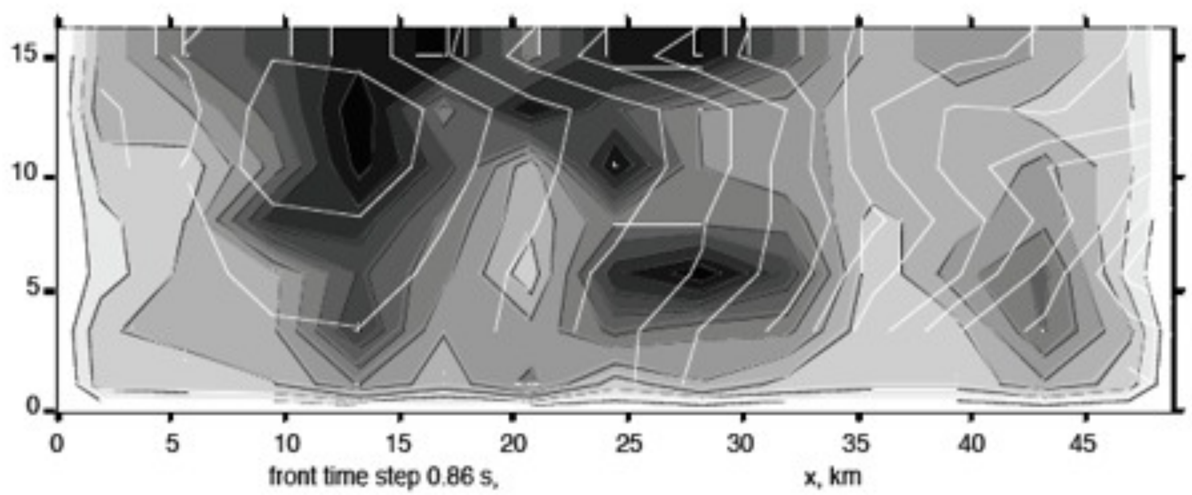

2-dimensional final slip distribution over a source rectangle

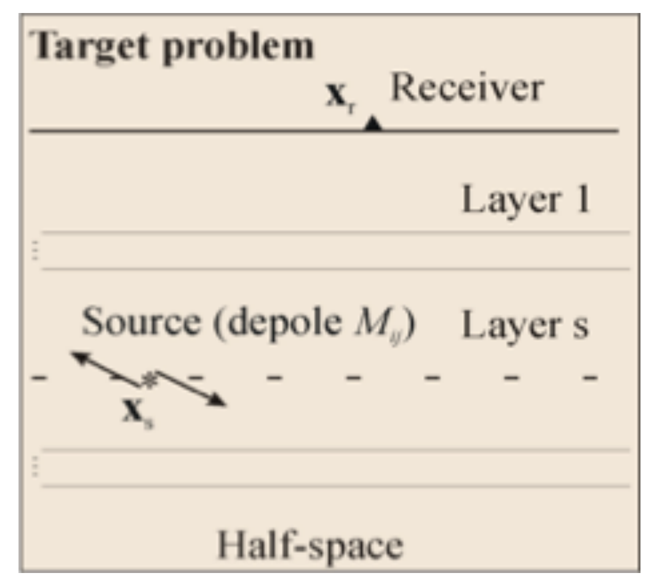

Computing time: about 1 hour for a 10Hz signal 40 s long (using 200 sub-sources)

10 Hz - Source definition

Source kinematic model

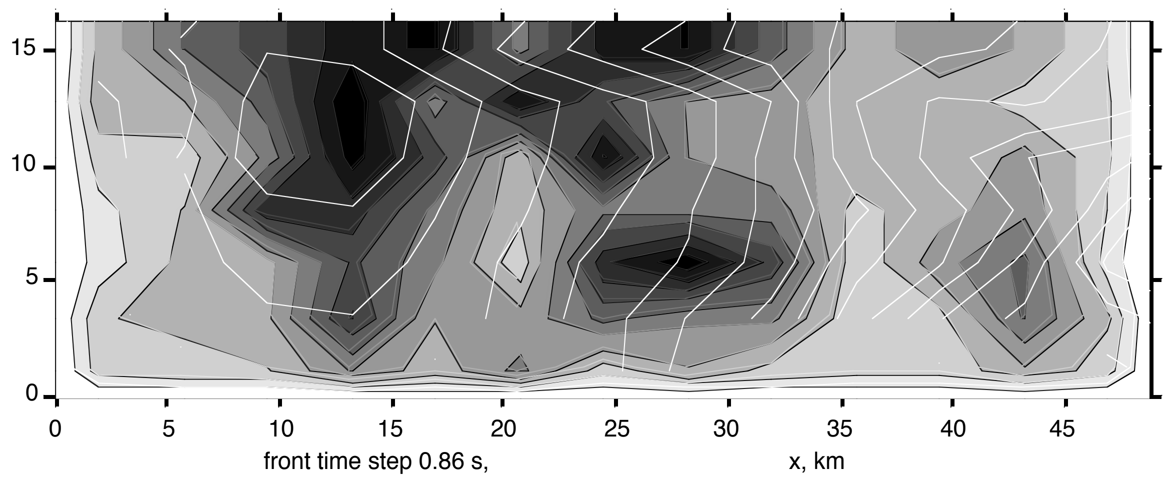

2-dimensional final slip distribution over a source rectangle, shown as a density plot (Mw=7.0).

Rupture front evolution was simulated kinematically from random rupture velocity field.

(Gusev, 2010)

Far-field source time histories and their spectra.

“Displacement” far-field functions (arbitrary scale) for the simulated case of mostly unilateral rupture propagation

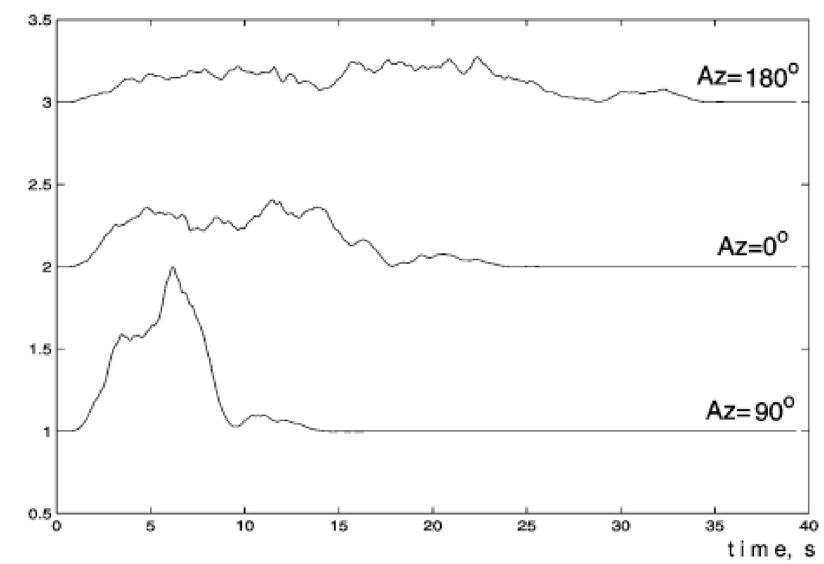

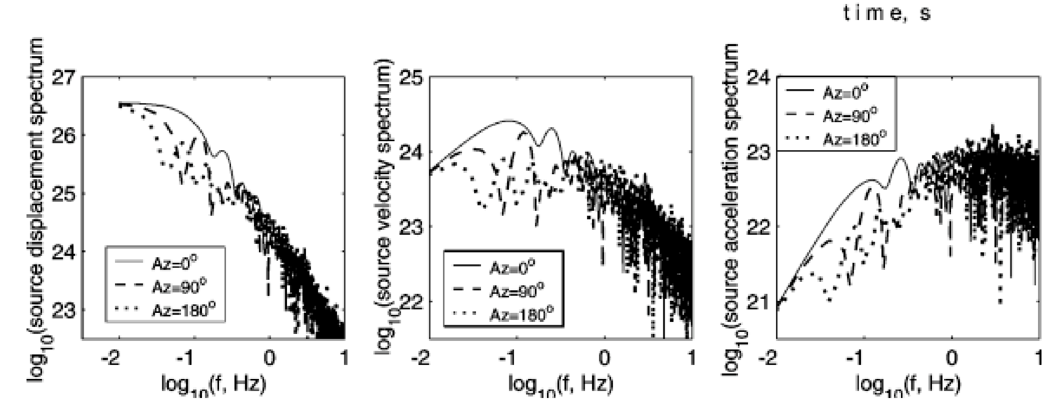

10 Hz - Example 1

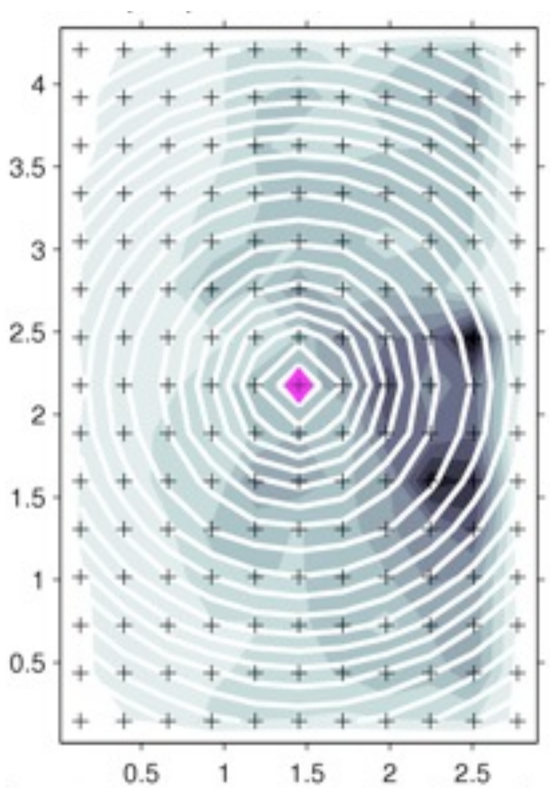

One examples (realization 123) of the 2D final slip function, shown as density over the fault plane. The purple square is the nucleation point. White contours are successive rupture front positions, simulated kinematically from random rupture velocity field. Crosses are positions of point subsources.

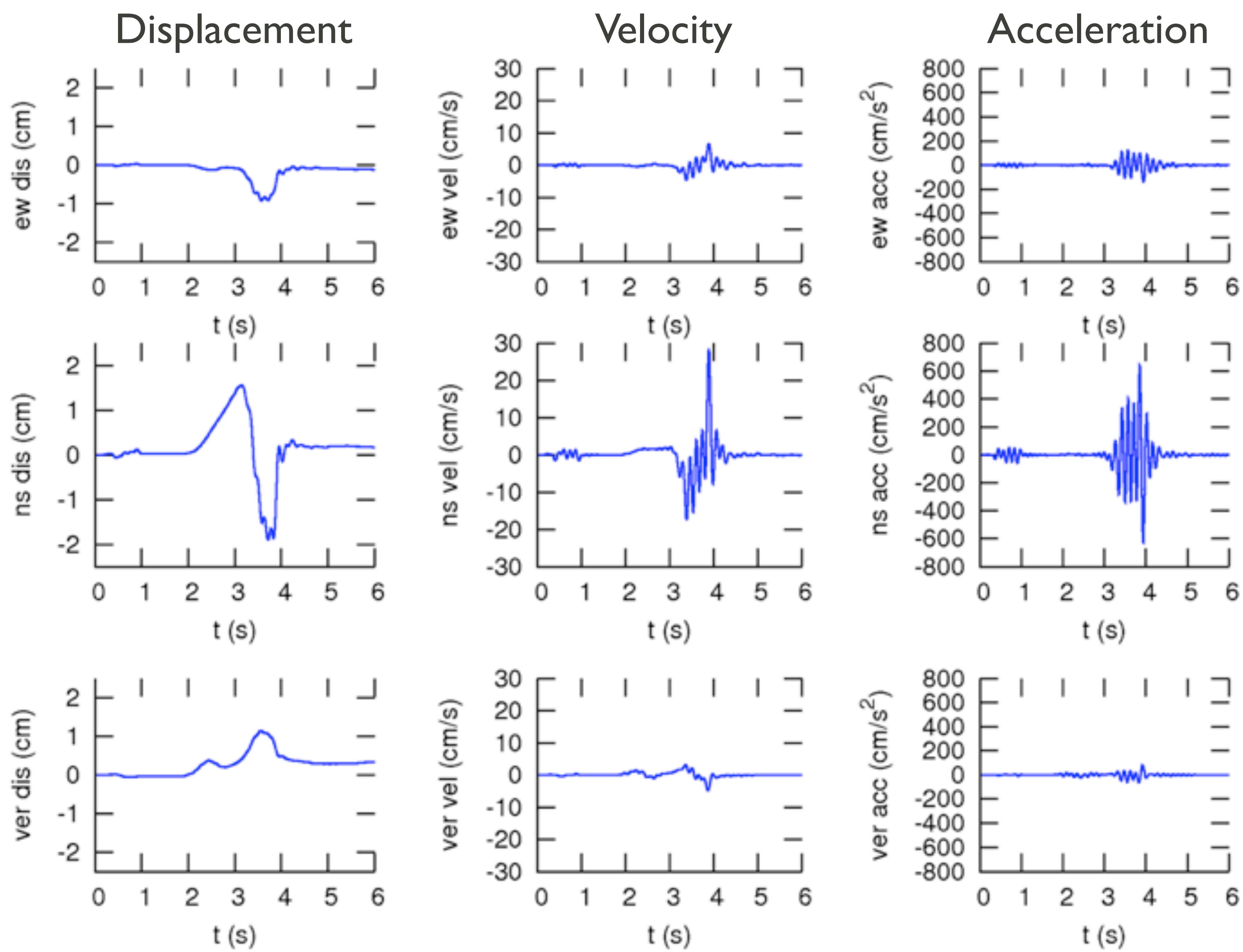

10 Hz - Example 2

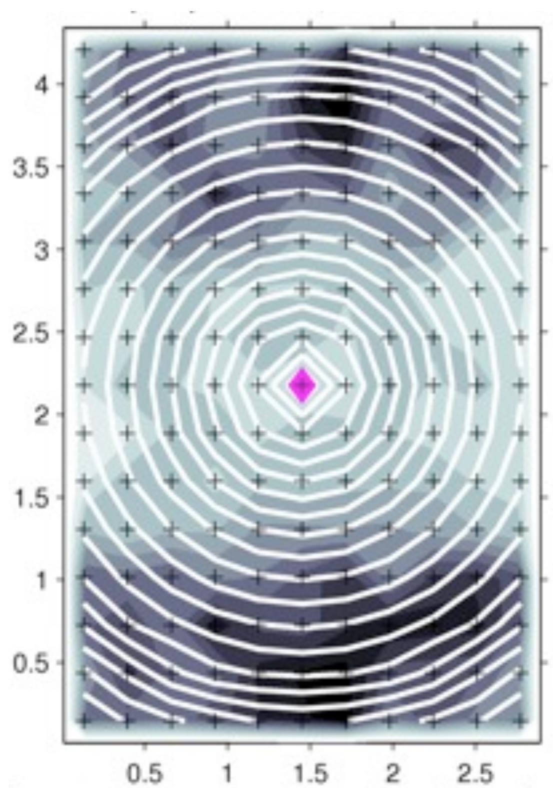

One examples (realization 155) of the 2D final slip function, shown as density over the fault plane. The purple square is the nucleation point. White contours are successive rupture front positions, simulated kinematically from random rupture velocity field. Crosses are positions of point subsources.

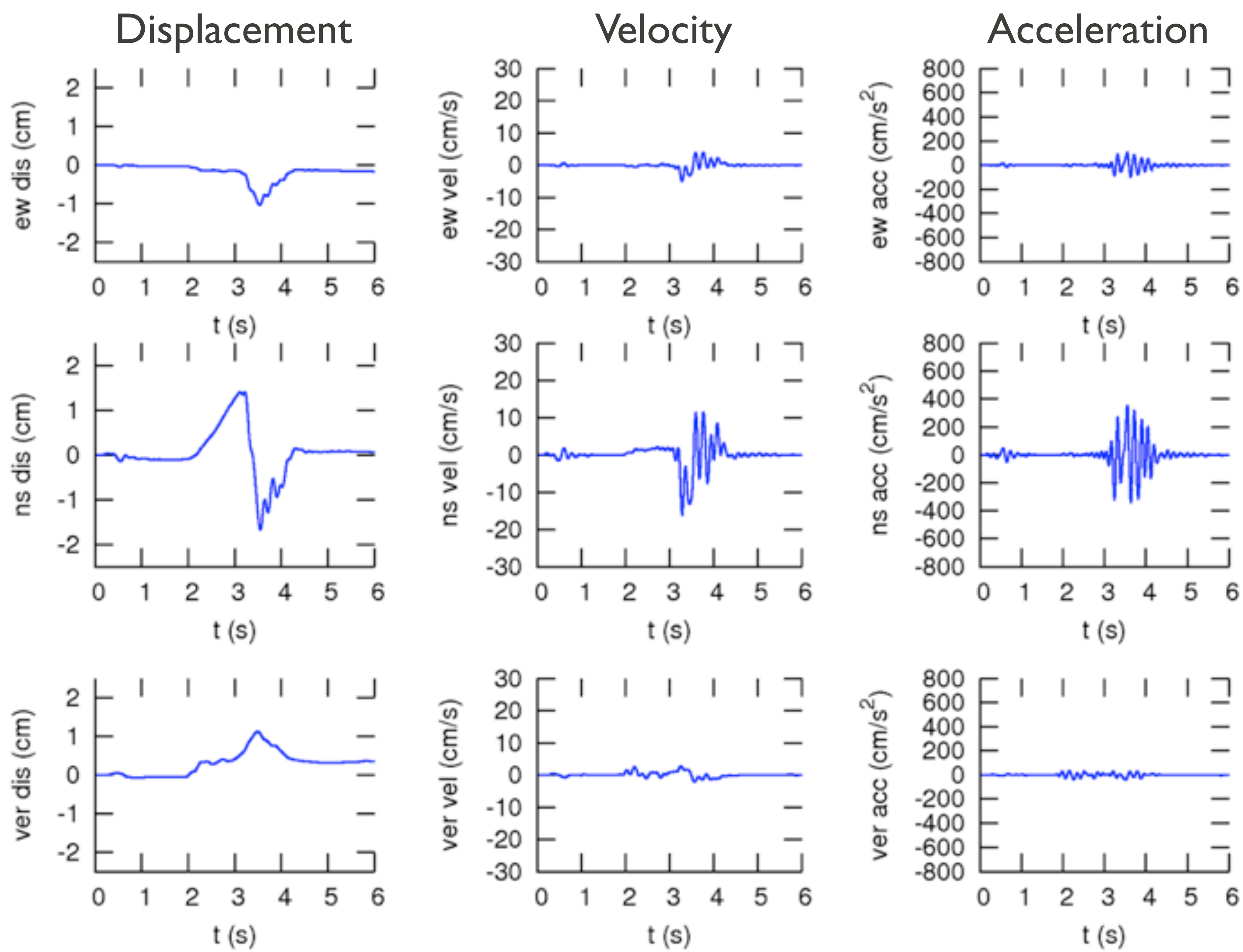

10 Hz - Dispersion of results

	E-W		N-S		Z	
	mean	σ	mean	σ	mean	σ
PGD (cm)	0.9	0.1	1.7	0.2	1.0	0.1
PGV (cm/s)	5.7	1.6	20	6	3.2	0.8
PGA (cm/s^2)	142	49	501	163	63	20

Average and standard deviation of the peak values for 200 different random realizations of the same source model.

Average and standard deviation of the acceleration response spectra (damping 5%) for 200 different random realizations of the same source model and examples of response spectra for two different realizations.

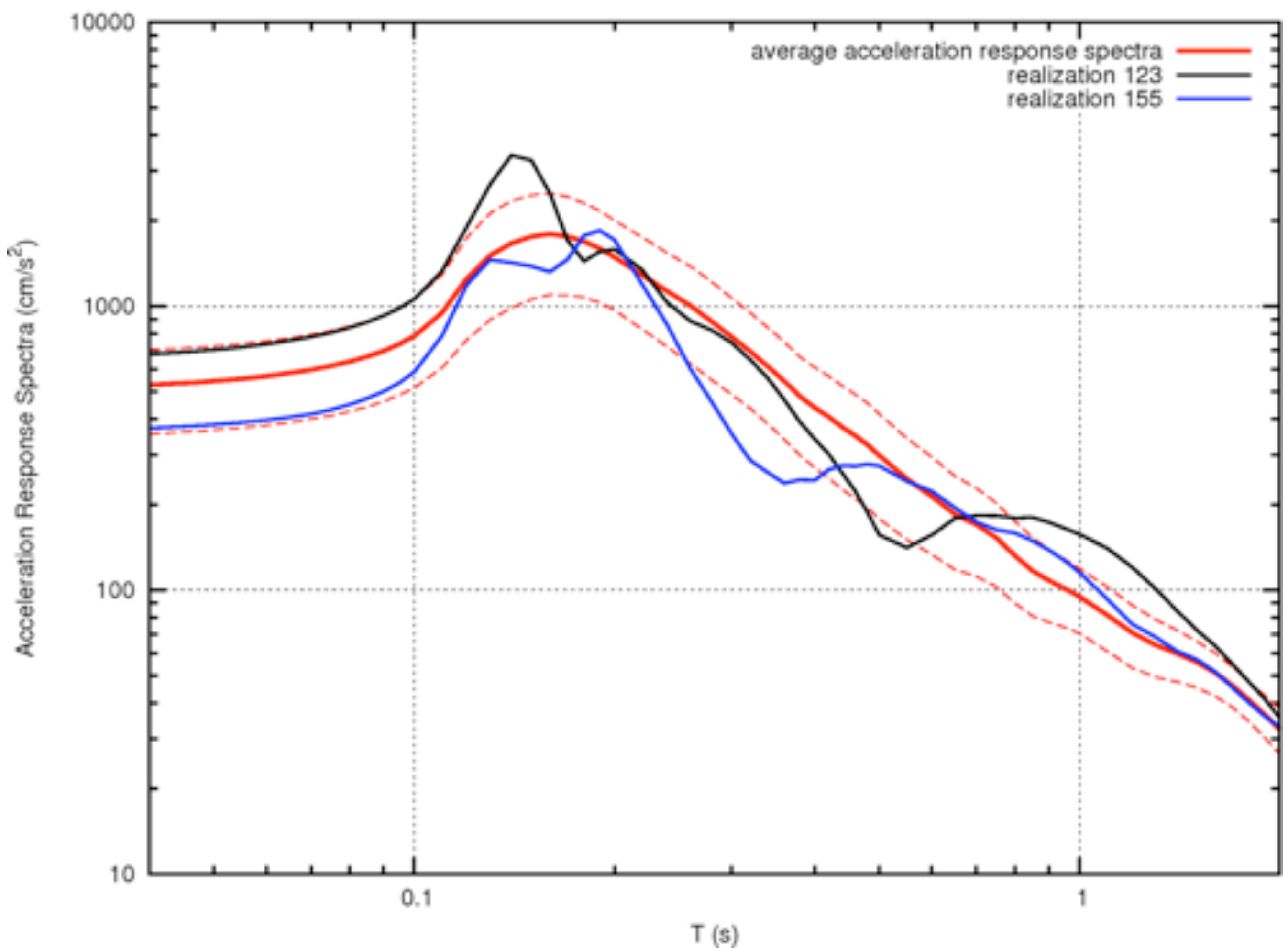

Road map

- Some remarks on sound SHA
  - Source & site effects
  - Integrated methodology
- A bird's eye on Scenario Based SHA
  - Scenarios at regional scale
  - Application to critical facility (real bridges...)

Road map

- Some remarks on sound SHA
  - Source & site effects
  - Integrated methodology
- A bird's eye on Scenario Based SHA
  - Scenarios at regional scale
  - Application to critical facility (real bridges...)
  - Tsunami physics

Tsunami
physics
research

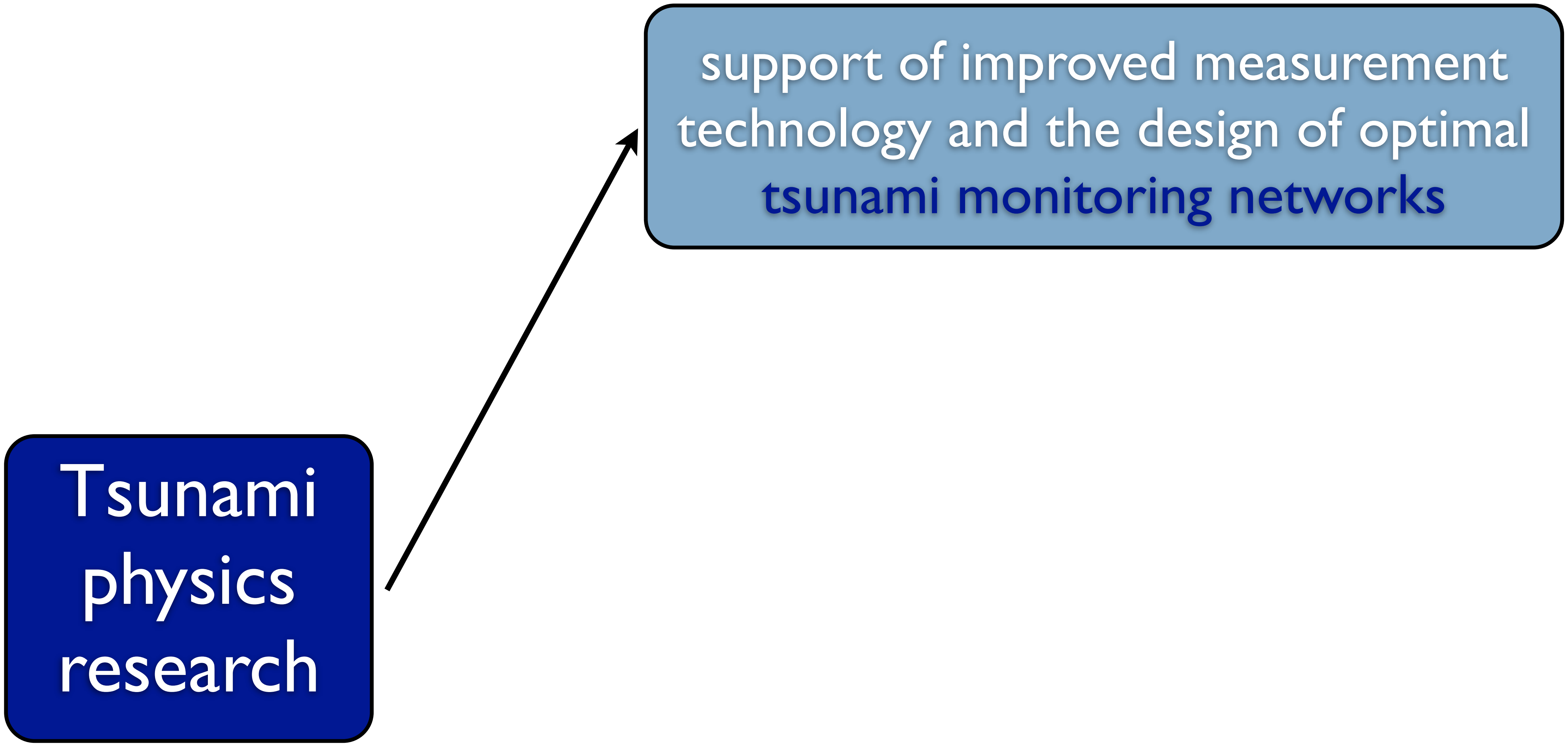
support of improved measurement technology and the design of optimal tsunami monitoring networks
Tsunami physics research

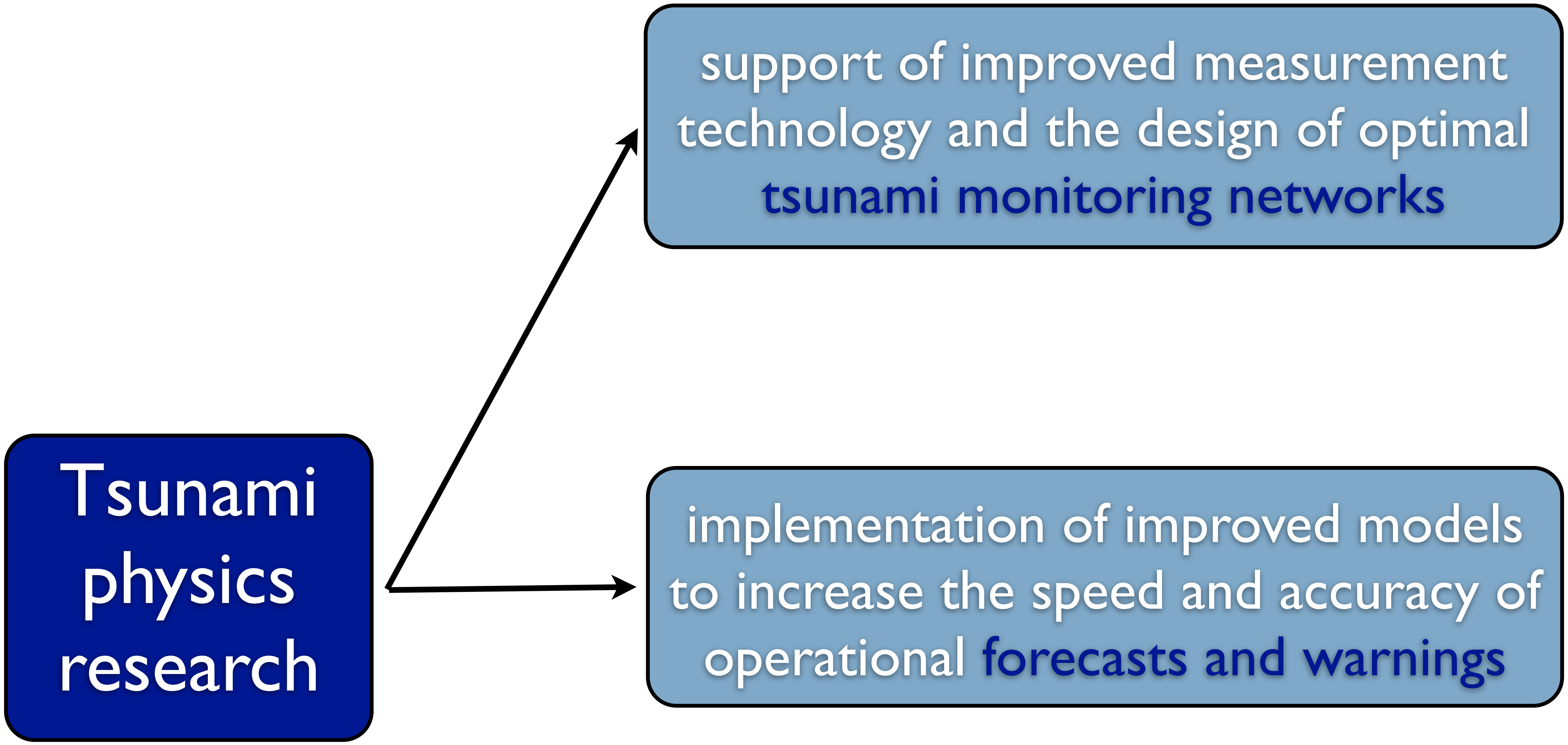
Tsunami physics research
support of improved measurement technology and the design of optimal tsunami monitoring networks
implementation of improved models to increase the speed and accuracy of operational forecasts and warnings

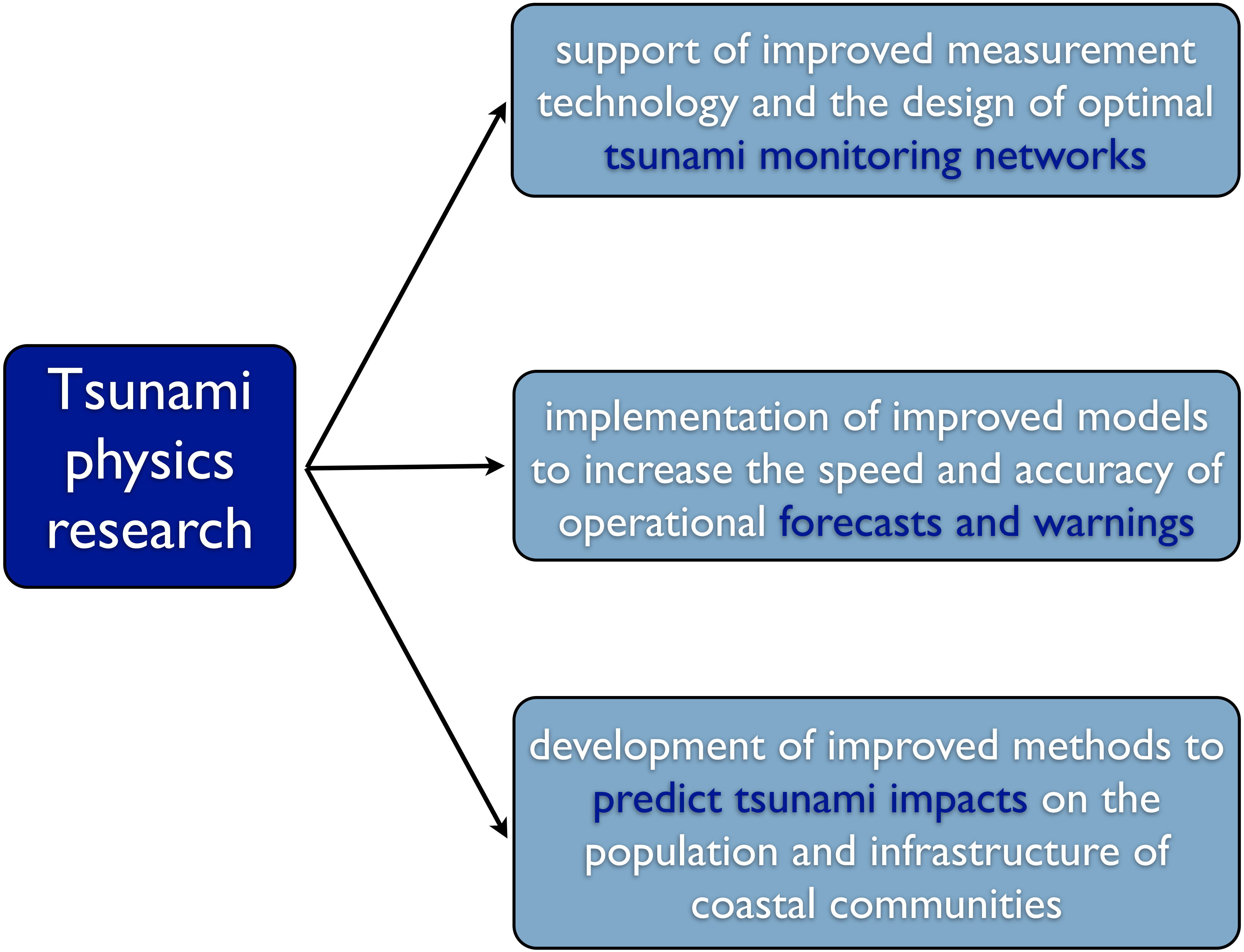
Tsunami physics research
support of improved measurement technology and the design of optimal tsunami monitoring networks
implementation of improved models to increase the speed and accuracy of operational forecasts and warnings
development of improved methods to predict tsunami impacts on the population and infrastructure of coastal communities

Scenario based tsunami hazard assessment

- Assess the potential threat posed by earthquake generated tsunamis on the coastlines.

Scenario based tsunami hazard assessment

- Assess the potential threat posed by earthquake generated tsunamis on the coastlines.

- Compilation a database of potentially tsunamigenic earthquake faults, to be used as input in the definition of scenarios.

Scenario based tsunami hazard assessment

- Assess the potential threat posed by earthquake generated tsunamis on the coastlines.
- Compilation a database of potentially tsunamigenic earthquake faults, to be used as input in the definition of scenarios.
- Each Source Zone includes an active tectonic structure with a Maximum Credible Earthquake and a typical fault.

Scenario based tsunami hazard assessment

- Assess the potential threat posed by earthquake generated tsunamis on the coastlines.
- Compilation a database of potentially tsunamigenic earthquake faults, to be used as input in the definition of scenarios.
- Each Source Zone includes an active tectonic structure with a Maximum Credible Earthquake and a typical fault.
- Provide information of the expected tsunami impact (e.g. height and arrival times) onto the target coastline; it can be progressively updated as knowledge of earthquake source advances.

Tsunami animation - NOAA

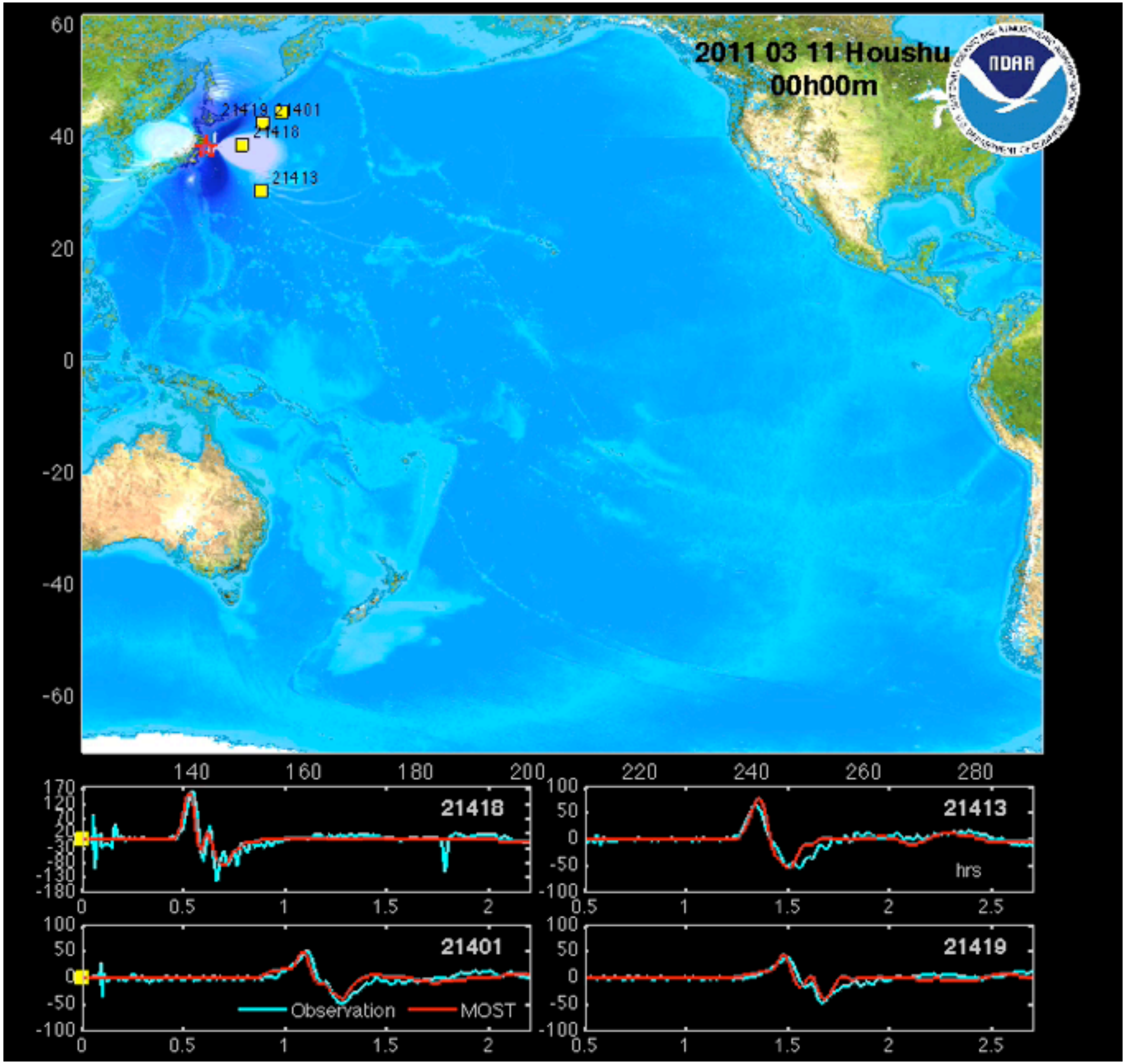

Tsunami travel times - NOAA

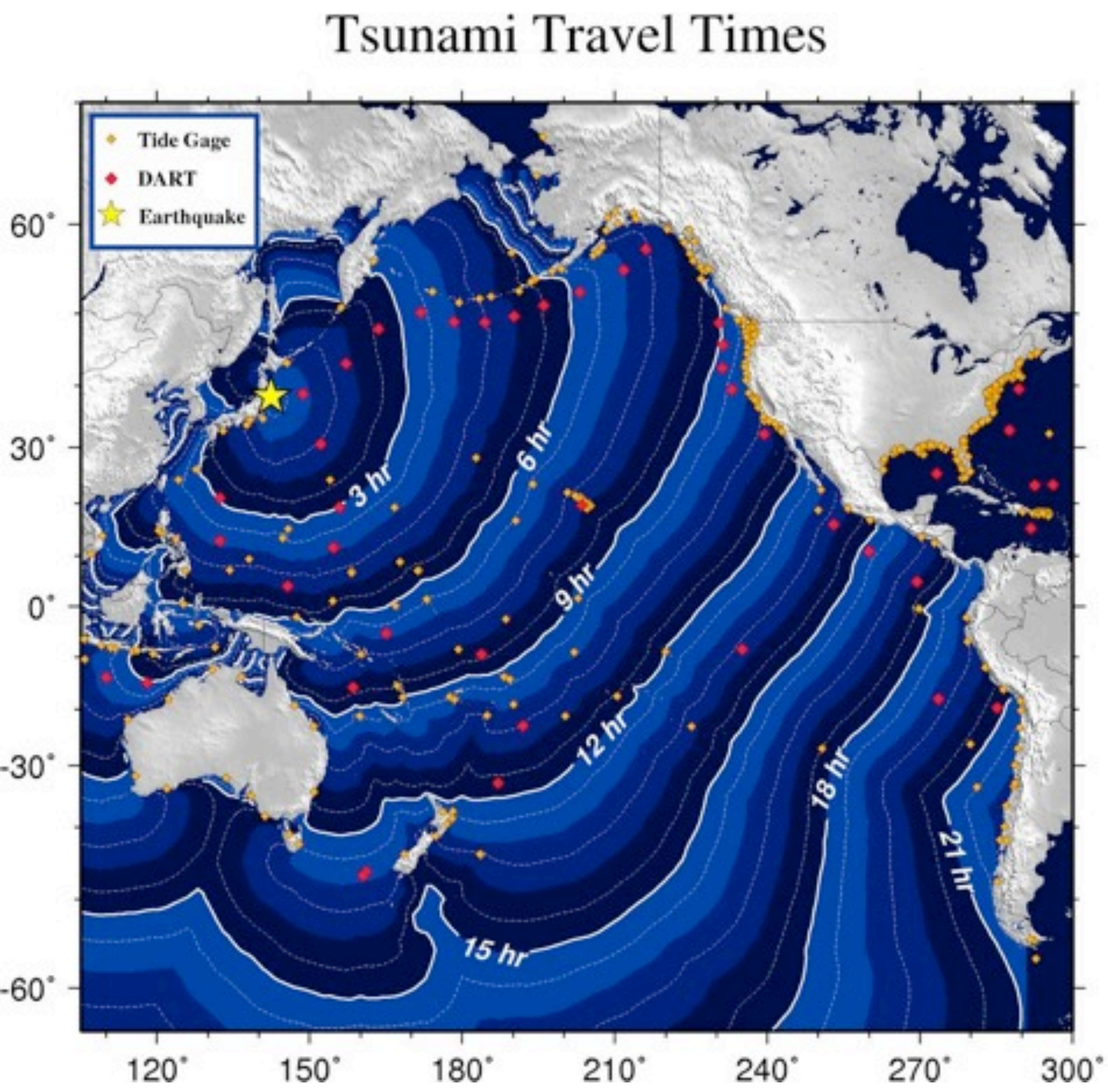

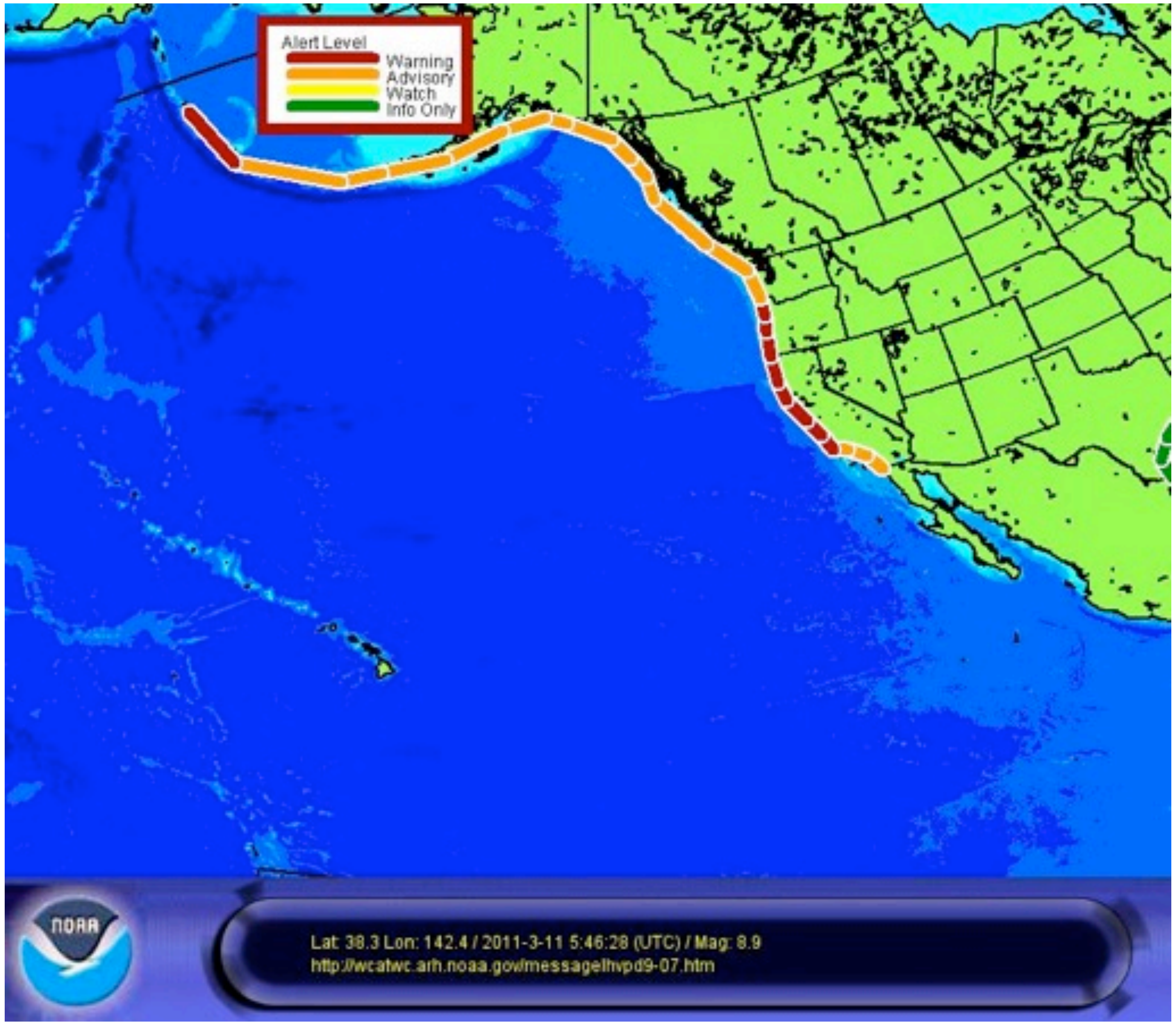

Ocean bottom data

The observation record of the ocean bottom pressure gauge. At around 14:46, the ground motion of the earthquake (M9) reaches the pressure gauge and at TM1 (coast-side), the sea level is gradually rising from that point.

The sea level rose 2 m, and after 11 minutes, the level went drastically up to 3m, which makes 5 m of elevation in total. At TM2: located 30km toward the land, a same elevation of sea level was recorded with 4 minutes delay from TM1.

釜石沖海底ケーブル式地震計システムで観測された海面変動

東京大学地震研究所

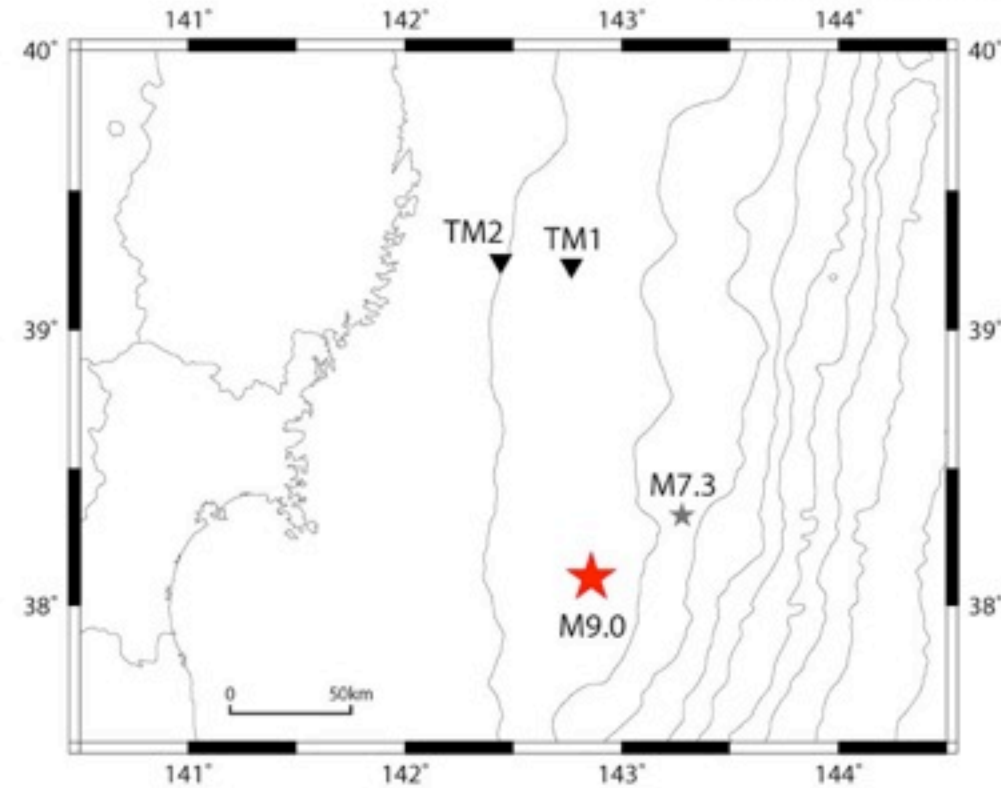

図１　釜石沖ケーブル式海底水圧計の位置

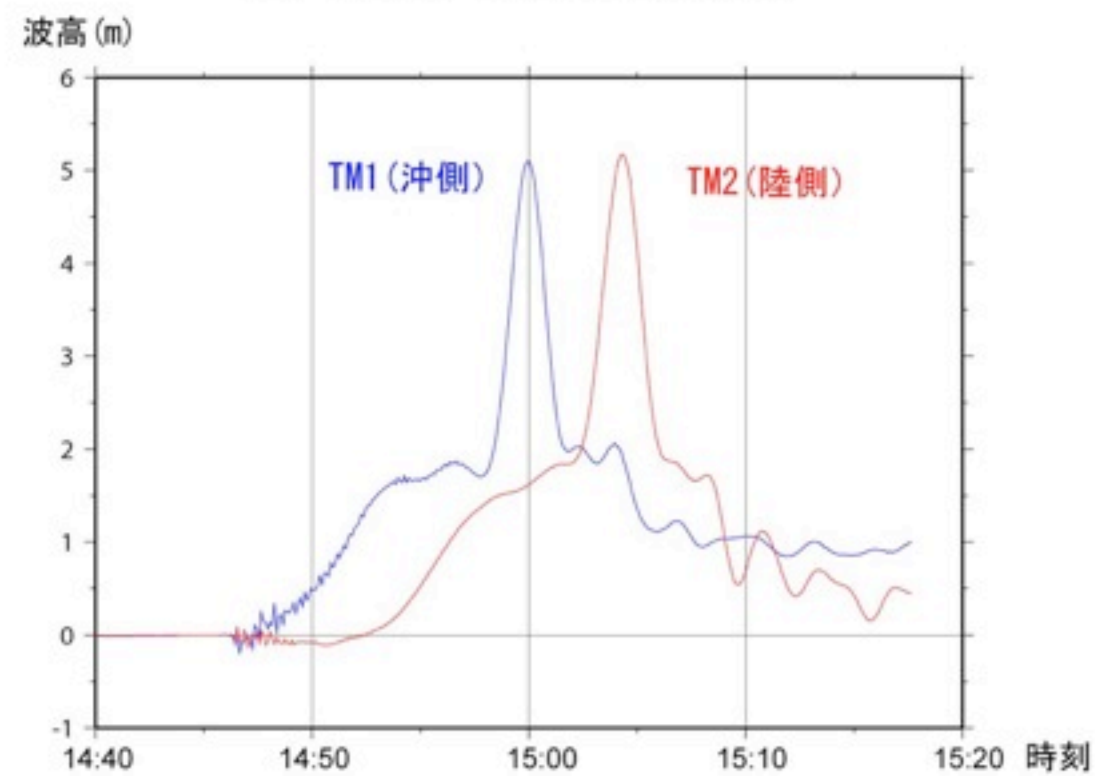

図２　海底水圧計の観測記録。14時46分頃、本震(M9.0)の振動が水圧計に伝わり、TM1(海寄り)では、その時から徐々に海面が上昇している。約２ｍ上昇し、約11分後にはさらに約3m急激に上昇し、合計約5m海面が上昇した。約30km陸寄りに設置されているTM2では、TM1から約4分遅れて同様の海面上昇を記録した。

Tsunami animation: time scales...

http://outreach.eri.u-tokyo.ac.jp/eqvolc/201103_tohoku/eng/

http://supersites.earthobservations.org/honshu.php

http://eqseis.geosc.psu.edu/~cammon/Japan2011EQ/

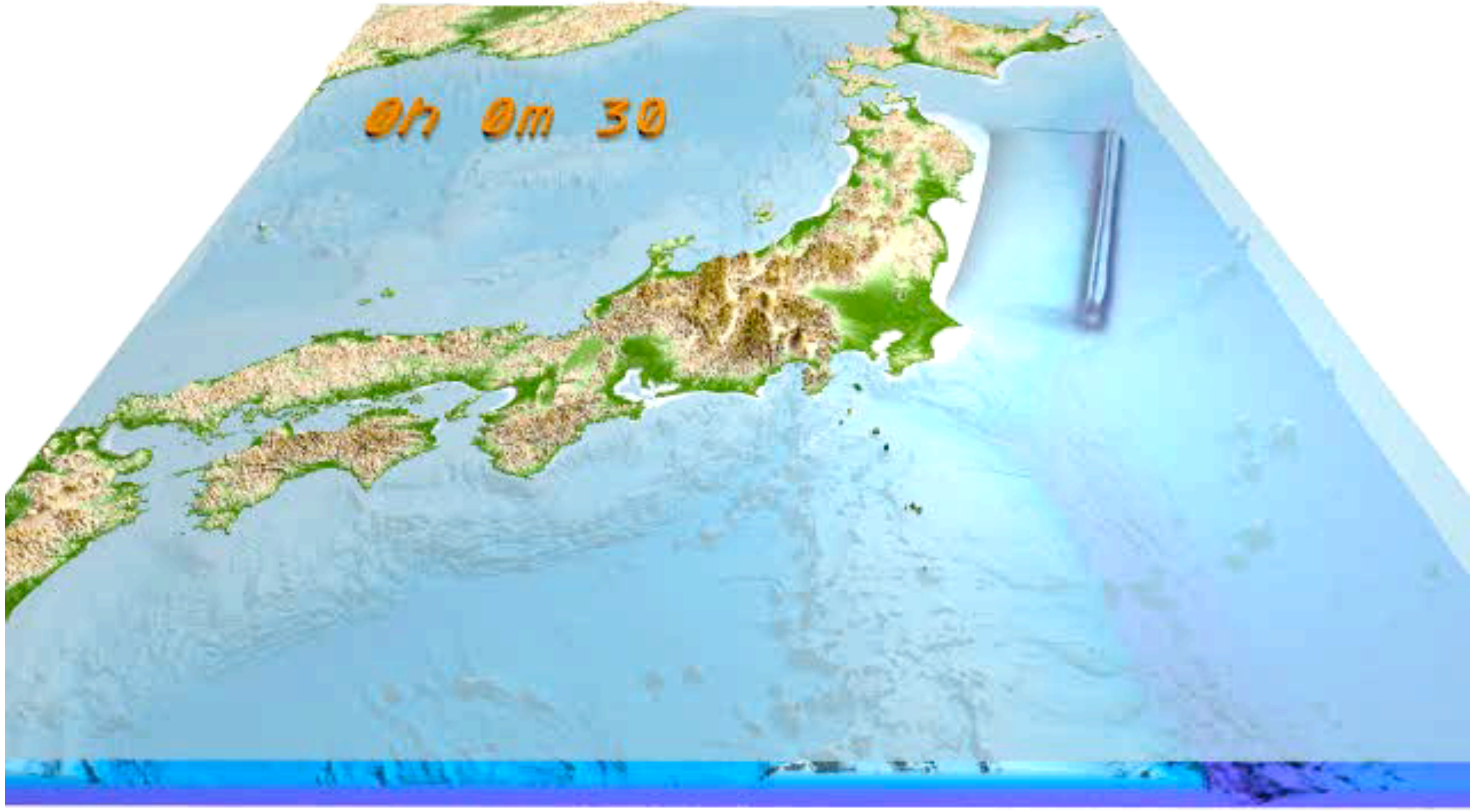

"Earthquake Research Institute, University of Tokyo, Prof. Takashi Furumura and Project Researcher Takuto Maeda"

Tsunami data and simulations: source

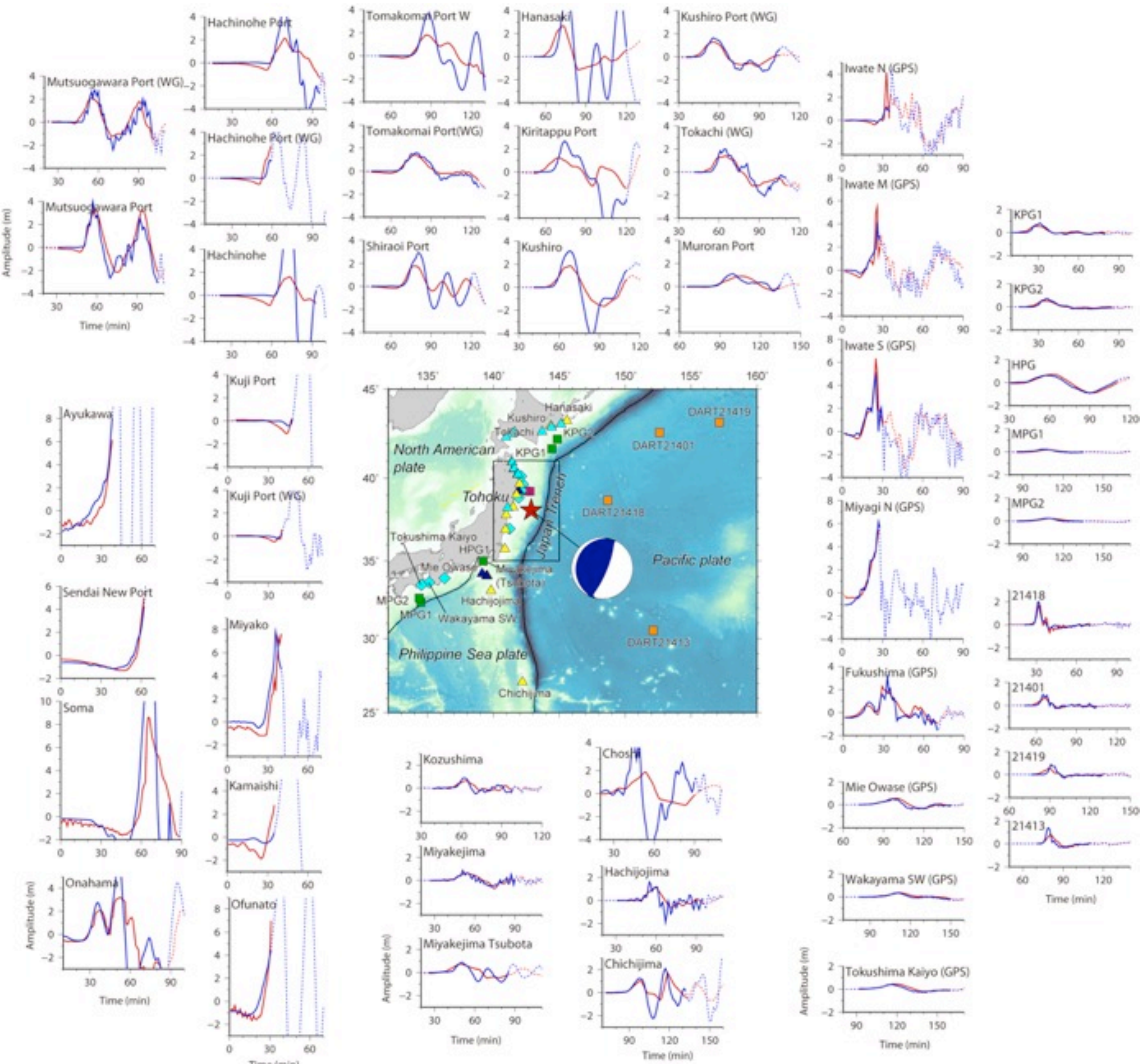

Simulated Tsunami around Japanese coasts

Red and blue lines indicate the observed tsunami waveforms at Japanese tide gauges and ocean bottom tsunami sensors and synthetic ones, respectively. Solid lines show the time windows used for inversion.

by Yushiro Fujii (IISEE, BRI) and Kenji Satake (ERI, Univ. of Tokyo)
http://iisee.kenken.go.jp/staff/fujii/OffTohokuPacific2011/tsunami_inv.html

Tsunami data and simulations: source

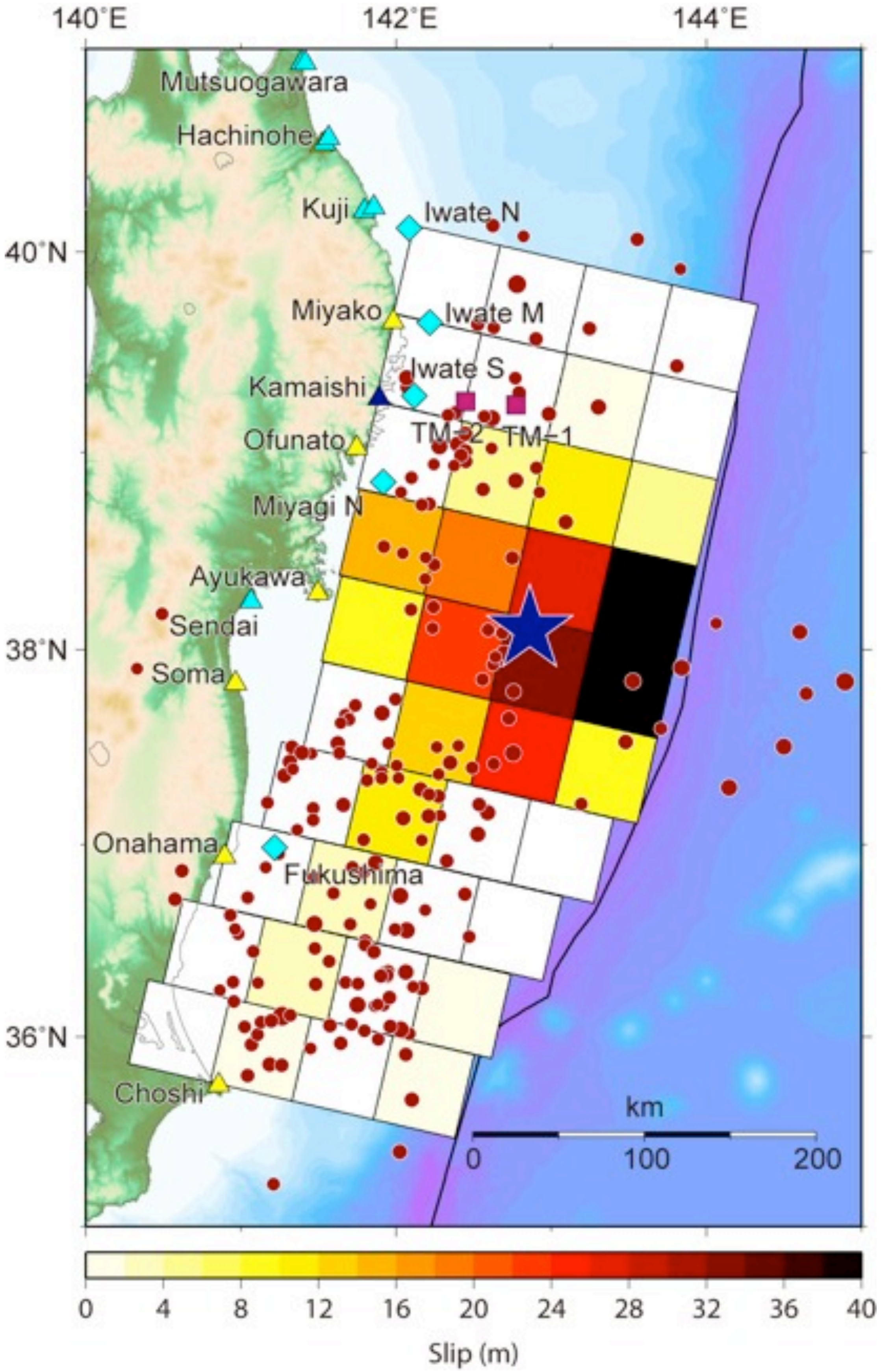

Slip distribution on the fault mode

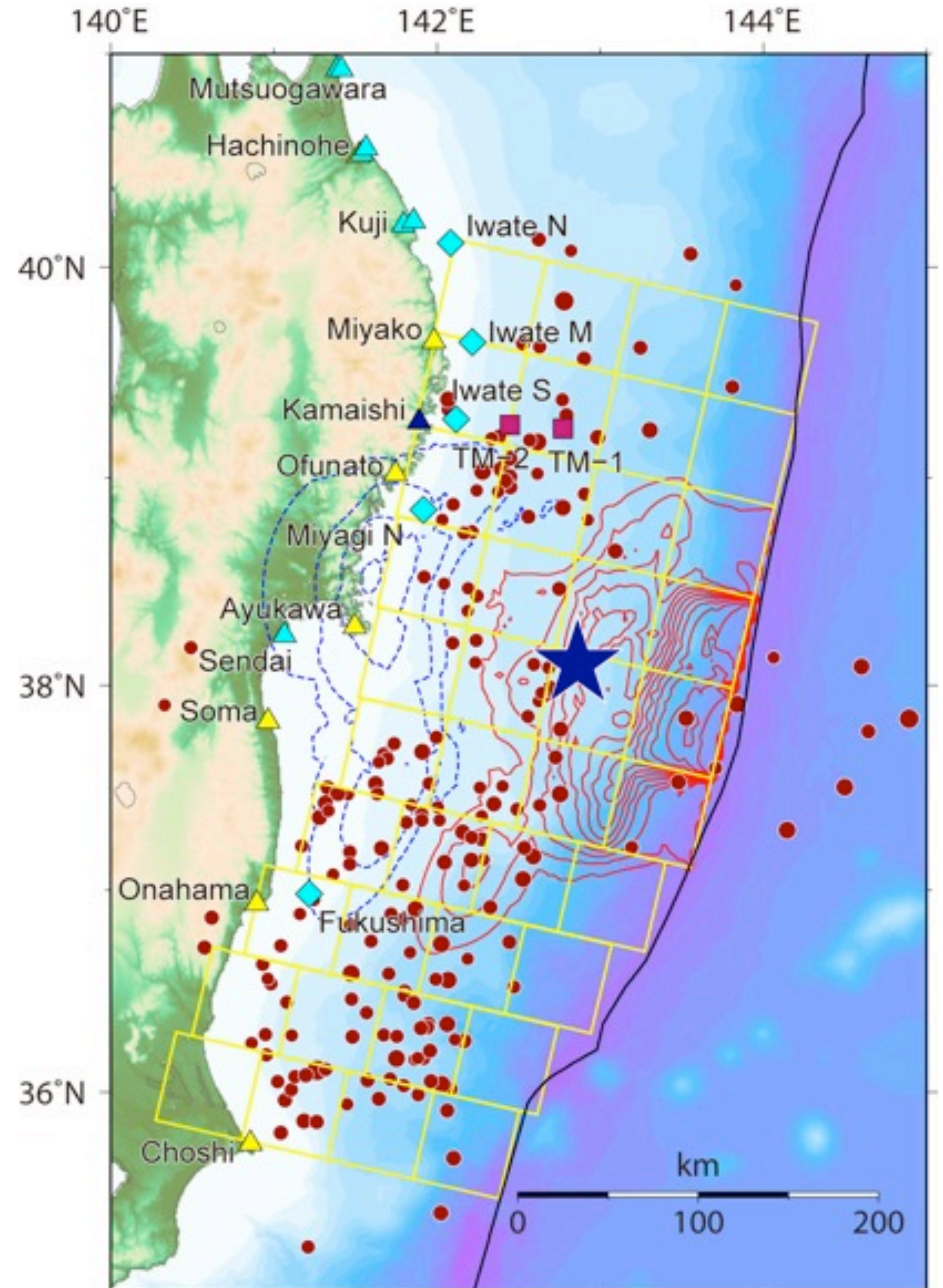

Calculated seafloor deformation due to the fault model

by Yushiro Fujii (IISEE, BRI) and Kenji Satake (ERI, Univ. of Tokyo)
http://iisee.kenken.go.jp/staff/fujii/OffTohokuPacific2011/tsunami_inv.html

Distribution of tsunami heights

Figure from the Headquarters for Earthquake Research Promotion
(at March 13)

http://www.jishin.go.jp/main/index-e.html

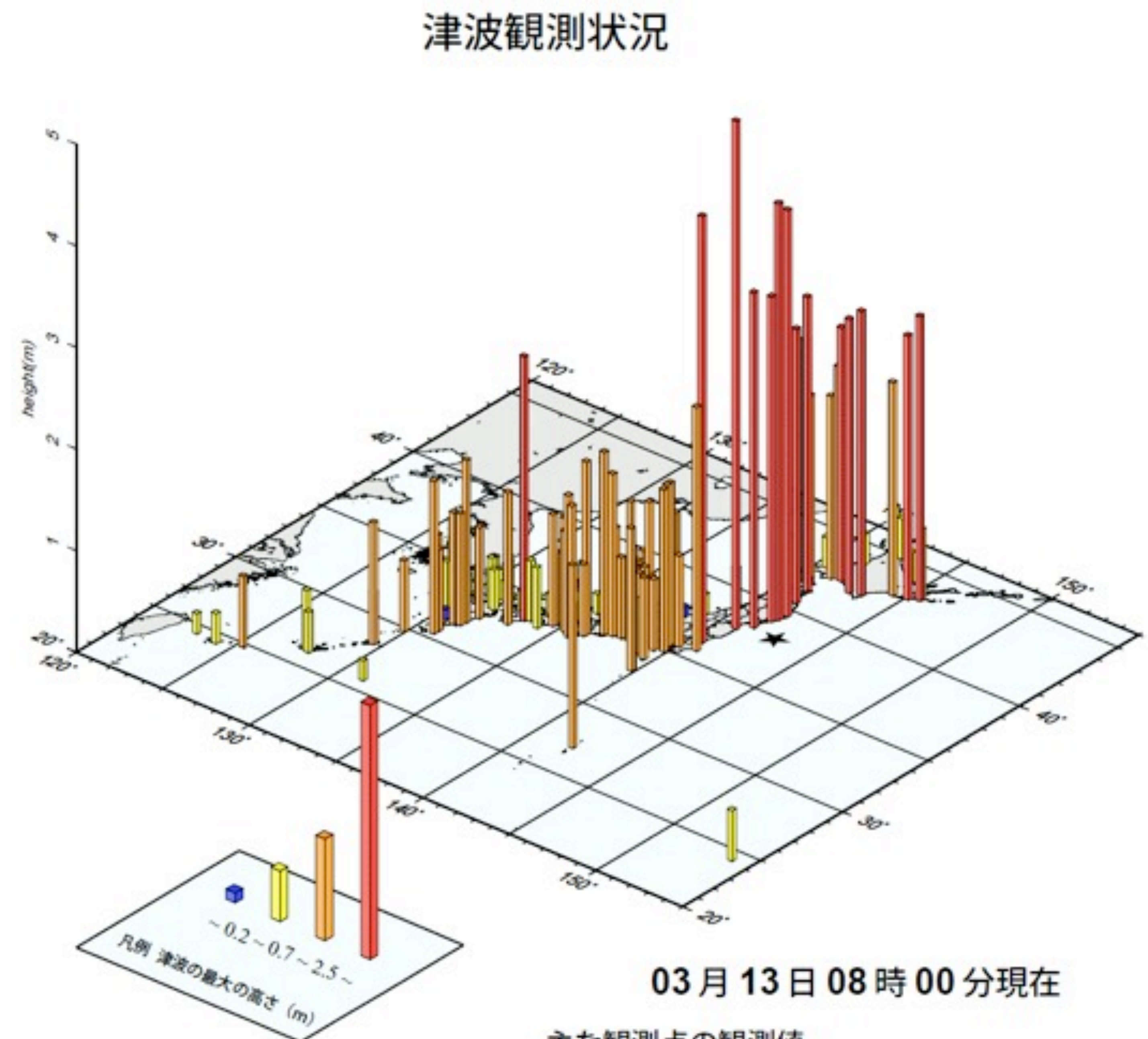

主な観測点の観測値

	第一波			最大波	
相馬	11日 14時 55分	押し	0.3m	11日 15時 50分	7.3m以上
大洗	11日 15時 15分	押し	1.8m	11日 16時 52分	4.2m
釜石	11日 14時 45分	引き	0.1m	11日 15時 21分	4.1m以上
宮古	11日 14時 48分	押し	0.2m	11日 15時 21分	4.0m以上
石巻市鮎川	11日 14時 46分	押し	0.1m	11日 15時 20分	3.3m以上
大船渡	11日 14時 46分	引き	0.2m	11日 15時 15分	3.2m以上
むつ市関根浜	11日 15時 20分	引き	0.1m	11日 18時 16分	2.9m
根室市花咲	11日 15時 34分	引き	微弱	11日 15時 57分	2.8m
十勝港	11日 15時 26分	引き	0.2m	11日 15時 57分	2.8m以上
浦河	11日 15時 19分	引き	0.2m	11日 16時 42分	2.7m

気象庁作成

Distribution of tsunami heights

Figure from the Headquarters for Earthquake Research Promotion
(at March 13)

http://www.jishin.go.jp/main/index-e.html

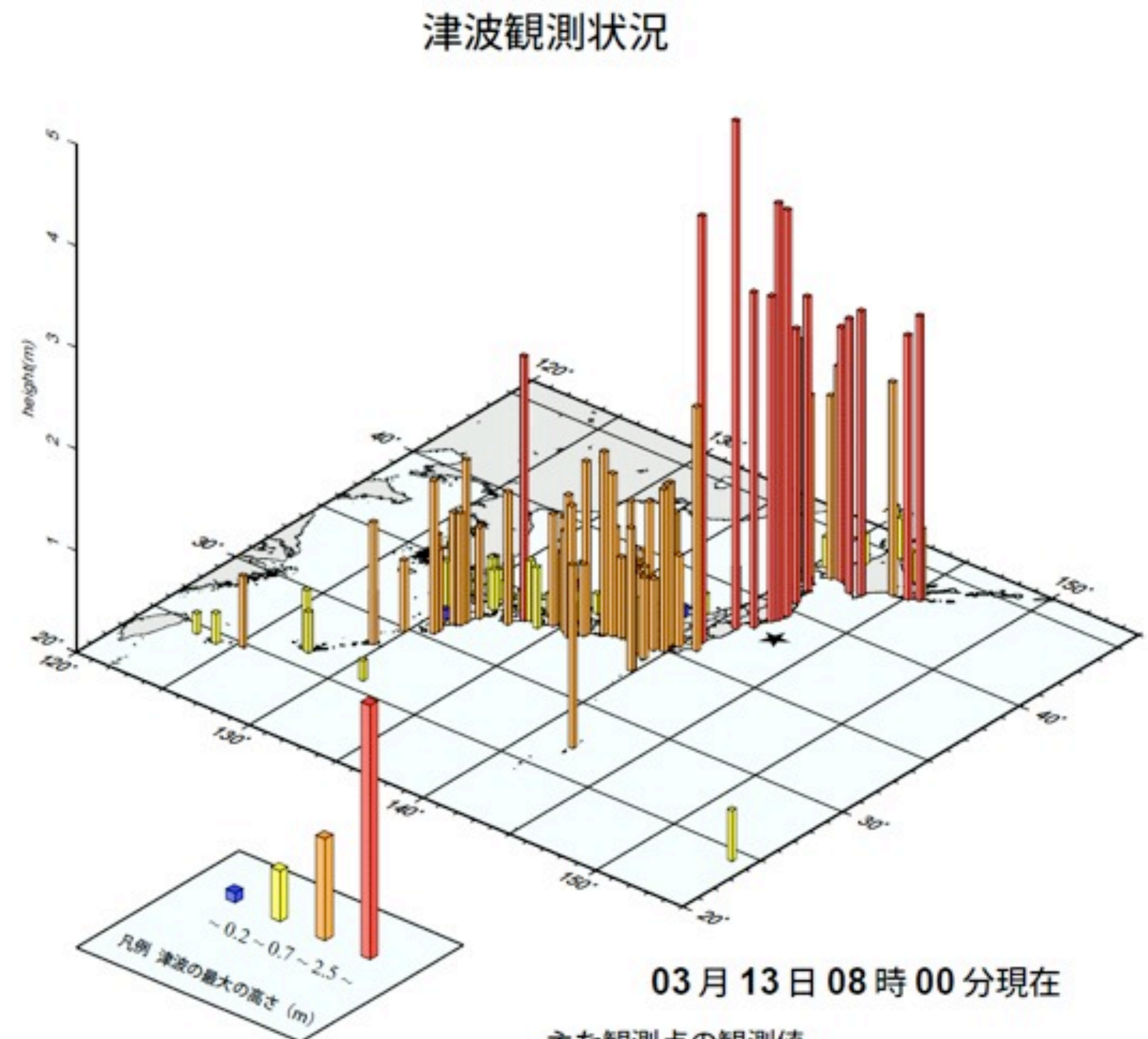

主な観測点の観測値

	第一波			最大波	
相馬	11日 14時 55分	押し	0.3m	11日 15時 50分	7.3m以上
大洗	11日 15時 15分	押し	1.8m	11日 16時 52分	4.2m
釜石	11日 14時 45分	引き	0.1m	11日 15時 21分	4.1m以上
宮古	11日 14時 48分	押し	0.2m	11日 15時 21分	4.0m以上
石巻市鮎川	11日 14時 46分	押し	0.1m	11日 15時 20分	3.3m以上
大船渡	11日 14時 46分	引き	0.2m	11日 15時 15分	3.2m以上
むつ市関根浜	11日 15時 20分	引き	0.1m	11日 18時 16分	2.9m
根室市花咲	11日 15時 34分	引き	微弱	11日 15時 57分	2.8m
十勝港	11日 15時 26分	引き	0.2m	11日 15時 57分	2.8m以上
浦河	11日 15時 19分	引き	0.2m	11日 16時 42分	2.7m

気象庁作成

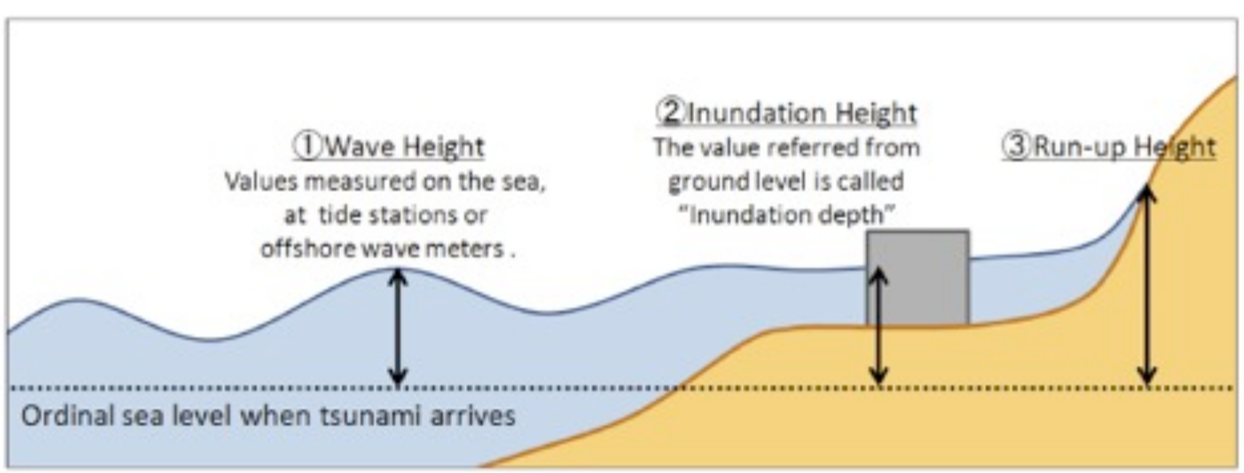

Sea gate in Hachinohe

http://minkara.carview.co.jp/userid/405365/car/375387/1923923/photo.aspx

Sea gate (9.3 m high)

http://ja2xt.mu-sashi.com/Numazu5.htm

Sea walls

Elevated platform used for tsunami evacuation that also serves as a high-elevation scenic vista point for tourist.
Okushiri Island, Japan. Photo courtesy of ITIC

Sea wall with stairway evacuation route used to protect a coastal town against tsunami inundation in Japan.

Photo courtesy of River Bureau, Ministry of Land, Infrastructure and Transport, Japan.

Deepest breakwater in Kamaishi (Iwate)

Tsunami walls...

The 2.4 km long tsunami wall in Miyako, Iwate Prefecture, was destroyed. The 6 m, 2 km long, wall in Kamaishi, Iwate Prefecture, was overwhelmed but delayed the tsunami inundation by 5 minutes.

The 15.5 m tsunami wall in Fundai, Iwate Prefecture, provided the best protection, but it is good to know that the original design was only 10 m. The village mayor fought to make it higher from information in the village historical records.

The biggest problem is that tsunami walls may give a false sense of security and other preparedness measures may NOT be undertaken.

Woody Epstein, 2011

Sea wall at Fudai

49 foot sea wall:
completed in 1967; floodgates were added in 1984.

Following the 1896 Meiji tsunami, village mayor Kotoku Wamura pressed for a seawall at least 15 meters high, often repeating the tales handed down to him growing up: that the devastating tsunami was 15 meters.

Miyako and Fudai…

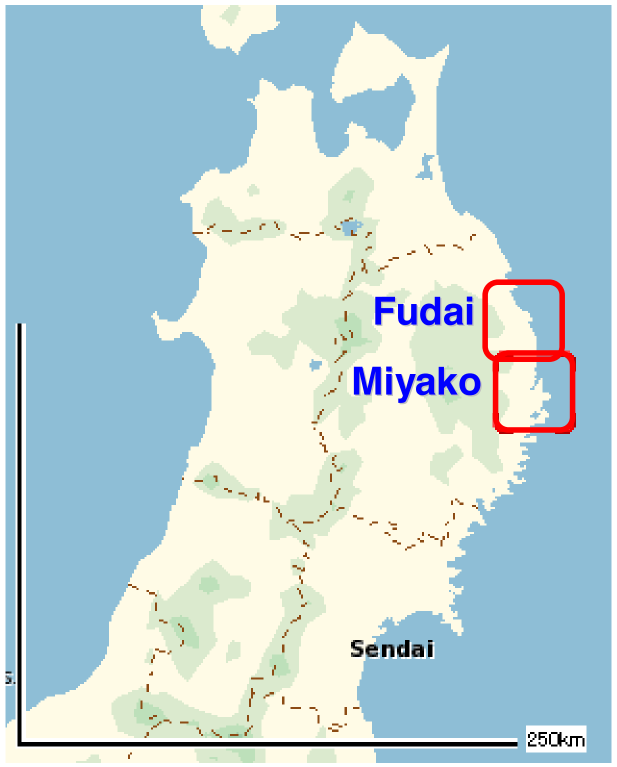

The 10m-high seawall was destroyed in Taro district, Miyako city, Iwate Pref.

The 15.5m-high seawall was undestroyed in Otabe district, Fudai village, Iwate Pref.

Fig. III-1-16 Difference of seawall heights resulting in different consequence.

A photo from the village's point of view (i.e. facing the coast)

A photo from a viewpoint of facing the village taken at the spot slightly below the stone monument

Tsunami stones (Tsunami-seki)

Expectations…

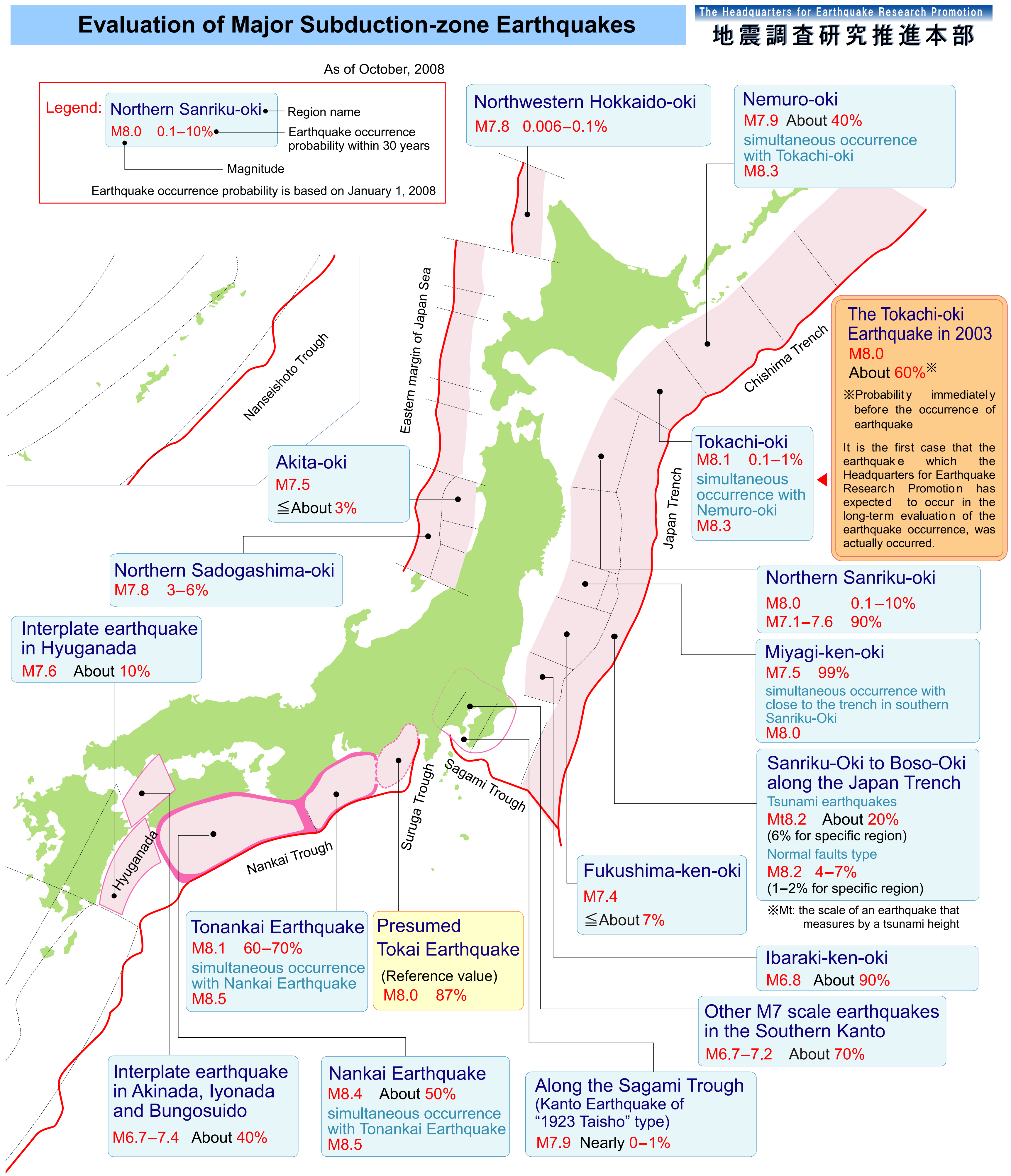

“Estimated magnitude and long-term possibilities within 30 years of earthquakes on regions of offshore based on Jan. 1, 2008.”

Expectations…

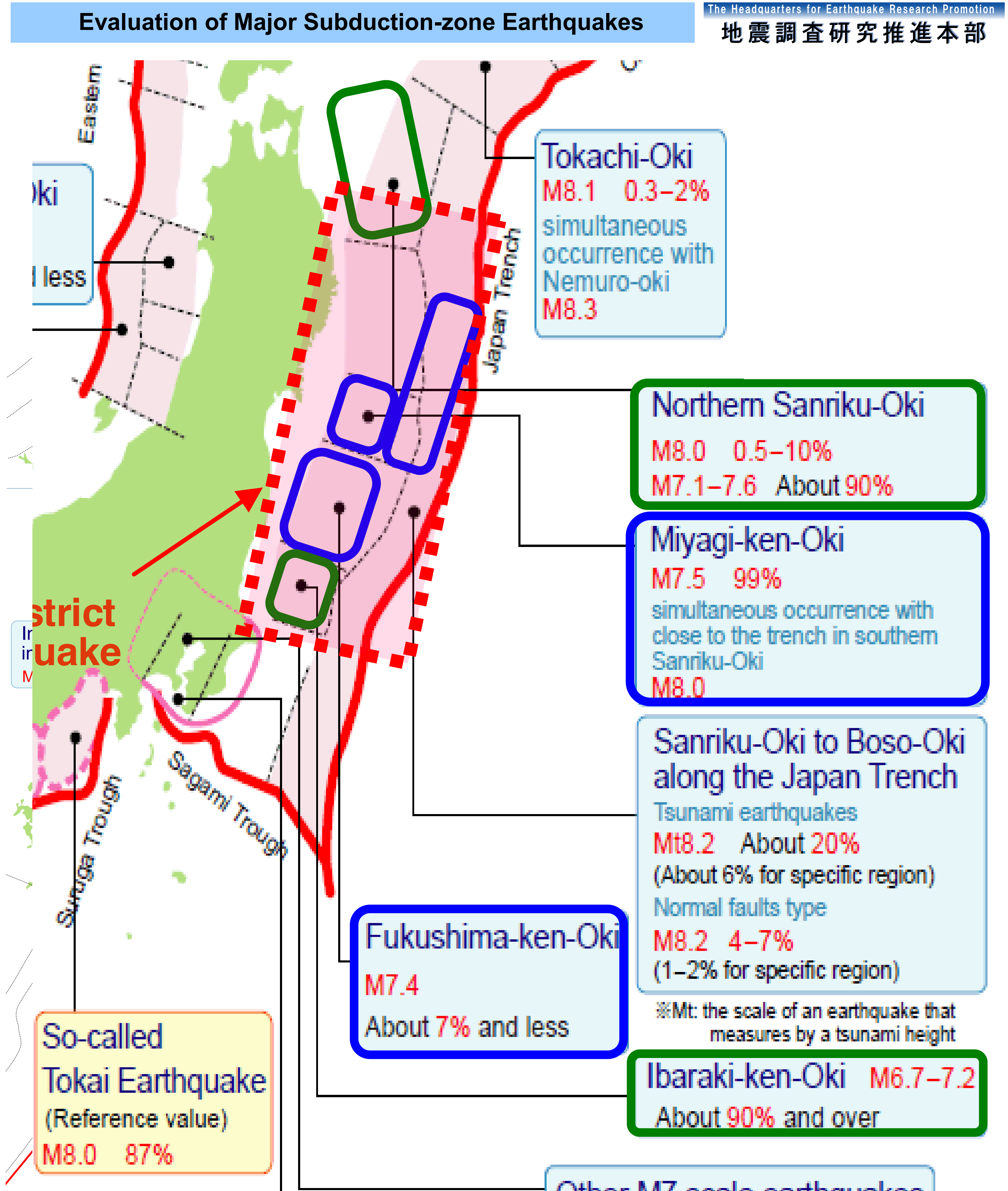

"Estimated magnitude and long-term possibilities within 30 years of earthquakes on regions of offshore based on Jan. 1, 2011."

"Estimated magnitude and long-term possibilities within 30 years of earthquakes on regions of offshore based on Jan. 1, 2008."

Reality...

Planning assumed maximum magnitude 8 Seawalls 5-10 m high

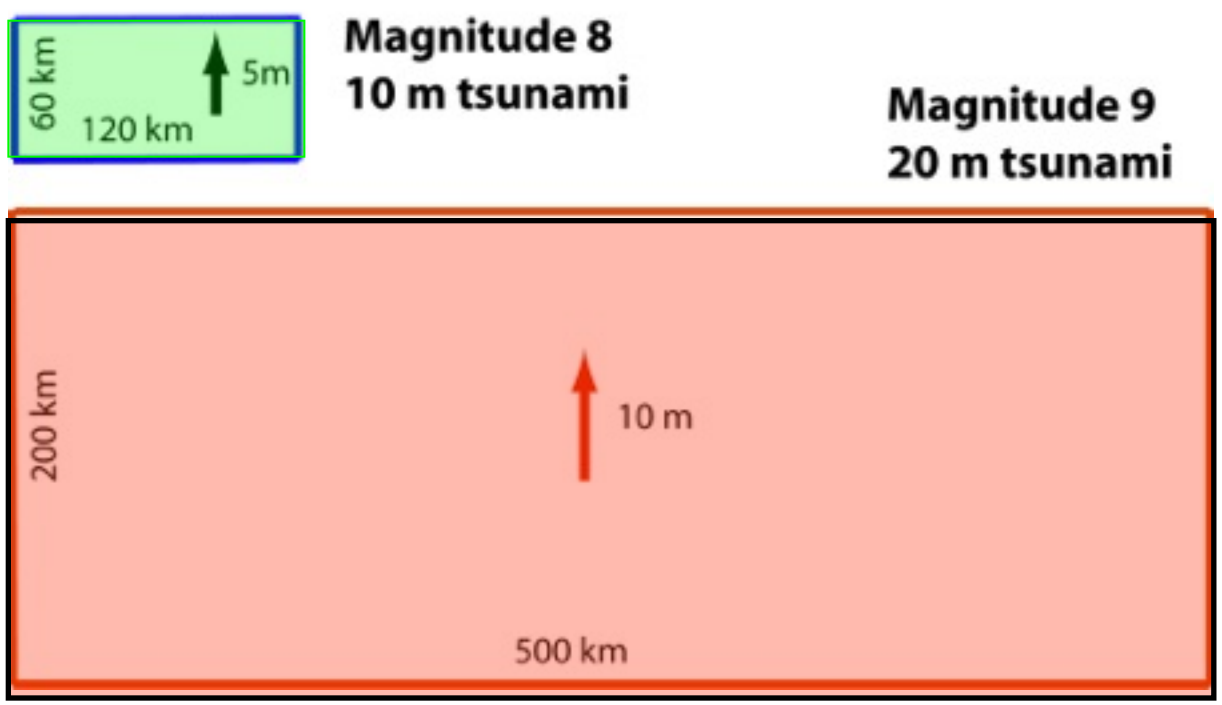

Tsunami runup approximately twice fault slip

M9 generates much larger tsunami

Stein, S. and E. Okal, The size of the 2011 Tohoku earthquake needn't have been a surprise, EOS, 92, 227-228, 2011.

Tsunami Assessment method for NPP in JSCE, Japan

The TSUNAMI EVALUATION SUBCOMMITTEE,
Nuclear Civil Engineering Committee, JSCE

Masafumi Matsuyama (CRIEPI)

Niigata meeting, November 2010
http://www.jnes.go.jp/seismic-symposium10/presentationdata/3_sessionB.html

Tsunami Assessment method for NPP in JSCE, Japan

The TSUNAMI EVALUATION SUBCOMMITTEE,
Nuclear Civil Engineering Committee, JSCE

Masafumi Matsuyama (CRIEPI)

History of TES

- Phase I 1999-2000
  The maximum and minimum water levels by deterministic method
  → "Tsunami assessment method for NPP in Japan」 (2002)"
- Phase II 2003-2005
  Probabilistic Tsunami Hazard Analysis for the max. and min. water levels
  Numerical simulation of nonlinear dispersion wave theory with soliton fission and split wave-breaking
  Tsunami wave force on breakwater
- Phase III 2006-2008
  Topography change due to tsunami
  Development of probabilistic Tsunami Hazard Analysis
- Now → Phase IV 2009-2011
  Revising of 「Tsunami assessment method for NPP in Japan」

Niigata meeting, November 2010
http://www.jnes.go.jp/seismic-symposium10/presentationdata/3_sessionB.html

Tsunami Assessment method for NPP in JSCE, Japan

The TSUNAMI EVALUATION SUBCOMMITTEE,
Nuclear Civil Engineering Committee, JSCE

Masafumi Matsuyama (CRIEPI)

History of TES

- Phase I 1999-2000
  The maximum and minimum water levels by deterministic method
  → "Tsunami assessment method for NPP in Japan」 (2002)"
- Phase II 2003-2005
  Probabilistic Tsunami Hazard Analysis for the max. and min. water levels
  Numerical simulation of nonlinear dispersion wave theory with soliton fission and split wave-breaking
  Tsunami wave force on breakwater
- Phase III 2006-2008
  Topography change due to tsunami
  Development of probabilistic Tsunami Hazard Analysis
- Now → Phase IV 2009-2011
  Revising of 「Tsunami assessment method for NPP in Japan」

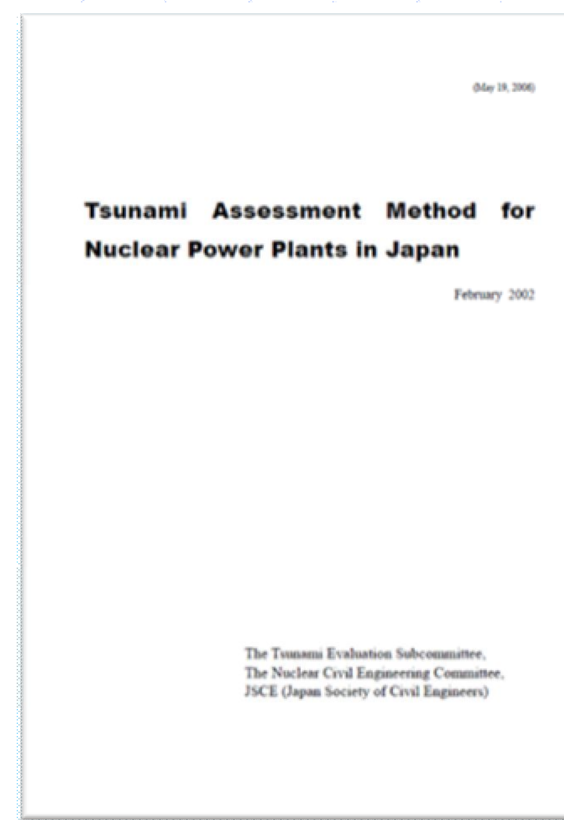
(May 19, 2006)

Tsunami Assessment Method for Nuclear Power Plants in Japan

February 2002

The Tsunami Evaluation Subcommittee,
The Nuclear Civil Engineering Committee,
JSCE (Japan Society of Civil Engineers)

Niigata meeting, November 2010
http://www.jnes.go.jp/seismic-symposium10/presentationdata/3_sessionB.html

Tsunami Assessment method for NPP in JSCE, Japan

The TSUNAMI EVALUATION SUBCOMMITTEE,
Nuclear Civil Engineering Committee, JSCE

Masafumi Matsuyama (CRIEPI)

Deterministic method (2002) Main flow chart

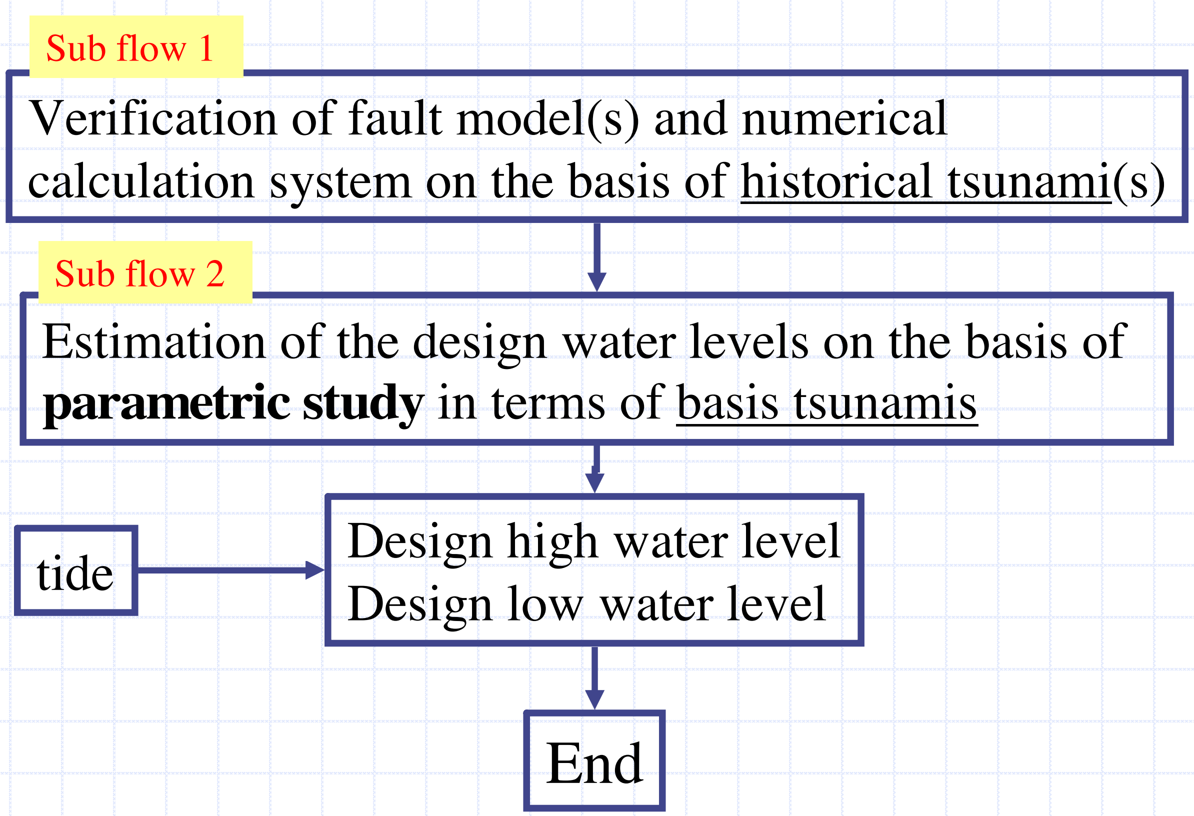

Niigata meeting, November 2010
http://www.jnes.go.jp/seismic-symposium10/presentationdata/3_sessionB.html

Tsunami Assessment method for NPP in JSCE, Japan

The TSUNAMI EVALUATION SUBCOMMITTEE,
Nuclear Civil Engineering Committee, JSCE

Masafumi Matsuyama (CRIEPI)

Deterministic method (2002)
Main flow chart

Sub flow 1

Verification of fault model(s) and numerical calculation system on the basis of historical tsunami(s)

↓

Sub flow 2

Estimation of the design water levels on the basis of **parametric study** in terms of basis tsunamis

↓

tide → Design high water level / Design low water level

↓

End

General parametric study in the near field

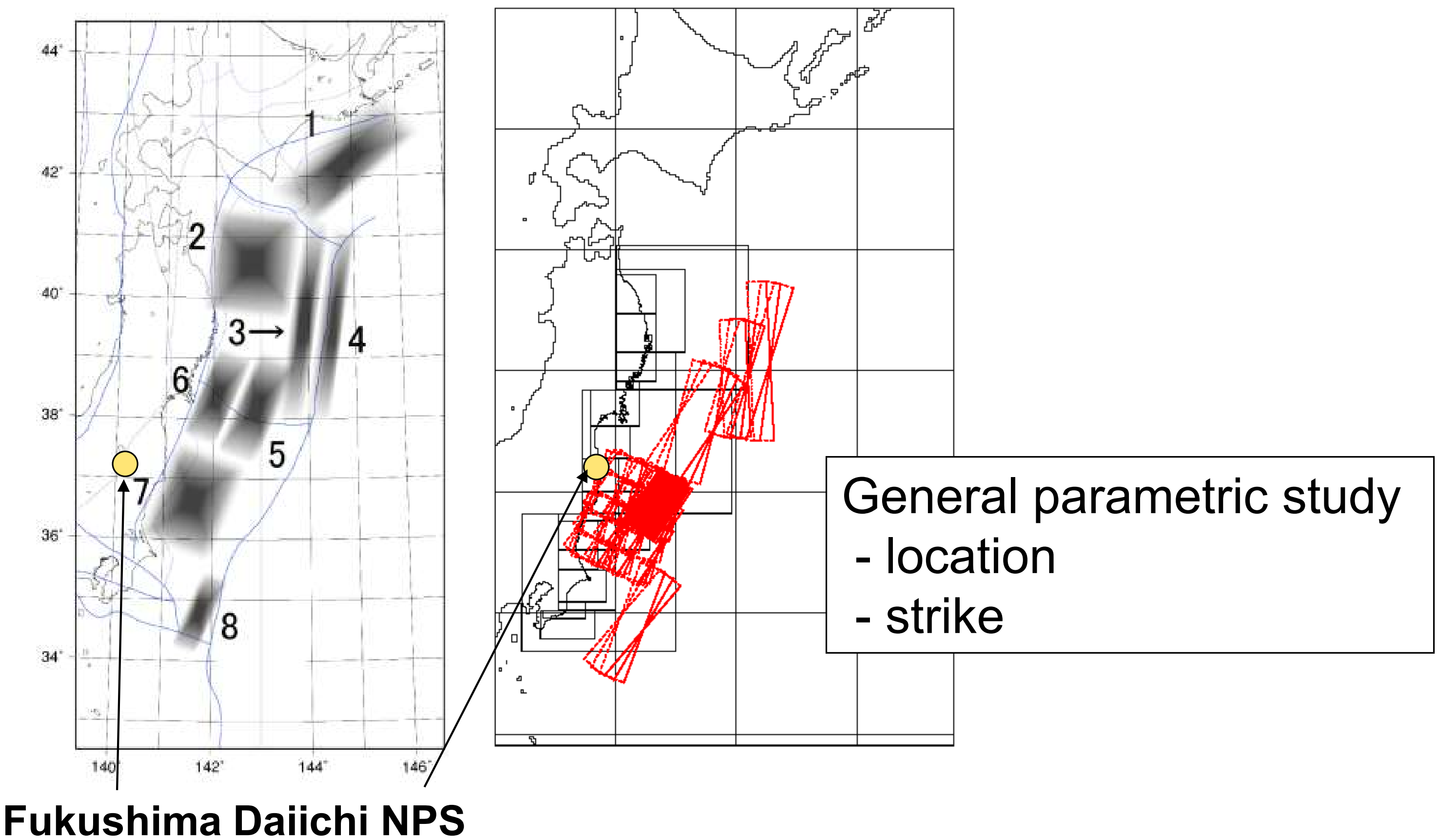

東京電力

All rights reserved. Tokyo Electric Power Co., Inc.

Niigata meeting, November 2010
http://www.jnes.go.jp/seismic-symposium10/presentationdata/3_sessionB.html

Tsunami Assessment method for NPP in JSCE, Japan

The TSUNAMI EVALUATION SUBCOMMITTEE,
Nuclear Civil Engineering Committee, JSCE

Masafumi Matsuyama (CRIEPI)

Deterministic method (2002)
Main flow chart

Sub flow 1

Verification of fault model(s) and numerical calculation system on the basis of historical tsunami(s)

↓

Sub flow 2

Estimation of the design water levels on the basis of **parametric study** in terms of basis tsunamis

↓

tide → Design high water level
Design low water level

↓

End

General parametric study in the near field

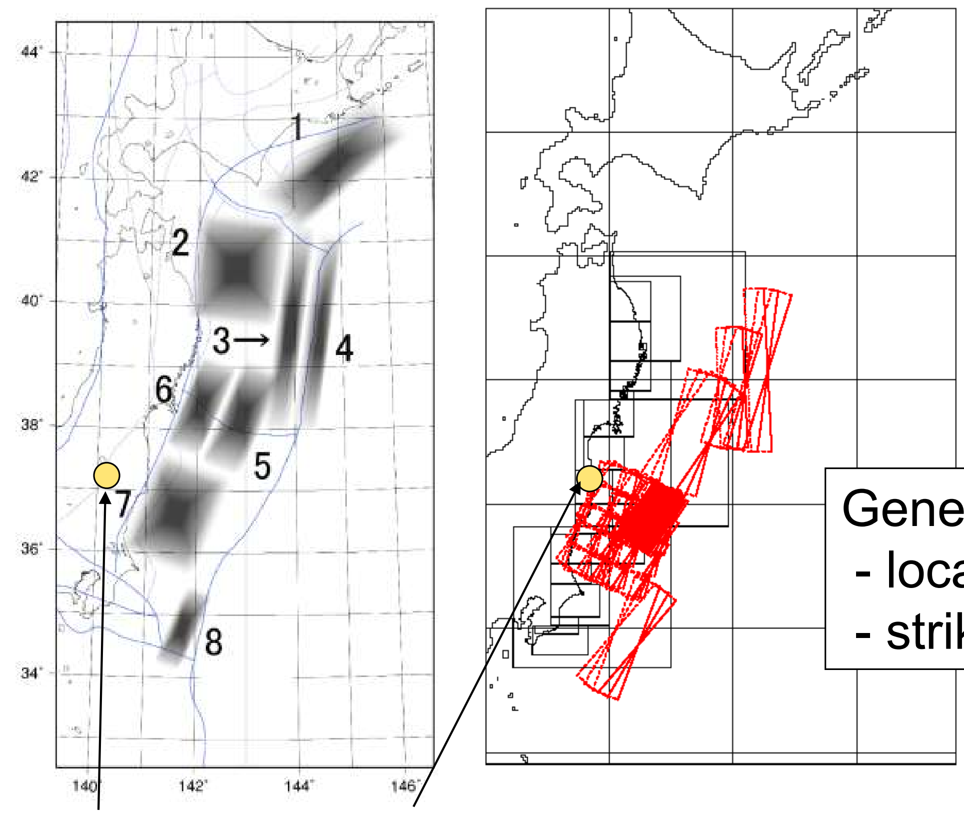

General parametric study
- location
- strike

Fukushima Daiichi NPS

Summary of Evaluation

Maximum water level = 4.4m + O.P.＋1.3m = O.P.+5.7m
Minimum water level = -3.6m – O.P.±0.0m = O.P.-3.6m

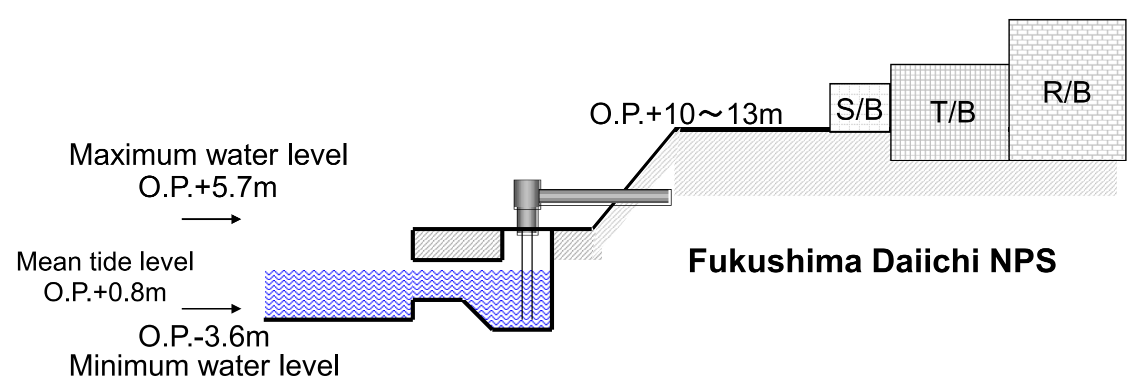

We assessed and confirmed the safety of the nuclear plants based on the JSCE method which was published in 2002.

Niigata meeting, November 2010
http://www.jnes.go.jp/seismic-symposium10/presentationdata/3_sessionB.html

Very basic tsunami physics...

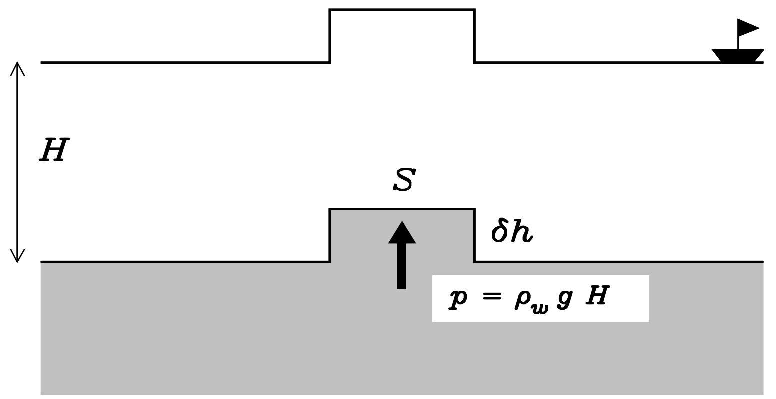

Bottom uplift
&
Waterberg
formation

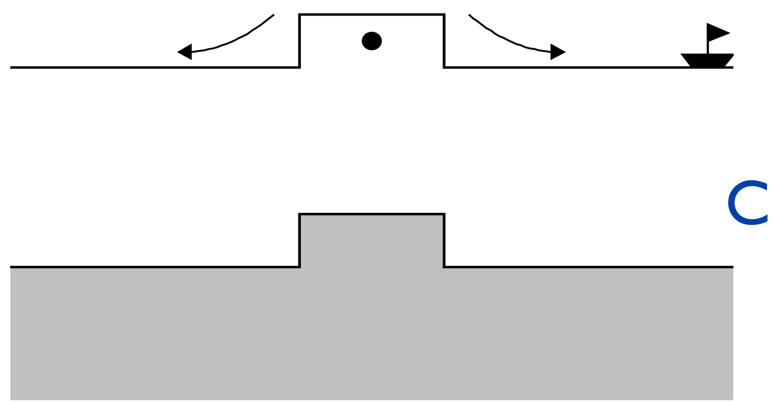

Center of mass falls...

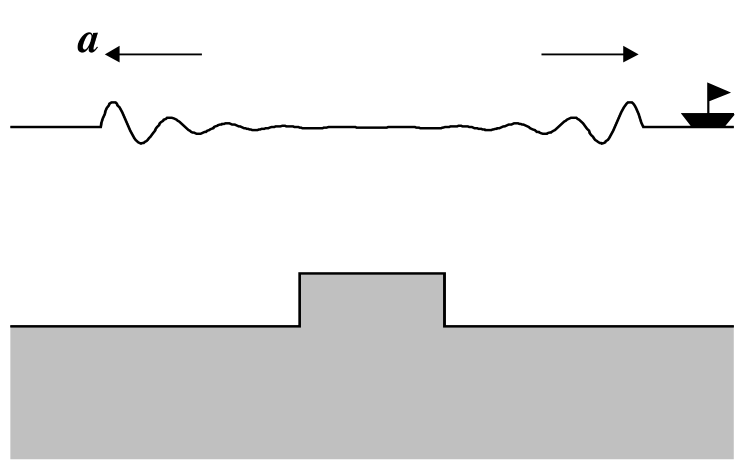

Potential
energy goes to
tsunami energy

Very basic tsunami physics...

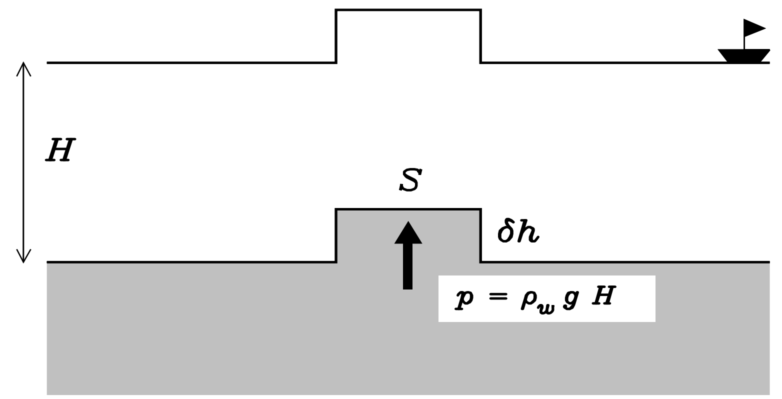

Bottom uplift
&
Waterberg
formation

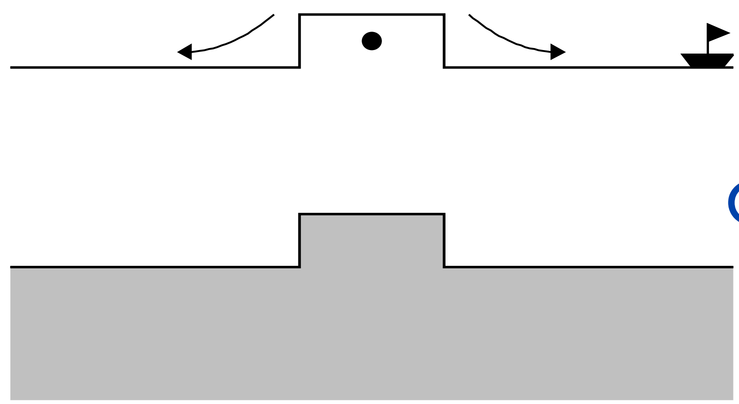

Center of mass falls...

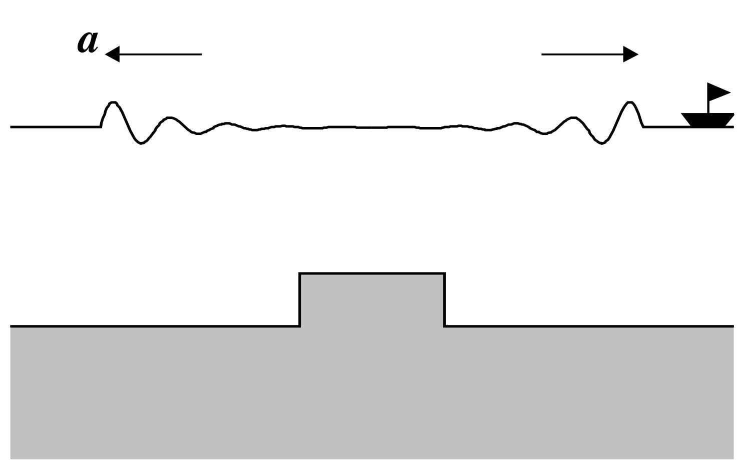

Potential
energy goes to
tsunami energy

Energy

$$E_R \approx 4.8 + 1.5M$$

$$E_T = \frac{1}{2}\rho g L \lambda (\delta h)^2$$

$$L \sim 10^6 m;\ \lambda \sim 10^4 m;\ \delta h \sim 5m$$

$$E_R \approx 10^{18} J \geq 10^2 E_T$$

Very basic tsunami physics...

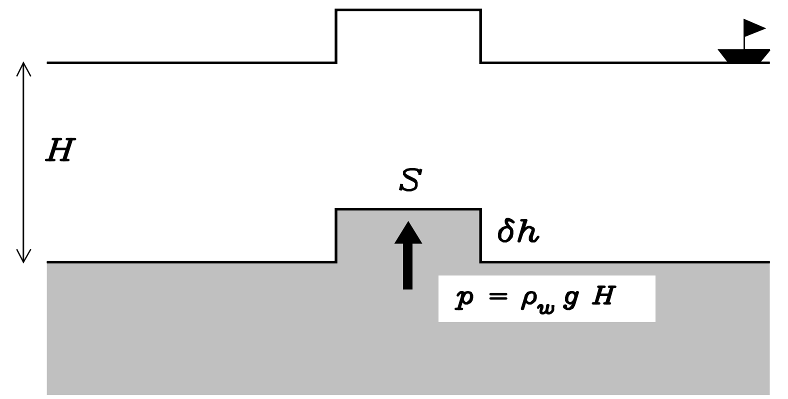

Bottom uplift
&
Waterberg
formation

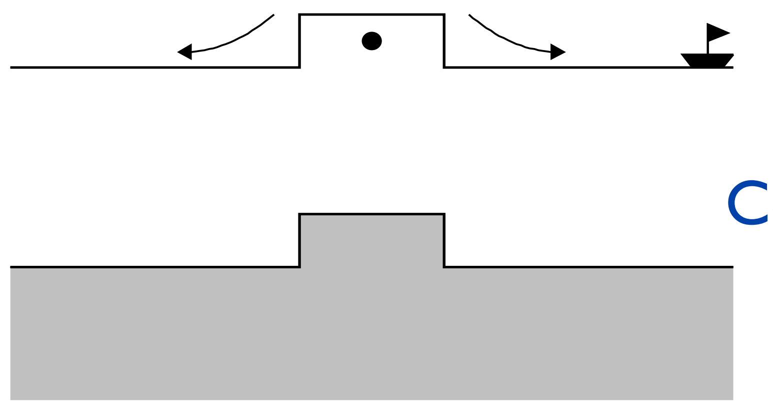

Center of mass falls...

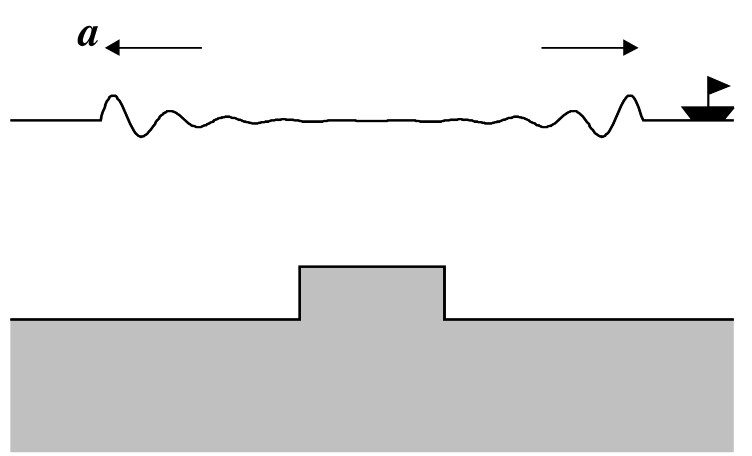

Potential
energy goes to
tsunami energy

Energy

$$E_R \approx 4.8 + 1.5M$$

$$E_T = \frac{1}{2}\rho g L \lambda (\delta h)^2$$

$$L \sim 10^6 m;\ \lambda \sim 10^4 m;\ \delta h \sim 5m$$

$$E_R \approx 10^{18} J \geq 10^2 E_T$$

Wavelength

$$\frac{\lambda}{H} \sim 40;\ \frac{H}{a} \sim 3 \cdot 10^3$$

$$\lambda >> H >> a$$

Very basic tsunami physics...

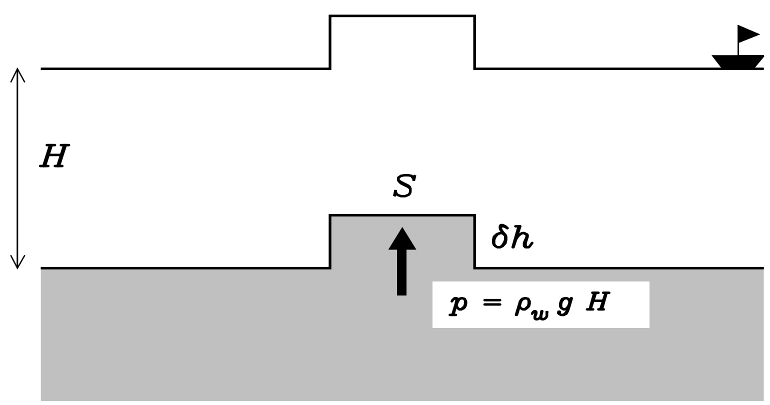

Bottom uplift
&
Waterberg
formation

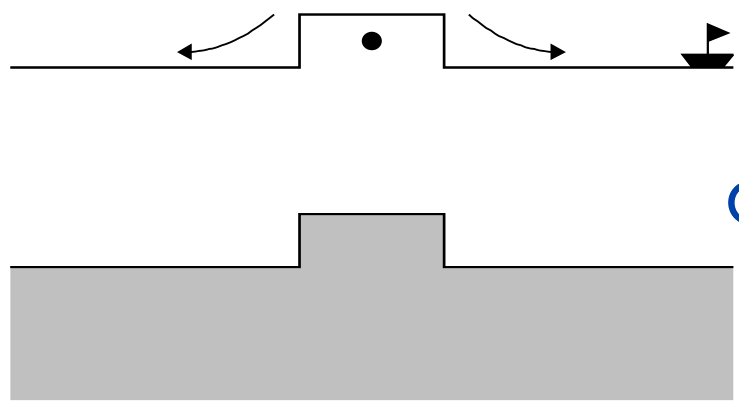

Center of mass falls...

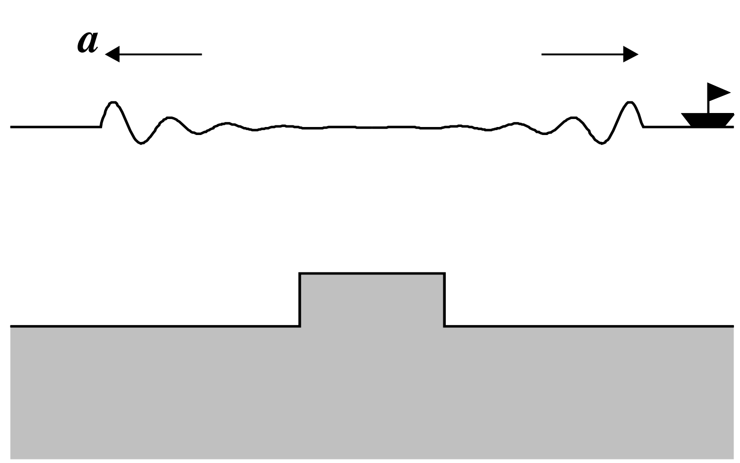

Potential
energy goes to
tsunami energy

Energy

$$E_R \approx 4.8 + 1.5M$$
$$E_T = \frac{1}{2}\rho g L \lambda (\delta h)^2$$
$$L \sim 10^6 m;\ \lambda \sim 10^4 m;\ \delta h \sim 5m$$
$$E_R \approx 10^{18} J \geq 10^2 E_T$$

Wavelength

$$\frac{\lambda}{H} \sim 40;\ \frac{H}{a} \sim 3 \cdot 10^3$$
$$\lambda >> H >> a$$

Tsunami is a shallow-water gravity wave with great wavelength and tiny amplitude

Navier-Stokes equations

Newton's law + Conservation of matter + Viscosity

$$\rho \frac{\partial \mathbf{v}}{\partial t} + \rho(\mathbf{v} \cdot grad)\mathbf{v} = -grad(P) - \rho grad(\phi) +$$
$$+\eta \Delta \mathbf{v} + (\eta + \eta')grad\left(div(\mathbf{v})\right)$$

Navier-Stokes equations

Newton's law + Conservation of matter + Viscosity

$$\rho\frac{\partial \mathbf{v}}{\partial t} + \rho(\mathbf{v}\cdot grad)\mathbf{v} = -grad(P) - \rho grad(\phi) + \\ +\eta\Delta\mathbf{v} + (\eta+\eta')grad\big(div(\mathbf{v})\big)$$

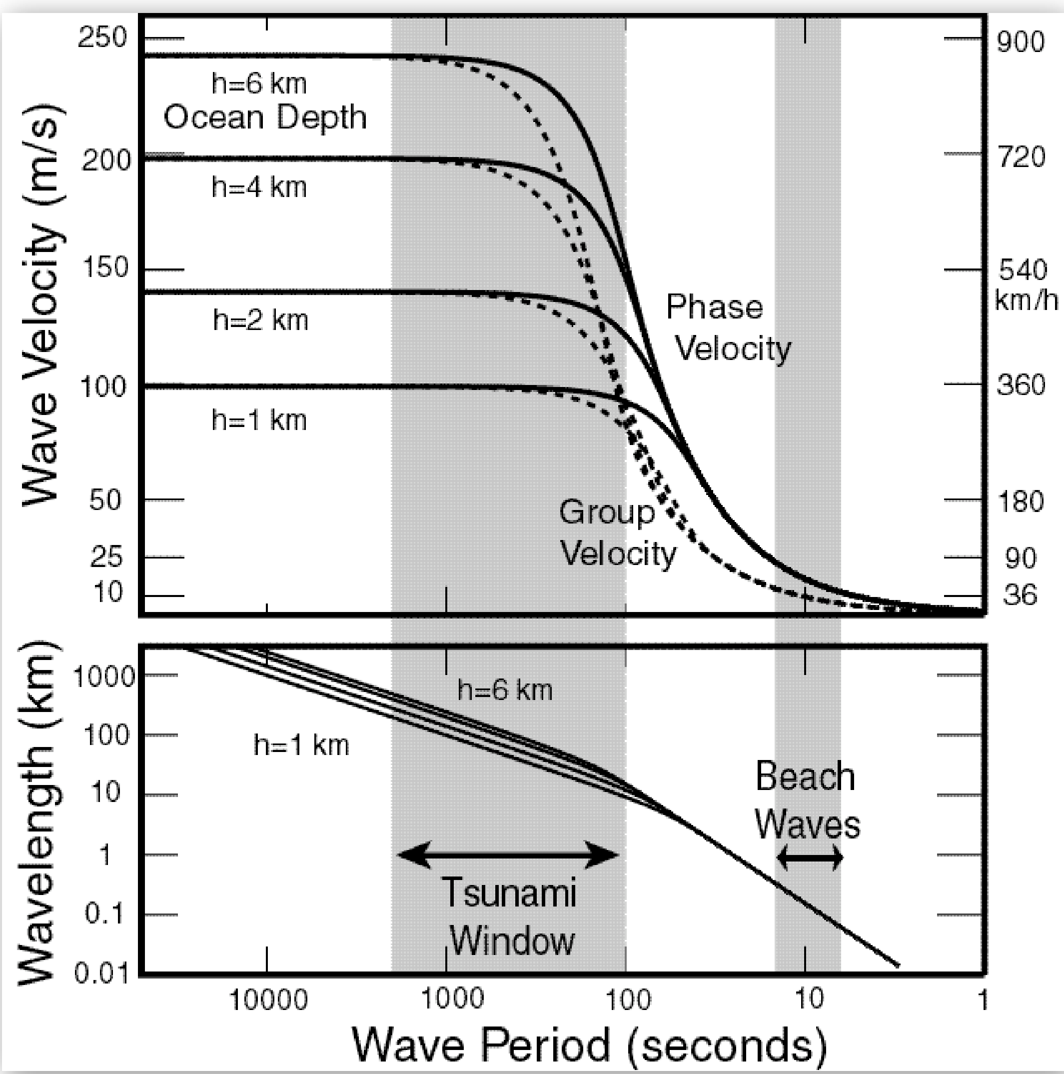

Navier-Stokes equations

Newton's law + Conservation of matter + Viscosity

$$\rho\frac{\partial \mathbf{v}}{\partial t} + \rho(\mathbf{v}\cdot grad)\mathbf{v} = -grad(P) - \rho grad(\phi) + $$
$$+\eta\Delta\mathbf{v} + (\eta+\eta')grad\left(div(\mathbf{v})\right)$$

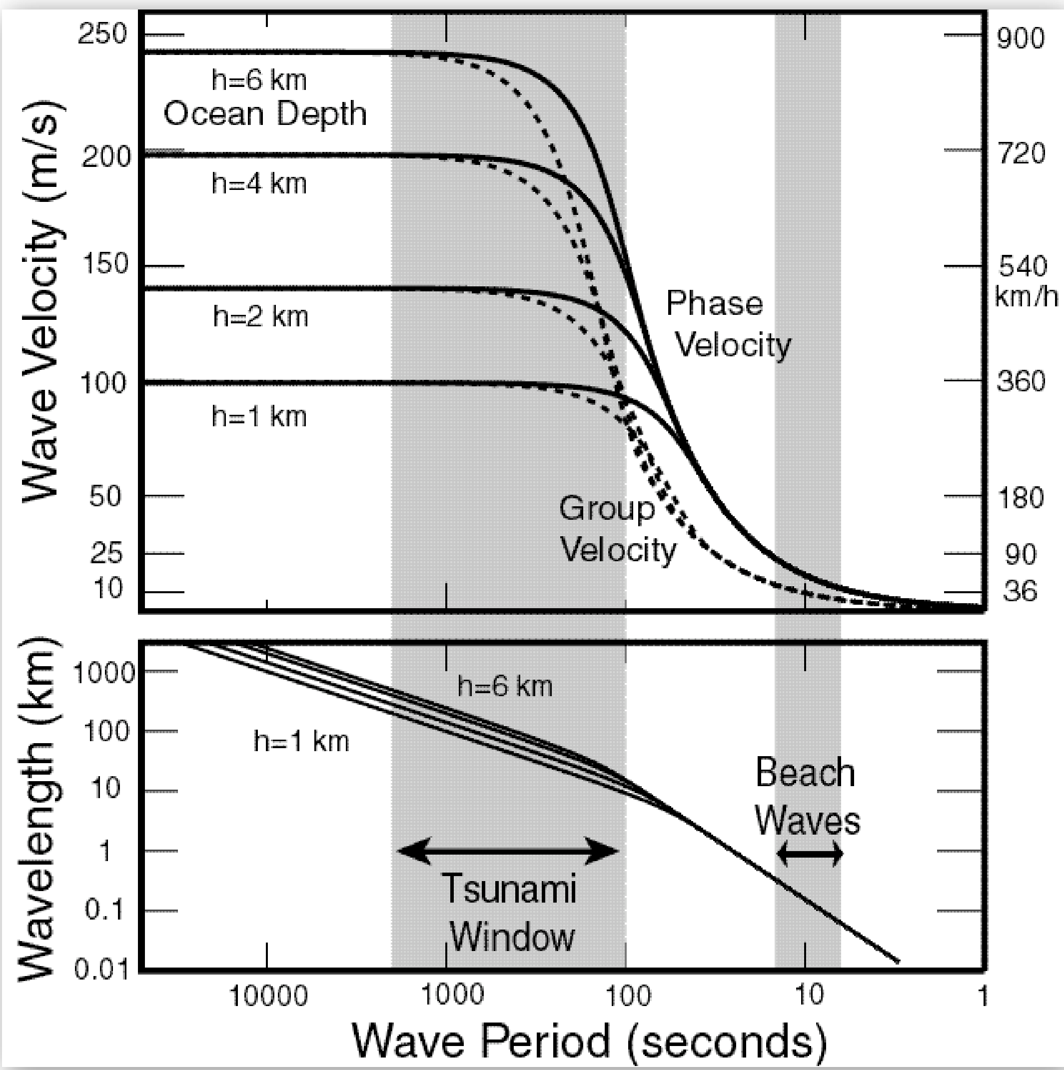

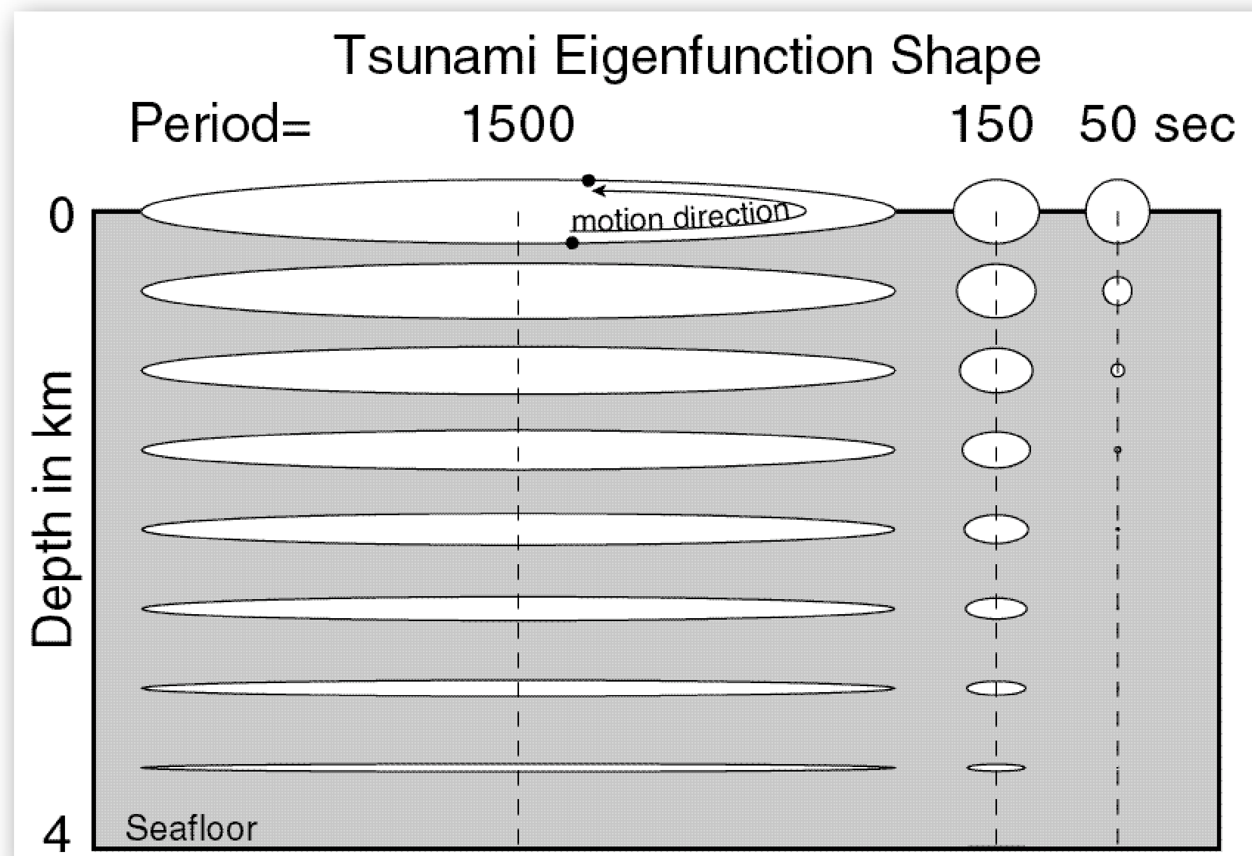

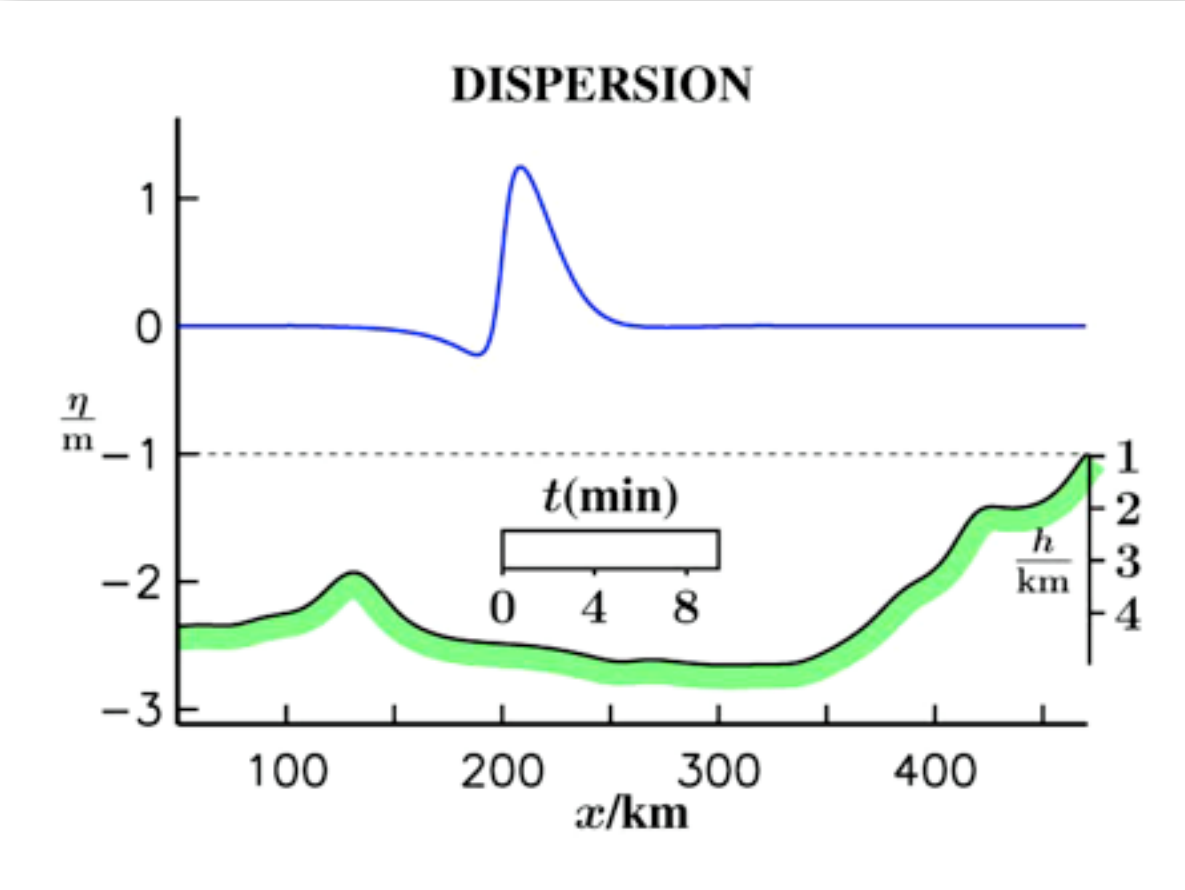

DISPERSION
1
0
η/m
−1
−2
−3
t(min)
0
4
8
h/km
1
2
3
4
100
200
300
400
x/km

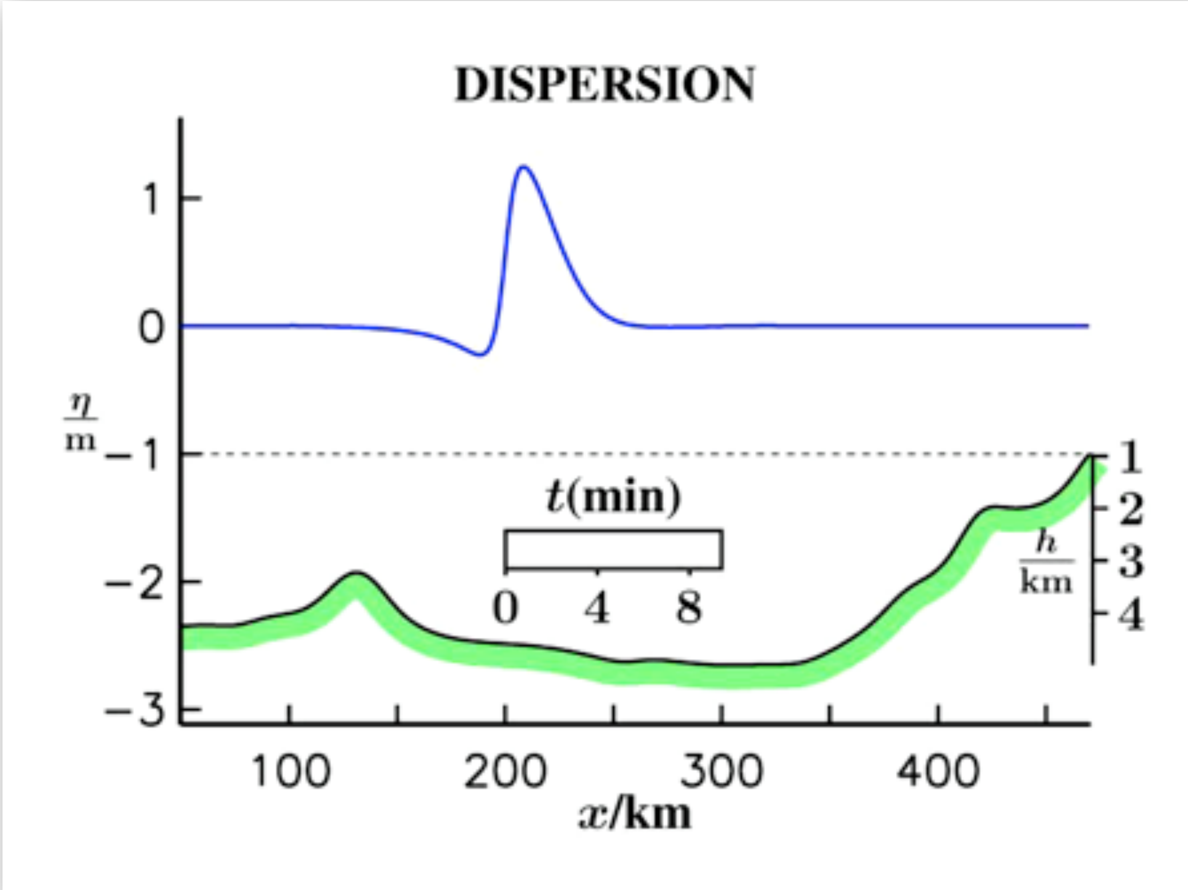
DISPERSION
1
0
−1
−2
−3
η/m
t(min)
0
4
8
h/km
1
2
3
4
100
200
300
400
x/km

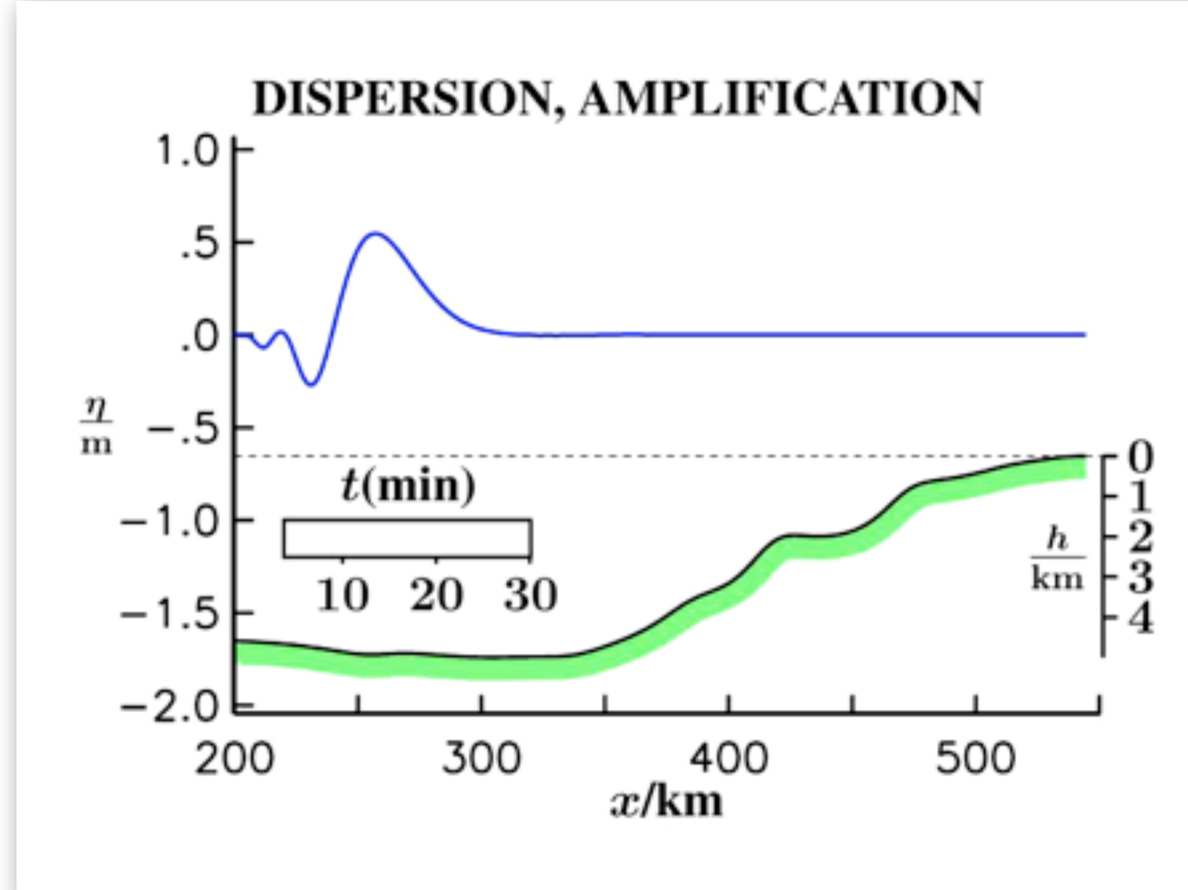
DISPERSION, AMPLIFICATION
1.0
.5
.0
−.5
−1.0
−1.5
−2.0
η/m
t(min)
10
20
30
h/km
0
1
2
3
4
200
300
400
500
x/km

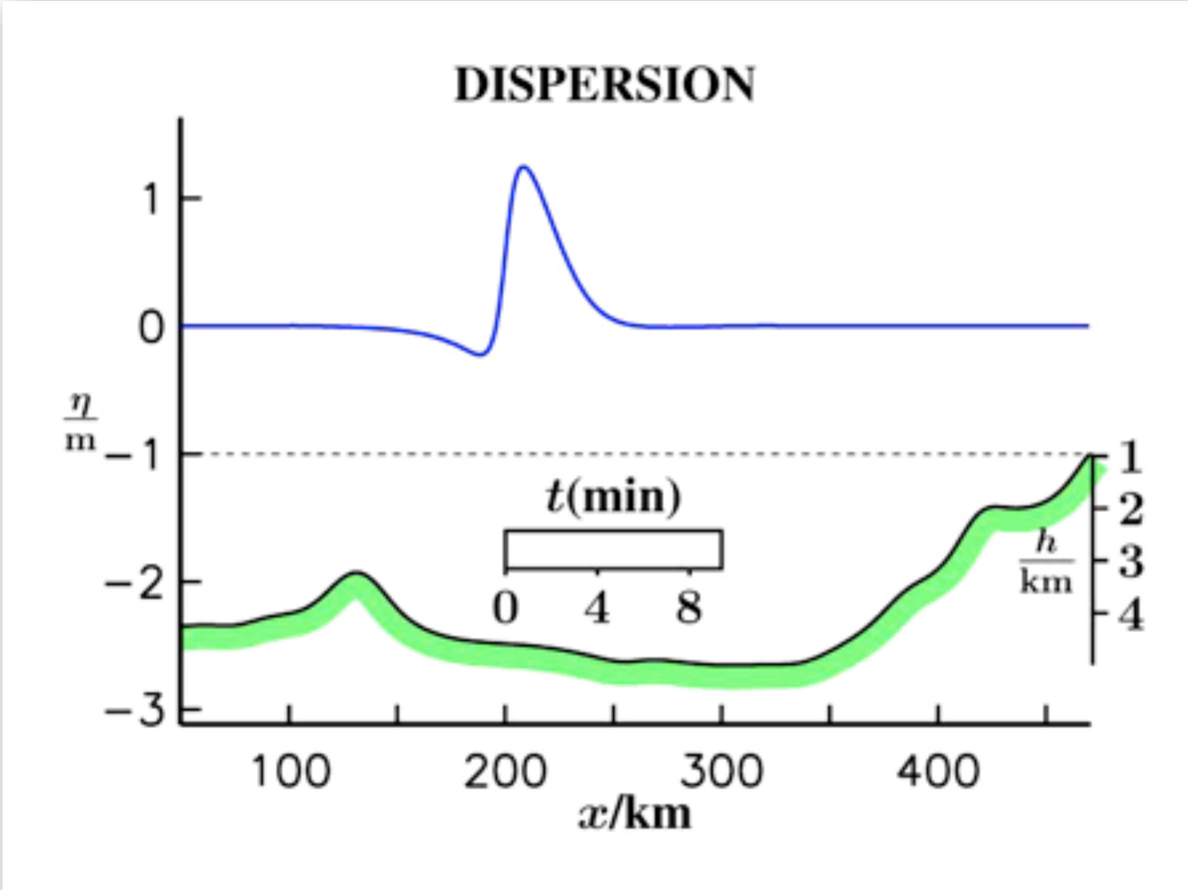
DISPERSION
1
0
−1
−2
−3
η/m
t(min)
0
4
8
h/km
1
2
3
4
100
200
300
400
x/km

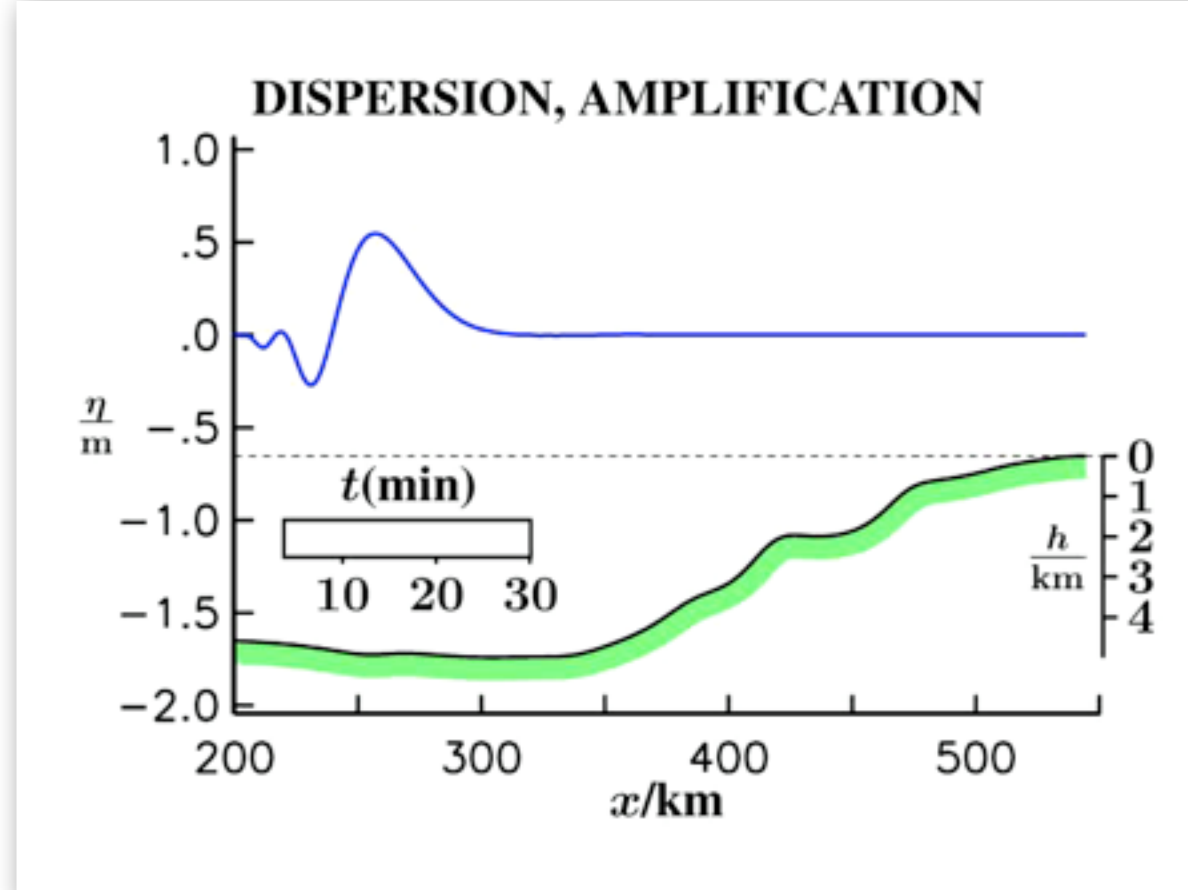
DISPERSION, AMPLIFICATION
1.0
.5
.0
−.5
−1.0
−1.5
−2.0
η/m
t(min)
10
20
30
h/km
0
1
2
3
4
200
300
400
500
x/km

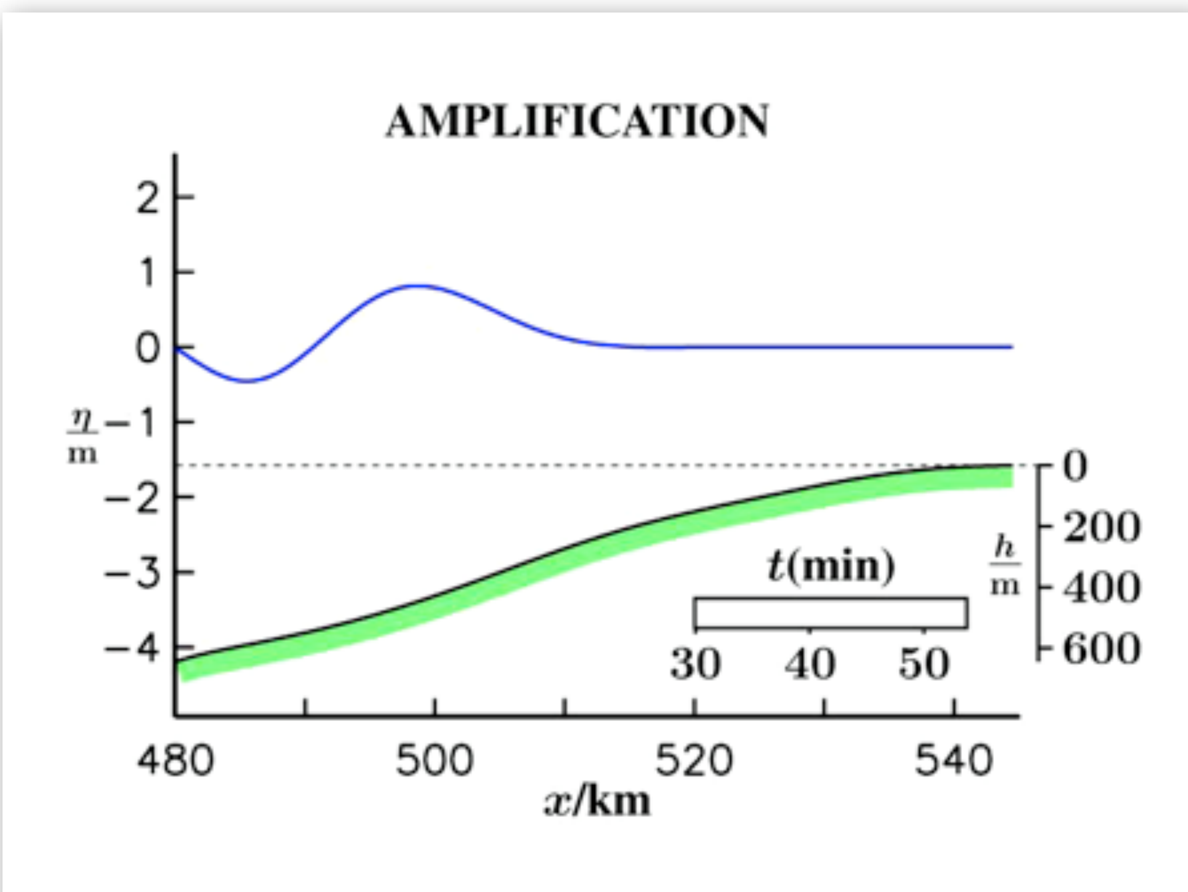
AMPLIFICATION
2
1
0
−1
−2
−3
−4
η/m
t(min)
30
40
50
h/m
0
200
400
600
480
500
520
540
x/km

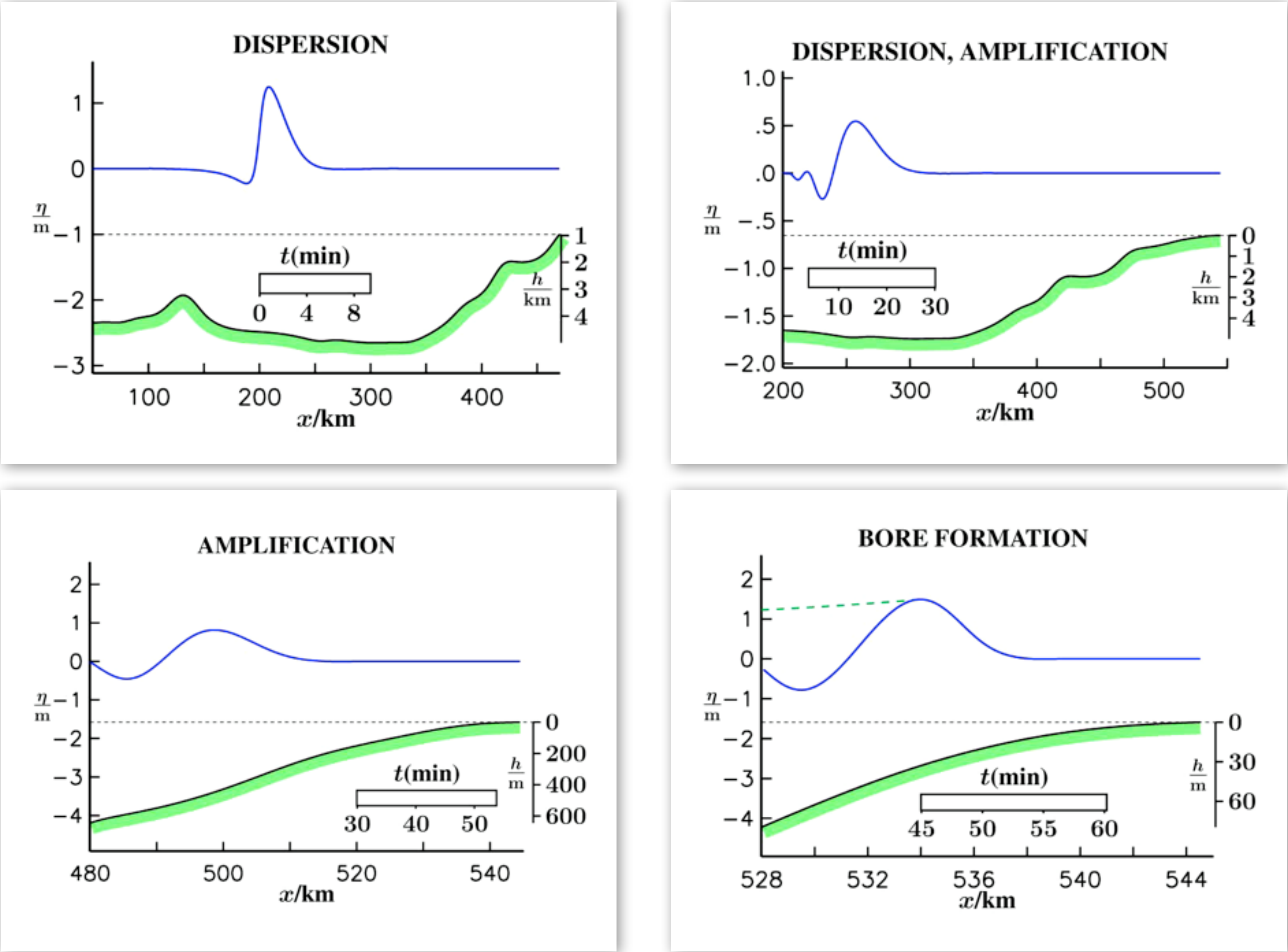
DISPERSION
1
0
η/m
−1
−2
−3
t(min)
0
4
8
h/km
1
2
3
4
100
200
300
400
x/km
DISPERSION, AMPLIFICATION
1.0
.5
.0
−.5
−1.0
−1.5
−2.0
η/m
t(min)
10
20
30
h/km
0
1
2
3
4
200
300
400
500
x/km
AMPLIFICATION
2
1
0
η/m
−1
−2
−3
−4
t(min)
30
40
50
h/m
0
200
400
600
480
500
520
540
x/km
BORE FORMATION
2
1
0
η/m
−1
−2
−3
−4
t(min)
45
50
55
60
h/m
0
30
60
528
532
536
540
544
x/km

Modal approach - sketch

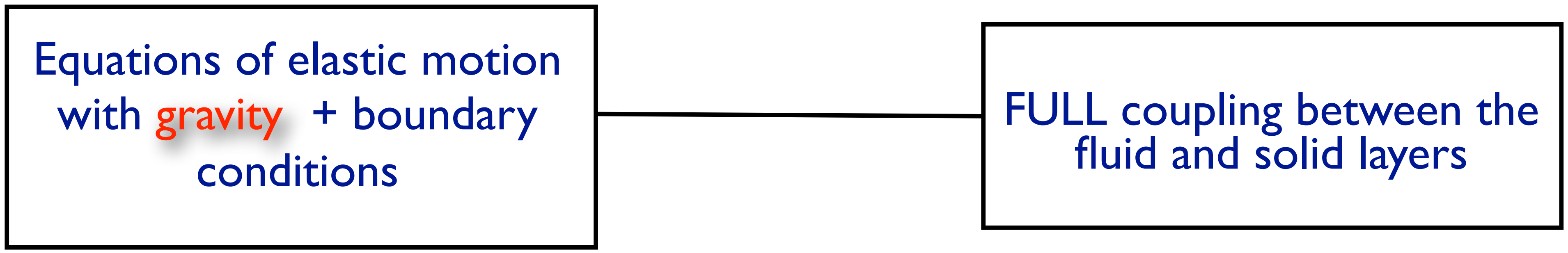

Modal approach - sketch

Equations of elastic motion with gravity + boundary conditions

FULL coupling between the fluid and solid layers

Eigenvalues
&
Eigenfunctions

Modal approach - sketch

Equations of elastic motion with gravity + boundary conditions

FULL coupling between the fluid and solid layers

Eigenvalues
&
Eigenfunctions

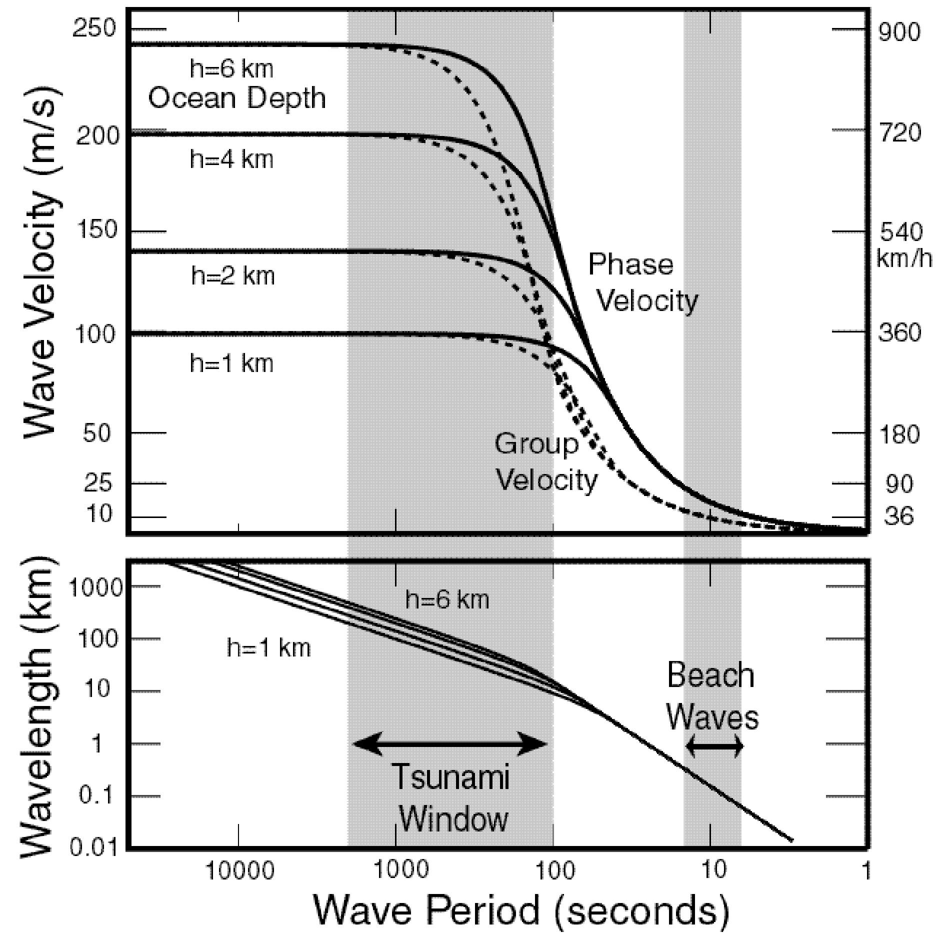

Modal approach - sketch

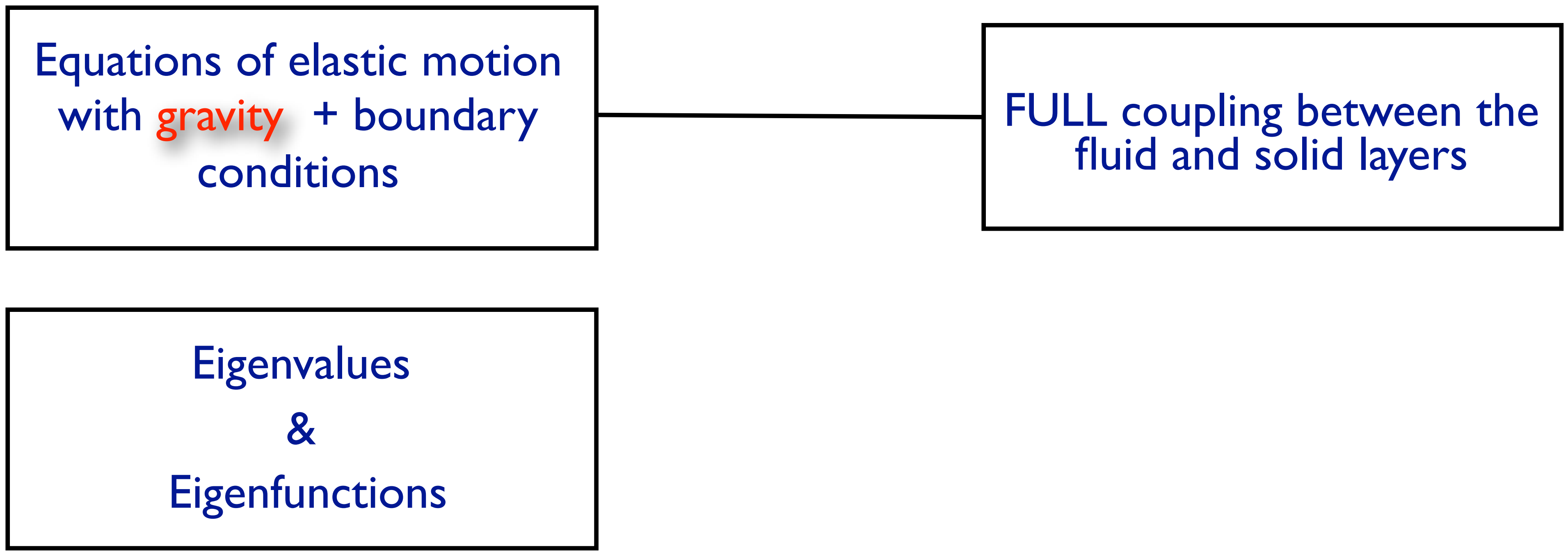

Modal approach - sketch

Equations of elastic motion with gravity + boundary conditions

FULL coupling between the fluid and solid layers

Eigenvalues
&
Eigenfunctions

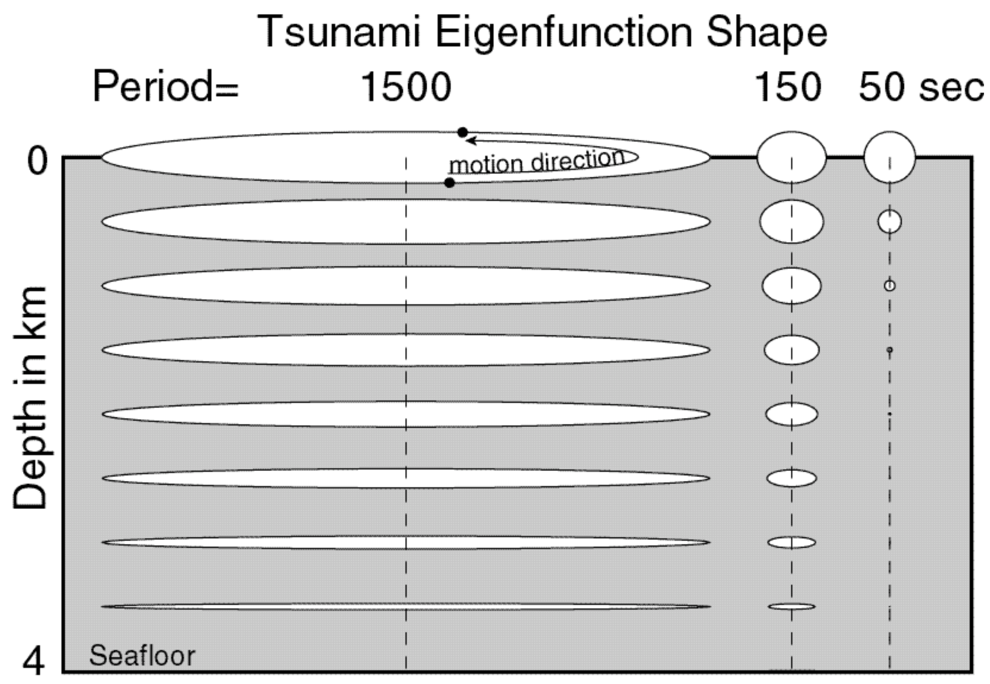

Modal approach - sketch

Equations of elastic motion with gravity + boundary conditions

FULL coupling between the fluid and solid layers

Eigenvalues
&
Eigenfunctions

Modal approach - sketch

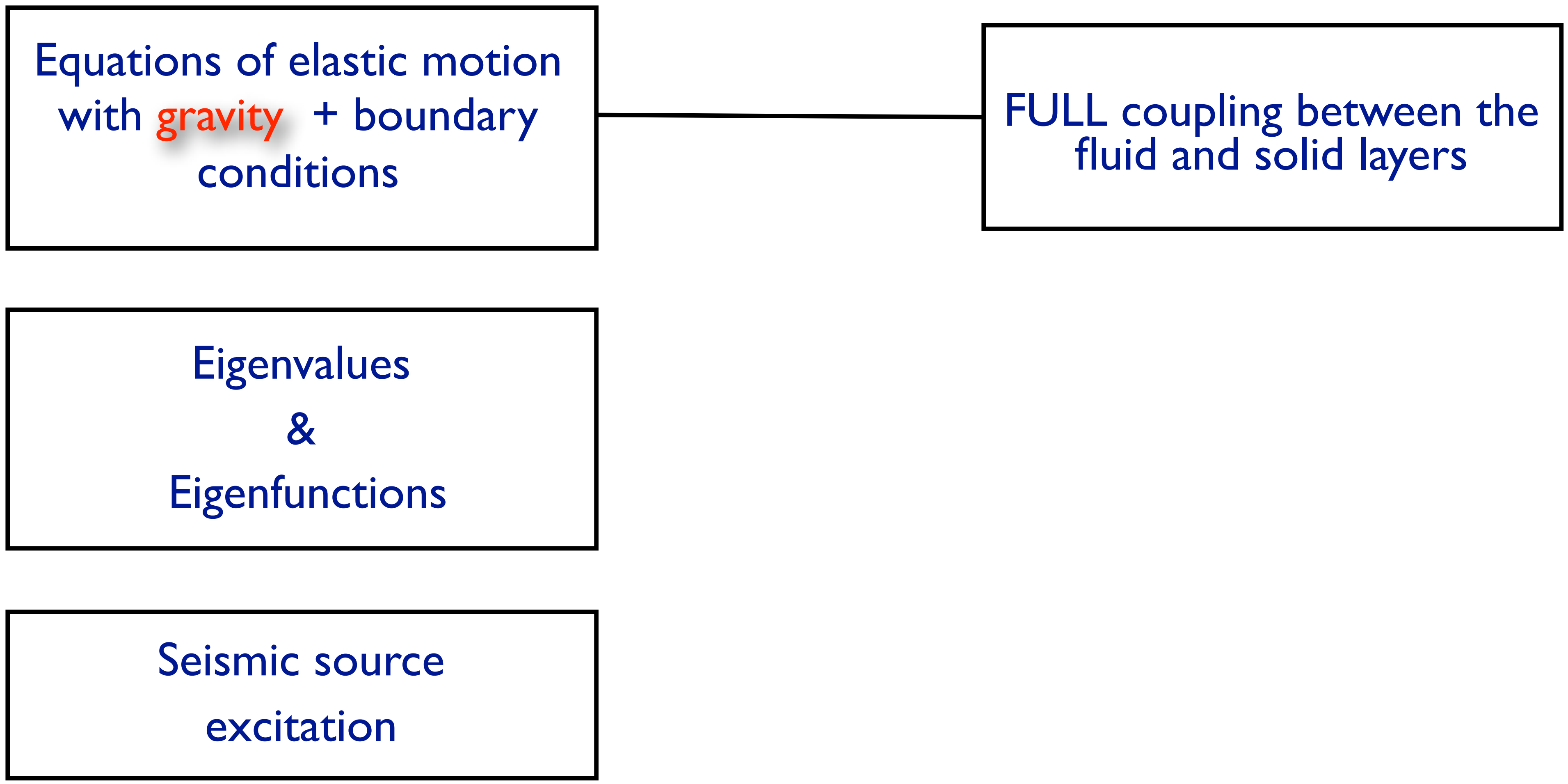

Modal approach - sketch

Equations of elastic motion with gravity + boundary conditions

FULL coupling between the fluid and solid layers

Eigenvalues
&
Eigenfunctions

Seismic source excitation

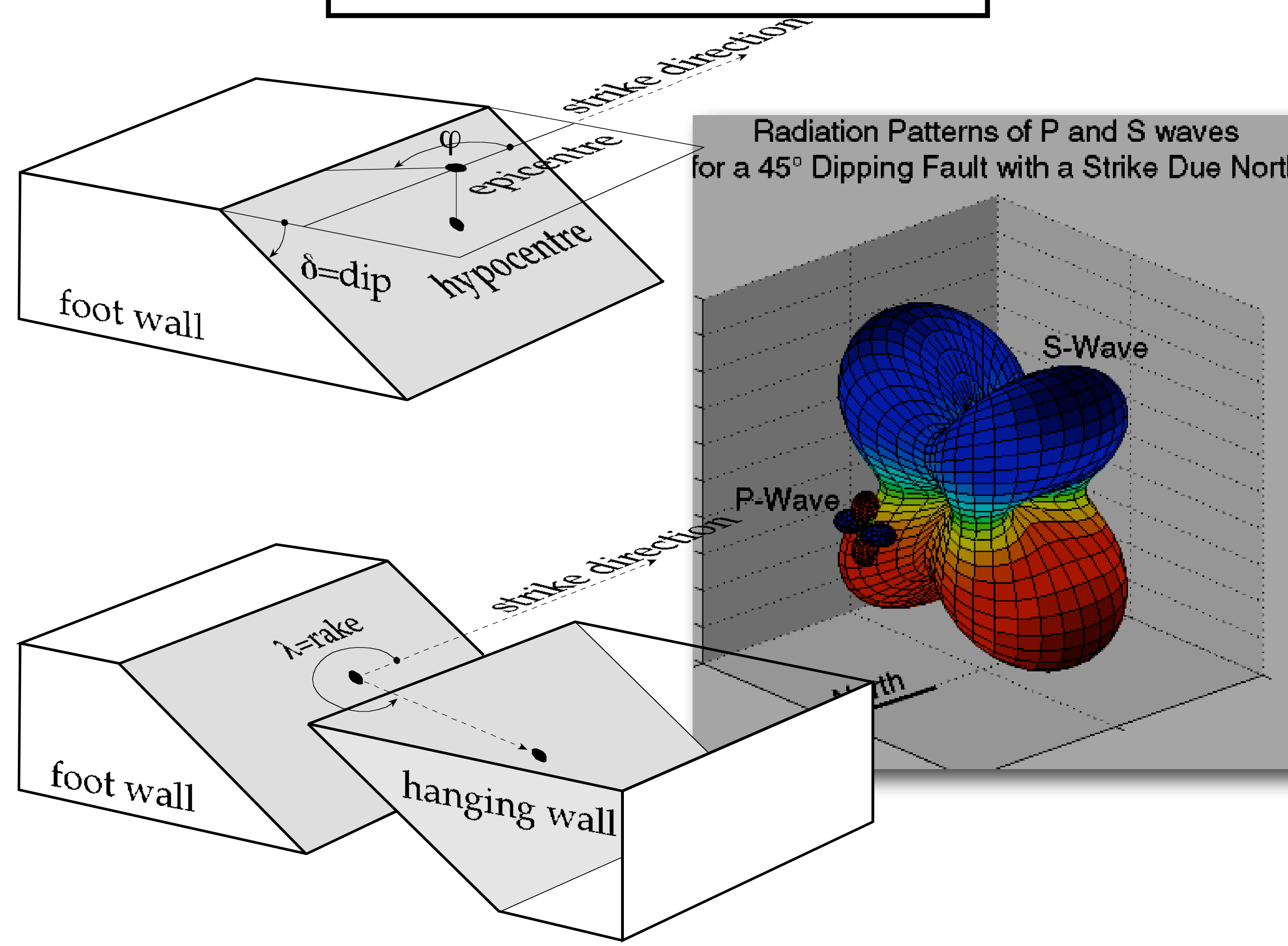

Modal approach - sketch

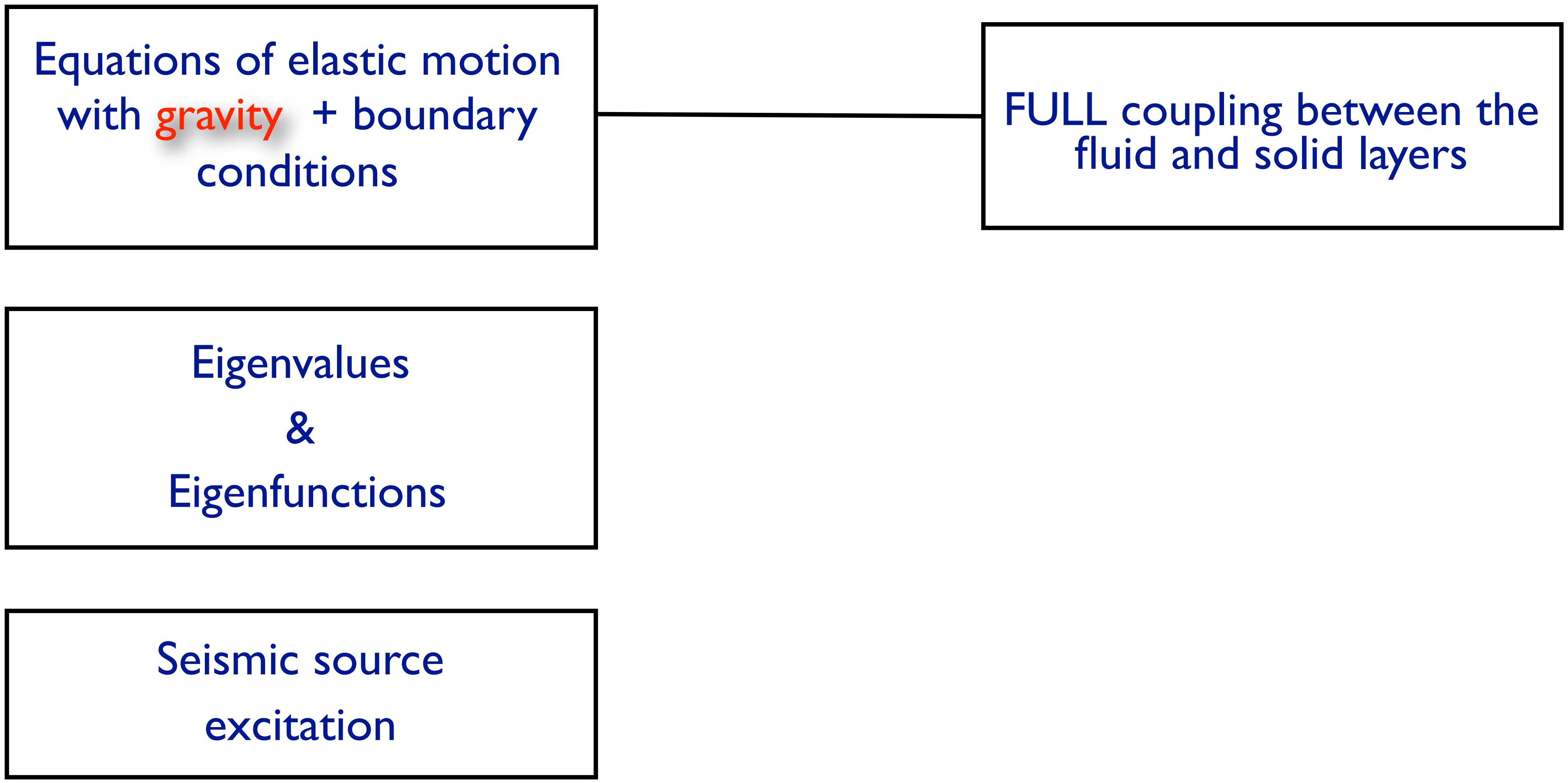

Modal approach - sketch

Equations of elastic motion with gravity + boundary conditions

FULL coupling between the fluid and solid layers

Eigenvalues
&
Eigenfunctions

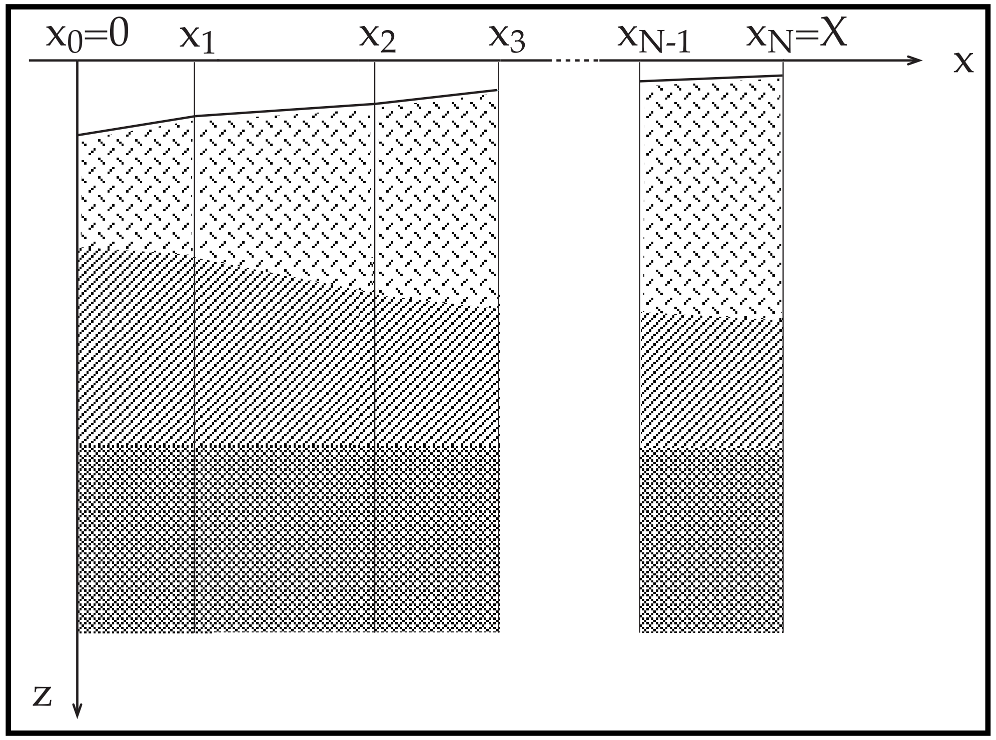

Seismic source excitation

Tsunami mode propagation in LHM

$$U(X,\varphi,z,\omega,t)=\frac{\exp(-i\pi/4)}{\sqrt{8\pi}}\,\frac{\exp[i\omega(t-\tau)]}{\sqrt{J}}\,\left.\frac{\chi(h_s,\varphi)R(\omega)}{\sqrt{\omega c\sqrt{v_g I_1}}}\right|_s\,\left.\frac{u(z,\omega)}{\sqrt{v_g I_1}}\right|_X$$

Modal approach - sketch

Equations of elastic motion with gravity + boundary conditions

FULL coupling between the fluid and solid layers

Eigenvalues
&
Eigenfunctions

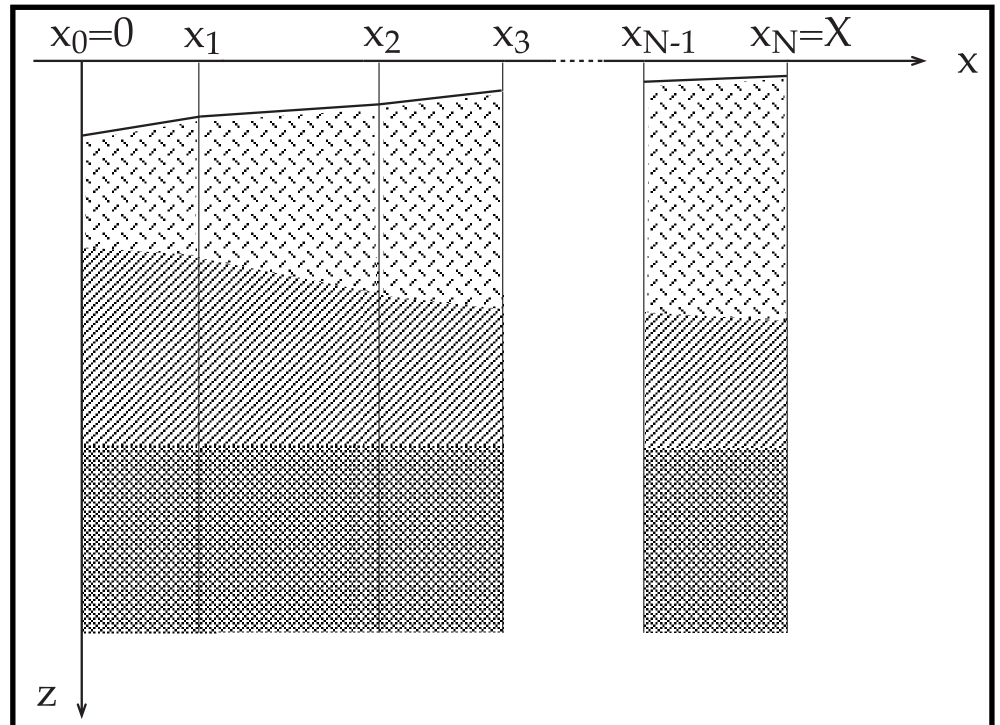

Seismic source excitation

Tsunami mode propagation in LHM

Propagation factor

Excitation factor

Receiver factor

$$U(X,\varphi,z,\omega,t)=\frac{\exp(-i\pi/4)}{\sqrt{8\pi}}\;\frac{\exp[i\omega(t-\tau)]}{\sqrt{J}}\;\left.\frac{\chi(h_s,\varphi)R(\omega)}{\sqrt{\omega c\sqrt{v_g I_1}}}\right|_s\;\left.\frac{u(z,\omega)}{\sqrt{v_g I_1}}\right|_X$$

Modal approach: formulation

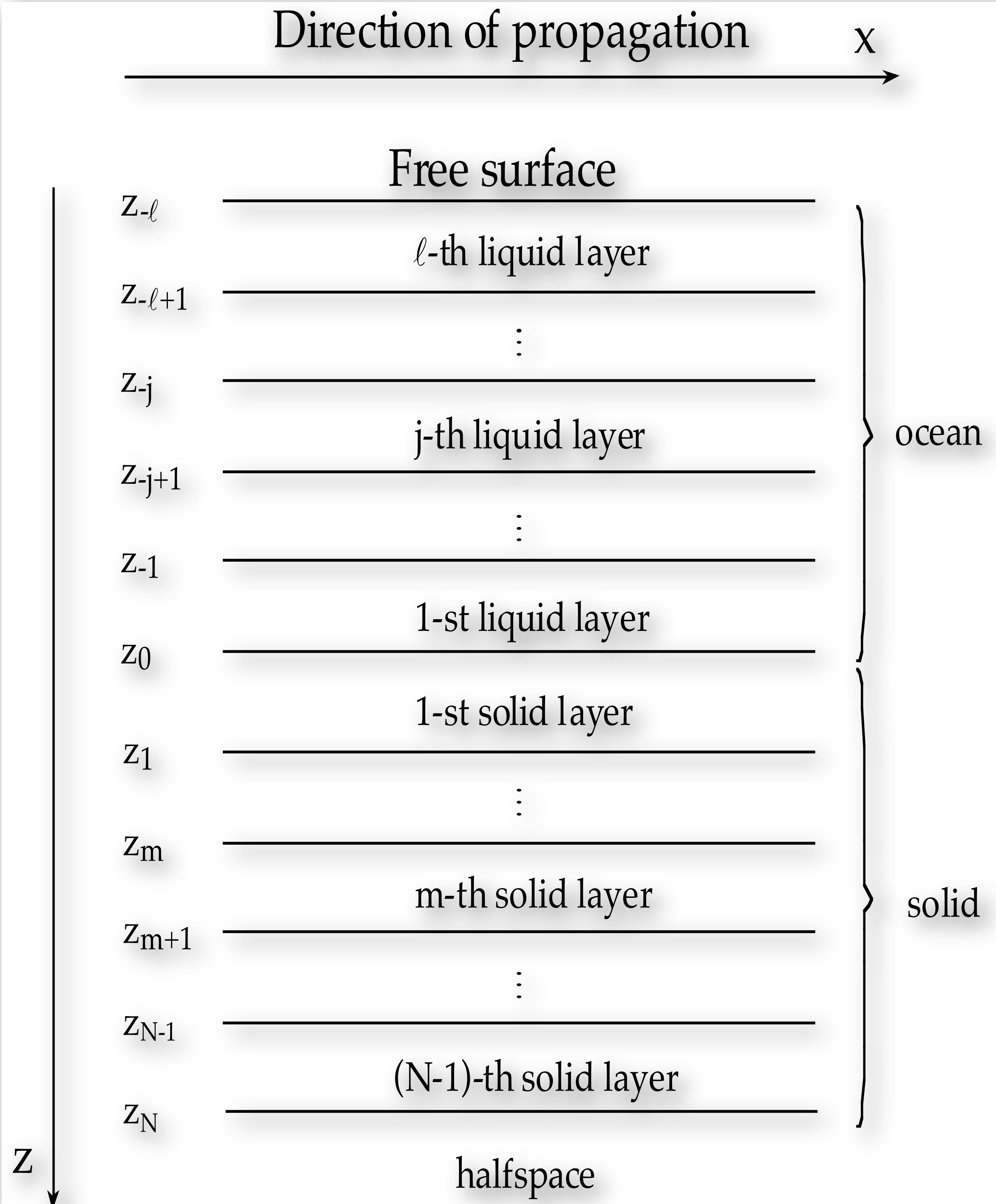

- **EQUATIONS OF MOTION**

$$\alpha^2\nabla(\nabla\cdot\mathbf{u}) - g\mathbf{e}_z\nabla\cdot\mathbf{u} = \frac{\partial^2\mathbf{u}}{\partial t^2}$$

$$\alpha^2\nabla(\nabla\cdot\mathbf{u}) - \beta^2\nabla\times(\nabla\times\mathbf{u}) = \frac{\partial^2\mathbf{u}}{\partial t^2}$$

- **BOUNDARY CONDITIONS**

$$\alpha^2\nabla\cdot\mathbf{u} - gw = 0$$

$$w_{-j}(z_{-j}) = w_{-j-1}(z_{-j}) \qquad u_{-j}(z_{-j}) = u_{-j-1}(z_{-j})$$
$$p_{-j}(z_{-j} + w_{-j}) = p_{-j-1}(z_{-j} + w_{-j-1})$$

$$w_{-1}(z_0) = w_1(z_0)$$
$$p_{-1}(z_0) = \sigma_1(z_0) \qquad 0 = \tau_1(z_0)$$

$$w_m(z_m) = w_{m+1}(z_m) \qquad u_m(z_m) = u_{m+1}(z_m)$$
$$\sigma_m(z_m) = \sigma_{m+1}(z_m) \qquad \tau_m(z_m) = \tau_{m+1}(z_m)$$

Modal approach: Eigenvalues

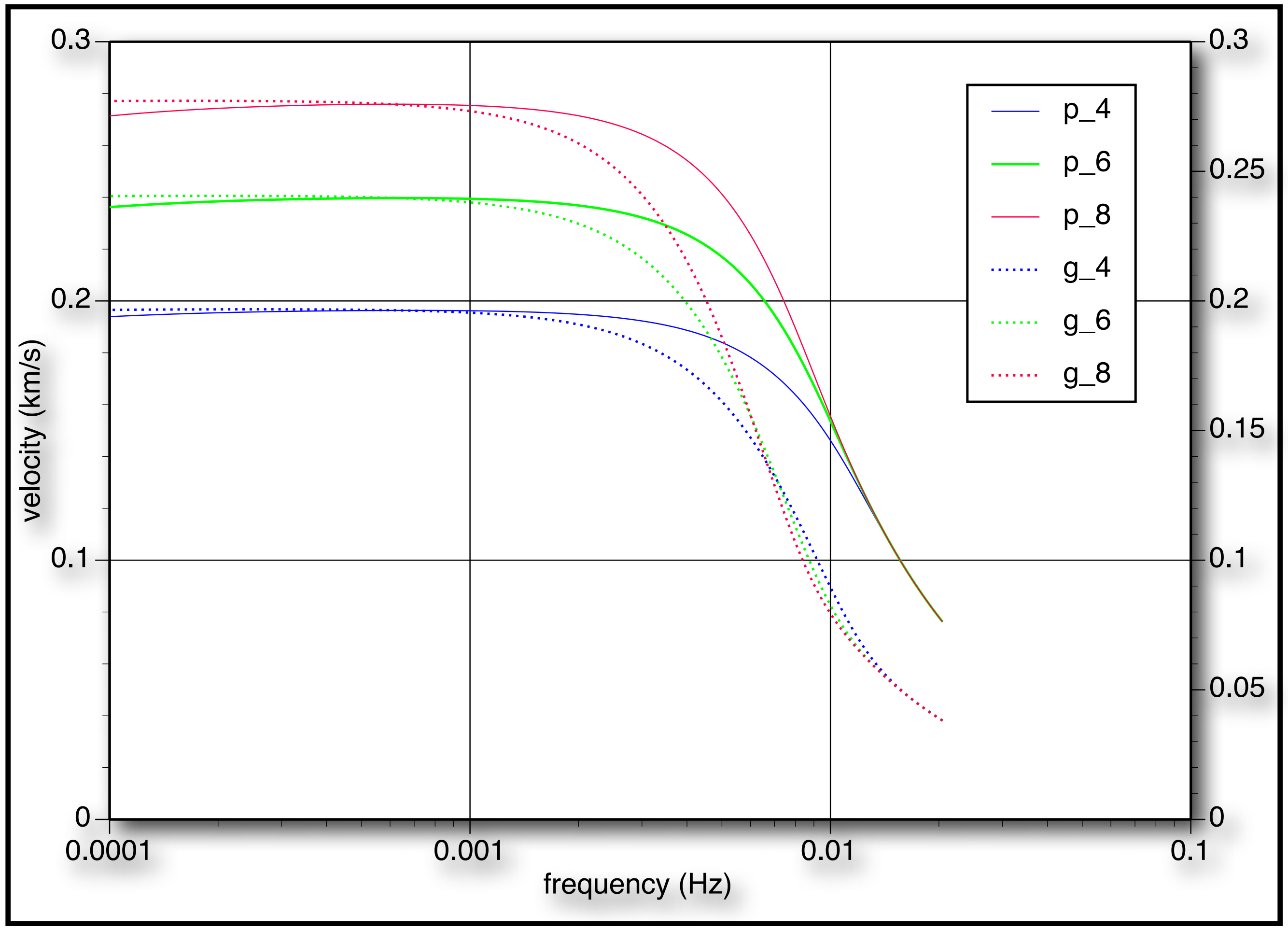

Modal approach: Eigenvalues

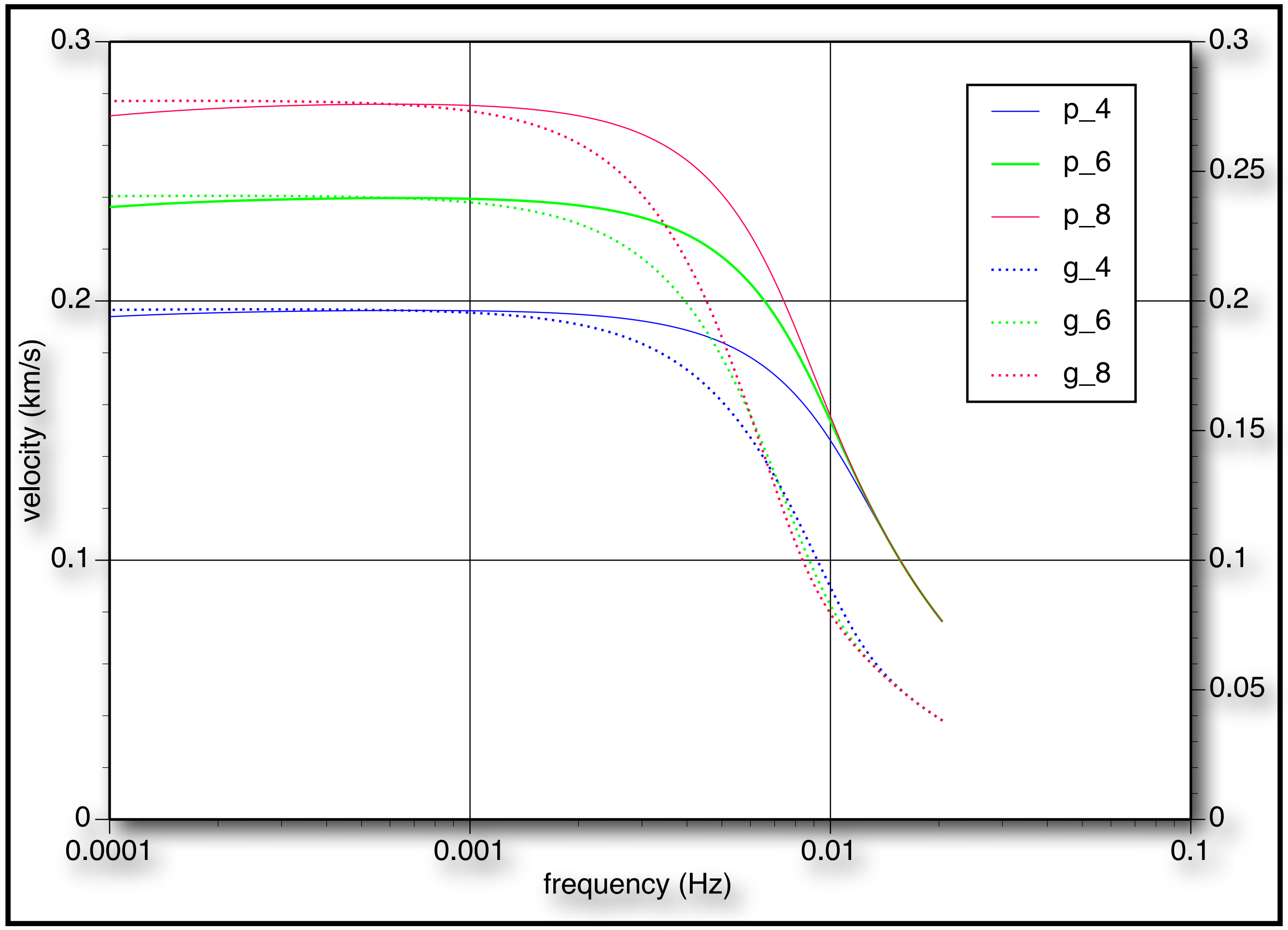

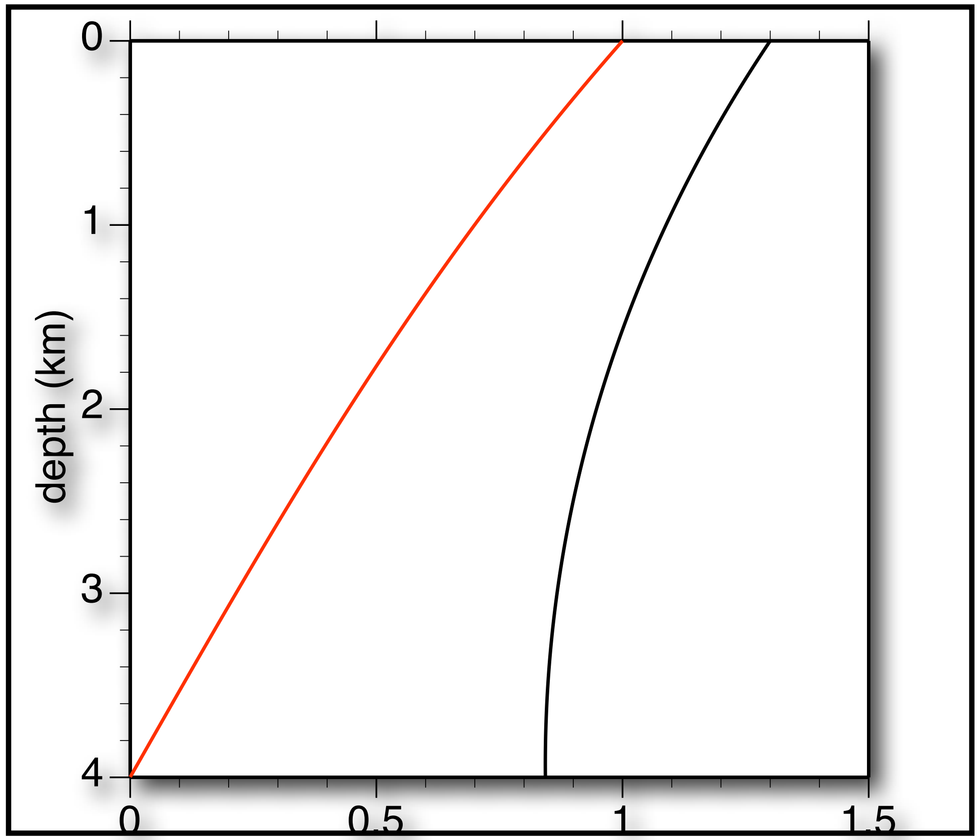

Eigenfunctions of the radial and vertical (normalized to 1 at the free-surface) component of motion at frequency equal to 0.007 Hz, in the fluid. The curves for three crustal models 1, 2 and 3, are totally overlapped; on the bottom, the eigenfunctions in the solid layers are shown

Modal approach: Eigenvalues

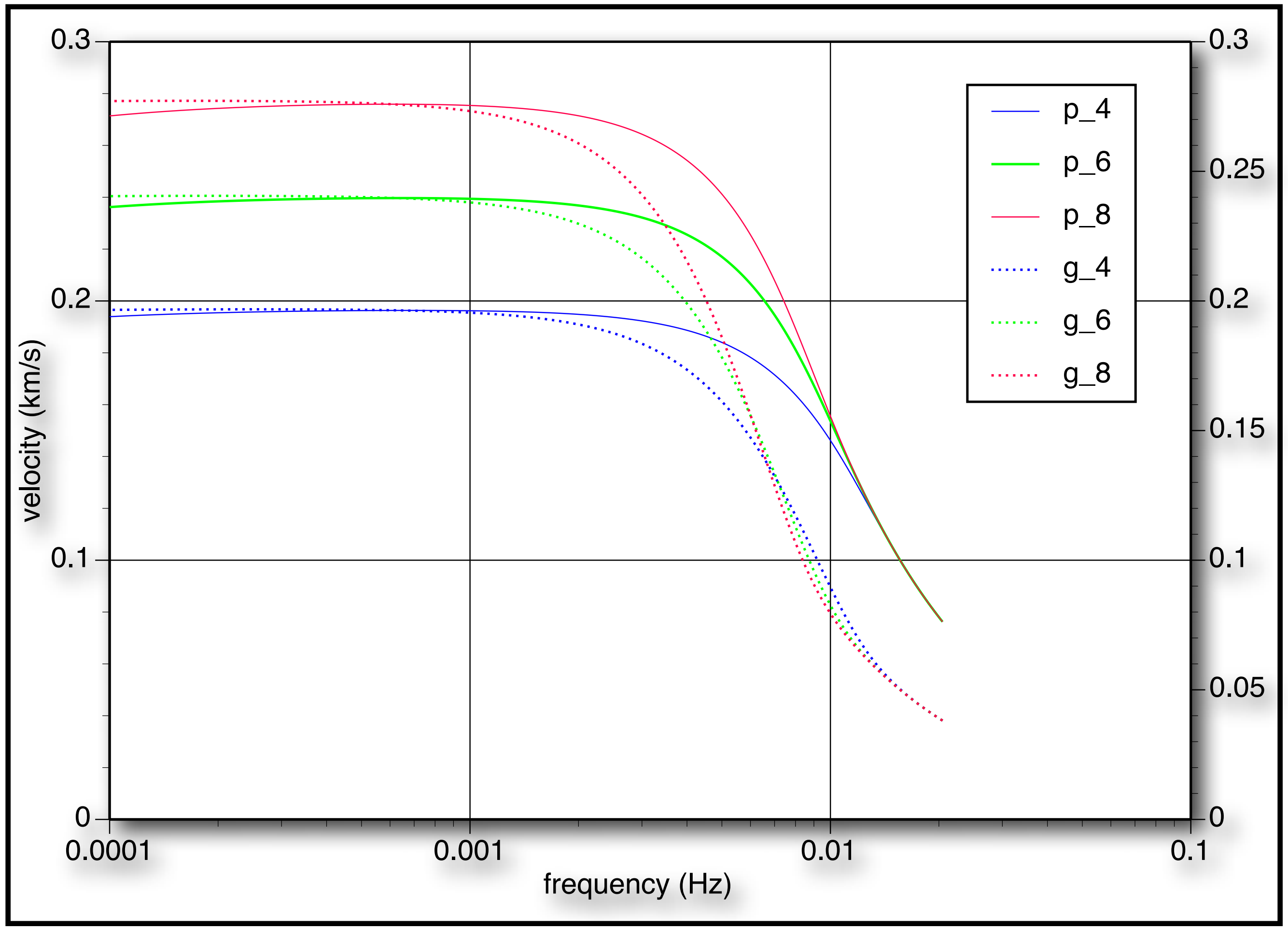

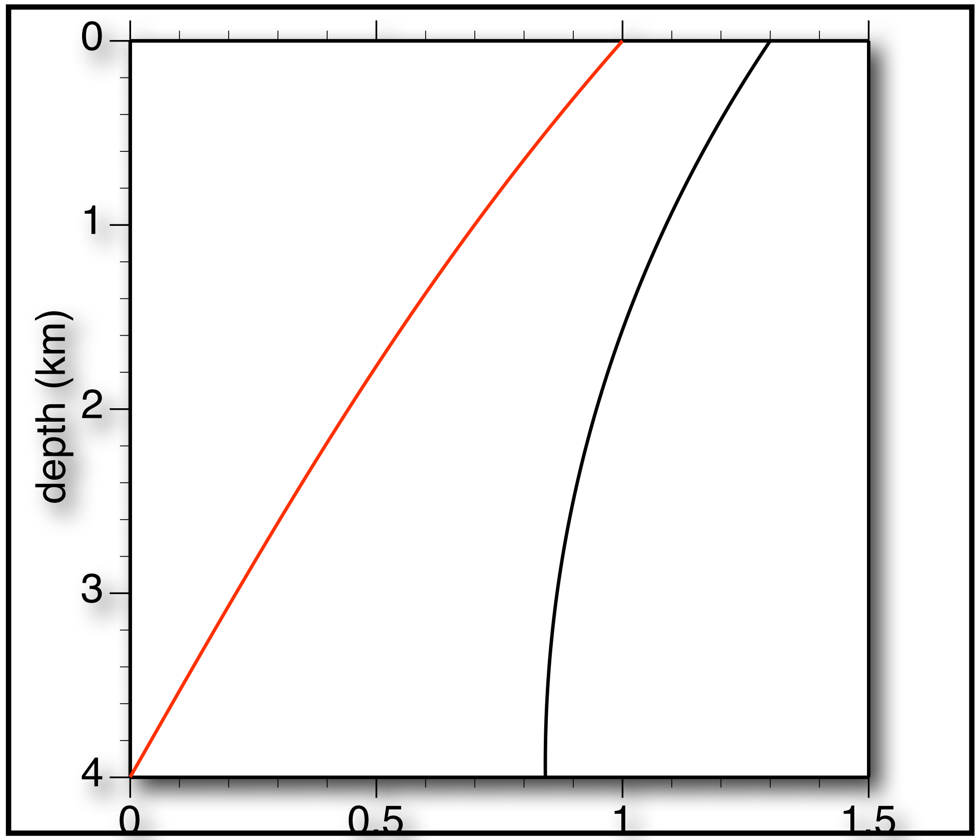

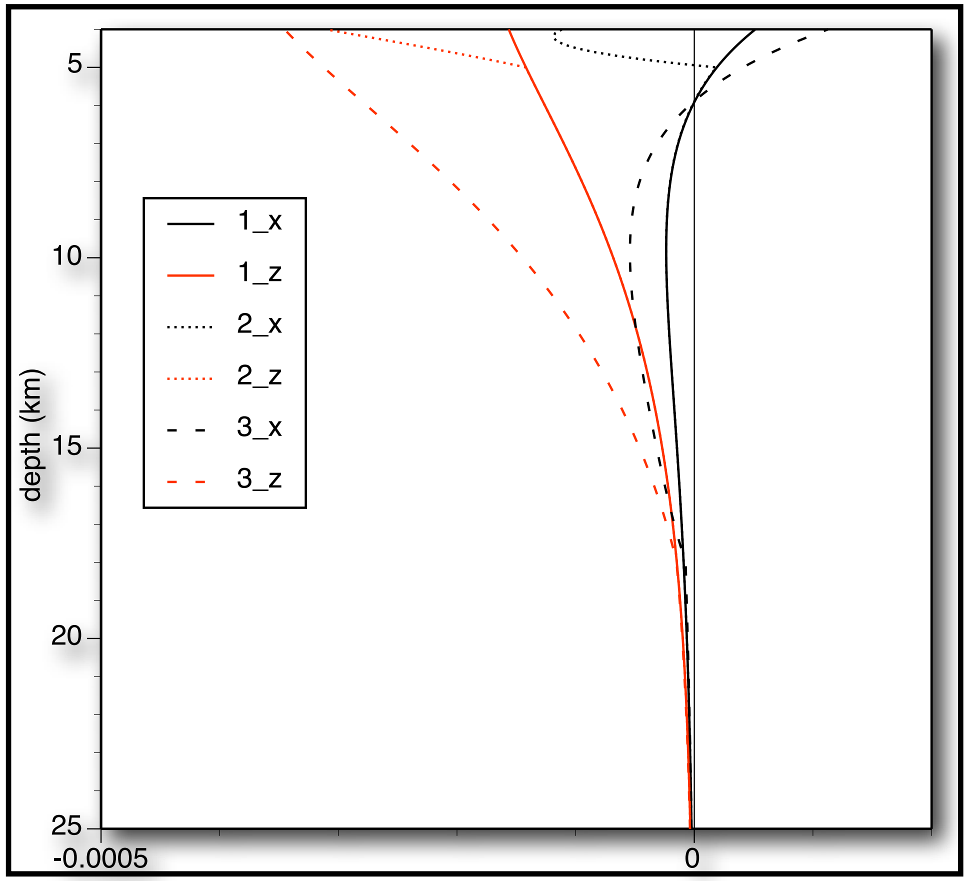

Eigenfunctions of the radial and vertical (normalized to 1 at the free-surface) component of motion at frequency equal to 0.007 Hz, in the fluid. The curves for three crustal models 1, 2 and 3, are totally overlapped; on the bottom, the eigenfunctions in the solid layers are shown

Modal approach: excitation spectra

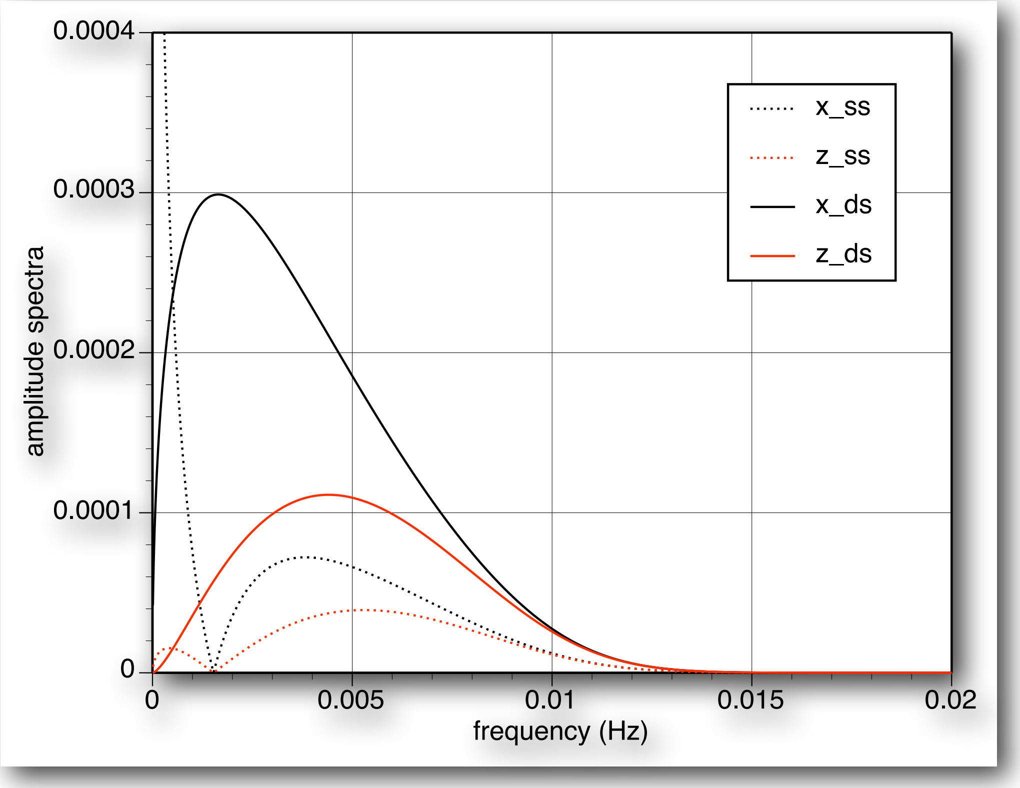

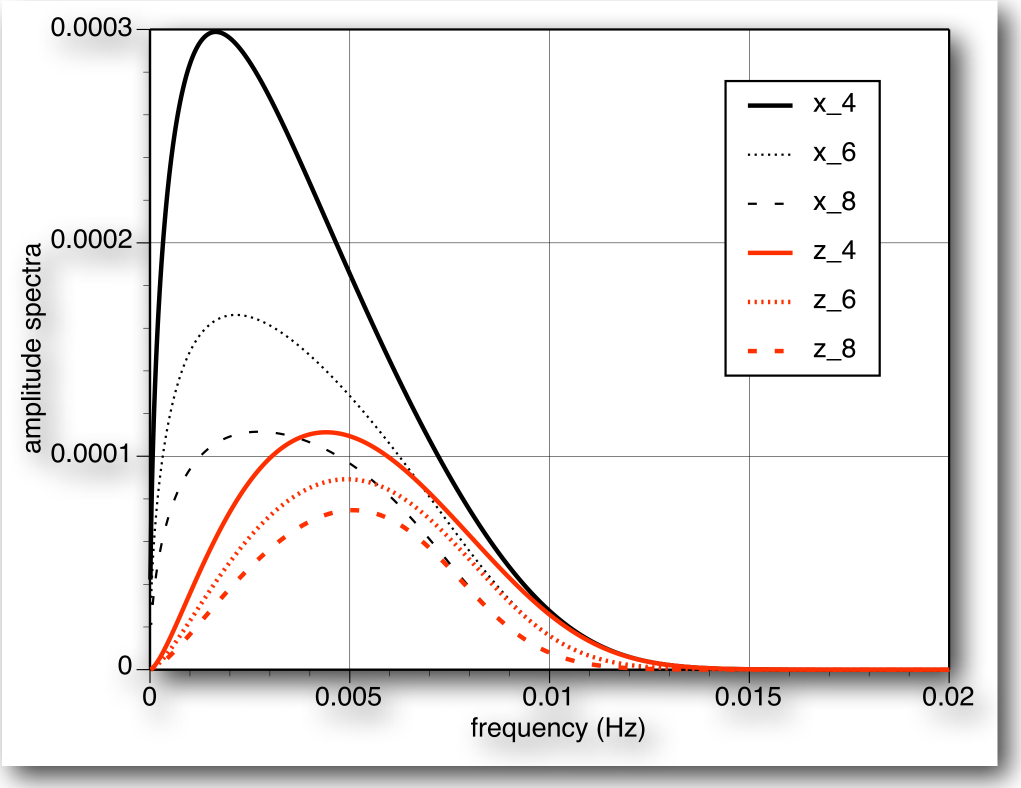

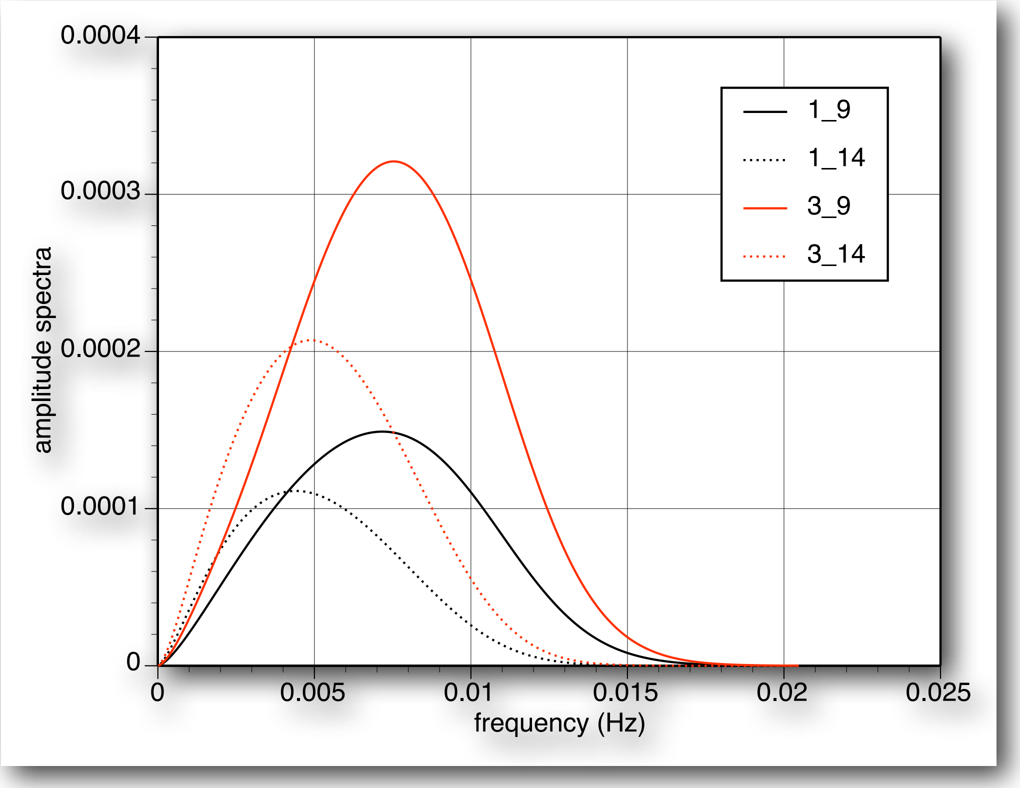

Modal approach: tsunami motion

$$\mathbf{U}(X,\varphi,z,\omega,t)=\frac{\exp(-i\pi/4)}{\sqrt{8\pi}}\frac{\exp[i\omega(t-X/c)]}{\sqrt{X}}\frac{\chi(h_s,\varphi)R(\omega)}{\sqrt{\omega c}\sqrt{v_g I_1}}\frac{\mathbf{u}(z,\omega)}{\sqrt{v_g I_1}}$$

- **SHOALING FACTOR**

$$\left|\frac{W(X_2,0,\omega)}{W(X_1,0,\omega)}\right|=\left[\frac{w(0,\omega)|_2\sqrt{v_g I_1}\Big|_1}{w(0,\omega)|_1\sqrt{v_g I_1}\Big|_2}\right]\frac{\sqrt{J_1}}{\sqrt{J_2}}\cong\sqrt[4]{\frac{H_1}{H_2}}$$

Modal approach: tsunami motion

$$\mathbf{U}(X,\varphi,z,\omega,t)=\frac{\exp(-i\pi/4)}{\sqrt{8\pi}}\;\frac{\exp[i\omega(t-X/c)]}{\sqrt{X}}\;\frac{\chi(h_s,\varphi)R(\omega)}{\sqrt{\omega c}\sqrt{v_g I_1}}\;\frac{\mathbf{u}(z,\omega)}{\sqrt{v_g I_1}}$$

$$\mathbf{U}(X,\varphi,z,\omega,t)=\frac{\exp(-i\pi/4)}{\sqrt{8\pi}}\;\frac{\exp[i\omega(t-\tau)]}{\sqrt{J}}\;\left.\frac{\chi(h_s,\varphi)R(\omega)}{\sqrt{\omega c}\sqrt{v_g I_1}}\right|_s\;\left.\frac{\mathbf{u}(z,\omega)}{\sqrt{v_g I_1}}\right|_X$$

- **SHOALING FACTOR**

$$\left|\frac{W(X_2,0,\omega)}{W(X_1,0,\omega)}\right|=\left[\frac{w(0,\omega)|_2\sqrt{v_g I_1}\Big|_1}{w(0,\omega)|_1\sqrt{v_g I_1}\Big|_2}\right]\frac{\sqrt{J_1}}{\sqrt{J_2}}\cong\sqrt[4]{\frac{H_1}{H_2}}$$

Modal approach: tsunami motion

$$\mathbf{U}(X,\varphi,z,\omega,t) = \frac{\exp(-i\pi/4)}{\sqrt{8\pi}} \frac{\exp[i\omega(t - X/c)]}{\sqrt{X}} \frac{\chi(h_s,\varphi)R(\omega)}{\sqrt{\omega c}\sqrt{v_g I_1}} \frac{\mathbf{u}(z,\omega)}{\sqrt{v_g I_1}}$$

$$\mathbf{U}(X,\varphi,z,\omega,t) = \frac{\exp(-i\pi/4)}{\sqrt{8\pi}} \frac{\exp[i\omega(t - \tau)]}{\sqrt{J}} \left.\frac{\chi(h_s,\varphi)R(\omega)}{\sqrt{\omega c}\sqrt{v_g I_1}}\right|_s \left.\frac{\mathbf{u}(z,\omega)}{\sqrt{v_g I_1}}\right|_X$$

- **SHOALING FACTOR**

$$\left|\frac{W(X_2,0,\omega)}{W(X_1,0,\omega)}\right| = \left[\frac{w(0,\omega)|_2 \sqrt{v_g I_1}\big|_1}{w(0,\omega)|_1 \sqrt{v_g I_1}\big|_2}\right] \frac{\sqrt{J_1}}{\sqrt{J_2}} \cong \sqrt[4]{\frac{H_1}{H_2}}$$

Modal approach: tsunami signals

Example: synthetic signals for the tsunami mode (vertical component) excited by a dip-slip mechanism with M_0=2.2 10^{21} Nm. h_s = 14 km; h_s = 34 km.

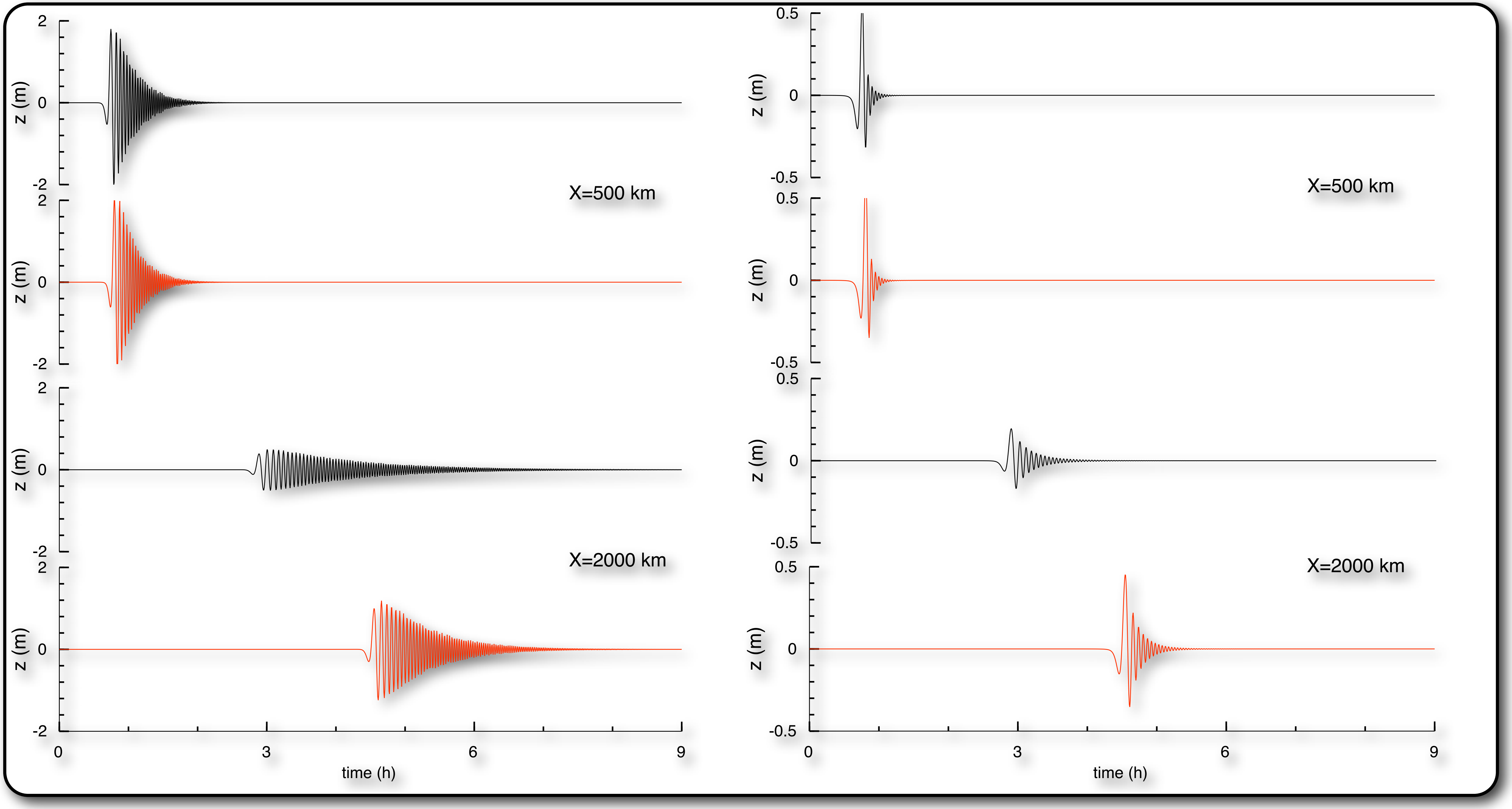

For each of the two source-receiver distances considered, the upper trace refers to the 1-D model and the lower trace to a laterally varying model. In the laterally varying model the liquid layer is getting thinner with increasing distance from the source, with a gradient of 0.00175 and the uppermost solid layer is compensating this thinning.

Modal approach: tsunami signals

Example:Sketch of a laterally heterogeneous model for a realistic scenario. Synthetic mareograms (vertical) calculated at various distances along the section.
The extension of zone C is 500 km.

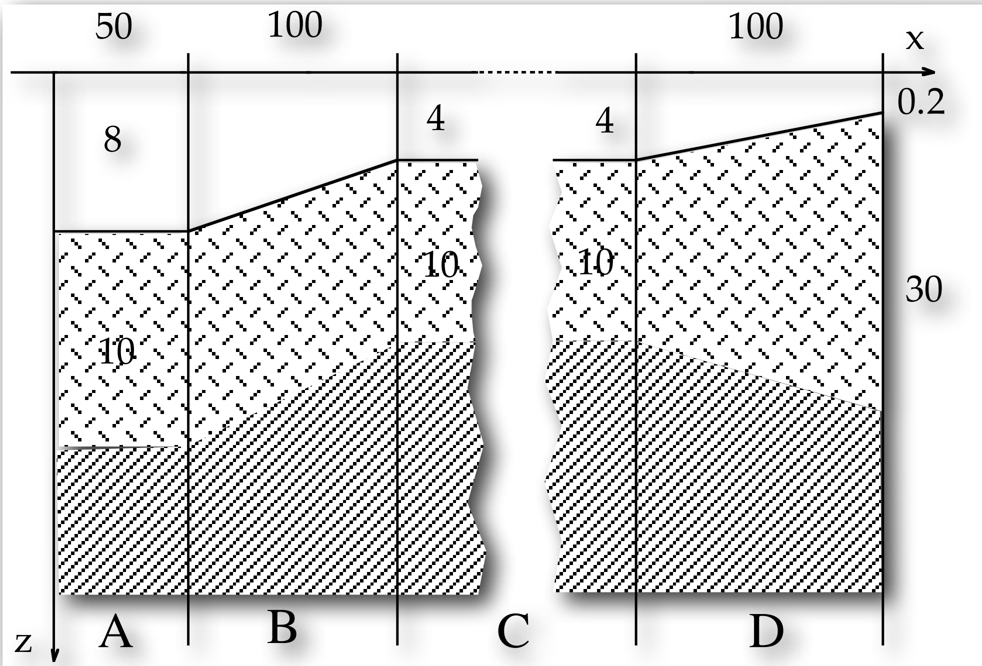

Modal approach: tsunami signals

Example:Sketch of a laterally heterogeneous model for a realistic scenario. Synthetic mareograms (vertical) calculated at various distances along the section.
The extension of zone C is 500 km.

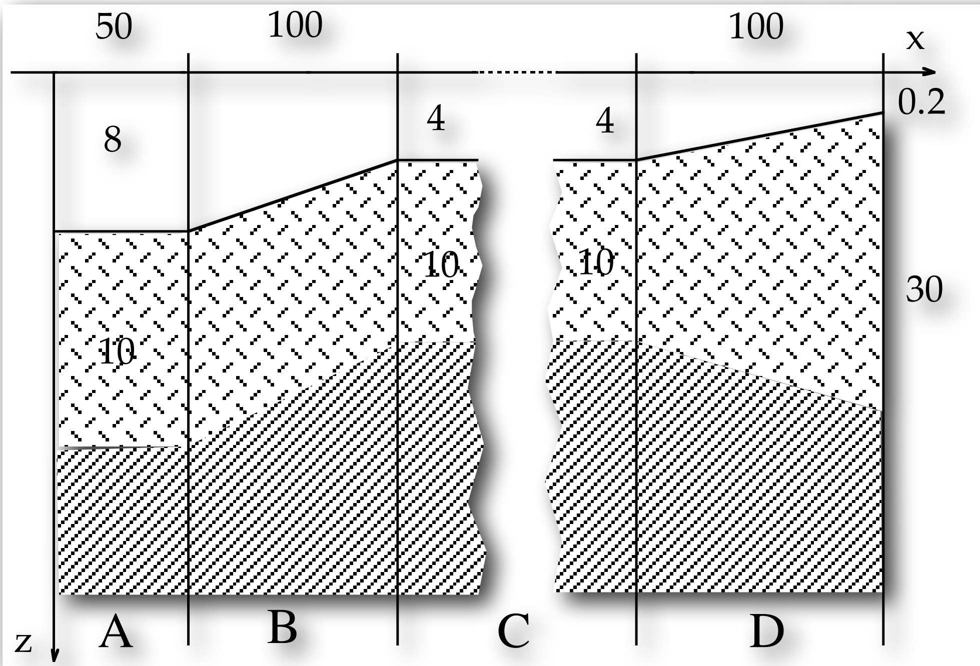

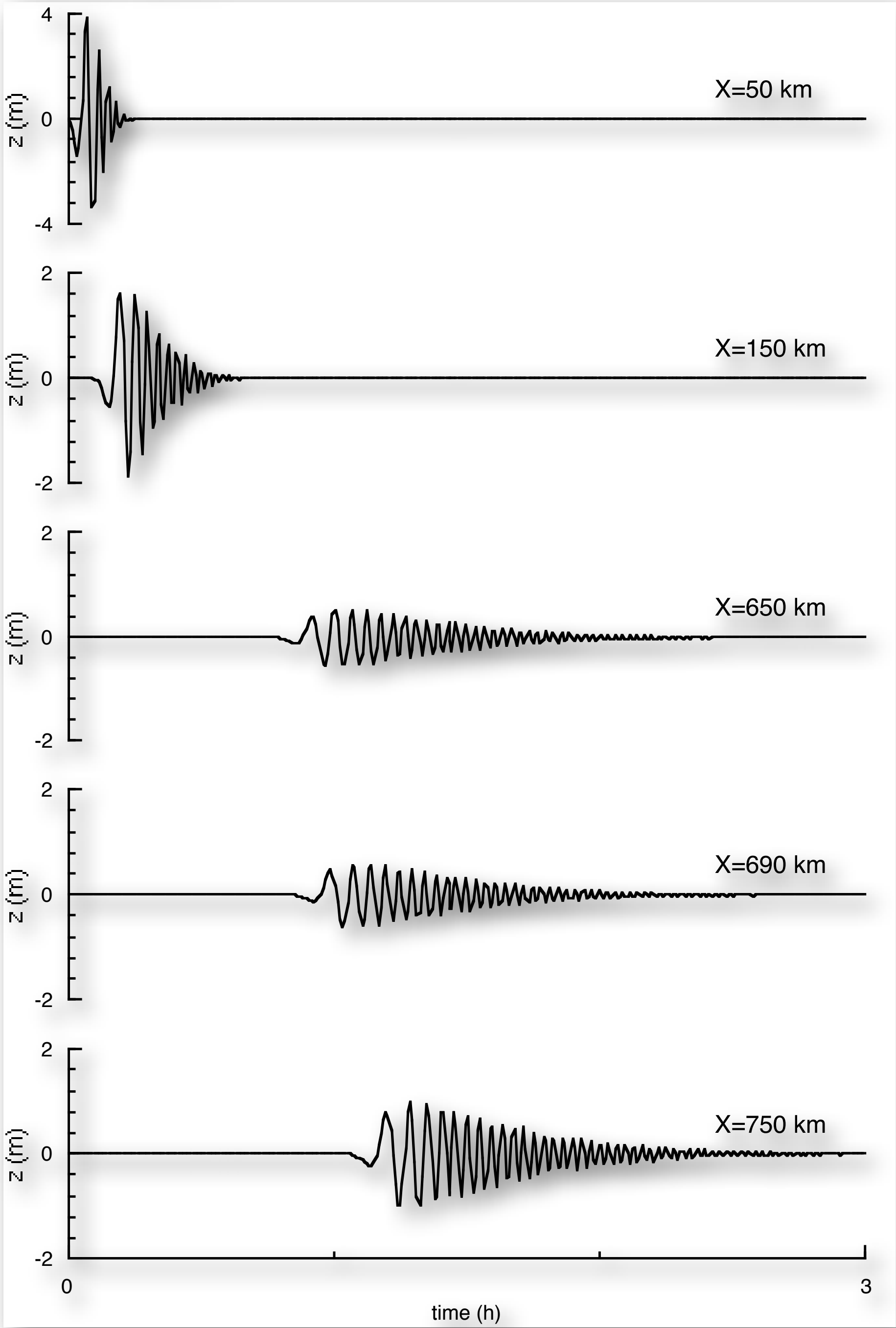

Modal approach: tsunami signals

Example:Sketch of a laterally heterogeneous model for a realistic scenario. Synthetic mareograms (vertical) calculated at various distances along the section.
The extension of zone C is 500 km.

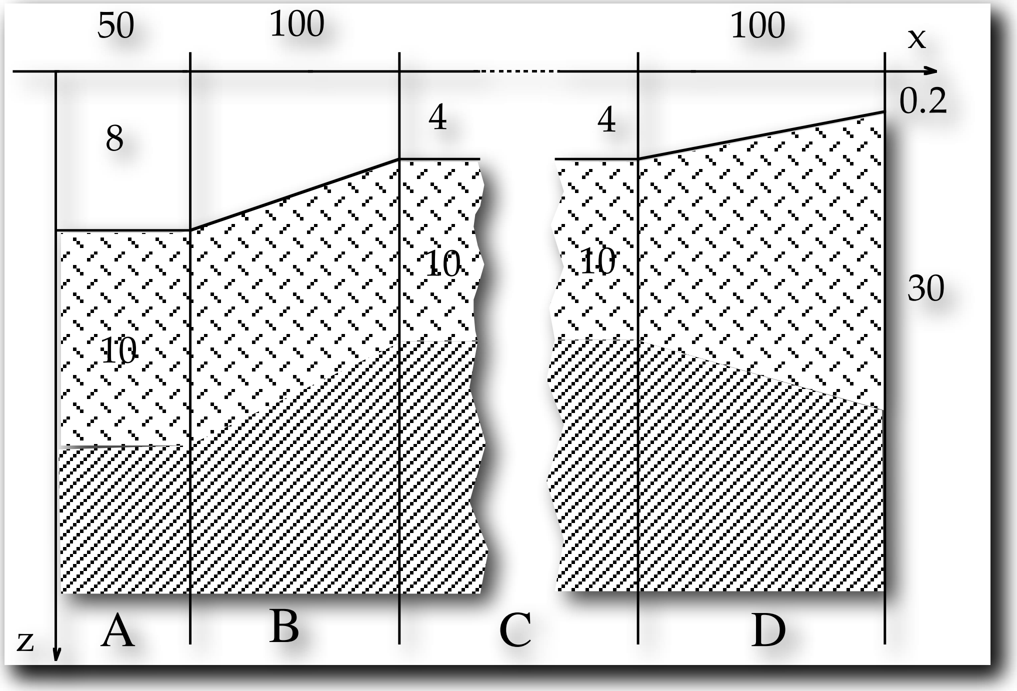

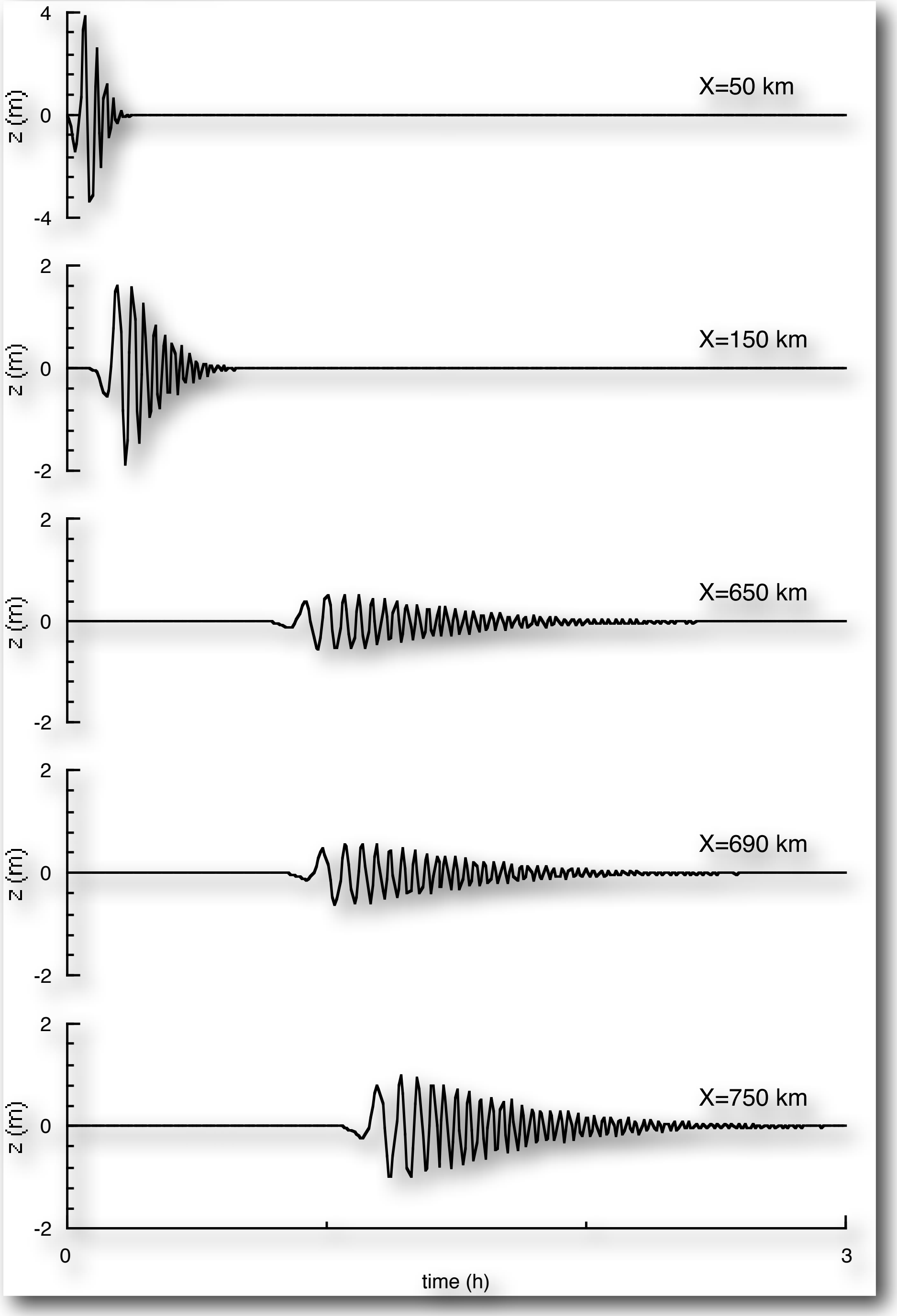

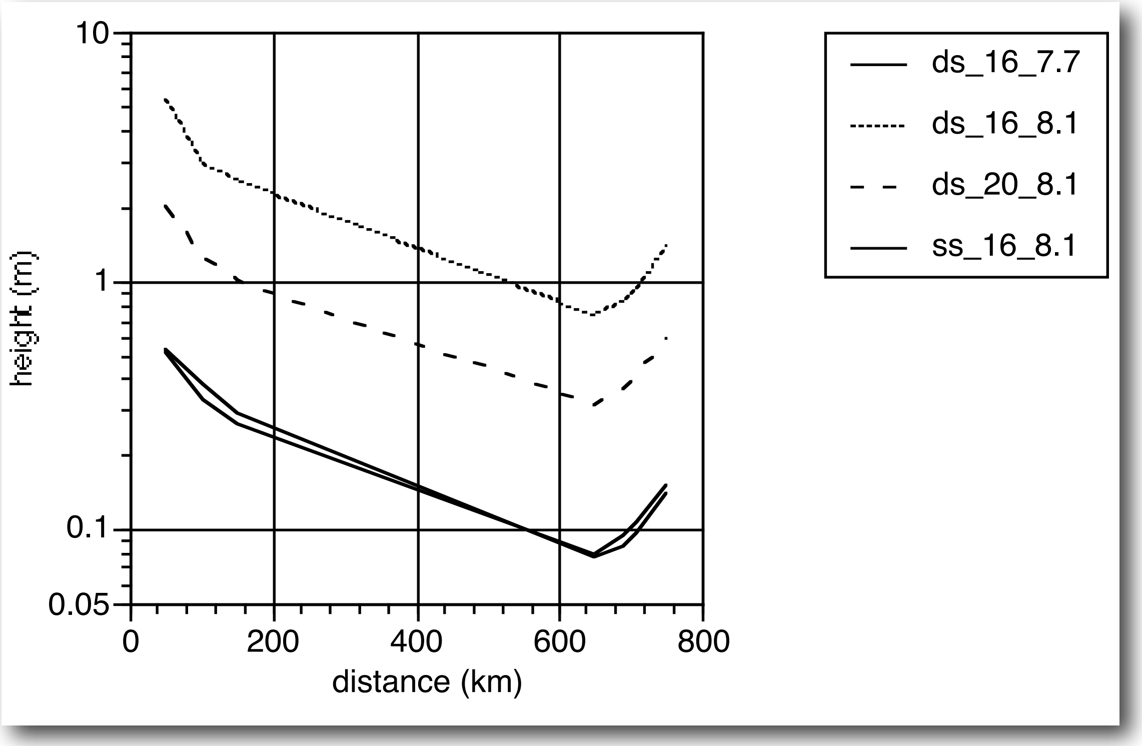

The Mediterranean Sea and Tsunamis

The Mediterranean Sea and Tsunamis

The Mediterranean Sea and Tsunamis

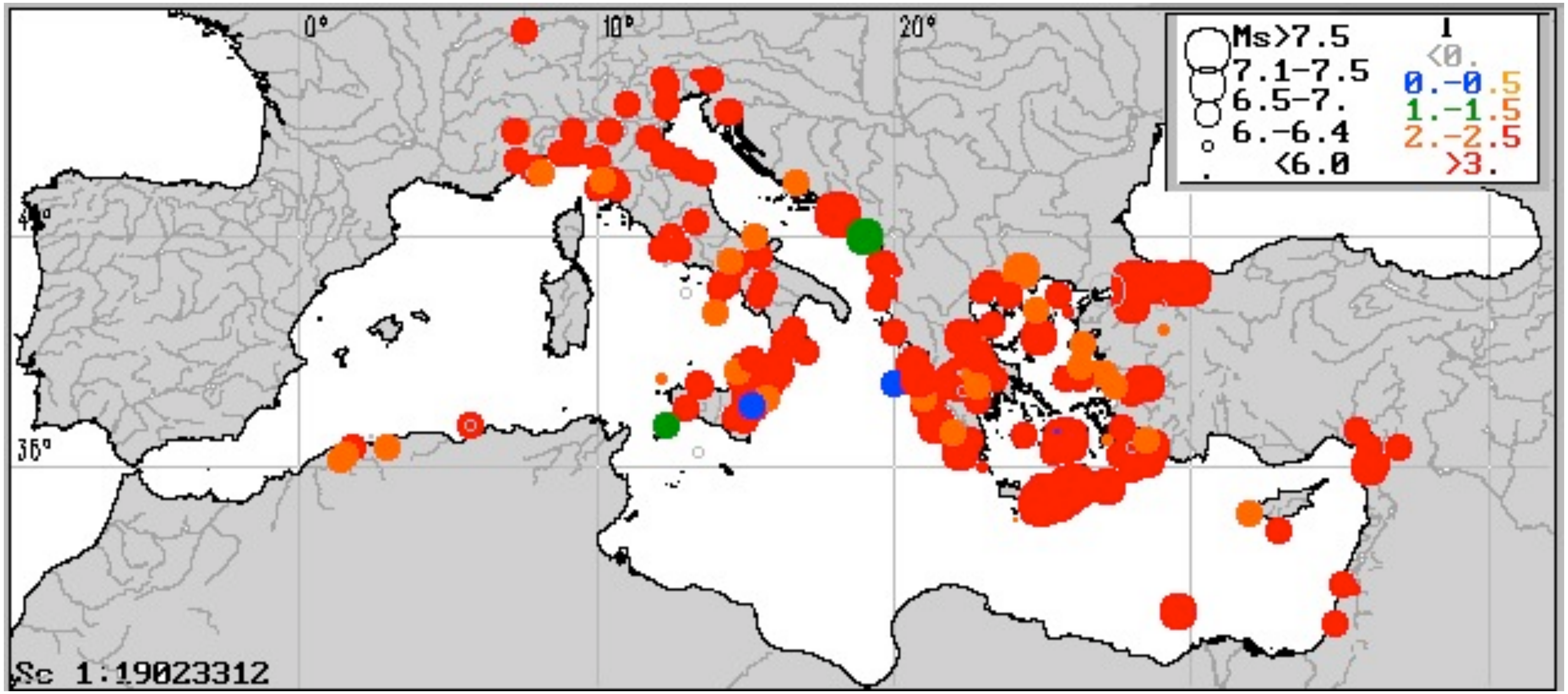

Map of epicenters of tsunamigenic earthquakes occurred since 1380 B.C. to 1996 within the Mediterranean region. The size of circles is proportional to the event magnitude, the color to the tsunami intensity

data from: 'Mediterranean Tsunami Catalog, from 1628B.C. to present of the Institute of Computational Mathematics and Mathematical Geophysics (Computing Center) Siberian Division, Russian Academy of Sciences. Tsunami Laboratory

Seismicity in the Adriatic basin

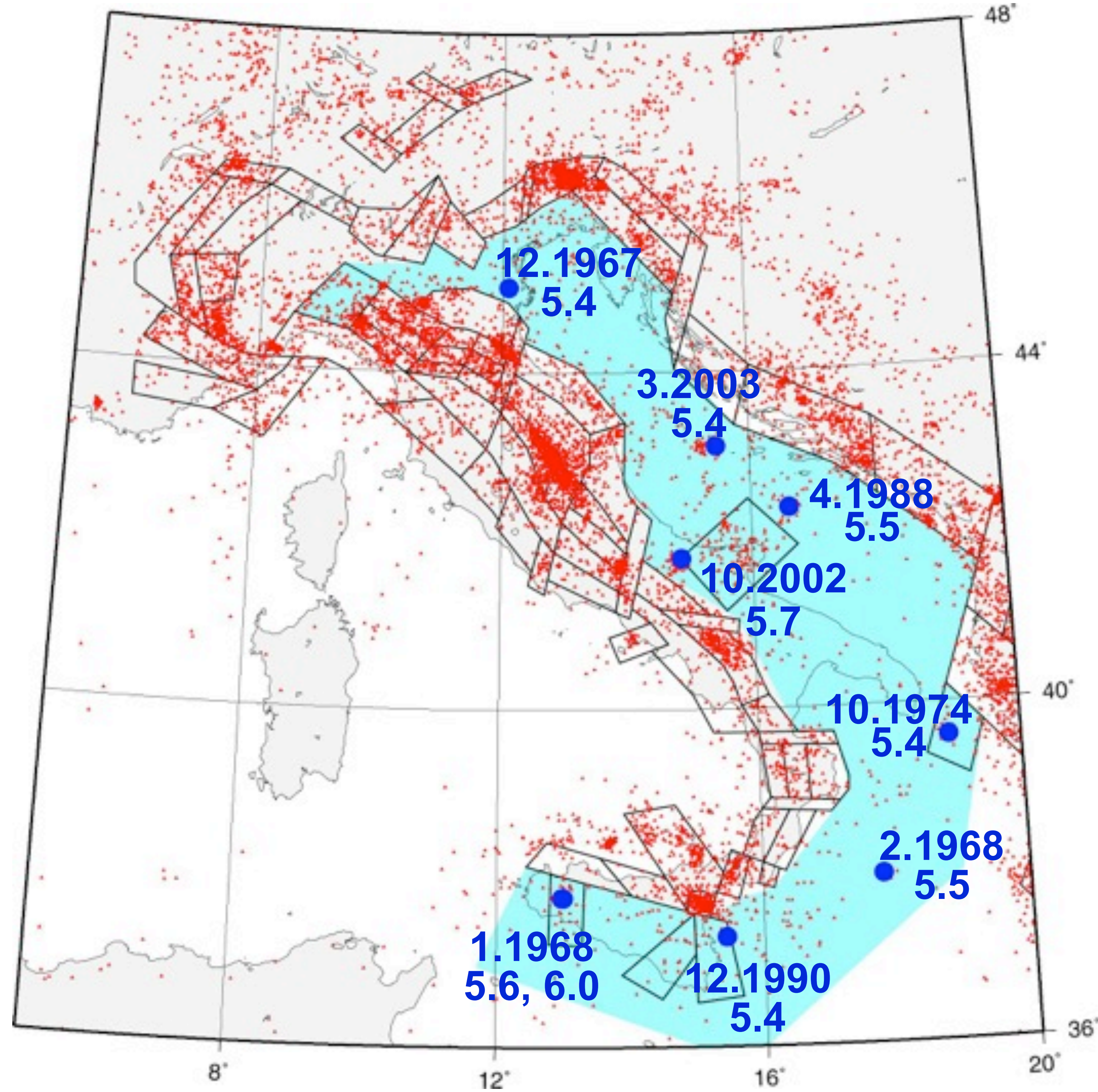

Earthquakes with M≥5.4 (1964-2004)

Historical tsunami in the Adriatic basin

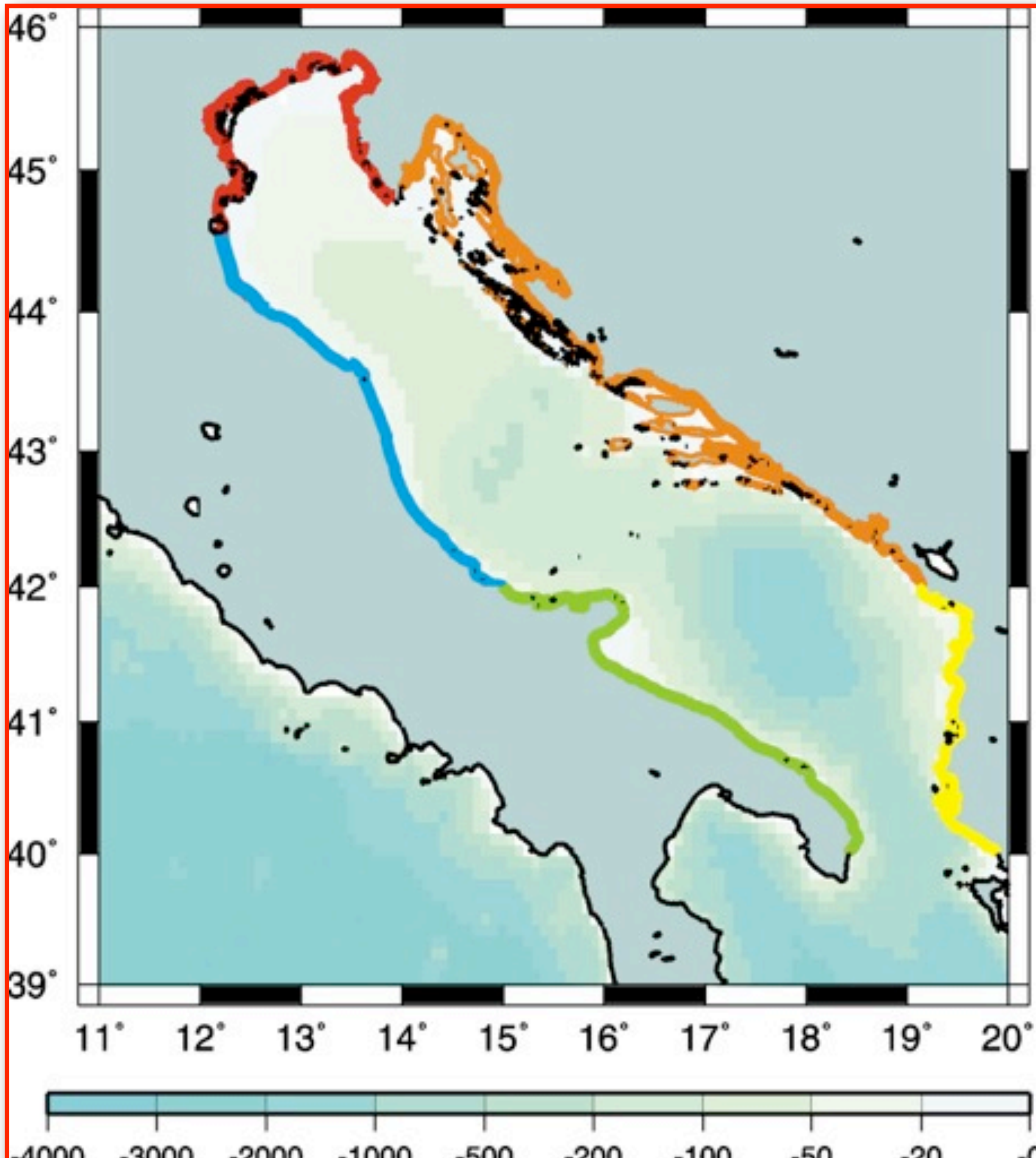

Tsunami reported in
ICTP Technical Report 2005:

CATALOGUE OF REPORTED TSUNAMI EVENTS IN THE ADRIATIC SEA
(from 58 B.C. to 1979 A.D.)

10	North-Adriatic coasts
14	Central-Adriatic Italian coasts
11	South-Adriatic Italian coasts
10	Croatian, Serbian and Montenegro coasts
13	Albanian coasts

Hazard scenarios for the Adriatic basin

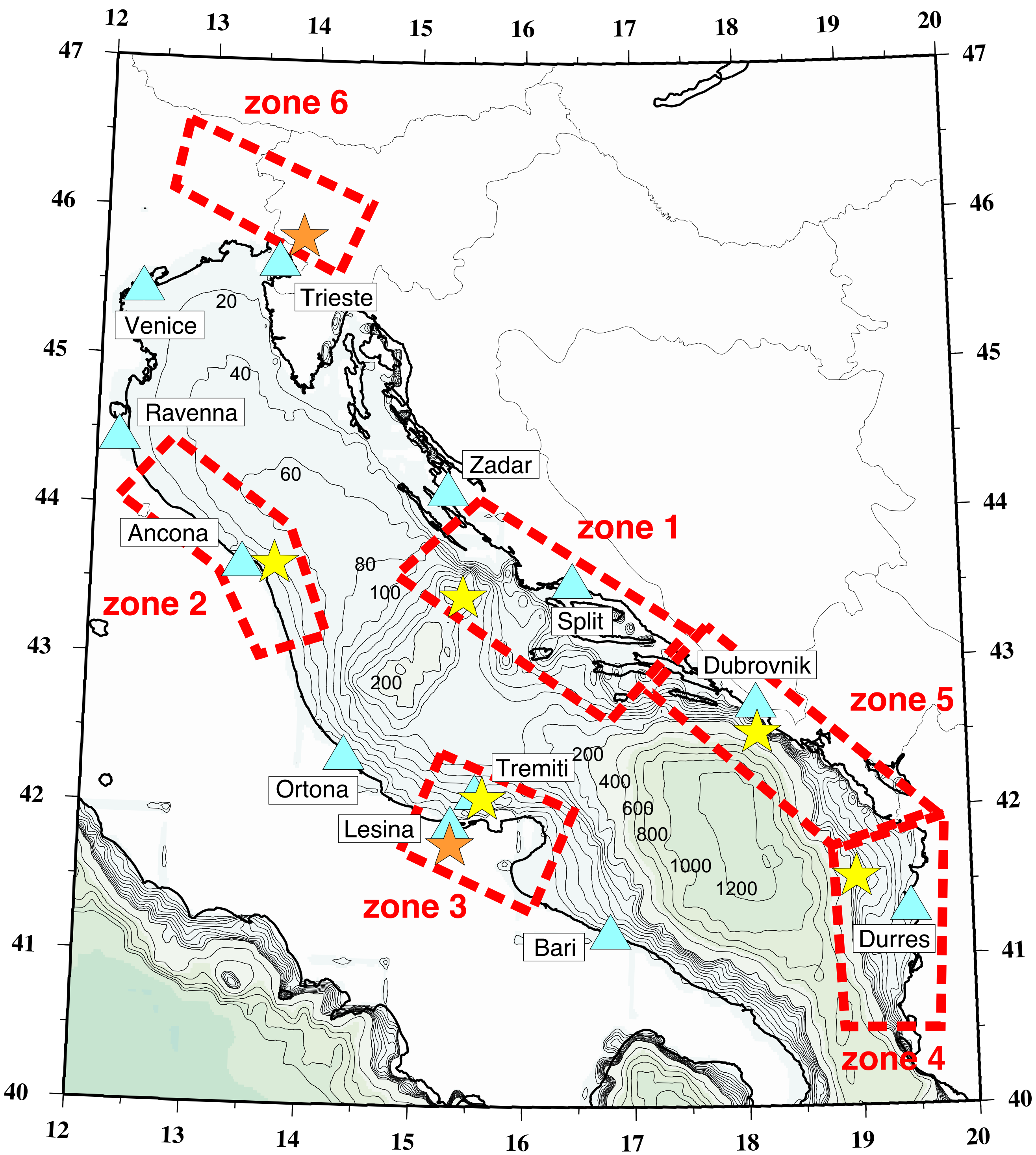

Bathymetric map of the Adriatic Sea. The bathymetric contours are drawn with a step of 20 m in the range from 0 to –200 m and with a step of 200 m in the range from –200 m to –1200 m.

The contours of the six tsunamigenic zones are shown in red, the blue triangles correspond to the 12 receiver sites, the stars correspond to the epicenters of the considered events (yellow: offshore, orange: inland).

Paulatto M., Pinat T., Romanelli F. , 2007. Tsunami hazard scenarios in the Adriatic Sea domain". Natural Hazards And Earth System Sciences (on line), vol. 7, pp. 309-325.

Tsunami scenarios in Adriatic Sea - Zone 1

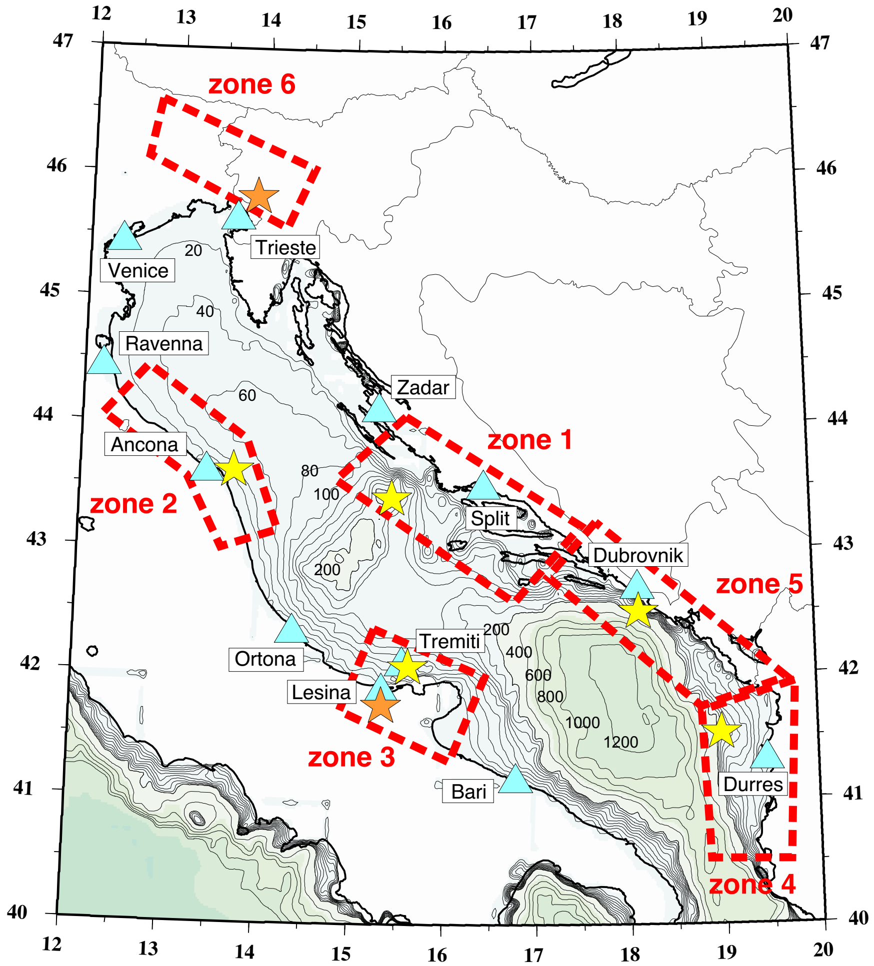

Tsunami scenarios in Adriatic Sea - Zone 1

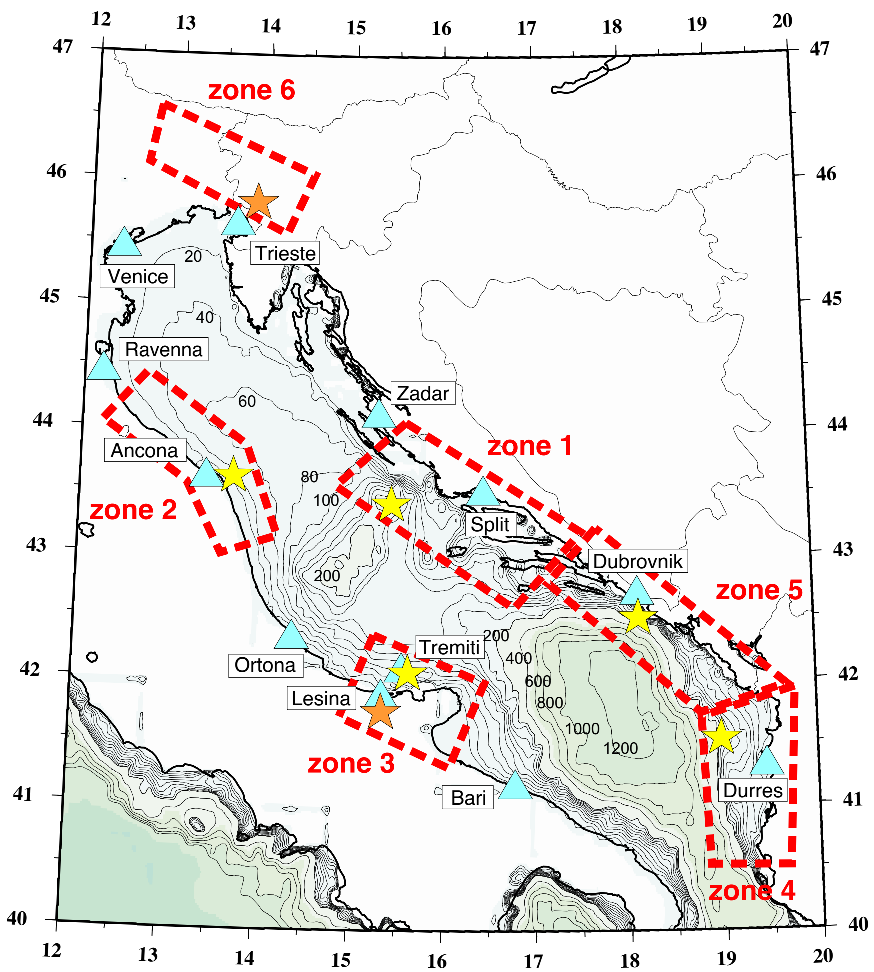

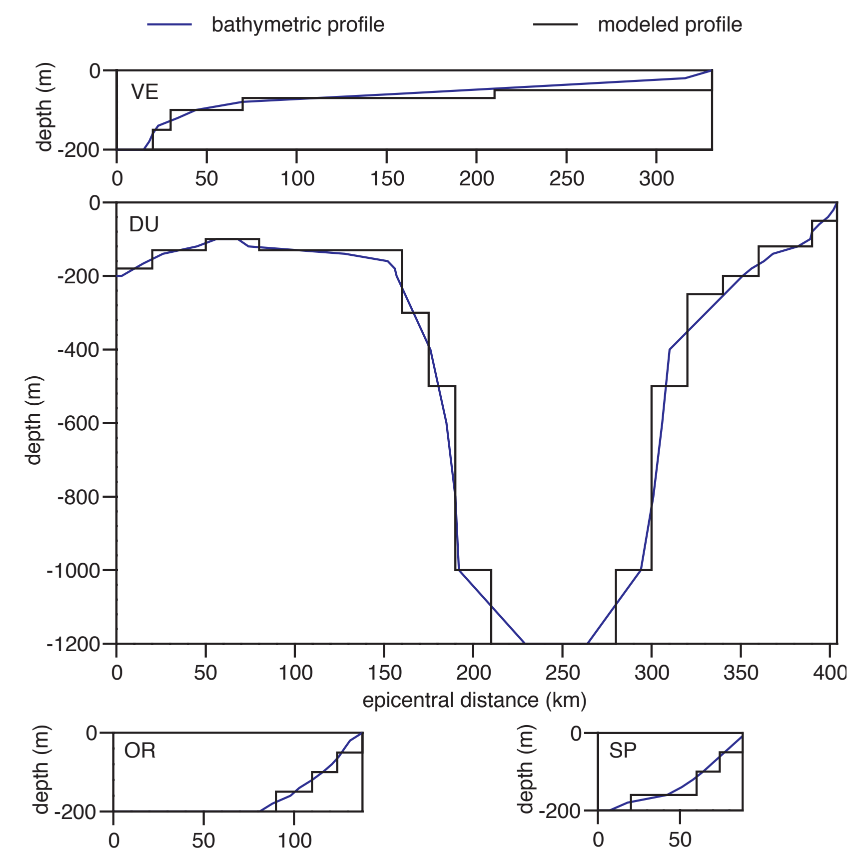

Bathymetric profiles to (from top) Venice (VE), Durres (DU), Ortona (OR) and Split (SP)

Tsunami scenarios in Adriatic Sea - Zone 1

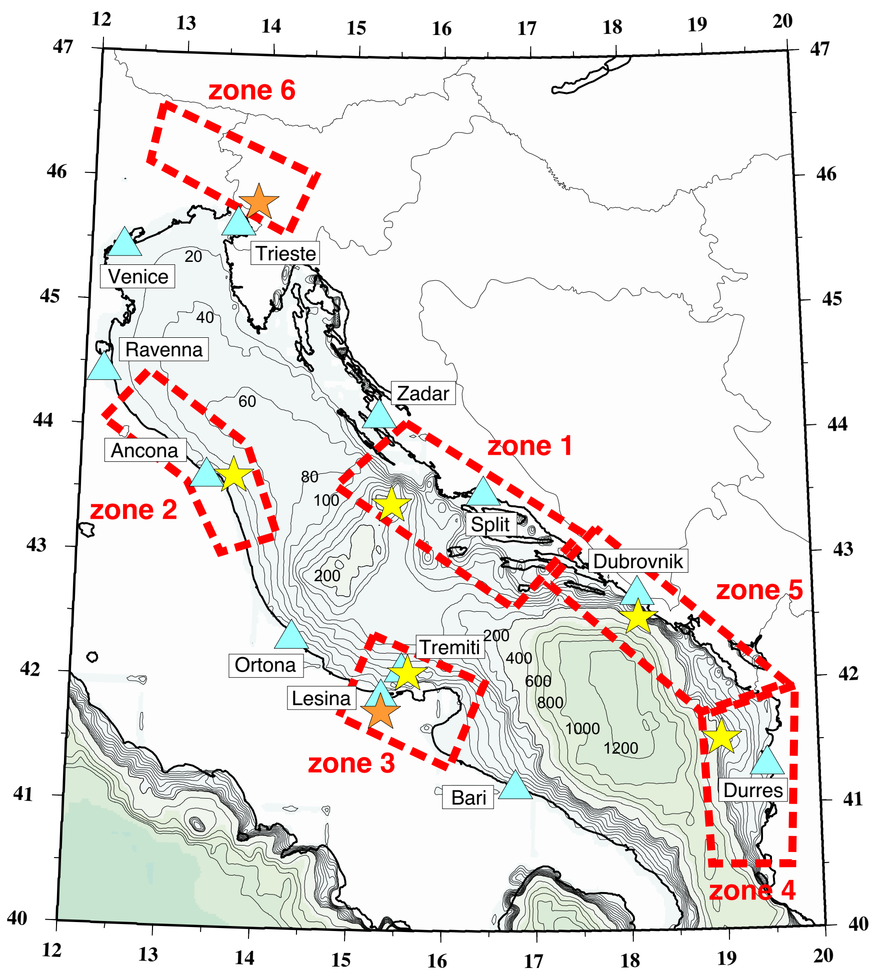

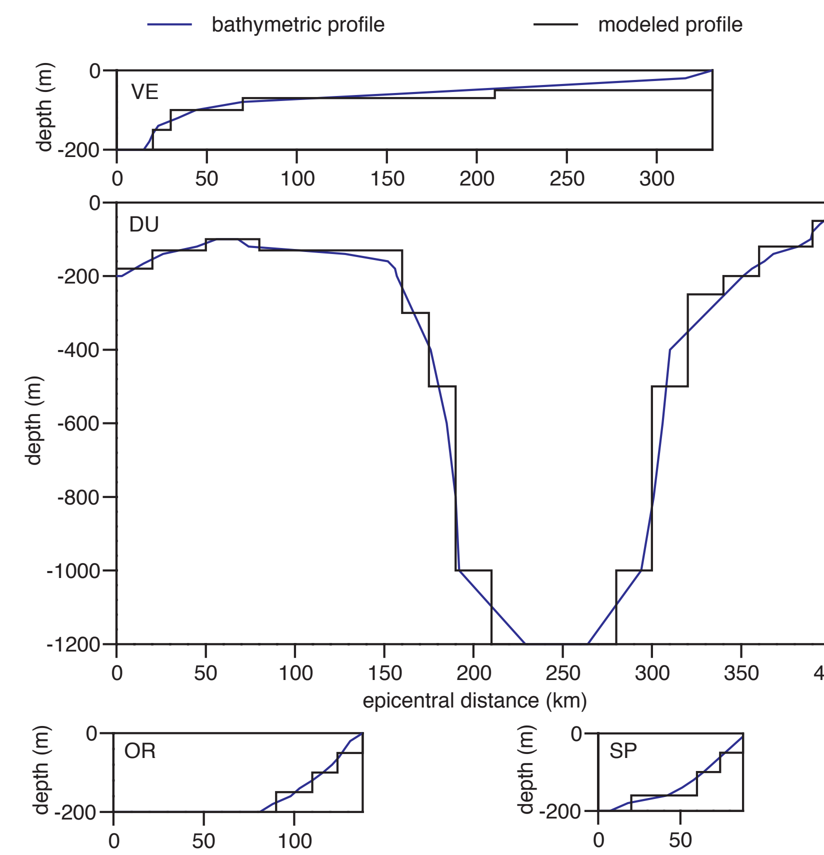

Bathymetric profiles to (from top) Venice (VE), Durres (DU), Ortona (OR) and Split (SP)

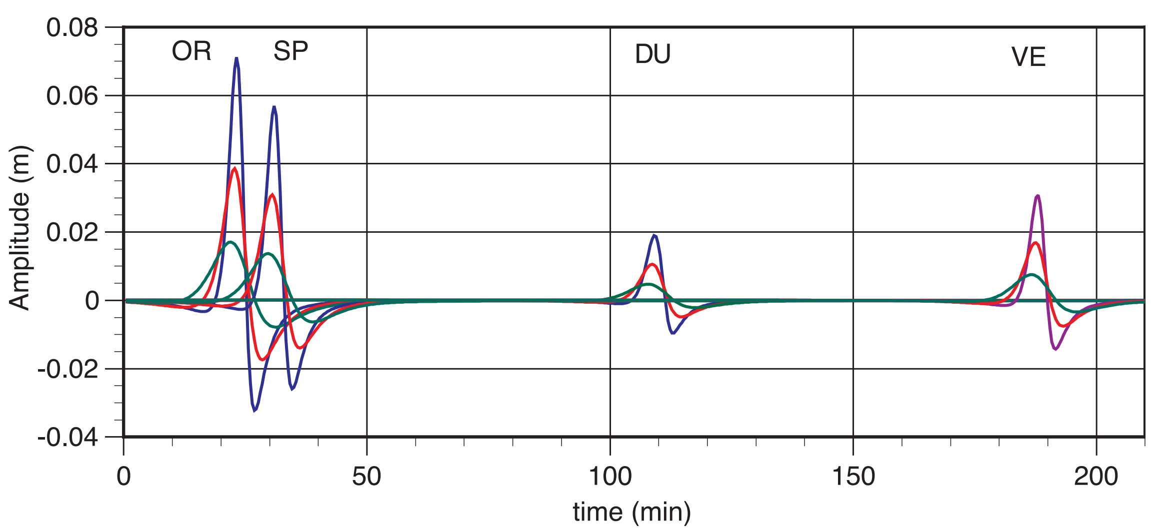

Synthetic mareograms for H =10 km (blue), 15 km (red), 25 km (green). Magnitude: M =6.5.

Adriatic

Tsunami scenarios in Adriatic Sea - Zone I

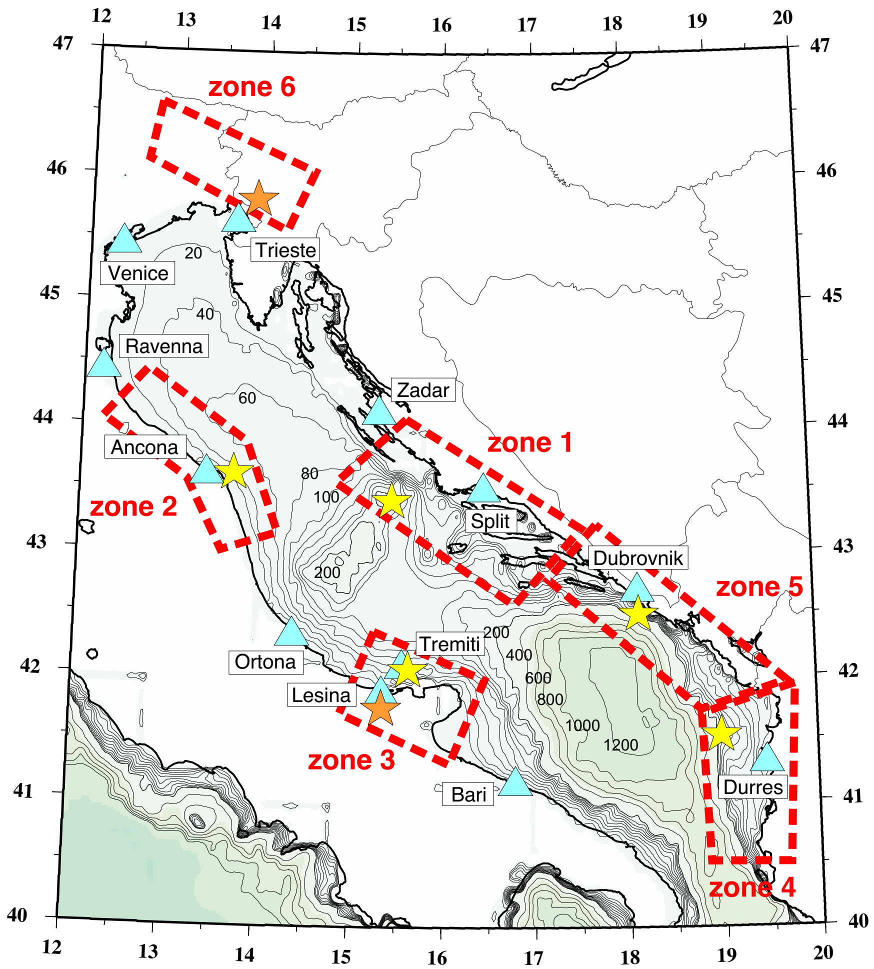

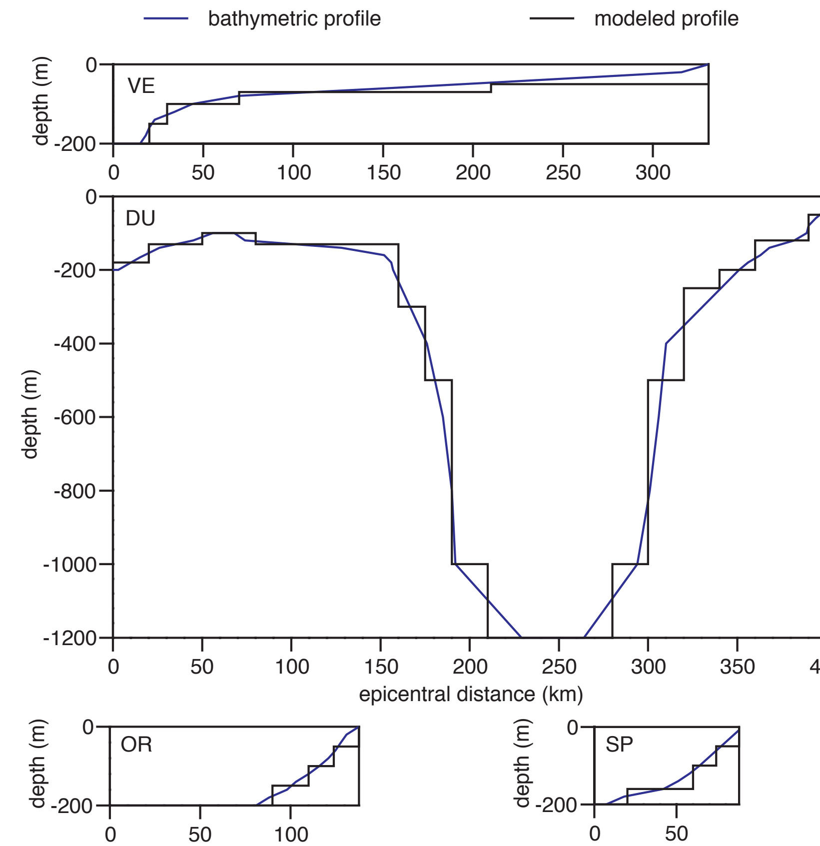

Bathymetric profiles to (from top) Venice (VE), Durres (DU), Ortona (OR) and Split (SP)

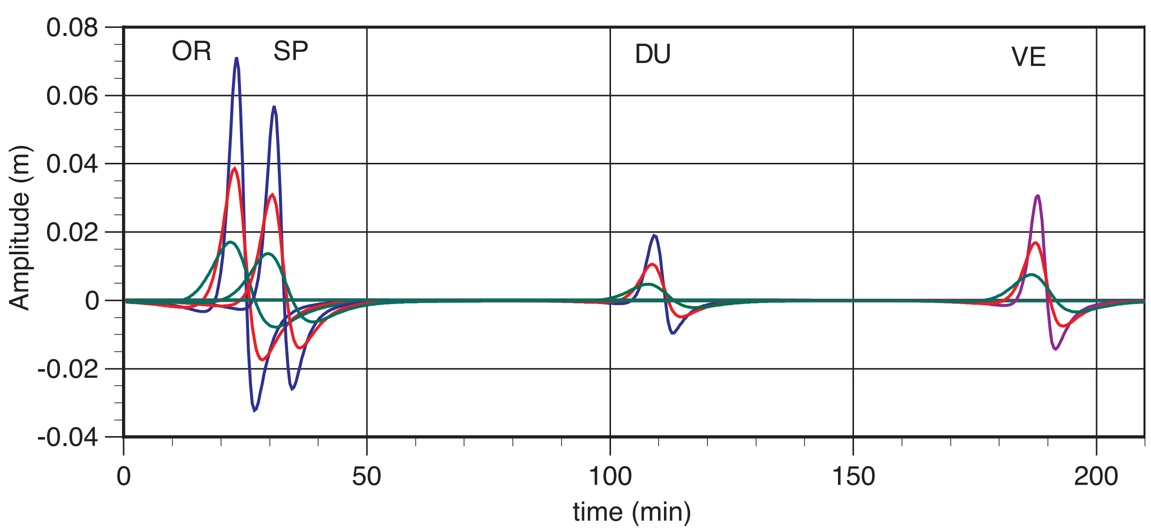

Synthetic mareograms for H =10 km (blue), 15 km (red), 25 km (green). Magnitude: M =6.5.

M		6.5			7.0			7.5		*Travel*
H (km)	10	15	25	10	15	25	10	15	25	*time (min)*
Durres	0.02	0.01	<0.01	0.11	0.06	0.03	0.60	0.33	0.15	*109*
Ortona	0.07	0.04	0.02	0.40	0.22	0.10	**2.25**	**1.22**	0.54	*23*
Split	0.06	0.03	0.01	0.32	0.17	0.08	**1.80**	0.98	0.43	*31*
Venice	0.03	0.02	0.01	0.17	0.09	0.04	0.97	0.53	0.24	*188*

Maximum amplitudes and related arrival times for different depths and magnitude

Tsunami scenarios in Adriatic Sea - Zone I

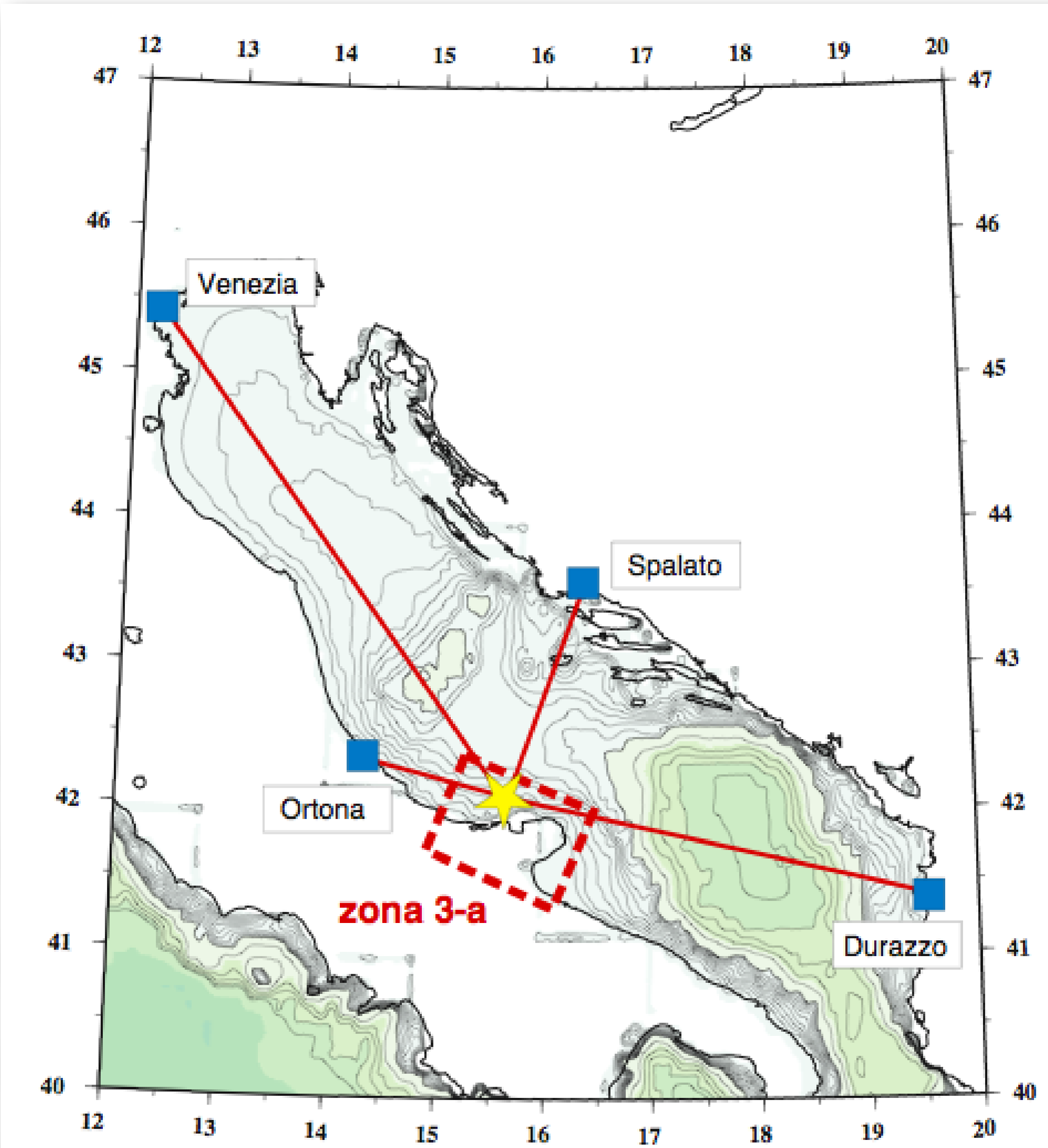

Zone boundaries (in red), the representative epicenter (yellow star), the four receivers (blue boxes) and their source-receiver paths (in red) are shown.

Tsunami scenarios in Adriatic Sea - Zone I

Tsunami scenarios in Adriatic Sea - Zone I

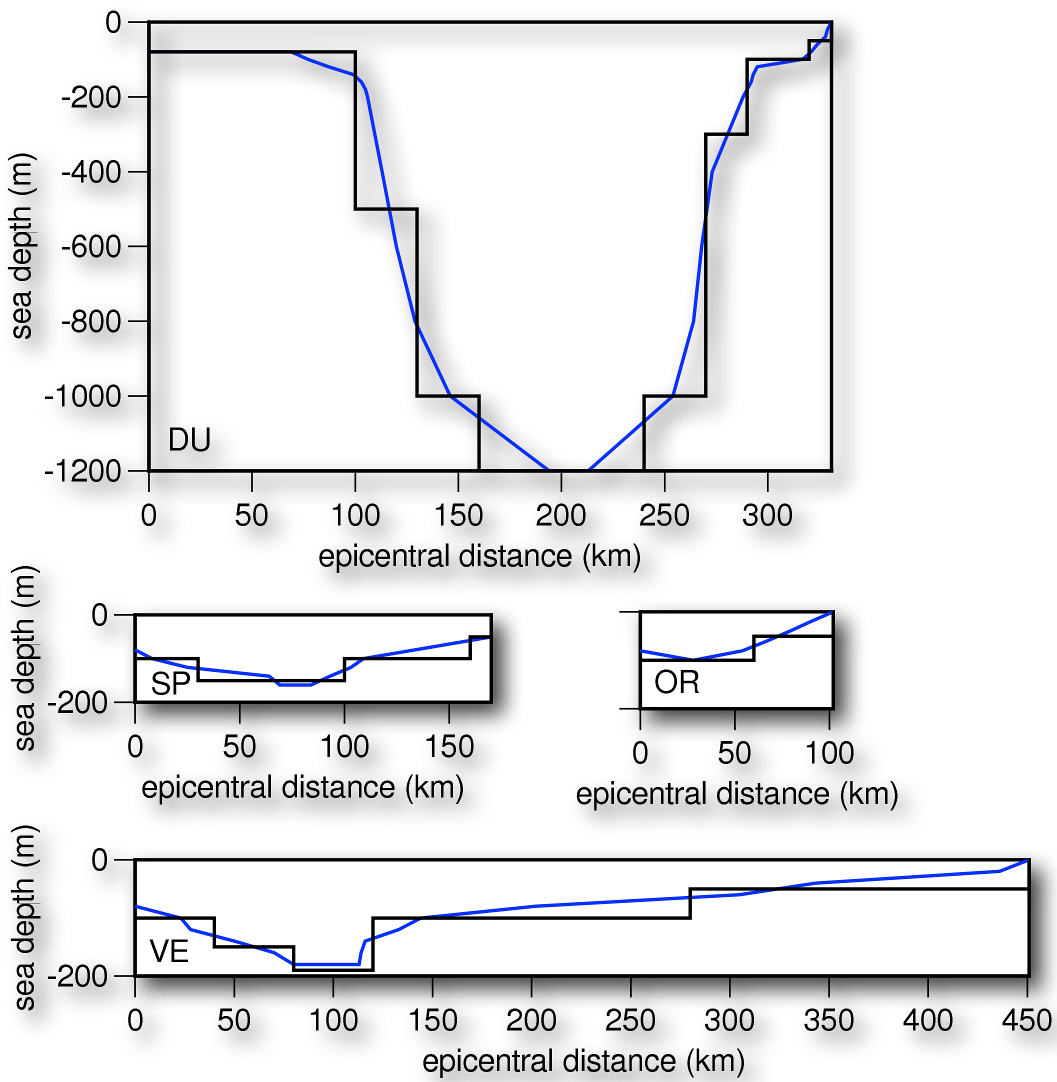

Fig. 9. Bathymetric profiles (in blue) along source-site paths and their parameterizations (in black) used for calculations for the four sites of Zone 3-a. From above: Durres (DU), Split (SP), Ortona (OR) and Venice (VE).

Tsunami scenarios in Adriatic Sea - Zone I

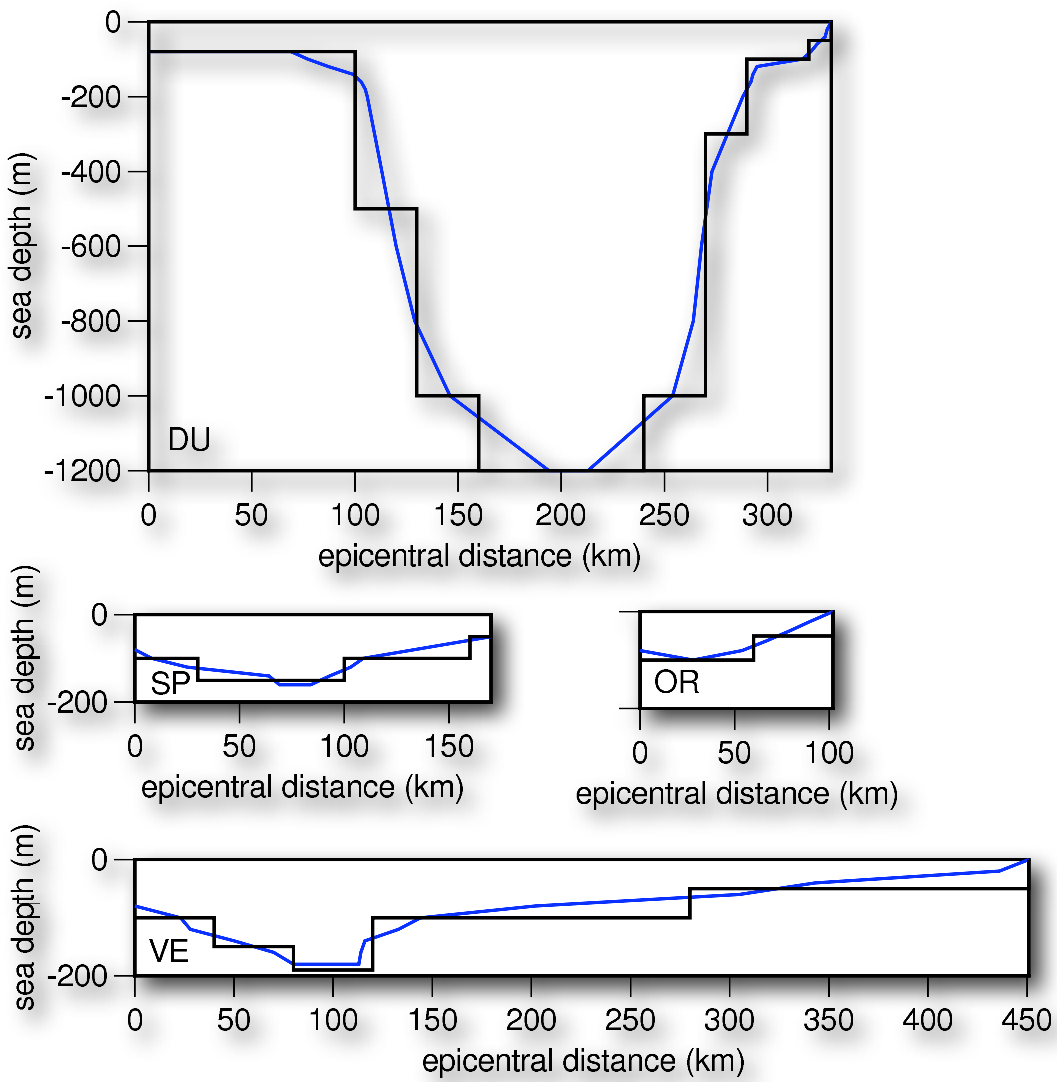

Fig. 9. Bathymetric profiles (in blue) along source-site paths and their parameterizations (in black) used for calculations for the four sites of Zone 3-a. From above: Durres (DU), Split (SP), Ortona (OR) and Venice (VE).

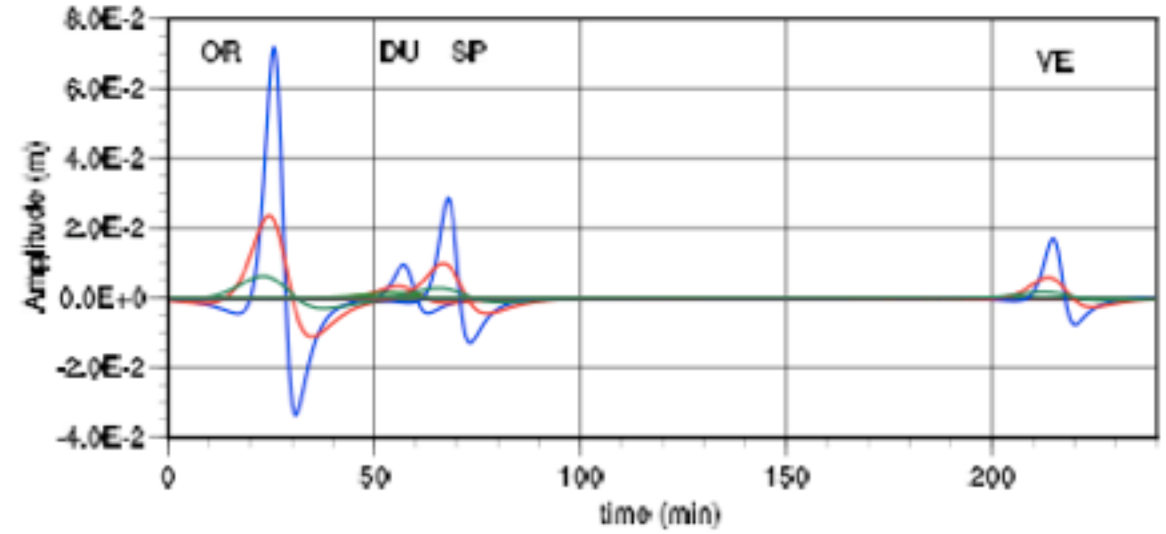

Synthetic mareograms for Zone 3-a. Focal depth: 10 km (blue), 20 km (green), 30 km (red). Magnitude: 6.5.

Tsunami scenarios in Adriatic Sea - Zone I

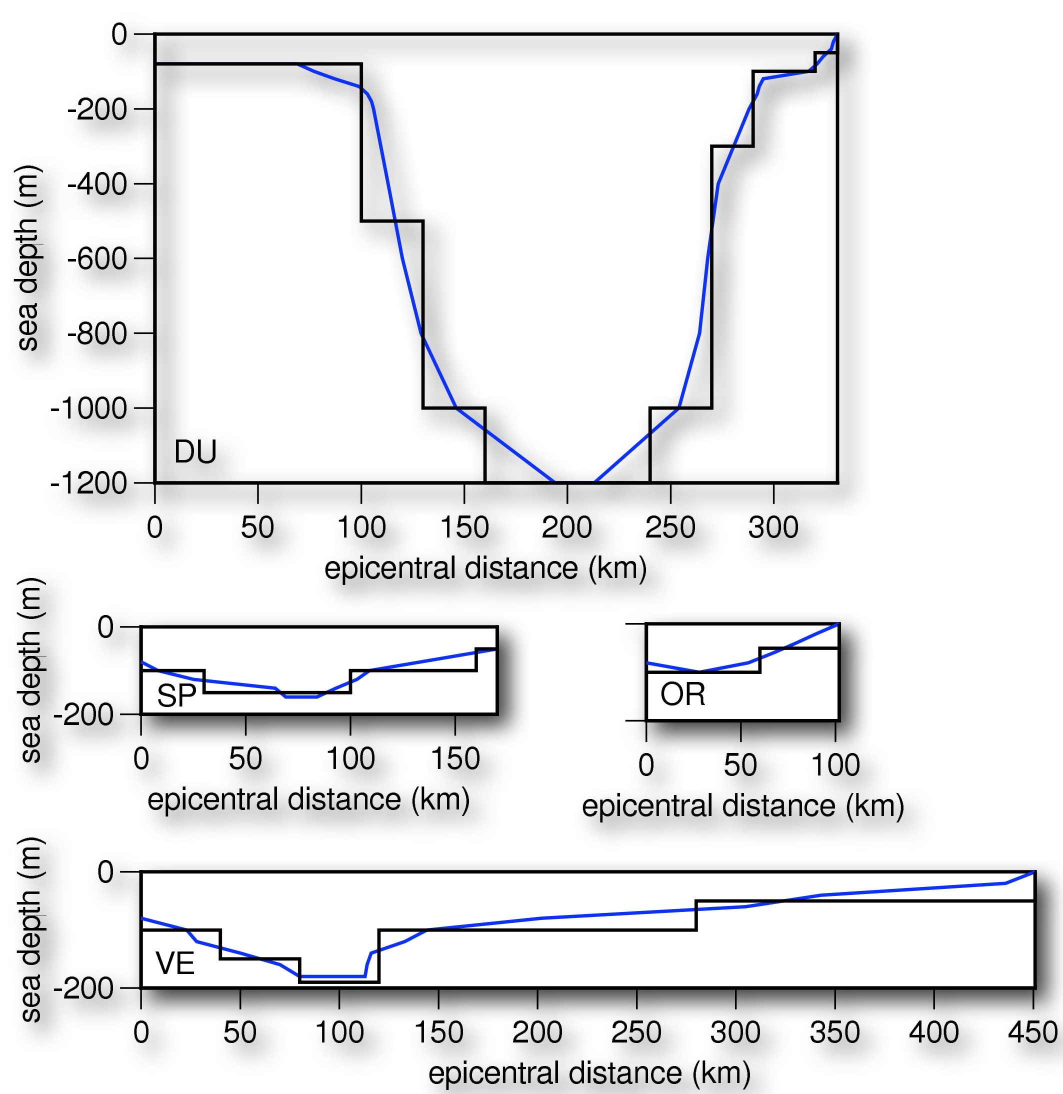

Fig. 9. Bathymetric profiles (in blue) along source-site paths and their parameterizations (in black) used for calculations for the four sites of Zone 3-a. From above: Durres (DU), Split (SP), Ortona (OR) and Venice (V

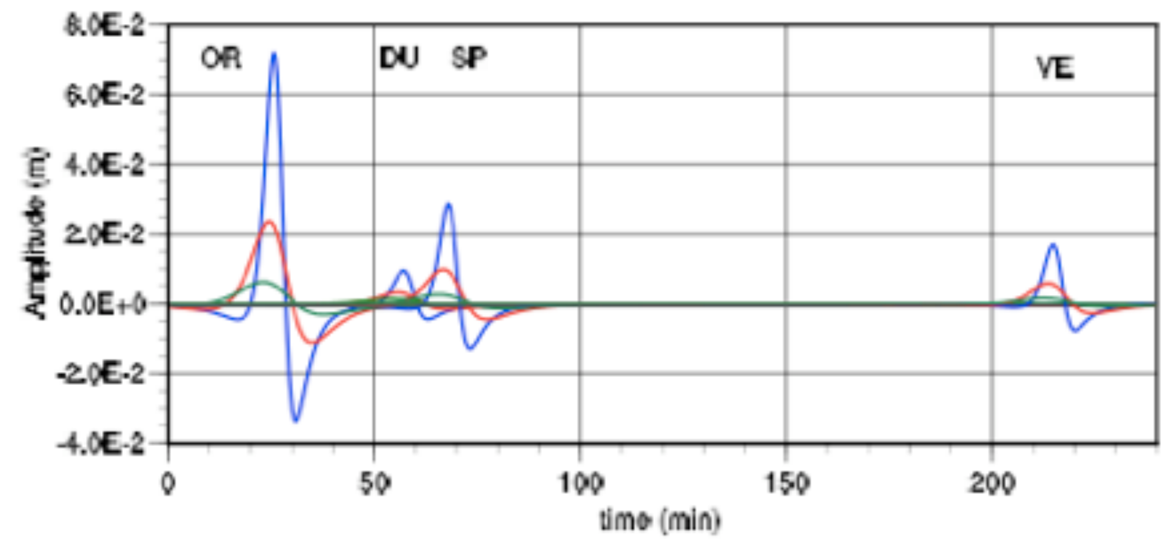

Synthetic mareograms for Zone 3-a. Focal depth: 10 km (blue), 20 km (green), 30 km (red). Magnitude: 6.5.

Table 10. Maximum amplitudes and travel times for the four sites of Zone 3, offshore source case. Scenarios are calculated for three values of magnitude, M=6.0, 6.5, 7.0, and three values of focal depth, H=10, 15, 25 km. Amplitudes are reported in meters. Amplitudes exceeding 1 m are written in bold style.

M		6.0			6.5			7.0		*Travel*
H (km)	10	15	25	10	15	25	10	15	25	*time (min)*
Durazzo	<0.01	<0.01	<0.01	0.01	<0.01	<0.01	0.05	0.02	0.01	57
Ortona	0.01	<0.01	<0.01	0.07	0.02	0.01	0.41	0.13	0.04	26
Spalato	0.01	<0.01	<0.01	0.03	0.01	<0.01	0.16	0.06	0.02	68
Venezia	<0.01	<0.01	<0.01	0.02	0.01	<0.01	0.10	0.03	0.01	215

Source 2 scenario

Inland source ⇒ Green-function approach

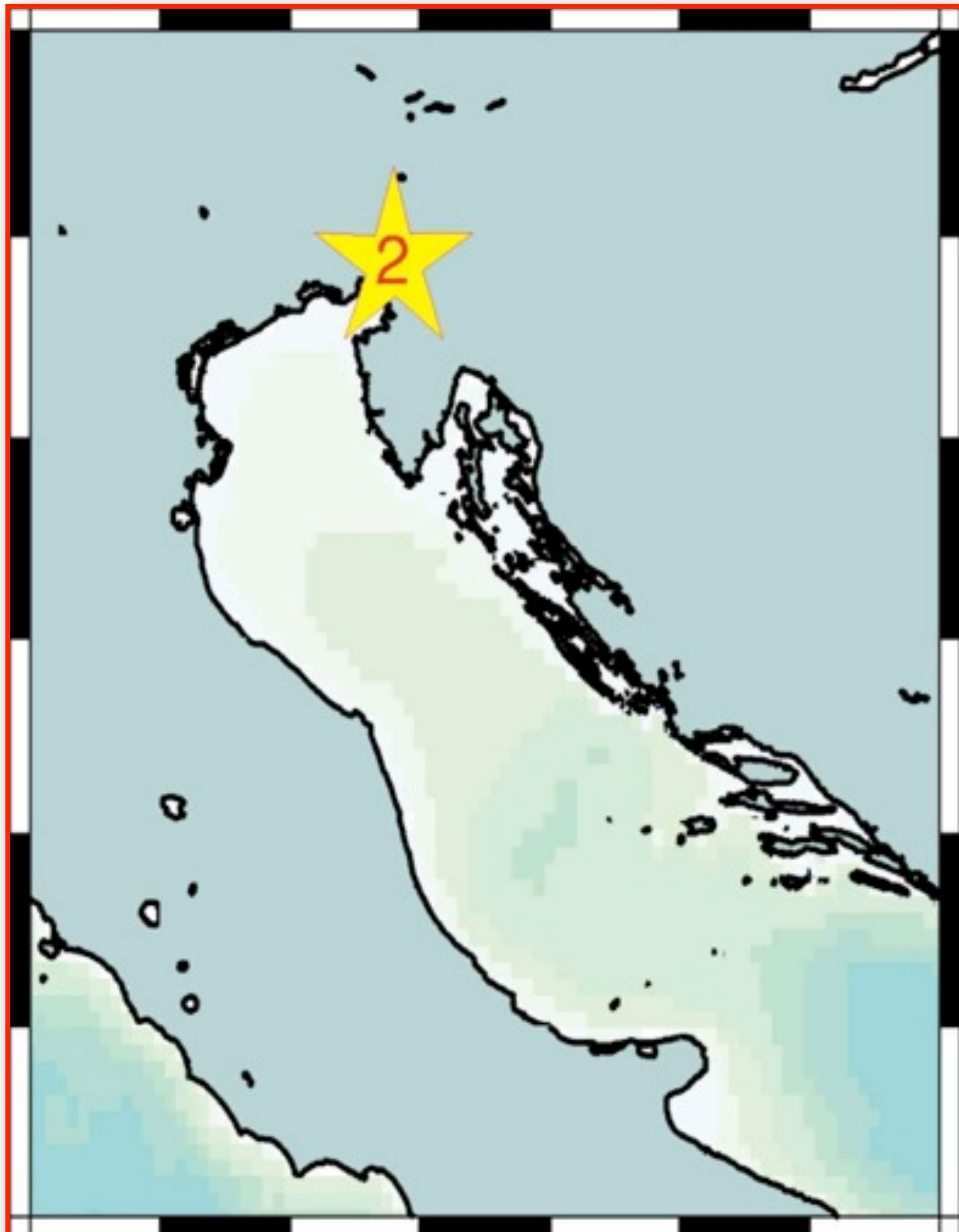

The recent re-evaluation of the 1511 earthquake by Fitzko, P. Suhadolc, A. Aoudia and G. F. Panza (2005) is consistent with a 6.9 magnitude single event rupturing 50 km of the Idrija right-lateral strike-slip fault with bilateral rupture propagation. This part of the Idrija fault stands 40 km far from the coastline.

Another seismogenic structure that needs to be considered is the the Rasa-Cividale right lateral-strike slip (Aoudia, 1998), that stands at 16 km from the coastline.

Source 2 scenario

Inland source ⇒ Green-function approach

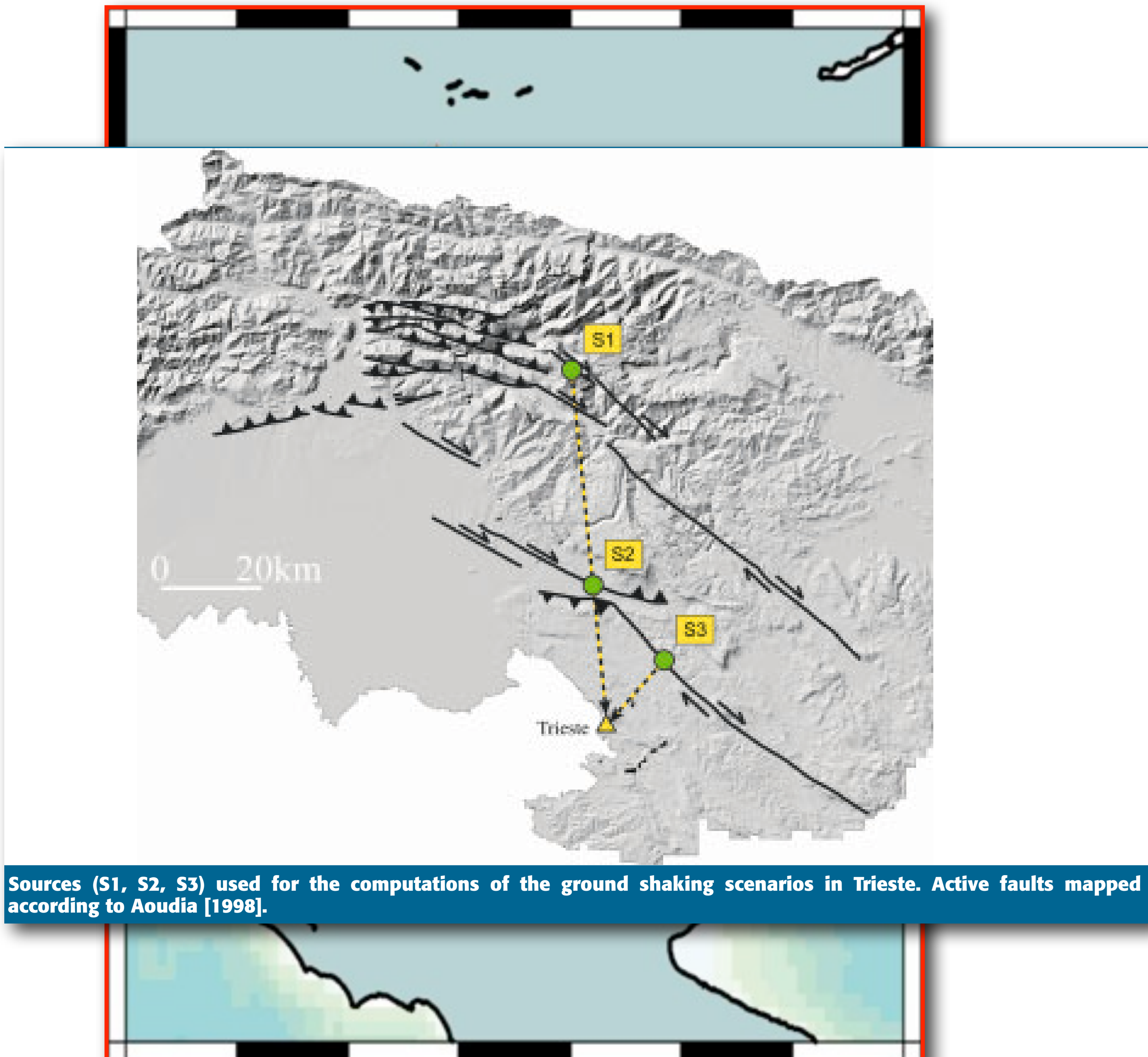

Sources (S1, S2, S3) used for the computations of the ground shaking scenarios in Trieste. Active faults mapped according to Aoudia [1998].

The recent re-evaluation of the 1511 earthquake by Fitzko, P. Suhadolc, A. Aoudia and G. F. Panza (2005) is consistent with a 6.9 magnitude single event rupturing 50 km of the Idrija right-lateral strike-slip fault with bilateral rupture propagation. This part of the Idrija fault stands 40 km far from the coastline.

Another seismogenic structure that needs to be considered is the the Rasa-Cividale right lateral-strike slip (Aoudia, 1998), that stands at 16 km from the coastline.

Tsunami scenarios in Adriatic Sea - Zone 6

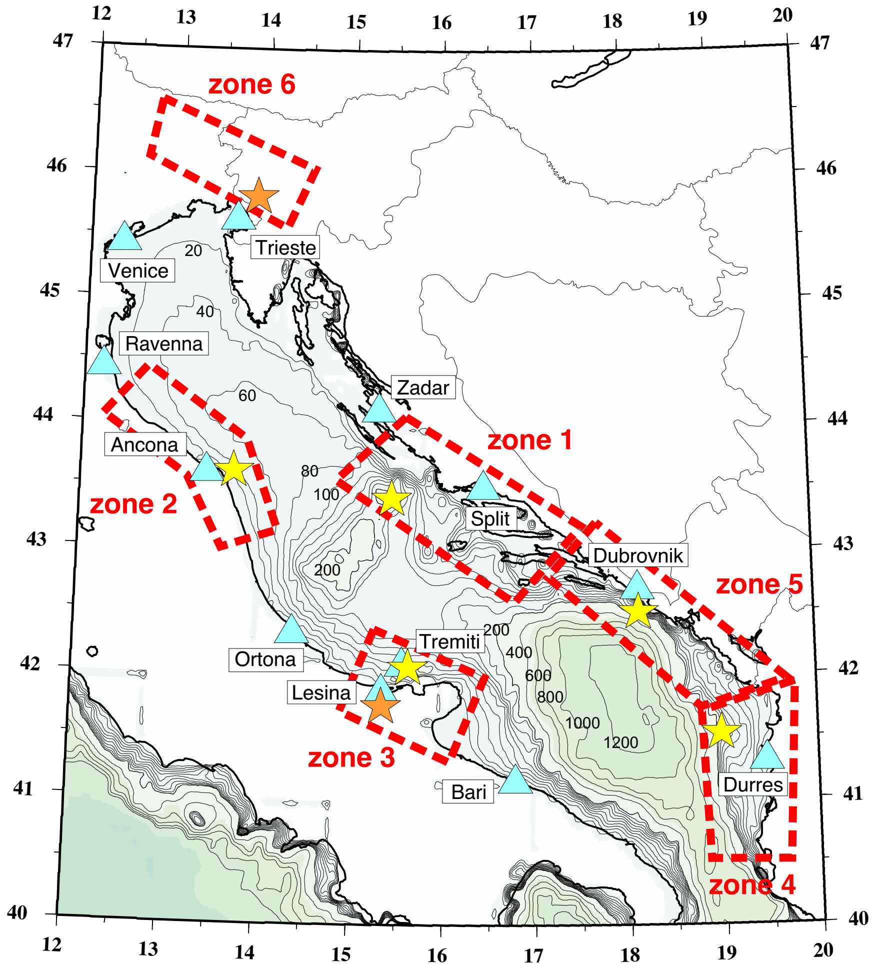

Tsunami scenarios in Adriatic Sea - Zone 6

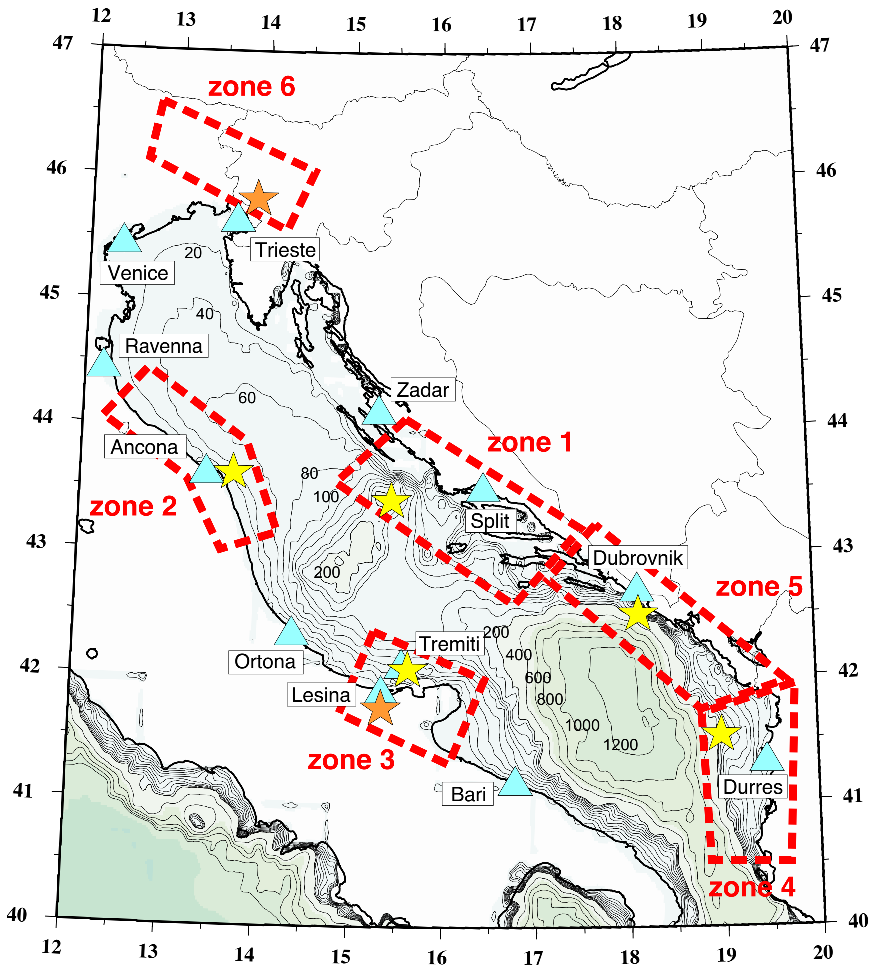

Table 7. Main parameters identifying the three sites of Zone 6.

Site	Latitude	Longitude	Epicentral dist. *R*
Trieste (TS)	45.67° N	13.77° E	30 km, 50 km
Venice (VE)	45.45° N	12.35° E	130 km, 150 km
Ravenna (RA)	44.42° N	12.20° E	210 km, 230 km

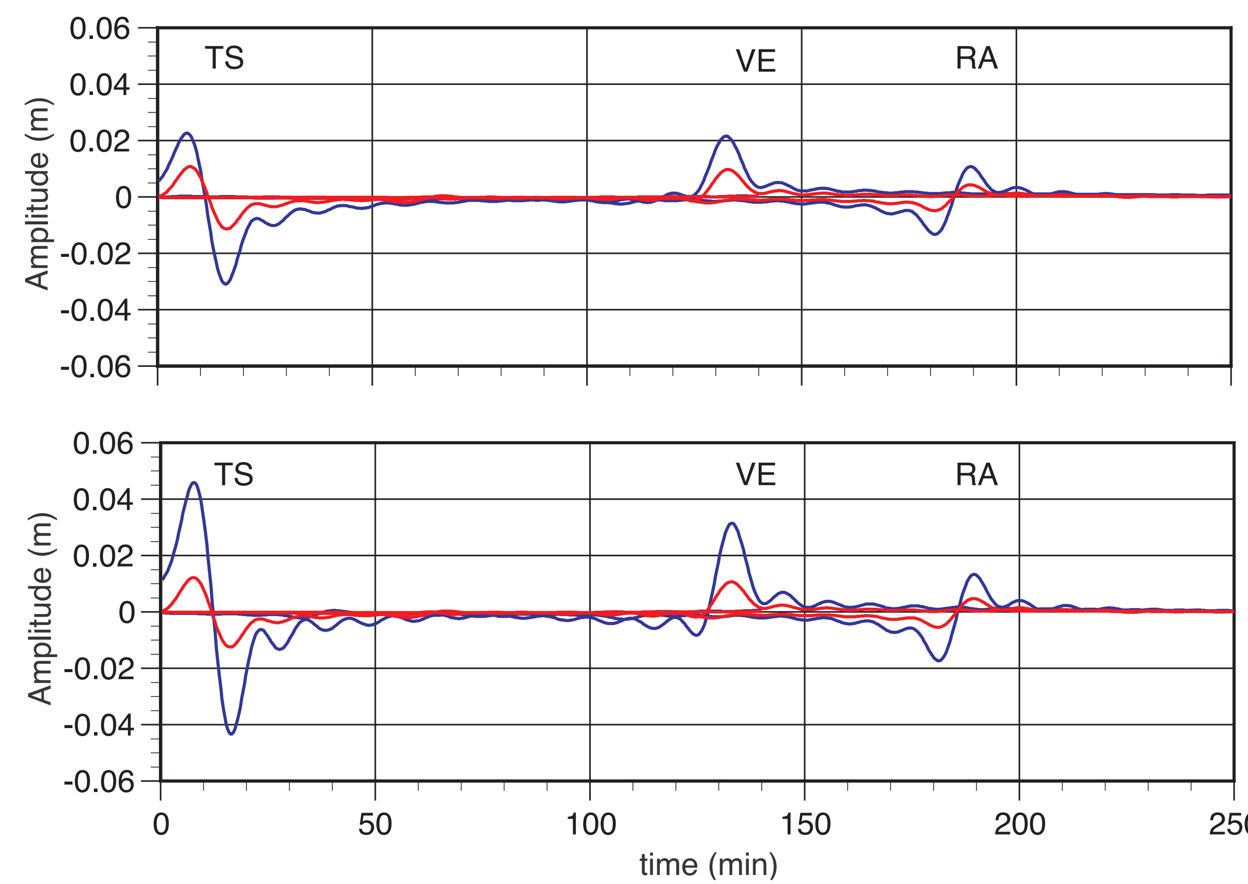

Synthetic mareograms for Zone 6, magnitude, M=7.0. Above: dip angle=45°; below: dip angle=30°. Blue line, d=20 km; red line, d=40 km.

Tsunami scenarios in Adriatic Sea - Zone 6

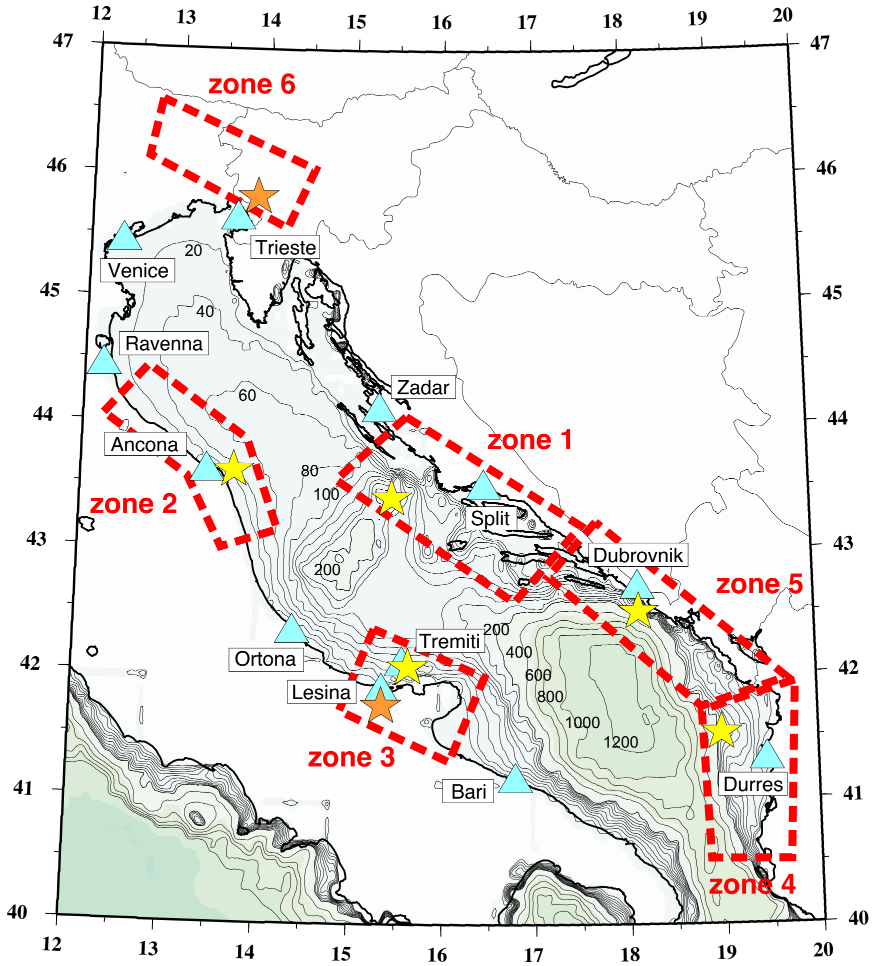

M	6.5		7.0		*Travel*
d (km)	20	40	20	40	*time (min)*
Trieste, dip = 45°	<0.01	<0.01	0.02	0.01	*7*
Trieste, dip = 30°	<0.01	<0.01	0.05	0.01	*8*
Venice, dip = 45°	<0.01	<0.01	0.02	0.01	*132*
Venice, dip = 30°	<0.01	<0.01	0.03	0.01	*133*
Ravenna, dip = 45°	<0.01	<0.01	0.01	<0.01	*189*
Ravenna, dip = 30°	<0.01	<0.01	0.01	<0.01	*189*

Maximum amplitudes and related arrival times for different depths and magnitude

Table 7. Main parameters identifying the three sites of Zone 6.

Site	Latitude	Longitude	Epicentral dist. *R*
Trieste (TS)	45.67° N	13.77° E	30 km, 50 km
Venice (VE)	45.45° N	12.35° E	130 km, 150 km
Ravenna (RA)	44.42° N	12.20° E	210 km, 230 km

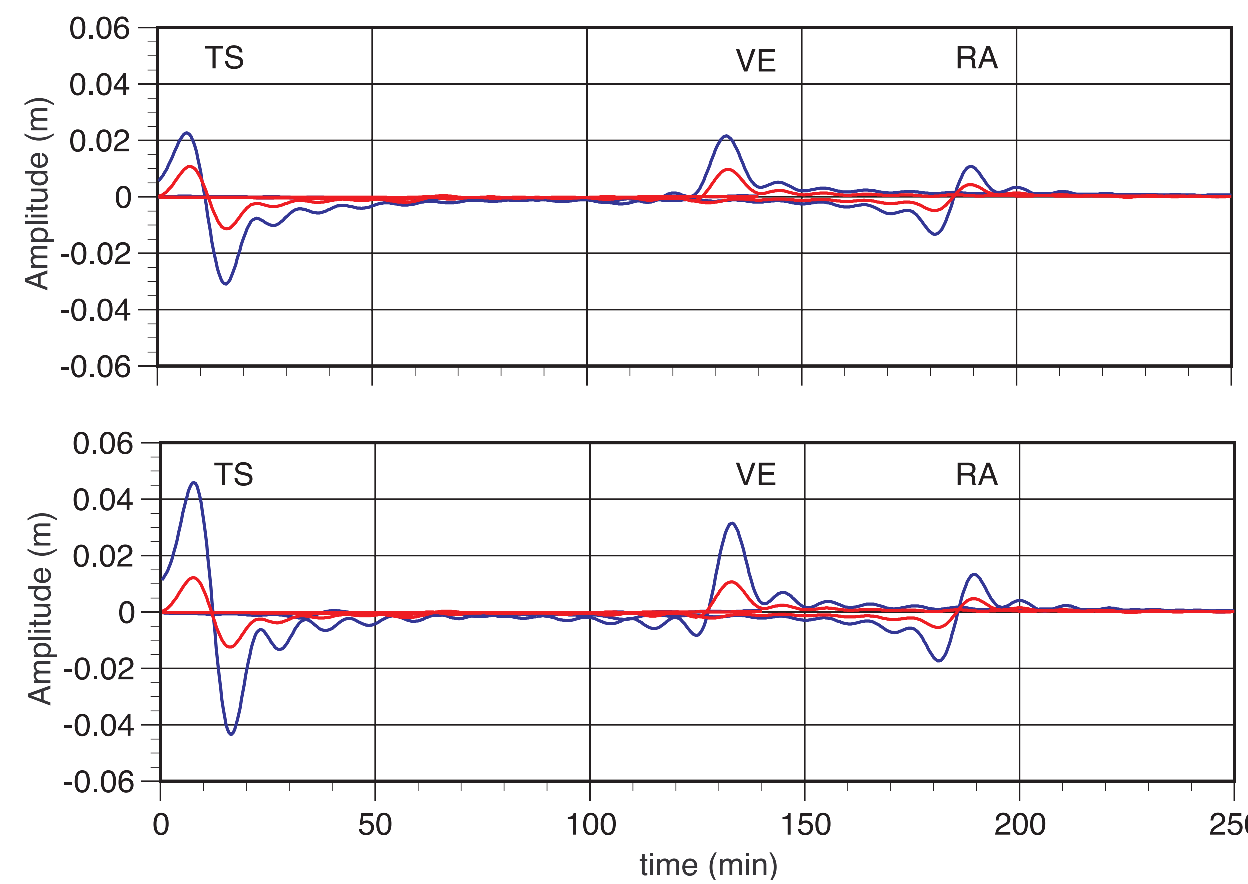

Synthetic mareograms for Zone 6, magnitude, M=7.0. Above: dip angle=45°; below: dip angle=30°. Blue line, d=20 km; red line, d=40 km.

Updating...

Tectonic sketch map of the Adriatic basin.

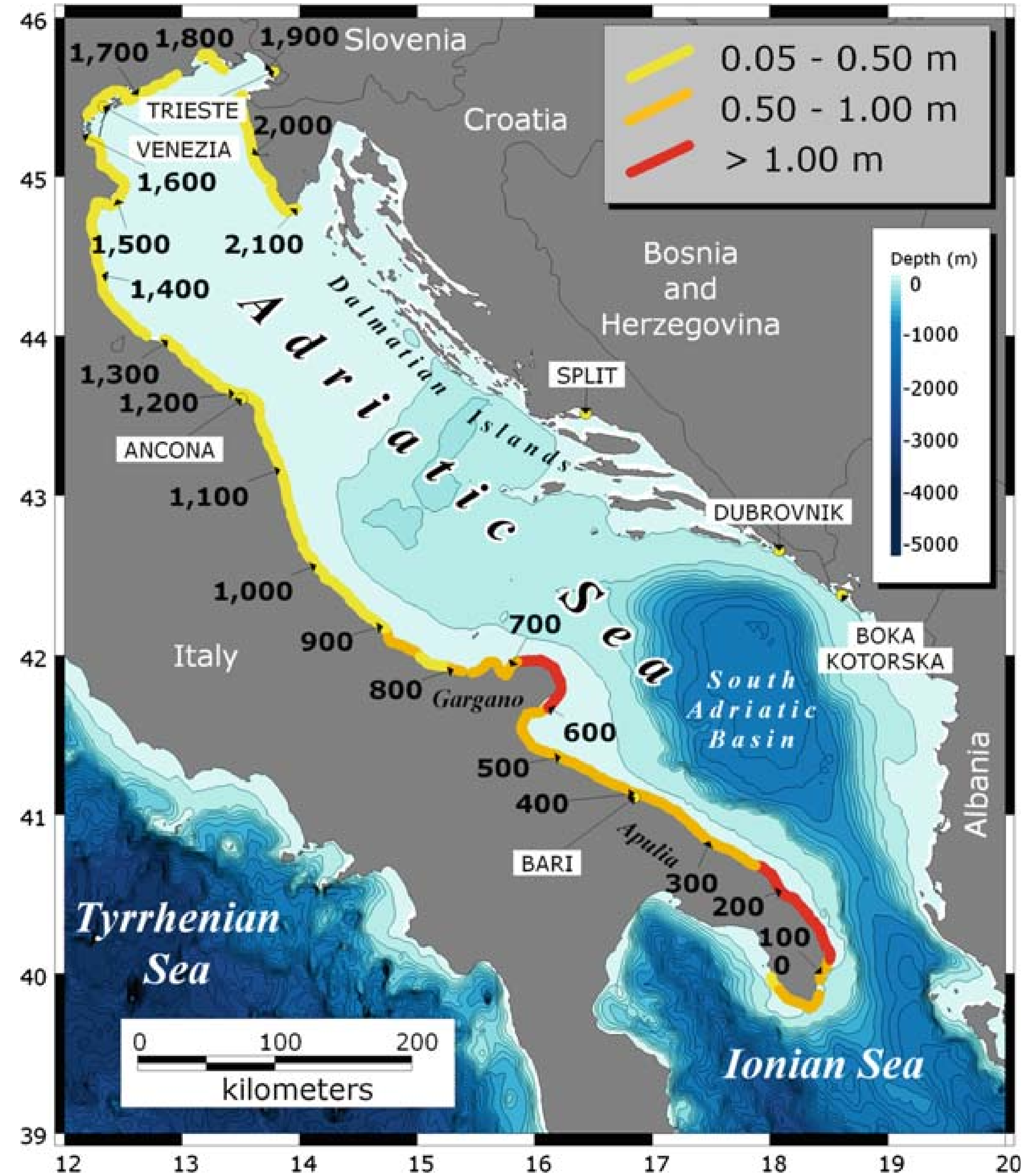

Combined threat levels posed by all SZs

Tiberti et al., 2009. Scenarios of Earthquake-Generated Tsunamis for the Italian Coast of the Adriatic Sea, Pageoph, 165, 2117–2142.

Building a culture of prevention is not easy.

While the costs of prevention have to be paid in the present, its benefits lie in a distant future.

Moreover, the benefits are not tangible; they are the disasters that did NOT happen.

Kofi Annan, 1999
(document A/54/1)

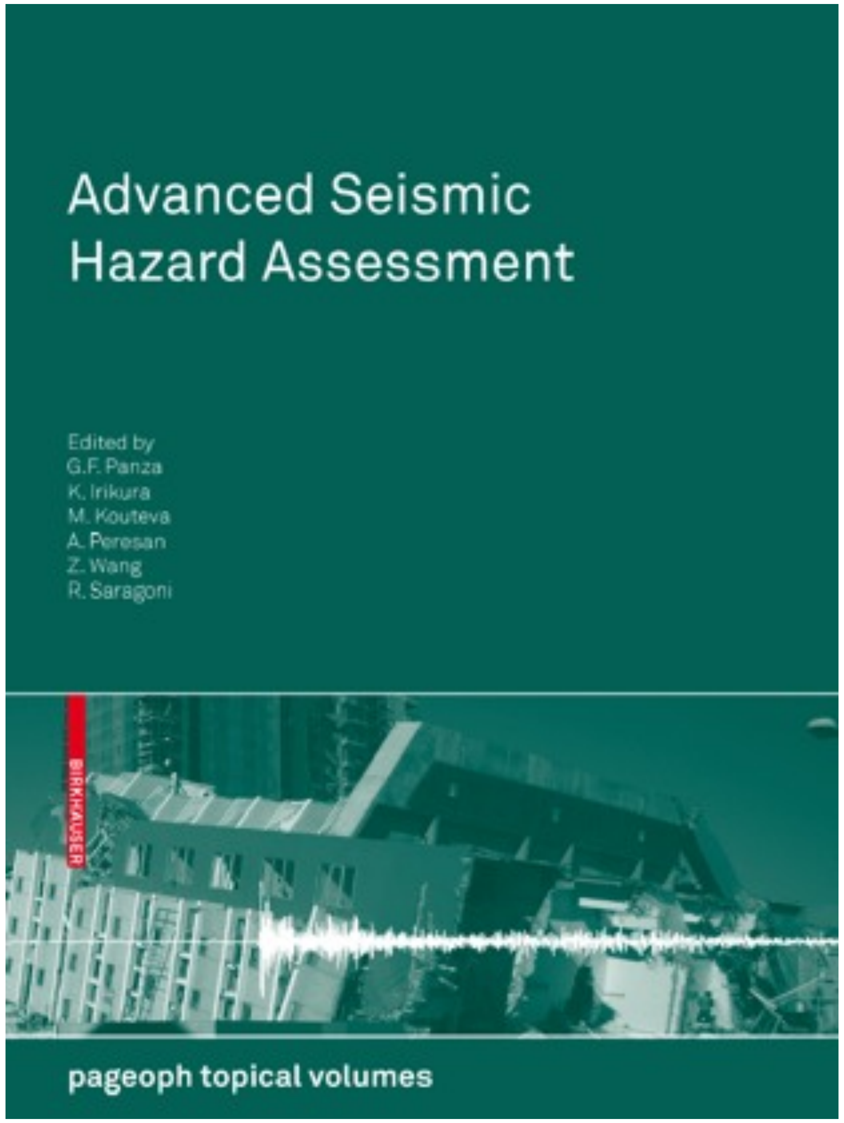

Pure and Applied Geophysics Topical Volume

Vol. 168, 2011

Part I: Seismic Hazard Assessment, ISBN 978-3-0348-0039-6
Part II: Regional Seismic Hazard and Seismic Microzonation Case Studies, ISBN: 978-3-0348-0091-4

Advanced Seismic Hazard Assessment

Editors: G.F. Panza (Italy), K. Irikura (Japan), M. Kouteva (Bulgaria), A. Peresan (Italy), Z. Wang (USA), R. Saragoni (Chile)

The aforesaid remarks and proposals are part of those contained in the Italian Parliament Resolution 8/00124, concerning recommended modifications of the Italian and European design rules for the isolated structures that has been approved (June 2011) at the Commission for the Environment, Territory and Public Works of the Italian Chamber of Deputies; the resolution explicitly mentions the need to resort to physically sound deterministic methods like NDSHA

References

- PANZA, G. F., ROMANELLI, F., VACCARI, F. (2001), Seismic wave propagation in laterally heterogeneus anelastic media: theory and applications to seismic zonation, Adv. Geophys. 43, 1–95
- ZUCCOLO E., VACCARI F., PERESAN A., PANZA G. F. (2010), Neo-Deterministic and Probabilistic Seismic Hazard Assessments: a Comparison over the Italian Territory, Pure Appl. Geophys. 168(1–2). doi: 10.1007/s00024-010-0151-8
- INDIRLI M., RAZAFINDRAKOTO H., ROMANELLI F., PUGLISI C., LANZONI L., MILANI E., MUNARI M., APABLAZA S. (2011). Hazard Evaluation in Valparaìso: the MAR VASTO Project. Pure And Applied Geophysics, pp 543-582, Vol. 168.
- PANZA, G. F., LA MURA, C., PERESAN, A., ROMANELLI, F., VACCARI, F. (2012). Seismic Hazard Scenarios as Preventive Tools for a Disaster Resilient Society, Advances in Geophysics, in press.